



## City Research Online

### City, University of London Institutional Repository

---

**Citation:** Divall, S. (2013). Ground movements associated with twin-tunnel construction in clay. (Unpublished Doctoral thesis, City University London)

This is the accepted version of the paper.

This version of the publication may differ from the final published version.

---

**Permanent repository link:** <https://openaccess.city.ac.uk/id/eprint/4785/>

**Link to published version:**

**Copyright:** City Research Online aims to make research outputs of City, University of London available to a wider audience. Copyright and Moral Rights remain with the author(s) and/or copyright holders. URLs from City Research Online may be freely distributed and linked to.

**Reuse:** Copies of full items can be used for personal research or study, educational, or not-for-profit purposes without prior permission or charge. Provided that the authors, title and full bibliographic details are credited, a hyperlink and/or URL is given for the original metadata page and the content is not changed in any way.

Ground movements associated with twin-tunnel construction in clay

by

Sam Divall

A dissertation submitted for the Degree of Doctor of Philosophy

City University London

Department of Civil Engineering

Geotechnical Engineering Research Group

May 2013



# CONTENTS

LIST OF TABLES .....	vii
LIST OF FIGURES .....	viii
ACKNOWLEDGEMENTS .....	xiv
DECLARATIONS .....	xv
ABSTRACT.....	xvi
LIST OF SYMBOLS .....	xvii
1 INTRODUCTION .....	1
1.1 General.....	1
1.2 Aims.....	3
1.3 Outline of the thesis .....	3
2 BACKGROUND .....	5
2.1 Scope of the research .....	5
2.1.1 Types of Tunnel Construction.....	5
2.1.2 Soil Structure .....	6
2.1.3 Prediction of tunnelling-induced ground movements .....	6
2.1.4 Assessment of damage to existing structures due to tunnelling.....	7
2.2 Research Method .....	8
2.2.1 Centrifuge model testing.....	8
3 TUNNELLING INDUCED GROUND MOVEMENTS.....	10
3.1 Introduction.....	10
3.2 Short-term ground movements in greenfield conditions.....	11
3.2.1 Volume Loss .....	11
3.2.2 Transverse Settlement Trough .....	12

3.3	Long-term Ground Deformations (Post construction) .....	15
3.3.1	Time-related tunnelling-induced settlement .....	15
3.3.2	Consolidation and Seepage .....	17
3.4	Tunnel Collapse .....	19
3.4.1	Failure Mechanisms .....	19
3.4.2	Undrained Stability .....	20
3.5	Summary .....	21
4	PREDICTION OF GROUND MOVEMENTS CAUSED BY TUNNELLING .....	23
4.1	Current practice for predicting ground movements above single tunnels.....	23
4.1.1	Predicting Short-Term Volume Loss .....	23
4.1.2	Transverse Surface Settlement Trough .....	24
4.1.3	Sub-surface Settlements .....	28
4.2	Modelling and Prediction of Twin Bored Tunnelling-induced Ground Movements..	30
4.2.1	Superposition Method .....	31
4.2.2	Overlapping Zones .....	31
4.2.3	Design Plots by Addenbrooke & Potts (2001) .....	32
4.2.4	Modification Method by Hunt (2005) .....	33
4.2.5	Conclusions from Twin-tunnel prediction methods.....	34
4.3	Field Observations .....	34
4.3.1	Heathrow Express (UK) – Side-by-side Tunnels.....	35
4.3.2	Lafayette Park (USA) – Side-by-side Tunnels.....	35
4.3.3	St James Park (UK) – Offset Tunnels .....	36
4.3.4	Docklands Light Rail Lewisham Extension (UK) – Side-by-side Tunnels .....	37
4.4	Summary .....	37

5	CENTRIFUGE MODEL TESTING .....	38
5.1	Introduction.....	38
5.2	Background to centrifuge model testing .....	39
5.2.1	Principals of centrifuge modelling.....	39
5.2.2	Scaling laws and time .....	40
5.2.3	Errors in Centrifuge Modelling.....	41
5.3	The London Geotechnical Centrifuge Testing Facility.....	43
5.3.1	The Acutronic 661 geotechnical centrifuge .....	43
5.3.2	Data Acquisition .....	44
5.3.3	Instrumentation and Calibration.....	44
5.3.4	Image Processing .....	45
5.4	Summary .....	47
6	APPARATUS DEVELOPEMENT .....	48
6.1	Previous Approaches to Tunnelling.....	48
6.2	Model Design.....	49
6.3	Common Elements to All Experiments .....	50
6.3.1	The soil.....	50
6.3.2	The model container (strong-box).....	51
6.3.3	Ground water supply .....	51
6.3.4	Location and fixing of instrumentation.....	52
6.4	Single tunnel Apparatus .....	52
6.4.1	Tunnel support system .....	52
6.4.2	Support window system.....	55
6.4.3	Fluid control system.....	55

6.5	Twin-Tunnel Apparatus .....	58
6.5.1	Twin-tunnel system.....	58
6.5.2	Twin-Tunnel support window system.....	60
6.5.3	Twin-tunnel back-wall/plug system.....	60
6.6	Summary .....	61
7	EXPERIMENTAL TEST SERIES .....	62
7.1	Experimental Procedure.....	62
7.1.1	Preparation of the clay in the model .....	62
7.1.2	Preparation of the model.....	63
7.1.3	Centrifuge Test Procedures.....	65
7.2	Tests Undertaken .....	67
7.3	Summary .....	68
8	CENTRIFUGE MODEL TEST RESULTS.....	70
8.1	Single Tunnel Apparatus Results.....	70
8.1.1	Surface settlements .....	70
8.1.2	Sub-surface settlement .....	73
8.1.3	Tunnel support pressure.....	78
8.1.4	Summary of experimental verification.....	79
8.2	Overall patterns from the twin-tunnelling tests.....	80
8.2.1	Surface settlement from twin-tunnels .....	80
8.2.2	Sub-surface Settlements from Twin-Tunnels.....	83
8.2.3	Tunnel support-pressure data from Twin-Tunnels.....	84
9	DISCUSSION .....	86
9.1	Increase in volume loss caused by second tunnel construction .....	86

9.2	Trough width parameter.....	88
9.3	Support pressure associated with Tunnel B construction .....	89
9.4	Application of the design charts.....	93
9.4.1	Surface settlements .....	93
9.4.2	Sub-surface settlements.....	95
9.5	Summary .....	96
10	CONCLUSIONS.....	97
10.1	Summary of work undertaken.....	97
10.2	Conclusions.....	98
10.3	Limitations of the results.....	99
10.4	Recommendations for further research .....	99
	REFERENCES .....	101
	TABLES .....	110
	FIGURES .....	124
	APPENDIX A.....	124
	APPENDIX B .....	228
	APPENDIX C .....	229
	APPENDIX D.....	234

## LIST OF TABLES

Table 2.1:	Relationship between category of damage and limiting tensile strain, $\epsilon_{\text{lim}}$ (after Boscardin & Cording, 1989)
Table 3.1:	Typical Values for Volume Losses (Hunt, 2005)
Table 4.1:	Volume loss prediction formulae (Macklin, 1999)
Table 5.1:	Centrifuge Scaling Laws (Marshall, 2009)
Table 6.1:	Summary of Tunnel Experimentation, (Meguid <i>et al.</i> , 2008)
Table 6.2:	Speswhite kaolin clay properties (Grant, 1998)
Table 7.1:	Summary of Tests undertaken
Table 8.1:	Summary of parameters from single tunnel tests
Table 8.2:	Summary of correlation factors
Table 9.1:	Summary of surface parameters from twin-tunnel tests
Table 9.2:	Summary of sub-surface parameters from twin-tunnel tests

## LIST OF FIGURES

- Figure 1.1:** Géotechnique artist impression of sub-surface congestion
- Figure 1.2:** Idealisations of the three twin-tunnelling scenarios in the y-z plane
- Figure 2.1:** Schematic diagrams of sprayed concrete lining tunnelling system, conventional shield and tunnel boring machines (Nyren, 1998).
- Figure 2.2:** Hogging or sagging zone and limited by a point of inflexion or extent of settlement trough (Mair *et al.*, 1996)
- Figure 2.3:** Damage category chart for  $L/H = 1$ , hogging mode (Mair *et al.*, 1996)
- Figure 3.1:** Settlement above an advancing tunnel heading (Attewell & Yeates, 1984)
- Figure 3.2:** Sources of tunnelling deformation for a shield driven tunnel (Cording, 1991)
- Figure 3.3:** Volume loss around a circular cavity (after Peck, 1969)
- Figure 3.4:** a) settlement trough (after Peck, 1969) and  
b) Gaussian fit to trough (after O'Reilly & New, 1982)
- Figure 3.5:** Variation in surface settlement trough width parameter with tunnels in clay (Mair & Taylor, 1997)
- Figure 3.6:** Settlement troughs with depth (Hunt, 2005 after Mair *et al.*, 1993)
- Figure 3.7:** Vector focus (Grant, 1998)
- Figure 3.8:** Observed failure mechanisms based on centrifuge model tests (Mair & Taylor, 1997)
- Figure 3.9:** Dependence of critical stability ratio on tunnel heading geometry (after Mair & Taylor, 1997; Mair, 1979 and Kimura & Mair, 1981)
- Figure 3.10:** Upper and lower bound stability ratios for plane strain circular tunnels (after Davis *et al.*, 1980)
- Figure 4.1:** a) Relationship between volume loss, tunnel heading geometry and stability number within  $C/D$  between 0.77 and 3.11 (after Macklin, 1999)

b) Upper and lower bound design lines for a relationship between volume loss and load factor for field monitoring data from overconsolidated clay sites (after Macklin, 1999)

**Figure 4.2:** Deformed tunnel shape given by (a) ground loss and (b) ovalisation (after Verruijt & Booker, 1996)

**Figure 4.3:** Definition of Gap parameter (after Rowe *et al.*, 1983)

**Figure 4.4:** Comparison of different methods for estimating surface settlement above an unlined shallow tunnel in moderately stiff clay

**Figure 4.5:** Variation of K with depth for sub-surface settlement profiles above tunnels in clay (after Mair *et al.*, 1993)

**Figure 4.6:** Comparison of different methods for estimating sub-surface settlement above an unlined shallow tunnel in moderately stiff clay

**Figure 4.7:** Example of Superposition method used to predict the surface settlement of two, 4m diameter, tunnels with a cover of 8m

**Figure 4.8:** Plastic zones induced by shield tunnelling in soft ground (after Fang *et al.*, 1994)

**Figure 4.9:** Design charts to find the increase in volume loss of the second tunnel's settlement profile (left) and an eccentricity of the maximum settlement (right). (Divall *et al.*, 2012 after Addenbrooke & Potts, 2001)

**Figure 4.10:** The modification factor for the settlement above the second tunnel (Hunt, 2005)

**Figure 4.11:** a) Plan schematic of the Piccadilly Line and Heathrow Express Tunnels  
b) Sub-surface settlement prediction for Tunnel 1 and Tunnel 2 of the Heathrow Express tunnels U.K. (Hunt, 2005)  
c) Surface vertical and horizontal ground displacement predictions for Lafayette Park, U.S.A. (after Cording & Hansmire, 1975)  
d) Surface vertical and horizontal ground displacements for St. James Park, U.K. (Nyren, 1998)

**Figure 5.1:** Principles of centrifuge modelling (after Taylor, 1995)



- Figure 5.2:** Stress distribution in a centrifuge sample (after Schofield, 1980)
- Figure 5.3:** Stress variation with depth in a centrifuge model, exaggerated (after Taylor, 1995)
- Figure 5.4:** Schematic diagram of the Acutronic 661 at City University London (Grant, 1998)
- Figure 6.1:** Schematic diagram of the centrifuge model layouts
- Figure 6.2:** Photograph and schematic of strong box container for single tunnel experiments
- Figure 6.3:** Photograph of consolidometer used for consolidation of slurry
- Figure 6.4:** Photograph of the ground water reservoir standpipe and tunnel pressure standpipe on the centrifuge swing bed
- Figure 6.5:** Schematic diagram of the LVDT gantry and spacing
- Figure 6.6:** Plan arrangement of apparatus on the swing bed for single tunnel testing
- Figure 6.7:** Cross-section through tunnel support apparatus
- Figure 6.8:** Schematic of single tunnel support window system
- Figure 6.9:** Details of the standpipe used to control the pressure in the tunnels
- Figure 6.10:** Photograph and schematic of fluid control apparatus
- Figure 6.11:** Photograph of solenoid and plug valve system and schematic (after McNamara, 2001)
- Figure 6.12:** Plan arrangement of apparatus on the swing bed for twin tunnel testing
- Figure 6.13:** Schematic of supporting window system (3D twin-tunnelling case)
- Figure 6.14:** Details of strong-box back wall and interchangeable inserts with variable spacing
- Figure 6.15:** Alterations to strong-box back wall to accommodate offset arrangements
- Figure 7.1:** Stress history of the model from slurry to moderately stiff clay
- Figure 7.2:** Jig for the creation of the twin-tunnel cavities on the bench during the model making stages of centrifuge modelling
- Figure 7.3:** Shelf for trimming the model to the correct height on the bench during the model making stages of centrifuge modelling

- Figure 7.4:** Holding nut for securing the tunnelling supporting system in place and the manifold for the tunnel pressure transducer
- Figure 7.5:** Comparison between circular footing and square footing on LVDTs with insert of clay surface slope
- Figure 8.1:** Comparison of centre-line vertical displacements in simulated single tunnel constructions with different support fluids
- Figure 8.2:** Raw settlement data from LVDTs (centre-line and '2D Check') after 3% volume loss in single tunnel tests of different support fluids
- Figure 8.3:** Gaussian curves fitted to the normalised settlement data from the single tunnel tests
- Figure 8.4:** Comparison of the water supported single tunnel settlement data (SD3) and various prediction methods for 3% volume loss
- Figure 8.5:** Typical CCD camera image taken during a test with known-coordinate markers circled
- Figure 8.6:** Sub-surface displacements displayed as vectors from air (top) and water (bottom) supported simulated single tunnel constructions for 3% volume loss
- Figure 8.7:** Sub-surface contours of SD2
- Figure 8.8:** Sub-surface contours of SD3
- Figure 8.9:** Calibration test investigating CCD camera vector movements for 5mm horizontal movement
- Figure 8.10:** Noise levels during apparent no movement during a centrifuge test
- Figure 8.11:** Movement at the tunnel centre-line measured by LVDT and Image Analysis for single tunnel air supported and water supported
- Figure 8.12:** Relationship between vertical displacement recorded by CCD Camera and LVDT (at known distances from the centre-line of the tunnel) for a water supported single tunnel simulated construction
- Figure 8.13:** a) Vertical Settlement at a depth of 2mm in a simulated single tunnel construction with water support, SD3

b) Vertical Settlement at a depth of 54mm in a simulated single tunnel construction with water support, SD3

c) Vertical Settlement at a depth of 75mm in in a simulated single tunnel construction with water support, SD3

**Figure 8.14:** Comparison of changes in pore-water pressure during tests SD2 and SD3

**Figure 8.15:** Twin-Tunnel vertical surface settlement from 1.5D spacing tests

**Figure 8.16:** Twin-Tunnel vertical surface settlement from 3D spacing tests

**Figure 8.17:** Twin-Tunnel vertical surface settlement from 4.5D spacing tests

**Figure 8.18:** Twin-Tunnel vertical surface settlement from 2.12D spacing test

**Figure 8.19:** Twin-Tunnel vertical surface settlement from 2.7D spacing test

**Figure 8.20:** Tunnel A and Tunnel B vertical surface settlement from 1.5D spacing tests

**Figure 8.21:** Tunnel A and Tunnel B vertical surface settlement from 3D spacing tests

**Figure 8.22:** Tunnel A and Tunnel B vertical surface settlement from 4.5D spacing tests

**Figure 8.23:** Tunnel A and Tunnel B vertical surface settlement from 2.12D spacing tests

**Figure 8.24:** Tunnel A and Tunnel B vertical surface settlement from 2.7D spacing tests

**Figure 8.25:** Sub-surface vertical displacement vectors presented as contours from tests SD13

**Figure 8.26:** Sub-surface vertical displacement vectors presented as contours from tests SD14

**Figure 8.27:** Sub-surface vertical displacement vectors presented as contours from tests SD15

**Figure 8.28:** a) Vertical Settlement at a depth of 9mm in SD13

b) Vertical Settlement at a depth of 39mm in SD13

c) Vertical Settlement at a depth of 60mm in SD13

**Figure 8.29:** a) Vertical Settlement at a depth of 8.5mm in SD11

b) Vertical Settlement at a depth of 40mm in SD11

c) Vertical Settlement at a depth of 60mm in SD11

**Figure 8.30:** a) Vertical Settlement at a depth of 8mm in SD15

b) Vertical Settlement at a depth of 39mm in SD15

c) Vertical Settlement at a depth of 60mm in SD15

**Figure 8.31:** a) Vertical Settlement at a depth of 7mm in SD18

b) Vertical Settlement at a depth of 38mm in SD18

c) Vertical Settlement at a depth of 58mm in SD18

**Figure 8.32:** a) Vertical Settlement at a depth of 7mm in SD17

b) Vertical Settlement at a depth of 37mm in SD17

c) Vertical Settlement at a depth of 58mm in SD17

**Figure 8.33:** Tunnel Pressures measured during 1.5D spacing tests

**Figure 8.34:** Tunnel Pressures and pore-water pressures measured during 3D spacing tests

**Figure 8.35:** Tunnel Pressures and pore-water pressures measured during 4.5D spacing tests

**Figure 8.36:** Tunnel Pressures measured during SD18 (2.12D spacing)

**Figure 8.37:** Tunnel Pressures measured during SD17 (2.7D spacing)

**Figure 9.1:** Volume loss of the second tunnel in respect to distance from the first (surface)

**Figure 9.2:** Volume loss of the second tunnel in regards to distance from the first (surface and sub-surface)

**Figure 9.3:** Volume loss of the second tunnel in regards to distance from the first (Design Chart)

**Figure 9.4:** K with depth for the settlement towards the existing tunnel

**Figure 9.5:** Pressure data during 1.5D spacing tests

**Figure 9.6:** Pressure data during 3D spacing tests

**Figure 9.7:** Pressure data during 4.5D spacing test

## ACKNOWLEDGEMENTS

My time within the Geotechnical Engineering Research Group (GERG) at City University London has been made enjoyable because of the supportive and nurturing Academic staff and the other group members. I am very fortunate to have been part of this group and grateful for the wonderful time I spent learning and conduct research here. A special thank you goes to those mentioned below.

Firstly, I would like to thank my supervisor Dr Richard Goodey. I will be forever indebted to him for the opportunities that were available to me during my studies, for making the process of research so enjoyable and the long hours spent educating me in academic writing. It has been an honour to be his first Ph.D. student.

I would also like to thank my second supervisor Professor Neil Taylor for being so generous with his help and time during my studies. Many insightful discussions about the research have been possible because of this and without his huge amount of geotechnical knowledge it is likely some of the problems presented during this research would have gone unsolved.

Additional thanks go to Professor Sarah Stallebrass for her nurturing nature and knowledge in soil mechanics. My research would have not been as successful without her invaluable input during my time at City University London. Thanks also to Dr Andrew McNamara for his good humour and technical expertise in centrifuge modelling. The procedure for preparing centrifuge models had benefited considerably from our discussions.

The apparatus used during the centrifuge experiments required a considerable amount of specialist skill and guidance from the technical staff at City University London. My sincere thanks go to Robert Cherry, to Jim Ford, to Melvyn Hayes and to Keith Osborne.

I wish to acknowledge the contributions of the research students from Cambridge University for their input in centrifuge modelling techniques and image analysis, in particular Michael Williamson. I am also grateful for the collaborations that took place during my studies that resulted in the furthering of my tunnelling knowledge including Dr Jamie Standing and Dr Ming Xu.

Thanks are also due to the other colleagues who have conducted research within the group during this period including Hitesh Halai, Neil Phillips and Alexis Rose. I would like especially to thank Rohit Gorasia for continually challenging me and pushing me to achieve my full potential.

I would like to give special thanks to my friends and family for their support and making me smile during the hardest parts of this research. Finally, thanks to Amy for her encouragement, support and love throughout my research because without her this thesis would not have been possible.

## **DECLARATIONS**

I grant powers of discretion to the University Librarian to allow this dissertation be copied in whole or in part without further reference to me. This permission covers only single copies made for study purposes, subject to normal conditions of acknowledgement.

## ABSTRACT

The rising population in urban environments comes with an associated demand for increased public transport. Due to the level of surface congestion an often utilised solution is to construct rapid transit systems within tunnels. Any sub-surface construction will generate ground movements which have the potential to cause damage to existing surface and sub-surface structures. Urbanisation and congested cities have driven the need for accurate predictions of tunnelling-induced settlements and has produced many publications (e.g. Peck, 1969; Cording & Hansmire, 1975; Clough & Schmidt, 1981; O'Reilly & New, 1982; Attewell & Yates, 1984; Cording, 1991; Mair *et al.*, 1993 and Mair & Taylor, 1997). Largely, however, these empirically based prediction methods are concerned with single tunnel greenfield, arrangements. Generally, mass rapid transport systems comprise of a pair of tunnels constructed within relative close proximity. This is known as twin-tunnel construction. A number of case studies have shown a relative difference in the settlements due to each tunnel construction (e.g. Cooper *et al.*, 2002; Cording & Hansmire, 1975 and Nyren, 1998). These were further investigated by numerical studies which support these observations (e.g. Addenbrooke & Potts, 2001 and Hunt, 2005). Analyses that use isotropic linear elastic-perfectly plastic soil models have tended to produce wider surface settlement troughs than observed by the Gaussian distribution (Mair *et al.*, 1981). It is that clear valuable insight could be gained from a physical model based study. Therefore, a series of plane strain centrifuge tests was carried out investigating twin tunnelling-induced settlements in overconsolidated clay. Apparatus necessary to perform these tasks required a significant amount of time to develop and was relatively complex. The main variables were the spacing between the tunnels, both horizontally and vertically, and the magnitude of volume loss. The tests were conducted at 100g where the cavities represented two 4m diameter tunnels at (usually) a depth of 10m at prototype scale. The tests utilised novel apparatus designed during the research to enable the simulation of the construction processes related to volume loss in separate sequential tunnels.

The results presented are in regards to the prediction of ground movements in the plane perpendicular to advancing tunnels and the significant findings of the research are as follows: -

1. Single tunnel surface and sub-surface settlement troughs are well represented by Gaussian distributions, however, the twin-tunnelling predictions can be improved by modifying the settlements solely due to the second tunnel construction.
2. The magnitude of volume loss from the new tunnel construction had increased due to the presence of the first tunnel. This effect was lessened by larger spacings between the tunnels.
3. Second tunnel settlements can be predicted using equations by Peck (1969), O'Reilly & New (1982) and Mair *et al.* (1993) but with the modifications. The surface and sub-surface settlement distributions towards the existing tunnel were observed to be wider than a single tunnel.

## LIST OF SYMBOLS

$\infty$	Infinity
A	Multiple of the trough width parameter (usually taken as 2.5 or 3) in a half settlement trough
a	Radius of a tunnel cavity
b	Radius of far field measurement (i.e. distance to surface)
C	Cover above the tunnel crown
$C_{\text{clay}}$	Depth of the low permeability soil above the tunnel crown extrados
$C_v$	Coefficient of consolidation
d	Centre-to-centre spacing of the tunnels
D	Bored tunnels diameter
DS	Normalised long-term settlements
E	Young's Modulus
g	Acceleration due to gravity
G	Secant stiffness
$G_0$	Arbitrary reference stiffness at r equals x
H	Distance over which the excess pore pressures are dissipated or drainage path length
i	Lateral distance from the tunnel centre-line to the point of inflection in the Gaussian distribution curve.
K	Dimensionless trough width parameter for Gaussian settlement troughs
$K_A$	Value of K in the region of the first bored tunnel



$k_l$	Tunnel lining mass permeability
$k_{soil}$	Equivalent isotropic permeability of soil
$L$	Length of a building
$LF$	Load Factor
$M$	Maximum modification factor described by Chapman <i>et al.</i> (2006)
$n$	Gravity scaling factor
$N$	Stability ratio
$NS_{c\ max(SS)}$	Normalised maximum surface settlement at the steady state long-term
$NS_{c\ max(SSI)}$	Normalised maximum surface settlement at the steady state long-term when the tunnel lining is fully impermeable
$NS_{c\ max(SSP)}$	Normalised maximum surface settlement at the steady state long-term when the tunnel is fully permeable
$R$	Radius of the bored tunnel
$R_p$	Radius, $r$ , of plastic zone
$RP$	Soil-lining relative permeability
$SF$	Seepage Factor
$S_{max}$	Theoretical maximum settlement at the tunnel centre-line
$S_{mod}$	Modified settlement
$S_u$	Undrained shear strength at tunnel axis level
$S_v$	Vertical settlement, at a defined horizontal point, in the $x$ - $z$ plane
$S_z$	Sub-surface vertical settlement from image analysis

$S_{z(mod)}$	Modified sub-surface vertical settlement
$S_{Z,max}$	Maximum sub-surface settlement (above the tunnel centre-line) at depth, Z
t	Time
$t_l$	Thickness of tunnel lining
$T_v$	Dimensionless time factor
u	Pore-water pressure
$U_R$	Radial deformation around the tunnel diameter
$U_r$	Radial movement at radius r
$U_t$	Dimensionless degree of consolidation
$V_L$	Volume loss expressed as a ratio
$V_{Lg}$	Volume loss in the ‘greenfield’ scenario
$V_S$	Volume of surface settlement trough
$V_T$	Volume of ‘ground lost’ around the bored tunnel
x	Lateral distance from a tunnel centre-line
$x_A$	Lateral distance from the centre-line of the first bored tunnel
$x_B$	Lateral distance from the centre-line of the second bored tunnel
z	Vertical distance from the un-deformed surface to the horizon analysed
$Z^*$	Vertical distance from the un-deformed surface to the tunnel axis level minus Vertical distance from the un-deformed surface to the horizon analysed ( $z_0-z$ )
$z_0$	Vertical distance from the un-deformed surface to the tunnel axis level
$\gamma$	Unit weight of soil

$\gamma_w$	Unit weight of water
$\Delta$	Maximum deflection between the building and tunnelling-induced settlements
$\delta$	Ovalisation ratio
$\Delta\rho_\infty$	Final surface settlement when all excess pore pressures have been dissipated
$\Delta\rho_t$	Surface settlement in respect to one-dimensional consolidation
$\varepsilon$	Radial strain
$\rho$	Density of the soil material
$\sigma_s$	Surface surcharge (if any)
$\sigma_T$	Internal tunnel support pressure (if any)
$\sigma_{TC}$	Internal tunnel support pressure at collapse
$a$	Radial acceleration
$r$	Radius from the centre of rotation
$\omega$	Angular velocity

### **Superscripts**

'        in terms of effective stress (i.e.  $\sigma'$  is effective stress)

### **Subscripts**

m	model
max	maximum
p	prototype
TA	Tunnel A
TB	Tunnel B

v        Vertical

z        Depth

### **Abbreviations**

BSP     British Standard Pipe (size scale for pipe fittings)

CCD     Charged Coupled Device (television cameras mounted on centrifuge swing)

CL       Centre-line

CNC     Computer Numerical Control machine

CSL     Critical State Line

CSSM   Critical State Soil Mechanics

DPI     Digital Pressure Indicator

EPBM   Earth Pressure Balance Machine

FD       Finite Difference (analysis)

FE       Finite Element (analysis)

ID       Internal Diameter

LVDT   Linear Variable Differential Transducer

NATM   New Austrian Tunnelling Method

OD       Outer Diameter

PPT     Pore Pressure Transducer

SCL     Shot Concrete Lining

TBM     Tunnel Boring Machine

**Note:** In general, standard SI (Système International) units are used.

# **1 INTRODUCTION**

The research addressed in this thesis concerns the ground movements generated by the construction of tunnels in close proximity within clay soils. In this introductory chapter the rationale and objectives for the work are presented. This is followed by an outline of the subsequent chapters.

## **1.1 General**

Underground construction has been used in a variety of applications since the first half of the 19<sup>th</sup> Century. The Thames Tunnel project was one of the earliest major underground construction projects and this still forms part of the London Underground Network (Skempton & Chrimes, 1994). As urban environments grew the available surface space became restricted and tunnelling in urban areas has since become an increasingly popular solution in response to the need for efficient transportation links, communication systems, water supply and waste disposal. In modern metropolises this has led to congestion of sub-surface space (illustrated in Figure 1.1) which places restrictions on new construction projects.

London is a perfect example of a congested urban environment with a long history of underground construction. London's sub-surface space is crowded with deep basements, deep foundations, service pipes and metro tunnels. In particular, the London Underground network services a large part of London and Greater London via a number of distinctly separate lines. Each line comprises two separate tunnels to facilitate east – west or north – south travel. The layout of these tunnels can take a number of different geometric arrangements such as side-by-side, stacked or offset (Figure 1.2). During the construction of each line, two tunnels can be constructed within a relatively short space of time and within a reasonably close proximity. These types of project will herein be referred to as twin-tunnelling projects.

Irrespective of the construction method or arrangement used, any underground construction will cause a change in the ground stress-state. This stress change is due to most excavation methods having unsupported soil at some point during the construction process. Consequently, ground

movements will arise which, if apparent at the surface can cause damage to buildings (Burland, 2001). Additionally, sub-surface movements may have a detrimental effect on existing buried services (Mair *et al.*, 1996). Damage assessments are based on predictions of deformations due to tunnelling and there is consequently a need for accurate prediction methods.

Due to time, cost or logistical constraints it is usual for the two tunnels to be created sequentially. This results in a construction delay between the tunnels and possibly a different ground response during the creation of the second cavity when compared with that produced by the first. On a number of twin bored tunnelling sites, such as St James Park in the UK (Nyren, 1998), Lafayette Park in the USA (Cording & Hansmire, 1975), and The Heathrow Express in the UK (Cooper & Chapman, 1998), ground movements and tunnel behaviour have been monitored. The observed ground movements in these case studies show a difference in the settlements generated by the first and second tunnels.

Barlett & Bubbers (1970) commented on the possibility of a weakening of the strata resulting in more pronounced settlement and distortions in the tunnel lining. Mair & Taylor (1997) stated that significant interaction effects must be evident when tunnels are very closely spaced. Finally, Cooper *et al.* (2002) noted that the ground movements above closely spaced parallel tunnel constructions can be significantly different from those observed above single tunnels, and this must have a significant impact on the settlement of structures and services in the vicinity. The tunnelling-induced ground movements and associated strains create a disturbance zone above the cavity. If the second tunnel produces another stress change in the already disturbed zone created by the first tunnel, a dissimilar set of movements could reasonably be expected. Previous research using various methods (e.g. Addenbrooke & Potts, 2001; Hunt, 2005 and Fang *et al.*, 1994) detail centre-to-centre spacings sufficient to ensure there would be no interaction between the tunnels.

Two similarly constructed tunnels could be assumed to give similar magnitudes and patterns of ground movements. However, this assumes that the construction of the first tunnel does not disturb the soil in the vicinity of the second tunnel. Therefore, it is the hypothesis of this thesis that the construction or existence of the first tunnel changes the stress history of the soil in the

area of the second tunnel construction. If this assumption is valid it might be assumed that the second tunnel construction would result in a dissimilar set of ground movements compared with those assumed for the first. It is clear that significant improvements in predictions may be achieved from a better understanding of the development of ground movements around closely constructed tunnels.

## **1.2 Aims**

The primary aim of the research was to develop an understanding of the effects of twin-tunnelling in clay through physical modelling techniques. To this end, a number of specific tasks were performed:

- i. the development of apparatus to simulate the ground response induced by tunnelling methods and of simultaneous/sequential tunnel constructions,
- ii. the implementation of a repeatable physical model to perform the events outlined above,
- iii. understanding and interpreting the mechanisms of short-term ground movements around twin tunnels, and
- iv. conducting a parametric study of short-term ground responses following various arrangements of twin-tunnelling scenarios in clay. The modelled ground responses are measured, recorded and normalised on presented charts.

## **1.3 Outline of the thesis**

This thesis describes the processes and outcomes of an investigation into ground movements caused by twin tunnelling. The purpose of Chapter 2 is to outline the scope of this thesis. This includes defining the type of tunnel construction being modelled, the framework of the soil mechanics being applied and a brief background into the prediction of damage assessment. Chapter 3 contains a review of the literature relating to the behaviour of clay during tunnelling practices. This includes short and long-term movements and field observations. Chapter 4 describes the current practices for predicting single and multiple tunnelling-induced ground movements. Details of the centrifuge testing practices are given in Chapters 5 to 7. Chapter 5

gives the background to typical tunnelling centrifuge modelling techniques which include the principals and relevant scaling laws. The facilities at City University London are also described in this chapter. Chapter 6 details the existing and newly designed apparatus used during this research. In addition to this Chapter 7 gives details of the entire testing procedure to perform the experiments for single and twin-tunnel arrangements. This includes the stress history of the soil, model making stages and simulation of construction. In Chapter 8 typical centrifuge model test results are presented and this chapter also contains a summary of all the tests undertaken. This includes such details as the calibrations of all the apparatus, the interpretation of the image analysis software and fundamental ground movement results. The results focus on the settlement trough width, ground movements, changes in pore pressures and tunnel pressures. The trends in the experimental results are analysed and discussed in detail in Chapter 9. Finally, Chapter 10 presents the conclusions to the thesis and includes the limitations of the thesis which leads to a series of suggestions for further work.



## **2 BACKGROUND**

This background chapter defines the type of tunnel construction being investigated; the framework of the soil mechanics applied and briefly covers the effects of tunnelling. This is followed by an outline of the methodologies applied during this research.

### **2.1 Scope of the research**

#### **2.1.1 Types of Tunnel Construction**

Methods of tunnel construction fall into one of two categories. Mair & Taylor (1997) defined these as open face and closed face tunnelling, where open faced tunnelling has easy access to the tunnel face and closed face tunnelling utilises a face support mechanism.

Open face tunnelling is normally adopted in dry, stiff soil conditions where the soil is self-supporting for a reasonable time period. The most common method of open face tunnelling is the Sprayed Concrete Lining (SCL) or New Austrian Tunnelling Method (NATM). This method involves a small unlined section being excavated, with sprayed concrete, known as Shotcrete, providing the support to the already constructed sections (Figure 2.1a).

Tunnel construction by means of tunnel boring machine (TBM) is usually preferred when the ground conditions are considered unstable (i.e. where face support is required temporarily or continuously). The main categories of TBM are shown in Figure 2.1b, 2.1c and 2.1d. TBMs have a circular face with cutting tools mounted on radial arms at the front. These are designed to accommodate disc cutters, picks or a combination of both depending on the geology. This cutting face is usually contained within a steel cylindrical shaped unit. The rear of the TBM is referred to as the tail and is smaller in diameter than the cutting face. The tail is responsible for the erection of the lining. These linings consist of either precast concrete or cast iron segments and are erected concurrently with the excavation. In particularly unstable ground lubrication slurry material is injected around the annulus of the tail and then replaced with a grout filling the gap between the unsupported soil and the lining. This is performed either simultaneously as the cutting face is thrust forward or at some distance behind the cutting face. Technological

advancements have made this a highly automated system with a high level of control. An Earth Pressure Balance Machine (EPBM) provides support pressure to the exposed face approximately equal to that within a pressure chamber. The rotating cutter face controls the entry of the excavated soil and water into this closed pressure chamber. Mair & Taylor (1997) stated that recent developments in the injection of slurries and foams have improved the control of these ground movements. Therefore, the rate of construction is controlled by the speed of the rotating cutter and the subsequent adjustment of face pressure. The work presented in this thesis is primarily concerned with the effects of TBM construction on ground movements.

### **2.1.2 Soil Structure**

London is an ideal example of a densely populated urban environment that has benefited from the use of TBMs for the construction of mass transit railway systems. This has been made technically possible because most of London's Underground tunnels are north of the River Thames and in the London Clay Formation. Withers *et al.* (2001) described the main body of London Clay as typically a very stiff, thinly laminated, very closely fissured, dark grey and grey-brown clay of very low to medium compressibility and high to very high plasticity. London Clay is considered a stiff overconsolidated clay making tunnelling relatively easy. Viggiani & Atkinson (1995) stated that the London Clay at Chattenden was subjected to a reduction in vertical effective stress due to erosion in the order of 1500kPa and therefore became overconsolidated. Consequently, the soil did not recover its original state. Field observations and laboratory tests by Viggiani & Atkinson (1995) showed stiffnesses at very small strain,  $G_0$ , measuring generally in the range of 10-30MPa, increasing slightly with depth. Gasparre *et al.* (2007) also conducted an investigation into natural London Clay and showed stiffnesses, resolved at a strain of approximately 0.01%, only slightly increasing with depth. During this thesis overconsolidated clay like deposits are considered in order to relate the work to construction in London.

### **2.1.3 Prediction of tunnelling-induced ground movements**

A fundamental stage in the design of any tunnelling system would be the assessment of ground movements and their effects on existing structures. Construction guidelines for surface

settlements have been largely based on research from single tunnel arrangements (e.g. Peck, 1969; Mair, 1979; Taylor, 1984 and Attwell & Yeates, 1984). Surface settlement predictions of twin-tunnels are often the superposition of two single tunnel predictions.

The prediction of sub-surface displacements and their effect on underground services is commonly based on extrapolations from surface measurements. However, relatively little is known about the sub-surface displacements surrounding a twin-tunnel construction or whether the same extrapolations are valid.

Hunt (2005) and Addenbrooke & Potts (2001) explored the influence of twin-tunnelling using the finite element method and proposed modifications to current semi-empirical solutions to account for the presence of the first tunnel. Using a different research methodology to give a better understanding of the development of ground movements around tunnels under construction could have considerable merit.

#### **2.1.4 Assessment of damage to existing structures due to tunnelling**

Although this research is concerned primarily with the soil movements, it is useful to contextualise the current research with work that has been carried out on assessing effects on surface and sub-surface structures. Surface settlement predictions are generally conducted due to concern over damage to existing structures. Existing tunnels and deep foundations also make it important to be able to predict the sub-surface movements and mechanisms of movement.

The positions of a building's foundations within the settlement trough are noted in the design procedures for new tunnelling systems and assessments of structural deformations are made. These assessments are based on damage to the building as a whole and not necessarily on individual structural details (Attwell & Yeates, 1984). Mair *et al.* (1996) stated that ground movements can lead to cracking and damage to buildings as a result of the generated tensile strains. A building's response to settlement was determined to be dependent on 'limiting tensile strains' and, based on this idea, Boscardin & Cording (1989) devised Table 2.1 which categorises a range of strains which may result in building damage. In order to relate these strains to the tunnelling process, Mair *et al.* (1996) stated that building damage could be

assessed in terms of a deflection ratio,  $\Delta/L$ .  $\Delta$  is shown in Figure 2.2 as the maximum deflection between the building and tunnelling-induced settlements across the length of the building,  $L$ , in either the hogging or sagging zone. Figure 2.3 shows building damage in the hogging zone for  $L/H = 1$  (where  $H$  is the height of the building excluding the roof). Mair & Taylor (1997) stated that, in practice, the evaluation of  $\Delta/L$  is easier than the evaluation of angular distortion or horizontal strain and therefore Figure 2.3 relates horizontal strain and  $\Delta/L$ .

During closely spaced tunnelling projects (where the current assumption is that no interaction between the tunnels is evident) an unconservative maximum deflection, as a result of greater differential ground settlements, could lead to higher values of strain for a building of length,  $L$ . Therefore, greater certainty related to twin-tunnelling induced settlement could provide greater assurances for designers.

## **2.2 Research Method**

Centrifuge model testing was the research method utilised in this work. Eighteen tests were completed at City University London using the Geotechnical Centrifuge. The centrifuge model testing series focused on monitoring ground movements caused by the construction of twin tunnels.

### **2.2.1 Centrifuge model testing**

Centrifuge modelling is an effective way of reproducing a soil with a known stress history and with repeatable boundary conditions (Schofield, 1980). Utilising careful experimental procedures it was possible to monitor soil movements in three tunnelling scenarios. Tests involved two simulated tunnel constructions at equal and differing horizons. The distances between the tunnels, in terms of centre-to-centre spacing, were varied during the experimental test series.

New apparatus was developed which, once validated in a single tunnel arrangement, was used in experimental procedures for twin-tunnelling. The model tests were conducted under plane strain conditions with circular tunnel cavities in overconsolidated kaolin clay. The tunnel cavities were supported with fluid filled rubber bags and removing a known amount of fluid

from these bags simulated the construction process. A set of complex apparatus was designed in order to accurately control two separate tunnel excavations. The data obtained were validated against established semi-empirical prediction methods, compared with published numerical analysis and also compared with particular observations from case studies.

### **3 TUNNELLING INDUCED GROUND MOVEMENTS**

This chapter discusses ground movements related to twin bored tunnelling. Published material describing the ground response in creating tunnelling excavations (short and long-term) is discussed. Case studies and field measurements supporting the need for the study are also presented.

#### **3.1 Introduction**

Many useful insights into bored tunnelling-induced ground movements in clay can be gained from investigations assumed to be “greenfield”, i.e. ground that is undeveloped as illustrated in Figure 3.1 from Attewell & Yeates (1984).

Tunnel construction using a TBM causes three-dimensional movements ahead of the tunnel cavity (illustrated in Figure 3.2). Mair & Taylor (1997) identified and lists the sources of these movements as:

- i. Deformation arising from ground loss due to movements towards the face,
- ii. Radial movements around the shield due to over-cutting,
- iii. Radial movements due to lack of support before lining is introduced known as “the tail void process”,
- iv. Closure of the under grouted annulus around the newly completed ring,
- v. Closure of the grouted annulus gap due to insufficient grout or loss of grout,
- vi. The long-term consolidation affecting the ground state, and
- vii. Permanent distortion of the lining.

Stages vi and vii describe long-term deformations and are the result of ground pore-water pressures regaining equilibrium with the ground water table. Normally stages iv and v can be negated through good working practices. However, stages i - iii can become significant in the short-term especially when working in clay.

Tunnelling is a three-dimensional problem. For analysis purposes, some studies have separated this into two, two-dimensional problems (see Figure 3.1). These are the transverse settlement

trough (x-z plane) and the longitudinal settlement trough (y-z plane). This research focuses primarily on the x-z plane, sometimes referred to as the plane-strain scenario.

## **3.2 Short-term ground movements in greenfield conditions**

This section outlines terms and current knowledge relating to movements in the short-term. Clays respond in the short term in an undrained manner because they have a low permeability (values of coefficient of permeability,  $k$ , are generally less than  $10^{-8}$  m/s). This behaviour generally relates to items i - iii raised in section 3.1 and are as a direct result of the cutting process by the TBM.

### **3.2.1 Volume Loss**

Due to the nature of the cutting process the bored shape of a tunnel will always be larger than the final shape creating a set of displacements towards the cavity (see Figure 3.3). This phenomenon has been described by the term “ground loss” or, the more frequently used, ‘volume loss’ (Peck, 1969).

The ground movements described by Peck (1969) were radial displacements towards the cross section and longitudinal displacements along the line of the tunnel. These two movements have proven difficult to separate, and therefore, assessments of volume loss have been determined by considering a plane-strain scenario.

In the undrained case the volume of ‘ground loss’ around a tunnel cavity should be equal to the volume of the surface settlement trough. Mair & Taylor (1997) stated that whenever necessary the volume loss should be expressed in terms of the volume of surface settlement trough. This is mainly due to difficulties in obtaining field measurements around the tunnel cavity whereas measurement of surface displacements is relatively straight forward. It is usual to denote these two volumes as:

$V_T$  is volume of ‘ground lost’ around the bored tunnel and

$V_S$  is the volume of surface settlement trough.

Therefore, in the undrained case  $V_T = V_S$ , and  $V_L$  is volume loss usually expressed as a percentage of the tunnel cross-sectional area. For the situation featured in Figure 3.3 the volume of the surface settlement trough can be expressed as;

$$V_S = \frac{V_L}{100} \left( \frac{\pi D^2}{4} \right) \quad (3.1)$$

where  $D$  is the bored tunnel diameter.

### 3.2.1.1 Typical Volume Losses for Clay

The precise magnitude of volume loss is governed by how the stress state in the ground is redistributed during tunnelling. The volume loss has been described as dependent on both the type of tunnel boring machine and the quality of the workmanship (Hunt, 2005). This, perhaps, is the reason volume loss around tunnels has been difficult to predict. It is therefore common practice to assume a value for volume loss based on engineering judgement, experience and previously published case studies. Table 3.1 lists literature publishing typical values of volume loss for different construction methods since the early 1980's. Mair & Taylor (1997) reviewed 35 papers and drew the following conclusions:

- i. During open face tunnelling in stiff clays volume losses are usually between 1 and 2%,
- ii. During effective sprayed concrete lined tunnelling (SPL) in stiff clays volume losses are largely between 0.5 and 1.5%, and
- iii. During closed faced TBM tunnelling volume losses have been proven to be approximately 0.5% in sands and 1 – 2% in soft clays.

### 3.2.2 Transverse Settlement Trough

The surface settlement trough is the manifestation of the movements from around the tunnel cavity. Assessing the direction and relative magnitude of surface displacements in clay could be based on theories by Peck (1969). These were based largely on surface settlement observations from case studies and the shape of the transverse settlement trough was found to be suitably described by a Gaussian distribution curve, illustrated in Figure 3.4a and Figure 3.4b. The



volume of this Gaussian distribution curve (per metre length),  $V_s$ , can be evaluated by Equation (3.2) from O'Reilly & New (1982);

$$V_s = \int_{-\infty}^{+\infty} S_{\max} \exp\left(\frac{-x^2}{2i^2}\right) dx \quad (3.2)$$

$$V_s = \sqrt{2\pi} i S_{\max} \quad (3.3)$$

where  $S_{\max}$  is the vertical maximum settlement,

$x$  is the horizontal distance from the tunnel centre-line and

$i$  is the horizontal distance to the point of inflexion.

From Equation (3.3) it is clear there are only two variables for determining the settlement trough by a Gaussian distribution curve ( $S_{\max}$  and  $i$ ). In this case,  $S_{\max}$  controls the magnitude of the settlement trough and  $i$  (or trough width) determines the extent. Methods for assessing for these parameters are discussed in Chapter 4.

### **3.2.2.1 Variations to Trough Width and Maximum Settlement**

Plotting a half space Gaussian surface settlement trough (Figure 3.4b) shows that the trough extends up to  $3i$  from the tunnel centre-line. The value of  $i$  therefore controls the overall width of the settlement trough. O'Reilly & New (1982) proposed an approximately linear relationship (see Figure 3.5) between the location of the inflection point,  $i$ , and the depth to the tunnel axis level,  $Z_0$ . This relationship is the most widely accepted. Moreover, this relationship was shown to be independent of the construction method and not very sensitive to the size of tunnel (when the cover is greater than the diameter). However, it is worth noting that the 'tail' of the settlement trough has been shown to not necessarily stay true to the Gaussian assumption after  $2.5i$  from the tunnel centre-line (Grant, 1998).

Many researchers have attempted to improve the understanding of settlement trough behaviour by investigating the trough width (specifically  $i$ ). The relationship between trough width and volume loss is complex. The trough width has been shown, variously, to both remain constant

and vary with volume loss. Grant & Taylor (2000) measured in their centrifuge tests in clay that the settlement trough had a constant width between volume losses of 2 - 20%. However, Hergarden *et al.* (1996) showed in centrifuge tests of mixed soil types (sand overlying clay) an increase in volume loss gave a decreased parameter  $i$ .

Although knowledge about ground deformations is derived from surface settlement data there are, of course, deformations below surface level. The Gaussian settlement trough shape can be observed throughout the depth of the soil above a tunnel (Mair *et al.*, 1993). This work analysed data from case studies and centrifuge experiments and showed troughs became narrower with depth but were similar in shape as seen in Figure 3.6. Essentially this figure shows the distribution of  $i$  with depth and that the relationship is linear. Therefore, the assumption is that the tangent of these settlements has a point of vector focus on the tunnel centre-line. The theory of points of vector focus by Mair *et al.* (1993) was modified by Grant (1998), as shown in Figure 3.7, and shows that dependent on the sub-surface region; the points of inflexion have three separate points of vector focus. In Zone 1 (near the surface) the tangent of the distribution of  $i$  gives a vector focus point above the tunnel centre-line. Zone 2 (between Zone 1 and just above the tunnel boundary) has a point of vector focus just below the tunnel. Finally, in Zone 3 the distribution of  $i$  from just above the spring line of the tunnel boundary show a point of vector focus well below the tunnel. Grant & Taylor (2000) also stated the relationship between  $i$  and depth was not applicable at a distance of  $0.5D$  above the tunnel crown. The magnitude of  $i$  in this case was found to be less than anticipated due to the tunnel. Moh *et al.* (1996) had taken measurements during the construction of Taipei Rapid Transit Systems. A relationship was subsequently developed for predicting  $i$  for sub-surface settlement troughs close to the tunnel by taking into account its presence.

A tunnel construction in clay is often considered an undrained event and therefore it is assumed that, per unit length of settlement trough, the volume loss remains unchanged with sub-surface regions. Therefore, the ratio of surface to sub-surface values of  $i$  with depth are inversely proportional to the ratio of sub-surface maximum settlement to surface maximum settlement (Figure 3.6). The maximum settlement at the crown should therefore be greater than the

maximum settlement at the surface. However, as discussed earlier the same relationship of  $i$  with depth was not appropriate at  $0.5D$  from the crown. Lo *et al.* (1984) reviewed several case studies and suggested a different linear relationship of 0.33 was appropriate in most cases for the ratio of surface maximum settlement to sub-surface maximum settlement.

### **3.3 Long-term Ground Deformations (Post construction)**

Although the tunnelling-induced settlements addressed in this project are assumed to be short-term, it is reasonable to assume that some degree of long-term movement could occur between tunnel constructions.

Time-related settlements refer to movements that develop post construction and in some cases may continue years after the initial construction has been completed. The causes of these long-term movements are the dissipation of excess pore pressures and creep. This research focuses on the movements related to the dissipation of excess pore pressures (consolidation) as these are generated during tunnel construction. Broadly, these settlements can be categorised into consolidation of the soil around the tunnel and permeability of the tunnel linings. In order to understand how long-term settlements develop an understanding of these processes is required.

#### **3.3.1 Time-related tunnelling-induced settlement**

The degree to which tunnel-induced settlements, in particular, are affected by consolidation and permeability is addressed in this section. In general, the long-term settlements occur because tunnels act like drains. These long-term movements are very complex given the amount of variables to consider. Hunt (2005) identified four main factors:

- i. Pre-construction pore water pressures and post-construction excess pore water pressures,
- ii. Depth and diameter of the tunnel,
- iii. Permeability of the soil and liner, and
- iv. Compressibility of the soil and the flexibility of the liner.

Points iii and iv relate to the permeability and stiffness of the tunnel liner when compared with the surrounding soil mass.

Mair & Taylor (1997) summarised the affects from consolidation and permeability, referring to the pore-water pressure state, in tunnelling-induced settlements. This work states that when the tunnel lining is of low permeability, compared with the clay, and positive excess pore pressures are generated; these exist within one tunnel diameter. This results in additional settlement in a similar pattern to the short-term. If the tunnel lining is of low permeability relative to the clay, in stiffer clays, negative excess pore pressures generally result from construction. This would result in swelling rather than consolidation due to the equilibrium pore water profile and would result in no discernible long-term settlements. If the tunnel lining is permeable relative to the clay, the tunnel will act as a drain. This will result in consolidation settlements and a significantly wider surface settlement trough than associated with the short-term.

Wongsaroj (2005) proposed a method of quantifying the relative permeability of the soil-liner using the dimensionless Equation (3.4). If  $RP < 0.1$  using Equation (3.4) then there will be no long-term settlement and if  $RP > 100$  the lining is totally permeable. Equation (3.4) is defined as;

$$RP = \frac{k_l C_{\text{clay}}}{t_l k_{\text{soil}}} \quad (3.4)$$

where  $RP$  is soil-lining relative permeability,

$k_l$  is tunnel lining mass permeability,

$C_{\text{clay}}$  is depth of the low permeability soil above the tunnel crown extrados,

$t_l$  is thickness of tunnel lining, and

$k_{\text{soil}}$  is equivalent isotropic permeability of soil.

$RP$  is used in conjunction with a range of design charts, featured in Wongsaroj (2005), for different  $C/D$  ratios. The design charts give a value of the Normalised long-term settlement,  $DS$ , which are substituted into Equation (3.5) to estimate the normalised maximum long-term settlement. Equation (3.5) is defined as;

$$DS = \frac{NS_{c \max(SS)} - NS_{c \max(SSI)}}{NS_{c \max(SSI)} - NS_{c \max(SSP)}} \quad (3.5)$$

where DS is normalised long-term settlements,

$NS_{c \max(SS)}$  is normalised maximum surface settlement at the steady state long-term,

$NS_{c \max(SSI)}$  is normalised maximum surface settlement at the steady state long-term when tunnel lining is fully impermeable,

$NS_{c \max(SSP)}$  is normalised maximum surface settlement at the steady state long-term when tunnel is fully permeable,

In addition, earlier work by Taylor (1984) investigated the phenomenon of ‘soil squeezing’ by performing a series of centrifuge tests around tunnels and trenches. It was shown that excavations in clay continued to increase their settlements with time. Taylor (1984) explained this with the aid of a seepage factor, SF. A high value of seepage factor implies that a high seepage gradient has been caused by the simulation of a tunnel construction. This suggests that only small time-dependent deformations would exist if the tunnel support pressure was high enough to prevent seepage into the tunnel.

$$SF = \frac{\gamma_w(C + D) - \sigma_T}{\gamma_w(C + D)} \quad (3.6)$$

Using an understanding of the theoretical aspects covered in this section it is possible to make a reasonable assessment of the long-term post construction ground movements before the construction of a tunnel. This understanding is vital for separating the long-term behaviour of the ground due to the presence of a tunnel from the ground movements directly related to the construction.

### 3.3.2 Consolidation and Seepage

During a twin-tunnel construction it is reasonable to assume some degree of consolidation of the soil could be possible between the individual constructions. Atkinson (1993) used Critical State

Soil Mechanics (CSSM) to examine the relation between consolidation and seepage flow. Seepage flow leads to volume changes that, in turn, are associated with the changes of effective stress as the excess pore pressures dissipate. Seepage will flow in a direction dependent on the polarity of the excess pore pressures when compared to the steady state pore pressure. This would also suggest that after some considerable time the seepage and volume changes will cease then the excess and hydraulic gradients become zero and pore pressures return to their steady state values.

To estimate the time taken for these excess pore pressures to dissipate fully an understanding of consolidation and some formulae are needed;

$$U_t = \frac{\Delta\rho_t}{\Delta\rho_\infty} \quad (3.7)$$

$$T_v = \frac{c_v t}{H^2} \quad (3.8)$$

and the general solution becomes;

$$U_t = \frac{2}{\sqrt{3}} \sqrt{T_v} \quad (3.9)$$

and using the  $\sqrt{t}$  (time) method;

$$\sqrt{T_v} = \sqrt{\frac{c_v t}{H^2}} = \frac{\sqrt{3}}{2} \quad (3.10)$$

$$c_v = \frac{3H^2}{4t} \quad (3.11)$$

where  $U_t$  is the dimensionless degree of consolidation,

$T_v$  is dimensionless time factor,

$\Delta\rho_t$  is the surface settlement in respect to one-dimensional consolidation,

$\Delta\rho_{\infty}$  is the final surface settlement when all excess pore pressures have been dissipated,

$c_v$  is coefficient of consolidation ( $\text{m}^2/\text{year}$ ), and

$H$  is the distance over which the excess pore pressures are dissipated (m).

Given standard values of  $c_v$  (taken from an oedometer test) and an estimated drainage length it would be possible, using the expressions above, to evaluate an amount of time for consolidation after an event. This is particularly important when considering time between tunnel constructions and the subsequent effect of any drainage or consolidation between the two tunnelling events.

### **3.4 Tunnel Collapse**

Adequate stability during construction is of primary concern in any tunnelling system. This is of particular importance when tunnelling through urban areas. The appearance of sink holes would cause catastrophic damage and possible fatalities as the result of tunnel collapse.

Although this investigation is concerned with pre-failure ground movements, it is useful to understand observed failure mechanisms. This is because most pre-collapse movements were determined via investigations into collapse; for example centrifuge experiments (i.e. Mair, 1979). Stability relationships have led to the estimation of volume loss based on face pressure controlling settlements. Stability is introduced here and the prediction of volume loss based on these concepts is covered in Chapter 4.

#### **3.4.1 Failure Mechanisms**

Geometries of tunnel failure mechanisms in clays have been well investigated using centrifuge modelling by Mair (1979), illustrated in Figure 3.8. Mair & Taylor (1997) stated that case studies of tunnel failures are generally consistent with the mechanisms shown. The mechanism is shown to propagate upwards and outwards from the tunnel invert to the surface. At the surface the settlement trough is significantly wider than one tunnel diameter.

### 3.4.2 Undrained Stability

For an advancing tunnel face Broms & Bennermark (1967) performed a series of laboratory extrusion tests and analysed field observations to introduce the concept of a stability ratio,  $N$ . Based on this, a critical stability ratio at collapse,  $N_c$  was proposed as;

$$N = \left( \frac{\sigma_s + \gamma(C + D/2) - \sigma_T}{S_u} \right) \quad (3.12)$$

where  $\gamma$  is unit weight of the soil,

$C$  is cover above the tunnel crown,

$D$  is bored tunnel diameter,

$\sigma_s$  is the surface surcharge (if any),

$\sigma_T$  is the internal tunnel support pressure (if any), and

$S_u$  is the undrained shear strength of the clay.

Mair (1979) extended this concept to determine the critical stability ratio ( $N_c$ ) and plotted Figure 3.9. This design chart shows  $N_c$  in terms of the dimensionless ratios  $P/D$  and  $C/D$  which were based on centrifuge model tests; where  $P$  is the length of tunnel boring face as shown in Figure 3.9. The formula given by Mair (1979) for predicting critical tunnel stability is defined as;

$$N_c = \left( \frac{\gamma(C + D/2) - \sigma_{TC}}{S_u} \right) \quad (3.13)$$

where  $\sigma_{TC}$  is the internal tunnel support pressure at collapse.

Tunnelling investigations carried out using a geotechnical centrifuge are often two-dimensional. Therefore, when using Figure 3.9 the line of interest is labelled ' $P/D \rightarrow \infty$ ' because the length of tunnel boring face is zero. Given a depth or  $C/D$  this figure shows that the critical stability ratio trends towards 4 for a circular cavity. Davis *et al.* (1980) investigated a number of upper and lower bound solutions into the stability of tunnels in clay. Significantly, this study investigated



a number of variations to the plastic collapse mechanism. The series of centrifuge tests on model shallow tunnels from Mair (1979) were used to verify these solutions. The optimum lower bound presented by Davis *et al.* (1980) is shown in Figure 3.10 for calculating the tunnel support pressure with respect to  $\gamma D/S_u$ . Using the relationships above it is therefore possible to estimate the pressure required to support a single tunnel during construction before a permanent lining is installed. This is necessary during a tunnel construction to avoid collapse and to understand the source of any small movements due to insufficient tunnel support.

Xu *et al.* (2013) conducted a series of centrifuge tests investigating the effect different arrangements of umbrella arches have on the stability of a single tunnel. The centrifuge tests were overconsolidated kaolin clay models with pressurised air supported rubber bags similar to those conducted by Mair (1979). However, different arrangements of resin tubes were cast around the annulus of the cavity. The different arrangements were intended to intersect the shearing planes from the plastic collapse mechanisms in Davis *et al.* (1980). These tests showed that placing the resin tubes at the sides, instead of at the crown, of the tunnel increased the stability. The relationship between tunnel support and settlement will be described in detail in Chapter 4.

### **3.5 Summary**

This chapter presented the sources of the tunnelling-induced ground movements. Previous work has been examined to establish typical ground movements which may result from the process of twin-tunnelling in clay.

The ground movements presented have been largely separated into three sections. The first of these focuses on short term movements. This was undertaken in order to gain an understanding into the behaviour of clay pre-failure. During this section important parameters of tunnel construction were highlighted that are required for adequate prediction of settlements (given in Chapter 4). This study was primarily concerned with the influence the first tunnelling event has on a second. This introduces a time aspect to the study and therefore an understanding of the sources of long-term settlements affecting tunnels was conducted. This is important for

understanding the soil behaviour during the delay between the tunnel constructions. The final section contains a brief description of tunnel failure including the plastic collapse mechanism observed during tunnelling research in clay.

## **4 PREDICTION OF GROUND MOVEMENTS CAUSED BY TUNNELLING**

Bored tunnel constructions cause ground movements. The assessment of the potential effects from these ground movements on infrastructure is an essential aspect of the planning, design and construction of a tunnelling project in an urban environment. Therefore, accurate assessments of these vertical and horizontal movements are required and have been explored by many authors (e.g. Peck, 1969; Cording & Hansmire, 1975; Clough & Schmidt, 1981; O'Reilly & New, 1982; Attewell and Yeates, 1984; Cording, 1991; Mair *et al.*, 1993 and Mair & Taylor, 1997). These authors have shown a number of methods for estimating ground movements based on tunnel diameter, tunnel depth, type of construction method and soil type. This chapter details current practice and various modelling techniques for estimating ground movements around single and twin-tunnels in clay.

### **4.1 Current practice for predicting ground movements above single tunnels**

Tunnelling construction guidelines have been developed based, largely, on research from single tunnel arrangements (e.g. Peck, 1969; Mair, 1979; Taylor, 1984 and Attwell & Yeates, 1984). These methods are generally based on the two-dimensional idealised case and some include a variety of parameters for prediction. The parameters to be determined were discussed in Chapter 3. This section outlines the prediction methods of these parameters firstly related to the magnitude of the ground movements (volume loss) and then the extent of these ground movements (trough width).

#### **4.1.1 Predicting Short-Term Volume Loss**

In Chapter 3 the concepts of the stability ratio,  $N$ , by Broms & Bennemark (1967) and critical stability ratio,  $N_c$ , by Mair (1979) were discussed. Kimura & Mair (1981) introduced the concept of a Load Factor (LF) and developed Equation (4.1) based on these concepts. This empirical formula was based on the stability of shallow tunnels in a number of centrifuge experiments taken to collapse.

Where;

$$LF = \frac{N}{N_c} \quad (4.1)$$

Investigations into volume losses in clays could have considerable merit when related to the load factor ratio, LF. In particular, Mair (1979) produced a plot of  $V_L$  verses LF and investigated the geometric variables of C/D and for P/D (illustrated by Figure 4.1a). Macklin (1999) collated prediction methods for estimating volume losses caused by single tunnels through over-consolidated clay (given in Table 4.1). These predictions of volume loss all use some of these stability parameters.

However, Macklin (1999) used these studies and drew on another by Atkinson & Potts (1977), (C/D ratio equal to 0.77) to propose a relationship between the logarithm of  $V_L$  and LF above the C/D ratio of 1 and for  $P/D \rightarrow \infty$ . Equation (4.2) was determined from a plot of an upper and lower bound design lines (Figure 4.1b).

$$V_L(\%) = 0.23e^{4.4(LF)} \text{ for } LF \geq 0.2 \quad (4.2)$$

This text also commented that Equation (4.2) was used for predicting volume losses during a reported case study and was found to be an adequate method for a 2.44m diameter tunnel constructed in London Clay. Once a prediction or estimate of the volume loss expected has been made consideration must then be given to how these settlements will be distributed at the surface and sub-surface.

#### **4.1.2 Transverse Surface Settlement Trough**

Many solutions have been developed for predicting the soil movement above tunnels. These have been separated into a number of categories with a wide range of complexity. The most commonly used solutions are based on empirical relationships. However, the selection of key parameters used in these solutions requires experience and judgement. These are represented by Mair *et al.* (1981) and Clough & Schmidt (1981) in this dissertation. Other solutions include a

Closed-form elastic solution proposed by Verruijt & Booker (1996) and a closed form semi-empirical elastic solution by Loganathan & Poulos (1998).

Finally, the most complex solutions are usually Finite element (FE) or Finite Difference (FD) numerical methods. The mathematics supporting these numerical analyses is outside the scope of this research and is therefore not included. It is worth commenting however, that the increased capacity of computing in recent years offers considerable possibilities for modelling many aspects of a bored tunnel construction. The stress-strain characteristics of overconsolidated clay are difficult to represent numerically and would necessitate the use of a complex constitutive model such as the 3-Surface Kinematic Hardening (3-SKH) model proposed by Stallebrass (1990). However, even these complex constitutive soil models are acknowledged to not necessarily represent all aspects of soil behaviour important to tunnelling. For instance, Grammatikopoulou *et al.* (2008) compared the settlement predictions obtained from a single tunnel finite element analysis using various advanced constitutive models with field measurements and the Gaussian distribution. It was shown that the predicted settlement troughs did not represent all of the features observed during an actual tunnel construction.

#### 4.1.2.1 Empirical Methods

A Gaussian distribution for ground movements was proposed by Peck (1969) and verified by many site measurements and centrifuge tests (e.g. Mair *et al.*, 1993). The semi-empirical approach has been adopted for calculating surface settlements based on this;

$$S_v = S_{\max} \exp\left(-\frac{x^2}{2i^2}\right) \quad (4.3)$$

where  $S_v$  is the vertical settlement, at a defined horizontal point, in the x-z plane,

$S_{\max}$  is the theoretical maximum settlement at the tunnel centre-line,

$x$  is the lateral distance from the tunnel centre-line, and

$i$  is the lateral distance from the tunnel centre-line to the point of inflection in the Gaussian distribution curve.

Integrating Equation (4.3) twice shows the relationship below;

$$V_s = \sqrt{2\pi} \cdot i \cdot S_{max} \quad (4.4)$$

where  $V_s$  is volume of surface settlement.

In order to determine the magnitude of settlements Equation (3.1) and Equation (4.3) can be combined to produce Equations (4.4);

$$S_{max} = 0.313 \frac{V_L D^2}{i} \quad (4.5)$$

where  $V_L$  is volume loss expressed as a ratio, and

$D$  is the bored tunnel diameter.

Given data on tunnel geometry and knowledge of  $V_L$  it only remains to estimate the parameter  $i$  which governs trough width. Many authors have suggested relationships between  $i$ , tunnel depth and tunnel diameter (e.g. (O'Reilly & New, 1982 and Clough & Schmidt, 1981). Notably, O'Reilly & New (1982) proposed the formula Equation (4.6) based on a survey of UK tunnelling data;

$$i = K \cdot z_0 \quad (4.6)$$

where  $z_0$  is the vertical distance from the un-deformed surface to the tunnel axis level, and

$K$  is a dimensionless trough width parameter.

The parameter  $K$ , in practical terms, was simplified to 0.5 for tunnels in clay. The data presented by Mair & Taylor (1997) commented that there was some scatter but generally  $i$  was found to be within the envelope bounded by  $i=0.4z_0$  and  $i=0.6z_0$ . Hence,  $K$  could vary between 0.4 and 0.6.

Clough & Schmidt (1981) proposed a formula based on the geometric parameters of the tunnel;

$$i = R \left( \frac{Z_0}{D} \right)^{0.8} \quad (4.7)$$

where  $R$  is the radius of the bored tunnel.

#### 4.1.2.2 Closed-form solution by Verruijt & Booker (1996)

Verruijt & Booker (1996) derive a closed-form solution by using isotropic, homogeneous elastic half space equations. These expressions include some effect of the tunnel deformation and compressibility of the soil (first suggested by Sagaseta, 1987). The tunnel deformation described consists of radial contraction and shape ovalisation (Figure 4.2). Compressible soils used a value of Poisson's Ratio,  $\nu$ , less than 0.5. Verruijt & Booker (1996) estimate settlement by;

$$S_v = 4\varepsilon R^2(1 - \nu) \frac{Z_0}{x^2 + Z_0^2} - 2\delta R^2 \frac{Z_0(x^2 - Z_0^2)}{(x^2 + Z_0^2)^2} \quad (4.8)$$

where the radial strain was given by;

$$\varepsilon = \frac{V_s}{4(1-\nu)} \quad \text{Sagaseta (1987),} \quad (4.9)$$

and the ovalisation ratio was given by;

$$\delta = \frac{U_R}{R} \quad \text{Verruijt & Booker (1996),} \quad (4.10)$$

and  $U_R$  is the radial deformation around the tunnel diameter.

#### 4.1.2.3 Semi-empirical closed-form solution by Loganathan & Poulos (1998)

Loganathan & Poulos (1998) proposed a semi-empirical elastic analytical method based on shallow tunnel volume loss scenarios due to Verruijt & Booker (1996) under predicting the maximum settlement. The reasons the authors gave for this were that soil exhibits non-linear behaviour and therefore the ground movement at the tunnel soil interface was not realistic. Loganathan & Poulos (1998) considers the situation when the ovalisation,  $\delta$ , had been equal to zero i.e. there is no deformation of the lining. Loganathan & Poulos (1998), therefore,

attempted to model construction conditions generated by a TBM and compared this ground movement monitoring data taken during construction of the Heathrow Express Trial Tunnel. This method uses a ‘gap’ parameter (originally from Rowe *et al.*, 1983) which defines the ground displacements prior to the installation of the lining. The ‘gap’ will depend on the tunnelling machine, soil type, and experience and skill of the tunnelling machine operators. In Figure 4.3 the ‘gap’ is shown to account for the physical clearance between the outer shield and the lining ( $G_p$ ), allowance for out-of-plane ground movements ( $u_{3D}$ ) and allowances for workmanship ( $\omega$ ). Rowe *et al.* (1983) assumed ‘gaps’ between 90 and 160mm. Loganathan & Poulos (1998) proposed the following expression to predict vertical settlement;

$$S_v = 4V_L(1 - \nu)R^2 \frac{z_0}{z_0^2 + x^2} \exp\left(-\frac{1.38x^2}{(z_0^2 + R^2)^2}\right) \quad (4.11)$$

#### 4.1.2.4 Summary of prediction methods

In order to compare the numerous methods for estimating surface settlement troughs a normalised plot has been generated. Figure 4.4 shows a comparison of the various methods outlined above for predicting surface settlement outlined and has both axis normalised in terms of tunnel diameter. The estimates shown were calculated based on a two-dimensional scenario with a 5m diameter single tunnel and a C/D equal to 2. Mair *et al.* (1981) and Clough & Schmidt (1981) agreed the shape of the settlement trough is best described by a Gaussian distribution curve, however, their determination of  $i$  was different. This difference gives a narrower and deeper trough when using Clough & Schmidt (1981). Loganathan & Poulos (1998) and Verruijt & Booker (1996) show very similar settlement troughs, however, they are shallower and wider than the empirical prediction methods.

#### 4.1.3 Sub-surface Settlements

It is increasingly important to provide accurate predictions of sub-surface movements as tunnels are often constructed in proximity to other services due to underground congestion in urban environments. These services could not only be other tunnels but also deep basements or foundations. Relatively few methods are available to estimate the tunnelling-induced sub-



surface settlements. Two methods of prediction are presented here; Mair *et al.* (1993), an empirical method, and Loganathan & Poulos (1998), a closed-form solution.

#### 4.1.3.1 Empirical Method

Throughout the depth of soil above the tunnel Mair *et al.* (1993) used the observations from centrifuge tests and sub-surface data from various tunnelling projects in stiff clay to show that the settlement distribution remained Gaussian in shape. An extended Gaussian distribution of the surface settlement gave a reasonable approximation for these movements (illustrated by Figure 4.5). Changes were made to the previously presented formulae and are as follows;

$$i = K(z_0 - z) \quad (4.12)$$

$$K = \frac{0.175 + 0.325 \left(1 - \frac{z}{z_0}\right)}{1 - z_0} \quad (4.13)$$

$$S_z = S_{z,\max} \exp\left(-\frac{x^2}{2K^2(z_0 - z)^2}\right) \quad (4.14)$$

$$S_{z,\max} = \frac{1.25V_L}{0.175 + 0.325 \left(1 - \frac{z}{z_0}\right)} \frac{R^2}{z_0} \quad (4.15)$$

where  $z$  is the vertical distance from the un-deformed surface to the horizon analysed,  
  
 $S_z$  is the sub-surface settlement in the  $x$ - $z$  plane, and  
  
 $S_{z,\max}$  is the maximum sub-surface settlement (above the tunnel centre-line) at depth,  $z$ .

#### 4.1.3.2 Closed-form solution by Loganathan & Poulos (1998)

Loganathan & Poulos (1998) modified Equation (4.11) to give a prediction of the sub-surface settlement profiles using the consideration that there is no deformation of the lining. This equation, similar to the surface prediction method, was compared with Verruijt & Booker (1996) and observations from the construction of the Heathrow Express Trail Tunnel. The

authors state that the modified equation gave smaller displacements at depth than the original. Presented below is their closed-form solution for estimating sub-surface vertical settlement;

$$S_z = V_L R^2 \left( -\frac{z - z_0}{x^2 + (z - z_0)^2} + (3 - 4\nu) \frac{z + z_0}{x^2 + (z + z_0)^2} - \frac{2z[x^2 - (z + z_0)^2]}{[x^2 + (z + z_0)^2]^2} \right) \exp \left[ -\left( \frac{1.38x^2}{(z_0 + R)^2} + \frac{0.69z^2}{z_0^2} \right) \right] \quad (4.16)$$

#### 4.1.3.3 Summary of prediction methods

Figure 4.6 shows a normalised comparison plot between the various methods for prediction sub-surface settlement outlined in sections 4.1.3.1 and 4.1.3.2. This figure is similar to Figure 4.4 in that the axes are normalised against tunnel diameter and is for a 5m tunnel with a C/D equal to 2. The settlement troughs are taken at a depth of one tunnel diameter below the ground surface level. Mair *et al.* (1993) gives a narrower and deeper settlement trough than Loganathan & Poulos (1998). This is a reflection of the difference observed at the surface level but is exaggerated as expected for sub-surface movements.

## 4.2 Modelling and Prediction of Twin Bored Tunnelling-induced Ground Movements

In this section a number of methods are outlined for the prediction of soil movements induced by twin bored tunnelling. Relatively little literature documenting the behaviour regarding twin-tunnels and their interaction has been published. It is because of this reason perhaps that few prediction methods exist. The complexity of any twin tunnel prediction method is further exacerbated by the near infinite possible geometric arrangements.

If the assumption is made that the tunnels are parallel then it could be stated that, generally, there are three twin tunnelling arrangements. Two-dimensional idealisations are shown in Figure 1.2. It can be seen that within these three variations side by side (1) geometry refers to multiple tunnels being constructed at the same horizontal axis depth. Stacked/Piggyback (2) arrangements consist of a second tunnel being constructed directly above or below the first. Offset (3) could be described as half way between the Side-by-side and Stacked arrangements.

This would be the arrangement when the tunnels' centre-lines have an offset in both the vertical and horizontal axis.

#### 4.2.1 Superposition Method

Superposition is a method for predicting surface settlement above any twin tunnel arrangement. A surface settlement prediction is produced using one of the methods outlined in section 4.1.2. Assuming that the second tunnel is of similar size and depth then the same distribution is positioned over the centre-line of the second tunnel ignoring any influence from the first. The summation of these two overlapping curves describes the total settlement. This is illustrated by Figure 4.7 and shows the superposition of two, 4m diameter, individual tunnel settlements. The settlement troughs are calculated for tunnels with 3% volume losses in a clay with cover of 8m.

O'Reilly & New (1982) provided a formula for twin tunnels by superposition;

$$S_v = S_{\max} \left[ \exp \left( -\frac{x_A^2}{2i^2} \right) + \exp \left( \frac{(x_A - d)^2}{2i^2} \right) \right] \quad (4.17)$$

where  $d$  is the horizontal distance between the two tunnels centre-lines, and

$x_A$  is the lateral distance from the centre-line of the first bored tunnel.

The expression above assumes the tunnels are parallel and have the same tunnel diameter, volume loss and settlement trough width. However, it is possible to take into account different depth of tunnel and trough widths by expansion of the expression. More importantly this expression implicitly ignores any interaction between the tunnels.

#### 4.2.2 Overlapping Zones

Fang *et al.* (1994) considered the displacements and strains associated with twin-tunnelling. The work considers a disturbed zone surrounding each of the tunnels created during a construction. If the second tunnel construction generates stresses within the zone created by the first construction a 'large and irregular' volume loss could be expected. Figure 4.8, originally from Hoyaux & Ladanyi (1970) and redrawn in Fang *et al.* (1994), used the finite element method to analyse the stress distribution surrounding tunnels driven through soft soils. This

study indicated the plastic zone was mainly influenced by the sensitivity of the soil deposit, diameter of tunnel and depth of tunnel. The varied sensitivity is represented by the two trends in the figure. These trends were derived from 22 twin-tunnel profiles which found the  $Z/R$  ratios varied from 3.2 to 18.1 and the  $d/D$  ratios varied from 1.3 to 2.7. However, when the tunnel spacing was sufficiently high the second tunnel would have little or no influence on the first. The authors postulated at what spacing between the tunnels can be considered large enough to avoid interaction. If the criterion of  $Z/R > 3$  has been used for insensitive clays then the plastic zones do not overlap and the interaction is negligible. Fang *et al.* (1994) also states that superposition could be used to estimate settlements above parallel tunnel construction if the interaction is negligible.

#### **4.2.3 Design Plots by Addenbrooke & Potts (2001)**

To investigate the influence of a second tunnel construction upon an existing tunnel Addenbrooke & Potts (2001) carried out an extensive numerical study. A series of finite element analyses were performed using a non-linear elastic-perfectly plastic constitutive model to represent the soil. Various geometric arrangements were considered, either side by side or piggy back, and all tunnels were modelled as having equal diameters. The analysis comprised the construction of the first tunnel over a short period, followed by some period of consolidation and the construction of the second tunnel. When considering side by side tunnel arrangements constructed using similar methods, this study predicted that the shape of the second tunnel's surface settlement profile was not 'too dissimilar' to the first (greenfield) tunnel. A method for adjusting the predicted settlement profile associated with the second tunnel was thus proposed. Two design charts were produced to find, firstly, an eccentricity of the maximum settlement and, secondly, the increase in volume loss of the second tunnel's settlement profile (Figure 4.9). The plots indicated that the volume loss resulting from the second tunnel increases as the spacing between the tunnels decreases. The increase in volume loss is given as a ratio of volume loss from the second tunnel construction,  $V_{L \text{ Tunnel B}}$ , over volume loss of the first (greenfield) tunnel construction,  $V_{L \text{ greenfield}}$ . Once the modified volume loss has been obtained the second tunnel settlements can be determined and can then be summed with those of the

unchanged first tunnel to predict the total settlement. As with the majority of the previous methods discussed this method is only applicable to surface settlements.

The design charts presented in the work are plotted in terms of the parameter ‘pillar width’. Pillar width is the horizontal distance between the tunnel’s centre-lines minus the sum of their radii expressed as a ratio of the average tunnel diameter. This allows for any possible distortion of the tunnel linings.

#### 4.2.4 Modification Method by Hunt (2005)

Hunt (2005) provided a different method for predicting movements above twin-tunnel constructions. This, finite element based, study used the modelling package ABAQUS applying a small strain-stiffness model and the modified gap parameter to analyse 2D plain strain undrained tunnel constructions in London Clay. Attempts were made to consider the construction delay by including a stiffness change with no consolidation. The results of these numerical analyses led the author to propose a Modification Factor to the semi-empirical tunnelling-induced ground movements caused by a second tunnel. This method was validated against a number of case studies.

This method modified the ground movements of the second tunnel in an ‘overlapping zone’, this soil is assumed to have been previously disturbed by the creation of the first tunnel. This is illustrated in Figure 4.10, taken from the study.

$$S_{mod} = FS_v \quad (4.18)$$

where  $S_{mod}$  is the modified settlement,

$S_v$  is the unmodified settlement above the second tunnel calculated by semi-empirical methods, and

$$F = \left\{ 1 + \left[ M \left( 1 - \frac{|d + x|}{AK_1 Z^*} \right) \right] \right\} \quad (4.19)$$

where  $Z^* = (z_0 - z)$ ,

A is the multiple of the trough width parameter (usually taken as 2.5 or 3) in a half settlement trough,

d is the centre-to-centre spacing of the tunnels,

$K_A$  is the value of K in the region of the first bored tunnel, and

M is Maximum modification factor described by Chapman *et al.* (2006).

The maximum relative increase in settlement,  $M=1.0$ , is aligned with the centre-line of Tunnel A and reduces to zero at some lateral distance from Tunnel A. Hunt (2005) concluded that the maximum percentage increase in settlement was usually 60 %.

As with Addenbrooke & Potts (2001) the method modifies the settlement profile above the second tunnel using Equations (4.18) and (4.19). The predicted total settlement is to add the modified second tunnel settlement with the unmodified first similar to that seen in Figure 4.7.

#### **4.2.5 Conclusions from Twin-tunnel prediction methods**

The twin-tunnelling investigations into the surface and sub-surface settlements have mostly been approached using finite element analysis in a 2D scenario. Single tunnel analyses that use isotropic linear elastic-perfectly plastic soil models tend to produce wider surface settlement troughs than observed on site (Mair *et al.*, 1981). However, predictions have been improved by using non-linear elastic, perfectly plastic models which give deeper and wider settlement trough predictions which compare more favourably with field observations. One limitation of these types of constitutive model is that the soils are represented as having isotropic behaviour. Much research has been conducted demonstrating the anisotropy of soils e.g. Al-Tabbaa (1987) and this highlights the potential difficulties of numerical modelling. It is clear that valuable insight could be gained from a physical modelling study which, as it uses real soil samples, inherently represents the actual behaviour.

### **4.3 Field Observations**

This section presents case studies concerned with the relative differences observed between single and twin tunnel settlements. Four twin-tunnelling case studies have been examined;

Heathrow Express, Lafayette Park, St. James' Park and Docklands Light Rail Lewisham Extension. The case studies are discussed in terms of geometric constants tunnel diameter, depth, and centre-to-centre spacing and in terms of settlement variables volume loss, maximum settlement and trough width.

#### **4.3.1 Heathrow Express (UK) – Side-by-side Tunnels**

Cooper *et al.* (2002) commented on the extensive monitoring conducted during the construction of the 9m diameter parallel tunnels either side of a concourse tunnel in London. These tunnels were bored below the existing Piccadilly line running tunnels. The settlement data was recorded using Electrolevels within the Piccadilly line tunnels which were 4m diameter and at a depth of 12.7m. The Heathrow Express tunnels were at a depth of 26m and were separated by a distance of 36.8m. The concourse tunnel was 15.9m from the 'Downline' tunnel and 20.9m from the 'Upline' tunnel. Figure 4.11a is a plan showing the arrangement of the Piccadilly line running tunnels and Heathrow Express tunnels.

Hunt (2005) showed the predicted greenfield settlement for the first tunnel (labelled as 1) with the actual settlement for another closely constructed tunnel (labelled as 3). The first tunnel prediction is based on a maximum vertical settlement of 29.3mm and a volume loss of 1.2% (Figure 4.11b). The same predicted settlement curve is positioned over the centre-line of the closely constructed tunnel. The actual maximum settlement of the closely constructed tunnel was 35mm and thus gave a higher volume loss than the first tunnel at 1.8%. There is a clear discrepancy between the settlement and the prediction method. Therefore, at this sub-surface level there was a significant disturbance of the soil shared by the two tunnel constructions. Cooper *et al.* (2002) noted that in order to fit the empirical relationship outlined by Mair *et al.* (1993) to the field data the trough width was modified. The half of the settlement trough, due to the second tunnel, towards the existing tunnel was wider than anticipated. This implies that there was some level of asymmetry in the settlements due to the second tunnel.

#### **4.3.2 Lafayette Park (USA) – Side-by-side Tunnels**

Cording & Hansmire (1975) analysed the surface and sub-surface settlement monitoring data of a side-by-side twin-tunnelling arrangement. 6.4m diameter tunnels were bored 14.6m below the

ground surface in clay. This text stated the surface settlement trough distribution curve, as proposed by Peck (1969), could be used to describe the shape displacements above a tunnel. However, for the twin-tunnels the settlement at the ground surface will be larger than the sum of the settlement for two single tunnels. In Figure 4.11c Hunt (2005) analysed the monitoring data from Cording & Hansmire (1975) which shows the first tunnel with a maximum vertical settlement of 52.7mm (3% volume loss). However, Cording & Hansmire (1975) gave the actual second tunnel maximum vertical settlement of 69.6mm and thus a volume loss of 3.63%.

It is, however, worth noting that the Modification Factor Method outlined by Hunt (2005) and featured in this literature review gave settlement profiles with very high agreement with this recorded case history when compared to routine superposition. However, the Modification Factor method was applied after  $K$  had been increased to fit the field data from Cording & Hansmire (1975).  $K$  towards the tunnel had been increased from 0.5 to 0.6 and reduced from 0.5 to 0.3 away from the tunnel. This implies that predictions may require the assessment of more parameters than just an increase in volume loss.

#### **4.3.3 St James Park (UK) – Offset Tunnels**

Nyren (1998) measured surface settlement displacements at the St. James's Park greenfield reference site. This site had been subjected to the driving of twin tunnels through London Clay. The first of these tunnels had been bored at a depth of 31m and gave an immediate transverse settlement trough profile. Volume losses of the westbound tunnel were 3.3% (maximum settlement of 20.4mm), unexpectedly high for the first tunnel which was thought to be due to a relatively rapid rate of advance (45 m per day).

The second tunnel, at a depth of 20.5m, was driven 250 days later and at half the rate. Nyren (1998) stated that the second eastbound tunnel was significantly influenced by the construction of the first tunnel. Figure 4.11d shows the asymmetry of the transverse settlement trough from the second tunnel construction. The half of the settlement trough towards the existing tunnel is significantly larger than would normally be assumed. Instead of the approximate 2.9% volume loss (maximum settlement of 23.4mm) Nyren (1998) stated a value of 2.2% would be a better estimate of the greenfield conditions had the westbound tunnel not been previously constructed.



#### **4.3.4 Docklands Light Rail Lewisham Extension (UK) – Side-by-side Tunnels**

Sugiyama *et al.* (1999) described the monitoring results of ground movements on the Docklands Light Rail (DLR) Lewisham Extension. This project had various geotechnical strata along the route of the twin tunnels. The predominate strata bored through was the Woolwich and Reading Beds (WRB). This is a complex soil formation ranging from very stiff to hard clays to dense sands and gravels. A slurry shield machine with a diameter of 5.85m was used. The clear separation between the two tunnels was approximately 15m. The C/D ratio over the 1km length of tunnel ranged from 1.6 to 2.5. Sugiyama *et al.* (1999) showed all the volume losses to be below 1%. However, at the majority of the monitoring sections the second, Northbound, tunnel appears to have a relatively much larger volume loss than the first, Southbound tunnel. One of the conclusions Sugiyama *et al.* (1999) drew was that the values for the points of inflexion were shown to be wider than those predicted. Therefore, the settlement troughs were wider and flatter than anticipated. It is perhaps the influence of the second tunnel on the first that has led to a difference in the points of inflexion and not due the misinterpretation of stiffness.

#### **4.4 Summary**

A number of prediction methods have been outlined in order to estimate the tunnelling-induced movements from single and twin tunnel arrangements. Firstly, routine single tunnel methods were outlined and their terminology applied to twin-tunnel prediction methods. The twin-tunnel methods short-comings have been critically analysed in order to appreciate the need for the presented research. The final section details a number of case studies, in various soils, showing evidence and need for an improvement to the current understanding of twin bored tunnel settlements.

## **5 CENTRIFUGE MODEL TESTING**

A brief introduction to the fundamental principles of centrifuge modelling is presented in this chapter. A review of the key aspects to consider when modelling this type of complex geotechnical scenario with a centrifuge is also explained. The centrifuge being used for this research project is the London Geotechnical Centrifuge located at City University London.

### **5.1 Introduction**

To understand complex geotechnical problems engineers must try to understand the engineering properties of soils and how they will interact with, on or in a proposed construction. Soil exhibits non-linear behaviour which requires complex methodology to form an understanding of its behaviour. The main method of investigation utilised in this research was the use of a geotechnical centrifuge. The focus of the test series was to examine the short-term surface and sub-surface deformations, in the plane perpendicular to twin bored tunnels in overconsolidated clay, after sequential simulated tunnel constructions,.

Experiments were performed in a plane strain strong box at 100g. Models consisted of a preformed circular cavity (or cavities) in overconsolidated clay. These were supported by either compressed air or water dependent on the particular test. Apparatus was developed to provide tunnel support using a fluid and to allow that fluid to be removed in order to simulate volume losses. Transducers were secured on a gantry above the model to monitor the vertical settlement at the surface. Ports are present in the back-wall for installation of pore pressure transducers and the fluid feed for the tunnels. During testing the front-wall of the strong box was replaced with Perspex windows enabling observation of the subsurface ground movements via digital image analysis.

A total of eighteen centrifuge tests were conducted with various geometries (cover and centre-to-centre spacing), alternative support fluids and varying volume losses. These tests would provide new insight into the behaviour of soil during twin bored tunnel constructions.

## 5.2 Background to centrifuge model testing

Physical modelling in geotechnics can be separated into three categories (1) full scale modelling, (2) reduced scale modelling under normal gravity conditions and (3) reduced scale modelling under increased gravities. Each has their own relative merits and disadvantages. With a centrifuge it is possible to create a stress distribution within the soil which increases with depth corresponding to the stress distribution in a full scale prototype.

### 5.2.1 Principals of centrifuge modelling

The general centrifuge scaling laws are described by Taylor (1995). The notations used in this text to describe these laws are also used in this thesis. In essence, Newton's laws of motion state the action of pulling a mass out of a straight flight path into a radial path would impose an inward acceleration on the mass towards the axis of rotation (Figure 5.1). This radial acceleration is a function of the angular velocity and radius from the centre of rotation.

Thus;

$$a = \omega^2 r \quad (5.1)$$

where  $a$  is the radial acceleration ( $\text{m/s}^2$ ),

$\omega$  is the angular velocity ( $\text{rad/s}$ ), and

$r$  is the radius from the centre of rotation ( $\text{m}$ ).

It is usual to describe the gravity scaling factor as;

$$n = \frac{\omega^2 r}{g} = \frac{a}{g} \quad (5.2)$$

where  $n$  is the gravity scaling factor, and

$g$  is the acceleration due to gravity ( $9.81\text{m/s}^2$ ).

Centrifuge testing is a method by which a soil with a stress distribution equal to that of the field or prototype can be reproduced consistently (illustrated in Figure 5.2). This fundamental principal can be written as;

$$\sigma_{vp} = \sigma_{vm} \quad (5.3)$$

$$\rho g h_p = \rho n g h_m \quad (5.4)$$

with the subscript of either m or p for model or prototype respectively.

where  $\rho$  is the density of the soil material, and

$h$  is the depth.

If we assume that the soil in the prototype and model are the same and that  $g$  is a constant, the scale factor for length in the model is therefore: -

$$h_m = \frac{1}{n} h_p \quad (5.5)$$

This implies that models accelerated at  $Ng$  give a stress equivalency with the soil to the full scale prototype. Table 5.1 is reproduced from Marshall (2009) and summarises other significant scaling laws important to geotechnical centrifuge modelling.

### 5.2.2 Scaling laws and time

It has previously been stated the importance consolidation has in understanding fundamental soil behaviour in this thesis. Consolidation events require a relationship for scaling time. This relationship needs to account for the dissipation of excess pore-water in the models. Tests performed with clay have a dimensionless consolidation time factor,  $T_v$ ;

$$T_v = \frac{c_v t}{H^2} \quad (5.6)$$

where  $C_v$  is the coefficient of consolidation,

t is time, and

H is the drainage path length.

For a degree of consolidation, in a soil, the model and prototype are equal.

$$c_{vp} \frac{t_p}{H_p^2} = c_{vm} \frac{t_m}{H_m^2} \quad (5.7)$$

Therefore;

$$t_m = t_p \frac{H_m^2}{H_p^2} \frac{c_{vp}}{c_{vm}} \quad (5.8)$$

$$t_m = t_p \frac{1}{n^2} \frac{c_{vp}}{c_{vm}} \quad (5.9)$$

This squared relationship implies that one hour of consolidation in a centrifuge at 100g equates to 416 days at prototype scale for the same soil.

### 5.2.3 Errors in Centrifuge Modelling

#### 5.2.3.1 Variations in stress level

Scaling laws, applied to a soil model in this way, indicate that within a centrifuge model the acceleration is not constant with depth. During testing this will vary linearly with the radius from the axis of rotation. Typical prototype against model vertical stress profiles are illustrated in Figure 5.3. To minimise the amount of under and over stress in the centrifuge model, an effective radius,  $R_e$ , is used. This effective radius gives the correct stress at a depth two-thirds of the model height from the surface. The error related to this modification in stress profile is in the order of 3%.

Considering this and Equation (5.2);

$$n = \frac{\omega^2 R_e}{g} \quad (5.10)$$

The effective radius is calculated by using the radius at the top of the sample,  $R_t$ :

$$R_e = R_t + \left(\frac{h_m}{3}\right) \quad (5.11)$$

### 5.2.3.2 *Radial Acceleration Field*

The acceleration field, through a centrifuge package, is radial and does not run parallel through the depth (shown in Figure 5.3). This introduces an error that increases with distances parallel from the model's centre-line. There is, therefore, a lateral component of acceleration, the effect of which needs to be recognised (Taylor, 1995). McNamara (2001) suggested the maximum horizontal components of acceleration are approximately 5% of the vertical (for the City centrifuge facility with a radius of 1.8m from centre to the swing bed a dimension of  $\pm 0.1$ m from the centreline). McNamara (2001) also stated this horizontal component, the error, can be minimised by orientating the strongbox such that the smallest dimension is in the same plane as the radial acceleration field. Stewart (1989) described in some detail the radial acceleration field and states as this passes through the centre-line of the model, and that measurements should be taken here, where the error due to the radial nature of the acceleration field is small. Taylor (1995) also stated it is good practice when designing a centrifuge model to place the geotechnical event around the central region of the model.

### 5.2.3.3 *Scaling Effects*

In general, the type of soil used in the centrifuge models will be of the same type as the prototype soil. This may lead to compatibility issues applying scaling laws to grain sizes, highlighted by Taylor (1995) and Philips (1995).

Taylor (1995) stated that it might be considered sensible to increase the particle size by the model scale applied to the prototype. This is flawed as clay would in some cases be scaled to represent fine sand. However, these two materials have different stress-strain characteristics. Philips (1995) commented that at least 30 particles must be in contact with a linear dimension of the model structure for the observed behaviour to be representative of the prototype behaviour. However, care must be taken when designing the model that the mechanical properties of the particles are not changed. Taylor (1995) mentioned the use of a ratio between grain sizes and an

important physical dimension and concludes that grain scaling is a problem when using relatively small scale models in relatively high acceleration with granular materials. Consequently, there should not be a grain size scaling effect if the previously outlined design parameters are followed.

#### **5.2.3.4 *Boundary Effects***

Philips (1995) described considerations for minimising boundary effects in models for geotechnical centrifuges. Initially, the concern was with side-wall friction. Although this is always present to some extent, it was suggested that models be significantly wide so that this friction is not a significant proportion of the resisting forces. It was suggested that models should be in the region of twice as long as the soil depth. Taylor (1995) suggested that for tunnelling models there should be at least one diameter space underneath the tunnel for base effects to be negligible.

### **5.3 The London Geotechnical Centrifuge Testing Facility**

#### **5.3.1 The Acutronic 661 geotechnical centrifuge**

City University London's centrifuge facility comprises of an Acutronic 661 geotechnical centrifuge, extensive details of which are given by Grant (1998). The important geometric details of the Acutronic 661 Centrifuge are shown in Figure 5.5. The radius of the swing bed is 1.8m and the effective radius for a model is typically between 1.5 and 1.6m. To balance the package on the swing bed a 1.45 tonne counterweight is used which can be adjusted radially when required using a screw mechanism. The maximum load capacity is a 400kg package tested at 100g and this reduces with accelerations to a maximum of 200kg at 200g. Therefore, the Acutronic 661 is a 40g/tonne centrifuge facility. The swing bed has dimensions of 500x700mm and a useable height of 970mm.

The centrifuge machine is situated within a reinforced concrete sided room opposite a preparation area. This arrangement lends itself to effective model making in contrast to housing the centrifuge in a pit. There are two significant explanations for this. Firstly, models need to be transported onto the centrifuge swing arm using a crane because they need to be lowered into

the pit. In addition access to the swing arm, for connecting pipes and instrumentation, is more problematic in a pit. However, the pit arrangement has been utilised successfully at other facilities (i.e. Cambridge and ETH research centres). City University London's centrifuge is situated inside a structured room to provide a safe environment, the centrifuge also in the centre of a fibre-glass clamshell which creates an aerodynamic chamber.

It is often necessary to allow overnight running of the Acutronic 661 and so the base has installed four strain gauged sensors for monitoring any out-of-balance loads. The centrifuge facility will shut down automatically if the sensors experience more than a 15kN out-of-balance load.

A stack of slip rings at the top of the Acutronic 661 supply connections of electrical and hydraulic components. 55 electrical and five, 15bar capacity, fluid slip rings are available. The remaining slip rings are used in the closed circuit television signals, supplying power for the lights or operating motors and solenoids. The fluid slip rings provide water, dense fluid (oil) or compressed air as required for each individual task.

### **5.3.2 Data Acquisition**

Permanently mounted junction boxes are used to receive signals from the instrumentation on the centrifuge swing which are then passed on to an on-board signal conditioning unit for filtering and amplification. The unit is located near the centrifuge axis within its own housing. The output from the transducers can be amplified by 1, 2, 10, 100, 500 or 1000 times depending on the individual requirements.

Data from the instrumentation on the model is sent to an on-board solid state computer via an A/D card. This is also located within the housing on the swing arm. The data is then sent via a RS232 serial link to a PC in the control room which displays the logged data.

### **5.3.3 Instrumentation and Calibration**

The main purpose of the instrumentation is to monitor the ground movements and pore-water pressures in the model. To monitor the vertical movements at the model's surface, several linearly variable differential transformers (LVDTs) were also used.



Twelve LVDTs were used with a range of  $\pm 15\text{mm}$ , with an output of  $\pm 5\text{V}$  or less at these limits. These transducers were calibrated individually within this range over 1mm steps using a screw micrometre within an instrument clamping block.

Miniature pore pressure transducers (PPTs) were used to measure the changes in pore-water pressure in the model during equalisation of pore-water pressures and during simulated tunnel constructions. These were PDCR81 miniature pressure transducers manufactured by Druck Limited, Leicester. The diaphragms of these PPTs are protected from the soil by a porous stone, glued to the instrument body. The PPTs are placed into a manifold which is then screwed into a de-airing chamber filled with distilled water and subjected to a vacuum in the order of  $-100\text{kPa}$ . This is vitally important for correct monitoring as the stones must be completely de-aired and saturated with water for correct operation. After de-airing the calibration involved applying pressure to this chamber using a Bishop ram. The transducers were calibrated against a Druck DPI101 Digital Pressure Indicator (DPI). Another two PPTs without porous stones were used in the model's standpipes to monitor the heads of water controlling the water table and tunnel pressure.

A sub-miniature flush diaphragm pressure transducer, model PX600-200GV series, supplied by Omega, Manchester, was used to measure either the air or water pressure in the tunnel apparatus. This transducer is also calibrated against the Druck DPI.

These transducers were calibrated before every test over the same range and used in the same channels and gains on the data acquisition system.

#### **5.3.4 Image Processing**

Grant (1998) was one of the first to use image processing at City University London and this system has since been used regularly to record displacement and strain data close to real time in centrifuge model testing. Primarily, the image processing was used to monitor the subsurface movements. Images for analysis were acquired, during the test, by a small charged couple device (CCD) camera that was mounted on the centrifuge swing-arm. This CCD camera was pointed at the centrifuge model through a Perspex window. Marker beads were placed into the

clay surface to allow the image processing software to track movements. For immediate viewing in the control room, signals from the CCD camera pass through the slip rings to a monitor. Images were also stored on a computer via a frame grabber.

The general theory and mathematics of close range geotechnical photogrammetry used within the custom written software is outside the scope of this thesis and, therefore, not presented. Image processing software and techniques are based on Taylor *et al.* (1998). However, a general overview of the procedure is described here.

The first stage was to record and track each target's movements in the image plane. A sequence of images was converted into a series of target positions. Specific parameters are needed in order to transfer the images from image plane to an object plane. Camera lens details (focal point and focal length etc.), camera position, camera orientation and the refractive properties of the Perspex window all need to be known. The position of the known target co-ordinates and specific known photogrammetric parameters are used to calculate the target positions (the change in movement is derived from the change in position). 'Known' co-ordinates were etched and painted black on the window side in contact with the soil model. The distortions due to the camera and the camera position have been calibrated out during the programme's computations, as has the refractive effect of the Perspex window. The vector movements can then be converted into millimetre movements in the object plane.

The analogue signal from the CCD camera passes through the slip rings and is converted to a digital image by a frame grabbing card within a PC. The target locations, calibration to co-ordinates in object space and calculations of strains were all conducted post-test. The quality of these measurements depends on the calibration and the precision to which the targets were located on the image plane. Each target has a number of pixels assigned to it. For an individual target, with dimensions of only a few millimetres across, this would take 6 or 7 pixels in the camera's view. The grey scale is applied over each target area and moving the target changes the intensity levels of the grey scale around this target. A level of tracking can be formed from this change in intensity level. With good lighting the amount of contrast over the image plan can improve the quality of the tracking.

Although in this procedure the camera position and orientation have been derived from the 'known' co-ordinates in the software, the procedures for calculating the camera position and orientation are common practice in digital photogrammetry and often require millimetre accuracy over very large areas. Grant (1998) commented that in the vertical direction the error in the target reading could have been in the order of 10-20 $\mu$ m. Although other methods are available White & Take (2002) shows the accuracy of the measurement as a whole is dependent on the resolution of the image. Therefore, different software packages should give the same movement and the same error.

## **5.4 Summary**

Outlined in this chapter was the background to the main methodology of this research. This included the fundamental principles behind the technique of geotechnical centrifuges. This was followed by a brief outline of the specific centrifuge facility available at City University London. The following sections detail the data acquisition, instrumentation and image processing capabilities of the facility. This was important because of the insight it gave to the subsequent development of new apparatus for this research.

## 6 APPARATUS DEVELOPEMENT

New apparatus was required to simulate and control two separate tunnel construction events. The apparatus necessary to perform these tasks required a significant amount of time to develop and was relatively complex. Previous approaches to centrifuge modelling of tunnelling problems, the model considerations and the arrangement of the apparatus are discussed in this chapter. A number of features of the apparatus were common to typical tunnelling centrifuge tests and are also described in this chapter.

### 6.1 Previous Approaches to Tunnelling

Modelling tunnelling procedures in clay using a geotechnical centrifuge can pose significant difficulties relating to accurate simulation of the construction process. The main difficulty is the simulation of, or actual removal of soil from the model to form the tunnel cavity. Methods have been developed by a number of research groups with varying degrees of complexity and success. A summary of physical modelling tunnelling methods reported in the literature is shown in Table 6.1.

Imamura *et al.* (1998) utilised an in-flight excavator to construct the tunnel cavity, the spoil from which was retained within the strongbox to avoid any out-of-balance loading. Whilst this approach would appear the most representative of the true construction process; the package size available at City University London would have made this type of system impractical to model. Additionally, the tests performed by Imamura *et al.* (1998) were in dry sand and therefore would not have behaved like materials analogous to London Clay.

Mair (1979) simulated volume loss in clay resulting from the overall tunnelling effects in a centrifuge. This method utilised a pressurised air-filled rubber bag within a circular tunnel cavity. This involved increasing the air pressure to equal the soil overburden in order to support the tunnel cavity during spin up and pore-water pressure equalisation and then decreasing this pressure to simulate a failure. Measurements of ground deformation correlating to particular volume losses were then made by inspection of the appropriate portion of the results set. Similarly, Wu *et al.* (1998) and Lee *et al.* (2006) used two pressurised bags at various centre-to-

centre spacings and covers in sand. The pressure within these bags was controlled during spin-up similar to the single tunnel tests by Mair (1979). However, to simulate a twin-tunnel construction the pressure within the tunnels was simultaneously reduced until collapse was observed. It may be argued that this is not a realistic interpretation of the construction process, as there was no delay between each tunnels construction where there would be in practice.

Jacobsz (2002) developed apparatus to enable modelling of small strain movements around a single tunnel in sand, close to another structure. Construction in-flight was simulated by draining water that was supporting the tunnel cavity. This allowed accurate control of the volume loss. However, Ng *et al.* (2012) described apparatus for simulating two advancing tunnel constructions in dry sand, sequentially. Each model tunnel consisted of five cylindrical rubber bags and between these was a rigid divider to control and separate the volume of water inside. This enabled the tunnel volume losses to be controlled independently. It was the approach by Jacobsz (2002) that the current twin-tunnel volume loss apparatus developed at City University London was based upon.

A considerable amount of literature relating to the ground movements around tunnels has been shown in Chapters 2 and Chapter 3 including a number of published monitored sites on ground movements associated with twin-tunnelling both at the surface and sub-surface. In order to predict these ground movements field studies, numerical analyses and physical model testing have provided the well-understood mechanisms of movement around single tunnels (Chapter 4). However, as shown above, significant insight could be gained from a physic model testing programme into ground movements around twin-tunnelling in clay. The design of a physical model and the development of the apparatus to perform these tests are detailed in the following chapters.

## **6.2 Model Design**

City University London had centrifuge apparatus capable of modelling a single tunnel collapse by the pressurised rubber bag method described by Mair (1979). This method of simulating a tunnel construction was also used by Grant (1998) with slight variations in the apparatus and

remains the usual method for conducting single tunnel centrifuge tests. Typically, models at City University London are made from kaolin clay and prepared in such a way as to have an undrained shear strength of between 35 and 55kPa (Rose, 2012; Begaj-Qerimi, 2009; McNamara, 2001; Grant 1998). The model tunnels are 50mm in diameter and usually tested at 100g. This relates, at prototype scale, to a tunnel of 5m in diameter. Grant (1998) first opted for this arrangement as it allows for up to 4D cover and a size of tunnel such that the deformations were reasonable for measurement. The tests are conducted in a plane strain configuration described in Section 6.3.2. All models detailed in this thesis consisted of a preformed circular cavities (or cavity) in overconsolidated clay. A generic schematic of the various models is shown in Figures 6.1. The function of the new apparatus was to provide support to these cavities (or cavity) during testing in a centrifuge model and allow for the simulation of the construction processes associated with volume loss. Two sets of apparatus (single tunnel and twin-tunnel) were developed for the experimental test series. The single tunnel apparatus, described in Section 6.3, was developed to prove the new system could be successful in modelling small, tunnelling-induced movements. A number of alterations are detailed, in Section 6.4 to enable twin-tunnel experimentation. The most notable difference between the sets of experiments is the change in tunnel diameter. The single tunnel apparatus has a 50mm diameter and the twin-tunnel apparatus have 40mm diameters. The reasons behind this difference in tunnel diameter are described in detail in Section 6.5.1.

## **6.3 Common Elements to All Experiments**

### **6.3.1 The soil**

This study is concerned with the fundamental mechanics of soil deformations associated with tunnelling and therefore a clay with well-established properties reconstituted from a slurry is appropriate (Mair, 1979). Speswhite kaolin clay was chosen because its engineering properties for physical modelling are well established (Grant, 1998). Viggiani & Atkinson (1995) stated that a limited investigation of London Clay showed that stiffness at small strain,  $G_0$ , was the same as for reconstituted samples at the same state. The engineering properties of Speswhite kaolin clay are presented in Table 6.2. Kaolin clay is often used for centrifuge modelling

because of its relatively high permeability and inert nature. These qualities are beneficial for relatively fast consolidation processes. The kaolin clay was supplied by Imerys', England in bagged powder form and was called Speswhite Quality China Clay.

### **6.3.2 The model container (strong-box)**

The test apparatus consists of a rectangular container referred to as a strong-box (Figure 6.2) which was first used for the purpose of centrifuge tunnelling research by Grant (1998). The strong-box contains the clay, the majority of the apparatus and all the instrumentation. The internal dimensions of the strong box are 550mm long by 200mm wide by 375mm deep which implies, at 200g, a maximum prototype scale ground volume of 110m long by 40m wide by 60m deep. The fully assembled strong-box comprises a base plate and four walls (two sides, front and back). The base plate has grooves cut to give a path for drainage (Figure 6.2) during the consolidation process using the pneumatic/hydraulic press (Figure 6.3). The front wall of the strong box can be removed and replaced with Perspex windows enabling observation of the sub-surface ground movements during testing during this experimental work. The clay would have been normally trimmed to give a C/D ratio equal to two or three. Oteo & Sagaseta (1982) suggested the wall boundaries should be 9D from the tunnel centreline in order to minimise any potential boundary effects. However, Kirmura & Mair (1981) performed a series of centrifuge tests in which the soil boundary was 3D from the tunnel centre-line. The authors concluded that their tests were sufficient in providing the detailed mechanics of a tunnel deforming under the self-weight of the surrounding soil. The strong boxes available at City University London have the boundary 5.5D from the tunnel centre-line and, therefore, it is assumed the influence of the boundaries will be minimal.

### **6.3.3 Ground water supply**

A standpipe arrangement on the centrifuge swing bed was used to set the level of the ground water table in the models during the tests (Figure 6.4). The ground water table was set to be 5mm below the surface of the clay. A second standpipe and reservoir was used to maintain the support pressure inside the tunnel and is discussed in Section 6.3.3. Water was supplied to both

stand-pipes via the fluid slip rings and the levels kept constant to a pre-determined height by overflow pipes.

#### **6.3.4 Location and fixing of instrumentation**

A rack of Linear Variable Differential Transformers (LVDTs) was bolted to the top of the strong-box for measuring vertical displacement at the surface. A row of nine LVDTs were placed across the centre-line of the sample at 0,  $\pm 45$ ,  $\pm 90$ ,  $\pm 135$  and  $\pm 180$ mm centres from the model centre-line (Figure 6.5). A second row of LVDTs at centres 0, 90 and 180 from the model centre-line, were set 45mm back from the centre-line of the sample to ascertain whether the model was behaving in plane strain. Holes are present in the back wall of the strong box for the installation of Pore Pressure Transducers (PPTs) within the clay sample and the fluid feed for the tunnels. At heights relative to the swing bed three pore-water pressure transducers were installed at 100, 120 and 220mm (Figure 6.1).

### **6.4 Single tunnel Apparatus**

The development of the single tunnel apparatus are given herein. The three main features are the Tunnel support system, Support window system and Fluid control system. These individual features were arranged on the swing as shown in Figure 6.6 for testing.

#### **6.4.1 Tunnel support system**

The tunnelling system was based on an arrangement first described by Jacobsz (2002) and is shown in Figure 6.7. The tunnelling system supports the preformed cavity during pore-water pressure equalisation and controls the magnitude of volume loss during the simulation of the tunnel construction. The cavity is supported by water (a virtually incompressible fluid) within a latex membrane. The main advantage of using water is that during ‘spin-up’ the water and soil are subjected to the same increase in g-level. The supporting water pressures within the cavities are, therefore, controlled by the standpipe at 1g and at the elevated g.

The water pressure inside the cavity is regulated by a separate system outlined in Section 6.4.3. The tunnelling system was designed to facilitate a wide range of volume losses which is



achieved by extracting a set volume of water from inside the latex membrane through a central hollow rod (described later in this Section).

In order to perform these two tasks, at the required g-level, the clay must be fully in contact with the latex membrane. In principal the cavities (or cavity) must ‘fail’ onto a fluid filled latex bag, the adequate water pressure within the bag prohibits soil movement and removal of this fluid generates the soil movement.

The depth of soil above the tunnels in the models has been determined in order to ensure the tunnels would ‘fail’ at the required g-level. The justification for this required the application of some known parameters of the soil and model dimensions to Equation (3.13). The equation below, taken from Mair (1979), has been modified to use model scale values and the gravity scaling factor,  $n$ . By using the model dimensions  $C/D=2$  and  $D=0.05\text{m}$  with the soil parameter  $\gamma=17.5\text{kN/m}^2$  it is possible to rearrange Equation (3.13) to show the conditions required for failure. However, it must be noted that the value for tunnel diameter is that of the single tunnel test.

$$N_c = \left( \frac{n\gamma(C + D/2) - \sigma_{TC}}{S_u} \right) \quad (3.12)$$

$$N_c S_u = Dn\gamma \left( \frac{C}{D} + 0.5 \right) - \sigma_{TC} \quad (6.1)$$

$$\sigma_{TC} = (100 \cdot 17.5 \cdot 0.05 \cdot 2.5) - N_c S_u \quad (6.2)$$

$$\sigma_{TC} = 218.75 - N_c S_u \quad (6.3)$$

Equation (3.12) must be used in conjunction with Figure 3.9, as described in Chapter 4, in order to obtain a value of  $N_c$ . Reading from Figure 3.9 using  $C/D=2$  and  $P/D=\infty$  gives  $N_c$  tending towards 4.  $P/D=\infty$  is used because this is a plane strain scenario. Inserting  $N_c=4$  and a suitable

value for  $S_u$  into the above derivation of Equation (3.12) means  $\sigma_{TC}$  must be greater than zero. Therefore, a positive support pressure is required to resist failure.

The framework of the tunnel system used to support the fluid filled latex bag consisted of a number of different structural elements. The system comprised two aluminium circular end pieces connected by a hollow rod acting as a mandrel. These pieces were set at either ends of the tunnel cavity. The end pieces were of 47 mm diameter and 6.5 mm thick. The diameter was chosen because the system needed to be placed within a preformed 50mm diameter cavity which utilised some of the existing apparatus for tunnel modelling. The thickness is of a size sufficient to provide for an o-ring groove around the circumference.

The end pieces secured a natural latex membrane in position (Figure 6.7, detail). The membrane was 50mm in diameter, 0.5mm in thickness and 240mm long. During the model making stage the bag was trimmed as appropriate after fitting.

The tunnelling system was sealed by placing 1¾" O.D. o-rings over the membrane at the recesses. The o-rings sat proud of the outer diameter and were clamped in place by tight fitting brass circular clasps. The clasps had an outer diameter of 49.9mm and internal diameters made to fit.

One of the end pieces was screwed onto the rod and sealed as previously outlined. The rod had a 6mm outer diameter and a 3mm internal diameter. Three 2.5mm diameter holes were drilled radially to allow for fluid flow. The opposite end piece was secured to a ¼" BSP threaded brass fitting. The fitting allowed a fluid supply through the strong box back-wall and supported the tunnelling system at one end during the testing stage. The fitting joined to the fluid controlling system (Section 6.4.3). Once assembled, the tunnel support system was filled with water prior to installation within the clay. A bleed screw, sealed with an o-ring, allowed the tunnel to be de-airing during the model making stage.

The overall length of the apparatus was 210mm as compared with the internal width of the strongbox which was 200mm. This required the end of the apparatus to sit within a recess cut into the front window of the strongbox. This feature was considered important as it ensured the

soil was solely supported by the fluid filled membrane and any observed soil movements would not be influenced by the stiff metal components.

#### **6.4.2 Support window system**

To observe the subsurface ground movement in a plane strain centrifuge model, it is usual practice to replace one wall of the strong box with a clear Perspex window. Cameras are used to record images at set intervals during the experiment and a digital image analysis system used to obtain subsurface movements (Taylor *et al.*, 1998). This process utilises a grid of reference targets etched onto the clay-facing side of the observation window.

The existing window was 83mm thick. Modifying this window to accommodate the various configurations of tunnels was considered uneconomical and therefore a second, inner Perspex window was used. This inner Perspex window was referred to as the support window (Figure 6.7). The support window is made from ½” Perspex sheet. It was positioned between the 83mm thick observation window and the strong box, clamped in position by bolts that pass through both windows. The support window had a 10mm deep circular recess for the end piece of the tunnelling system. As this was a blind recess, seepage of pore water from the model was prevented. The control targets for the image analysis were machined onto the support window using a CNC mill and their positions were therefore known to a high degree of accuracy. A test investigation any possible influence of this additional supporting window to the accuracy of sub-surface displacement measuring software is given in Chapter 8.

#### **6.4.3 Fluid control system**

The fluid control system was based on a similar arrangement described by Jacobsz (2002). The system can be divided into two parts (Figures 6.9 and 6.10) for different stages of the testing process. These parts were:

- The tunnel support pressure standpipe
- The fluid removal equipment.

The pressure within the preformed tunnel cavity was controlled by a standpipe situated on the swing-bed next to the ground water supply reservoir. The overflow was set at a level to provide

a pressure at the tunnel axis level equal to the soil overburden. In order to determine the pressure required a calculation similar to the one below must be performed.

$$\gamma \left( C + \frac{D}{2} \right) = \text{Soil overburden} \quad (6.4)$$

If  $C/D=2$ ,  $D=0.05\text{m}$ ,  $\gamma_w=9.81\text{kN/m}^2$  and  $\gamma=17.5\text{kN/m}^2$  is inserted into the above expression then,

$$17.5 \left( 2 \cdot 0.05 + \frac{0.05}{2} \right) = 2.19\text{kPa at } 1g \quad (6.5)$$

Therefore, the following expression determines the head of water required to also give a pressure of 2.19kPa.

$$\frac{2.19}{9.81} = 0.223\text{m} \quad (6.6)$$

Therefore; the overflow pipe was set at a 223mm above the tunnel axis level. The centre-line of the tunnel was 120mm from the swing-bed and therefore the total height of the overflow pipe above the swing bed should be equal to 343mm (or 120+223).

The fluid extraction system (Figure 6.10) comprised a Bishop ram driven by a 48V servo motor. The Bishop ram acted as a syringe and provided storage for fluid withdrawn from the tunnelling system. The Bishop ram was controlled remotely by the servo motor which drove a cog secured to the lead screw of the Bishop ram via a toothed bar. Use of the toothed bar accommodated the lead screw of the Bishop ram moving upwards as fluid was withdrawn. The pressure at the outlet of the Bishop ram was measured using a Druck 810 pressure transducer fitted within the outlet pipe.

The fluid controlling system was connected to the tunnelling system and the standpipe by 1/8" pipe. Stainless steel pipe was chosen because plastic or rubber tubing may have collapsed or

kinked at elevated g, impeding the flow of fluid within the apparatus. The control of the fluid in these pipes to the tunnels was achieved using in-line quarter-turn plug valves controlled by rotary solenoids. The position of the valves segregated the flow of fluid between the standpipe and the remainder of the apparatus. The plug valves were supplied by Hoke (model number 7312G2Y) and had 2.63mm diameter orifices. The solenoids were 50mm diameter 24V DC type D proportional rotary solenoids supplied by Magnet-Schultz. As the rotary solenoids were DC operated when the current was reversed it would provide a contra-rotation action and allowed an off/on action.

McNamara (2001) used this arrangement of plug valve and rotary solenoid for a similar application successfully at 100g. However, this work noted a necessary change in the operational method of the rotary solenoids because of the reduced reliability in an enhanced g field. Although the rotary solenoids were rated to 24V this did not provide sufficient torque to enable the instantaneous action required. The rotary solenoids were only operated for a short period of time and so McNamara (2001) increased the voltage to 70V to ensure the action. The same approach was adopted in the current work.

The rotary solenoid and plug valve arrangement was housed in a compact square aluminium section. The plug valve sat on top of the square section and was connected to the shaft of the rotary solenoid within the square section by a brass sleeve (Figure 6.11). The brass sleeve had sufficient clearance to allow for any out of alignment owing to the additional self-weight of the plug valve in an enhanced g field. The compact nature of this arrangement allowed it to be positioned outside of the strong box.

The completed system was calibrated prior to testing to ascertain the volume of fluid moved in a single revolution of the servo motor. This was performed by piping the outward orifice of the Bishop Ram to a burette and then requesting a series of single revolutions of the motor. One revolution was determined to withdraw 1.08 ml. The calibration of the fluid removal equipment is presented in Appendix A. A sample calculation of the volume of fluid to be removed for a single tunnel model is featured below. The calculation is based on the model being 200mm in length with a cavity of 50mm diameter along this entire length.

$$\frac{\pi}{4}D^2 \cdot l \quad (6.7)$$

$$392.5 \times 0.03 = 11.78ml \quad (6.8)$$

3% of the total volume of this cavity was calculated and requested for removal to simulate a tunnel construction equal to a 3% volume loss.

$$\frac{\pi}{4}5^2 \cdot 20 = 392.5ml \quad (6.9)$$

## 6.5 Twin-Tunnel Apparatus

The development of the twin-tunnel models involved a number of modifications to the above described apparatus. Figure 6.12 illustrates the layout of the modified apparatus for controlling individual tunnels. The overall concept for the system was identical (i.e. fluid support that could be removed to simulate volume loss) and each part performed similar functions to those previously discussed. Modifications were applied to three key elements in order to facilitate twin-tunnelling in parallel and offset arrangements.

### 6.5.1 Twin-tunnel system

As well as the obvious need to have two tunnel systems a number of other modifications were made to the previously described design. Principally, the outer diameter of the tunnels was changed to 40mm, however, structurally the tunnel support system is as shown in Figure 6.7. This change was to ensure the observed movements were not affected by boundary conditions due to the restricted size of the strong box.

If the diameter was too small then a higher g-level would have been required to reach a prototype scale where the tunnel would be analogous to an underground railway line. In addition smaller tunnels are relatively more difficult to prepare during the model making stage. Therefore, a similar justification to the boundary conditions of the single tunnel (Section 6.3.2) was required for the twin-tunnel model. In Chapter 3 it was stated that the surface settlement

trough could be best described as a Gaussian distribution curve. The maximum reach of a settlement trough at the surface is  $3i$  on each side of a tunnels centre-line. If the twin-tunnel model parameters ( $C/D=2$  and  $D=0.04m$ ) are applied to Equation (4.6) an indication of the possible maximum extent of settlements can be determined:

$$i = K \cdot z_0 \quad (4.6)$$

$$i = 0.5 \cdot 0.1 = 0.05 \quad (6.10)$$

$$3i = 6 \cdot 0.05 = 0.15m \quad (6.11)$$

The internal width of the strong box is equal to 550mm, therefore, the maximum distance between the tunnels centre-lines are:

$$550 - (2 \cdot 3i) = 250mm \quad (6.12)$$

$$\frac{250}{40} = 6.25D \quad (6.13)$$

Hence, for this case, the strong box can cater for spacings smaller than  $6.25D$  when the tunnel diameters are 40mm. The maximum spacing tested was 4.5 times the diameter and the extent of the settlement troughs are not well below that predicted to reach the side walls of the strong box.

The two end pieces for each tunnel are of a similar design to that described in Section 6.4.1 for a single tunnel but with an outside diameter of 37mm. Once again a latex membrane was secured at either end with an o-ring and brass clasp. Additionally, the centre support rod was extended by another 10mm to give an overall length equal to 220mm. Combined with a recess machined into the rear face of the strong box this modification avoided the soil being in contact with

anything except the latex membrane. This was designed to completely remove any influence of the rigid components on the soil movements.

Finally, the same verification procedures applied to the single tunnel arrangement were repeated for the twin-tunnel arrangements as shown in Section 6.4.1. The 40mm diameter modified Equation (3.13) to give  $\sigma_{TC}=174.4 - N_c S_u$ . A tunnel pressure would still, therefore, be required when applying the same soil conditions as in the single tunnel case. A new height of standpipe also needed to be calculated as shown in Section 6.4.2. The new diameter meant a soil overburden of 1.75kPa at 1g needed to be supported by the tunnelling support apparatus. This was equal to 178.4mm of hydrostatic head above the tunnel axis level or a total height of 298.4mm (or 120+178.4). The different tunnel diameter also requires a different amount of fluid to be removed from within the tunnel support apparatus. The calculation from Section 6.4.3 was repeated and shows that to achieve a 3% volume loss the tunnel support apparatus would need to remove 7.54ml of water.

### **6.5.2 Twin-Tunnel support window system**

A number of twin-tunnel support Perspex windows were fabricated. The new windows had external dimensions equal to the first (Figure 6.13). This was fixed to the strong box with the same pattern of bolt holes as described in Section 6.2.2. In total five twin-tunnel windows were fabricated for three parallel arrangements (1.5D, 3D and 4.5D) and two offset arrangements (2.12D and 2.7D).

### **6.5.3 Twin-tunnel back-wall/plug system**

A modified strong box back-wall was designed to support the tunnel apparatus. The strong box's rear wall was fabricated from 1" thick aluminium plate. The new back-wall was designed as a direct replacement for the existing wall and contained an insert to allow for variations in the centre-to-centre tunnel spacing (Figure 6.14). A series of bolts secured this insert within the modified strong box back-wall and sealed against an o-ring. The system was observed to have worked effectively in ensuring no water leaked from the model because no material could be witnessed on the swing bed post-test. This arrangement was beneficial as it allowed different



inserts to be manufactured rather a series of replacement walls for the strong box. The insert is of a size that can allow variation in tunnel centre-to-centre spacing.

A third circular recess was built into the back-wall to allow for the offset twin-tunnel arrangement testing. This recess was identical to those in the plug however was offset 60mm directly above the right-hand recess (Figure 6.15). A fitting, shown in Figure 6.15, was also manufactured to fully seal the recess when not being used during testing. The plugs from the parallel test could be reused in order to give three offset arrangements.

## **6.6 Summary**

This chapter detailed the elements of the centrifuge testing apparatus specifically developed for this research study. This was first achieved by outlining existing tunnel research techniques, apparatus (this is referred to as the common features) and then the requirements of any new apparatus. The new apparatus had to be developed by first the introduction of a prototype single tunnel apparatus system and then the adaptations for twin-tunnel testing. In addition, example calculations are included with detailed figures to fully illustrate how the novel apparatus works.

## **7 EXPERIMENTAL TEST SERIES**

### **7.1 Experimental Procedure**

The preparation of each centrifuge experiment was extremely complicated and required a number of stages. This section describes the preparation of models, the individual stages of testing during a single tunnel experiment and during the sequential tunnel experiments.

#### **7.1.1 Preparation of the clay in the model**

Speswhite kaolin clay powder was mixed with distilled water to produce slurry with a water content of 120% in an industrial ribbon blade mixer. Mair (1979) first used Speswhite kaolin clay slurry at this water content because it is twice the liquid limit and had similar undrained shear strength as Spestone kaolin clay powder mixed to 160%. The Spestone slurry was replaced with Speswhite because of the limited availability of the material. The reason for pouring the slurries at these water contents is because it minimises trapped air pockets during pouring.

Prior to placing the slurry within the strong-box the walls were lightly coated with grease to minimise wall friction in the finished sample. Mair (1979) stated for a 300mm high sample, up to 10% of the vertical stress was lost owing to wall friction. However, and was improved by the use of water-pump grease. A sheet of porous plastic was placed at the bottom of the strong box underneath a sheet of filter paper. The clay slurry was placed within the strong box to a sufficient depth dependent on the test. The amount of slurry was calculated to give a finished sample height 10-20mm more than required. Care was taken to prevent the entrapment of air bubbles within the clay slurry during pouring. Finally, a sheet of filter paper was placed on top of the slurry followed by a sheet of porous plastic.

To consolidate the clay slurry a loading platen, attached to a computer controlled pneumatic/hydraulic press was used to apply the pressure required in pre-determined stages (Figure 7.1). Drainage was allowed via three drainage holes in the platen at the top and taps screwed into the bottom plate of the strong box. Initially, the press was set to apply 10kPa

overnight. This was increased to 50kPa the next morning and 100kPa in the afternoon. At similar times the following day the applied pressure was increase to 250kPa and 500kPa. This pressure was held for three days and swelled back to 250kPa on the fourth. The same press and routine was used for consolidating all samples to ensure consistency.

### **7.1.2 Preparation of the model**

The pore-water pressures in the clay sample during in flight consolidation and testing were monitored by Druck pore pressure transducers (PPTs). These were installed during the swelling stage under the consolidation press. The PPTs were installed through holes in the strong box back wall. A specially fabricated guide was screwed into the hole and a hypodermic tube was used to remove a clay core half the model width (100mm). Once the PPTs were placed into the model, the cavity was back filled with de-aired clay slurry to a water content of 120% and a special fitting installed to seal round the wire as it exited.

Before the model could be removed from the consolidation press the water from above the platen was removed and the drainage taps disconnected. After the sample was removed it was imperative to ensure it did not dry out. Usual practice was to seal the exposed surfaces of the clay before and during model making as quickly as possible with silicone oil.

The front-wall of the strong box was removed to gain access to the front clay surface. A specially fabricated jig was clamped to the front of the strong box (Figure 7.2) and a sharpened aluminium box cutter used to trim excess clay from the surface. To bore the tunnels a frame was fitted to the front of the strong box (Figure 7.3) and corresponding plugged holes in the back wall removed. During twin-tunnel model preparation the cutter guide could be slid along the frame to the required horizontal position allowing accurate boring of the tunnel cavities. Stops on the frame allowed the guide to be repeatedly set to the same position. A 50mm outer diameter circular stainless steel seamless tube cutter was used during the single tunnel experiments and a 40mm outer diameter cutter was used during the twin-tunnel experiments. The clay from inside the cavities remained inside the tunnel cutters for easy removal from the model. Once the tunnels were bored another jig was clamped to the front of the strong box so that image analysis target beads could be pressed into the front surface of the clay. The jig

enabled the targets be accurately and effectively positioned in a 10x10mm grid in the face. At this stage the preparation of the clay model was complete.

The tunnel apparatus was placed inside the tunnel cavity/cavities. Every precaution was taken to bleed the air out of the tunnel systems before placement. This was carried out by partially filling the membranes with water. If the tunnel systems were completely filled it became very difficult to slide them inside the cavities. Screwed to the back of the tunnel apparatus were fittings allowing for fluid in-feed. These fittings also contained pressure transducers to monitor the internal tunnel pressures at the centre-line. The tunnel system was secured to the strong-box by large nuts (see Figure 7.4).

Prior to being bolted in place, the support window was lubricated with a high viscosity, clear silicone oil to reduce interface friction. The support and observation windows were placed carefully onto the front of the strong box. The fluid controlling apparatus could be placed onto the side and bolted securely through the windows. The piping was connected and de-aired. The tunnel membranes were de-aired by allowing water through the ¼”BSP fitting and allowing trapped air to exit through a bleed valve in the aluminium circular end piece. Finally, the tunnel membranes were topped-up with water so that they completely filled the cavity/cavities. This was carried out using a syringe attached to an outlet of the Bishop ram. This was to ensure that the tunnel membranes were in contact with the walls of the cavities and that there was no air in the connecting pipes. This was performed, primarily, to be certain the tunnels are 40mm in diameter. If this is not done the reliance of the apparatus is placed on the tunnels being filled with water from the standpipe faster than the soil can swell during the pore-water equalisation. Since the piping was 1/16” ID this was considered unlikely. In addition, any trapped air between the membranes and the cavities could affect the performance of the apparatus. This is because the air would have to be squeezed out during the in-flight consolidation. If the bag is not fully in contact with the membrane the air may be supporting the soil and not the fluid support.

The rack containing the Linear Variable Differential Transformers (LVDTs) was bolted to the top of the strong box to measure vertical surface settlement. The model was then weighed and

placed on the swing bed. The final tasks were the positioning of stand-pipes for the water feeds, installation of a PPT in the aquifer stand-pipe, positioning of the CCD cameras and lighting, checks of the signal amplification gains, positioning of the LVDTs to their electrical zero, connections of all the power supplies, solenoid valves and transducers to the junctions boxes, connection of the fluid supplies to the stand-pipes and strapping down the various cables around the model.

450ml of silicone oil was poured onto the top surface to prevent evaporation of pore water from the clay during the experiment. This quantity of silicon oil would be distributed over the plan area of the model (550x200mm) and have a uniform depth of 4mm at 1g. However, in flight the radial gravity force would create a curved surface which would have a minimum depth of 0.5-1mm at the centre-line. This overburden would therefore be negligible.

When the balance calculation, counter-weight positioning, water supply initiated and final checks made the centrifuge was started.

To support the cavity during spin-up the tunnels support pressure was supplied by the tunnel standpipe and, therefore did not need to be regulated manually. When the model reached 100g the pressurised tunnels were isolated from the standpipe using the plug valve and left, at least overnight, for the pore-water pressures within the soil to reach equilibrium with the standpipe. The tunnel excavation simulations were not started until the model had reached this stage. The full test procedure is outlined in further sections. From when the model left the consolidation press the model making procedure took approximately 4 hours and a further hour once on the swing-bed.

### **7.1.3 Centrifuge Test Procedures**

#### ***7.1.3.1 Testing for simulated single tunnel excavation (Apparatus A)***

Before the tunnel construction was simulated the data logger and image capture sequence was set to record at approximately one reading per second. Once a number of reference readings were taken the test could begin. To simulate a tunnel construction fluid was drained from within the cavity using the fluid control equipment. 3% of the total volume of the cavity was

removed. In order to achieve 3% volume loss for a single tunnel with a 50mm diameter; 7.54ml had to be removed which took approximately one minute. The centrifuge was usually run for at least an hour post-test to allow for any longer term movements to develop.

#### ***7.1.3.2 Testing for simulated sequential tunnel excavations (Apparatus B)***

As in the single tunnel tests, before any tunnel constructions were simulated, the data logger and image capture sequence was set to record at approximately one reading per second. The valve to the second tunnel (Tunnel B) was closed allowing the first tunnel (Tunnel A) to be solely controlled by the fluid controlling system. 3 or 5% of the total volume of the cavities were removed in the twin-tunnel tests. Water was drained from Tunnel A to simulate a tunnel construction. Once the toothed bar had finished rotating the valve connected to Tunnel A was closed and a time period representing a construction delay was observed.

Addenbrooke & Potts (2001) specifically addressed the effect construction delays had on their twin-tunnel settlement data. Two construction delays, called ‘rest periods’ in the work, were explored in this numerical study; 7 months and 3 weeks. Addenbrooke & Potts (2001) compared these two construction delays with the field study settlement data for Regents Park, London which had a 2 – 6 weeks construction delay. The average scatter from this surface field data was found to be in good agreement with the 3 week numerical study construction delay. The field settlement data in Barlett & Bubbers (1970) was observed after a construction delay of 2 weeks. The times in these two studies were used to determine an appropriate construction delay to adhere to during the centrifuge twin-tunnelling tests.

A construction delay to be used during the centrifuge test series was calculated using the consolidation related scaling laws (see below) and using the parameters of  $n=100$ ,  $C_v = 0.18\text{mm}^2/\text{sec}$  or  $648\text{mm}^2/\text{hour}$  (for Kaolin clay) and 3 weeks = 504 hours.

$$t_m = t_p \cdot \frac{1}{n^2} \cdot \frac{C_{vp}}{C_{vm}} \quad (5.9)$$

$$t_m = 504 \cdot \frac{1}{100^2} = 0.0504hrs \quad (7.1)$$

Equation (5.13) indicates a seepage time of 0.0504 hours or 3 minutes. Therefore, 3 weeks consolidation at prototype scale in the centrifuge (at 100g) can be represented by 3 minutes.

When the simulation of Tunnel B was required, the valve to Tunnel B was opened and the fluid draining was initiated simultaneously. In every test the same amount of fluid was requested from both tunnels. Once the fluid was drained the valve was closed and the centrifuge was left to run to allow for any longer term movements to develop.

## 7.2 Tests Undertaken

The key aim of the research was to investigate the surface, sub-surface movements and tunnel stability of twin bored tunnel constructions in stiff clay. The main variables were the lateral and vertical spacing of the tunnels. Table 7.1 presents a summary of the eighteen centrifuge tests. The tests are split into three categories; single tunnel, development and twin-tunnel experimentation.

The first two tests were of a preliminary nature and designed to gain experience with using the apparatus. These were single tunnel tests at different C/D ratios. Although these were preliminary tests, where the support pressure was air and taken to collapse, useful data was obtained for comparison. The following two tests were repeats of the first but with water as the supporting fluid. However, the test SD4 failed due to the latex membrane not sealing correctly. These four tests were to examine the success of the new modelling techniques to City University London.

Tests SD5 - SD9 were carried out to develop the twin-tunnel apparatus. All of these tests had a spacing of 1.5D but varied in their stress histories. In tests SD7 and SD8 the pre-flight consolidation pressure was only 350kPa (and swelled to 250kPa). This was to increase the rate of testing in order to increase the rate of apparatus development. During the testing of SD5 air

bubbles were observed being squeezed from within the tunnel cavities. To address this issue the tunnel cavities, prior to spinning-up, were completely filled with water using a syringe as explained in Section 7.1.2.

Tests after and including SD6 had rectangular pads instead of circular attached to the legs of the LVDTs to improve the monitoring ability of the LVDTs and, therefore, improve the surface data recorded. In order to ensure that the cores of the LVDTs do not punch through the surface of the clay they were originally equipped with a small circular plastic footing to distribute the load. It was noted upon completion of the experiments up to SD5 that these feet were of a size that could reduce the accuracy of the data especially in areas where the clay surface was sloping (Figure 7.5). To reduce this potential inaccuracy, the circular footings attached to the LVDT rods were changed to a rectangular shape. This shape was beneficial because in regions of maximum curvature (i.e.  $\pm 45\text{mm}$  from the tunnel centre-line) the narrowest side of the rectangle spread over a smaller region of settlement trough (see Figure 7.5).

In tests SD7 and SD8 the rotary solenoids were unable to operate. It was discovered subsequent to the tests that this was because of the orientation of the rotary solenoids on the swing. The direction of the elevated  $g$  prohibited the shaft from turning. Therefore, the rotary solenoids were repositioned so the shaft was facing vertically instead of horizontally.

Tests SD10 – SD12 were conducted for a volume loss of 3% with similar stress history and C/D. Three centre-to-centre parallel tunnel spacings were investigated. These were 1.5D, 3D and 4.5D. These geometries were then repeated for a volume loss of 5% in order to verify the patterns of movements as a result of tunnel spacing (SD13 – SD15). Tests SD17 and SD18 were offset arrangement tests and therefore had lateral centre-to-centre spacings of 1.5D and 2.25D and all were offset vertically by 1.5D.

### **7.3 Summary**

The purpose of Chapter 7 was to give full details of the methodology to the centrifuge experimentation. Full details of model preparation, model making and the testing procedure are



described. The second section of this chapter briefly an outline of each test performed which includes details of purpose, geometry, stress history and problems associated with each test.

## 8 CENTRIFUGE MODEL TEST RESULTS

This chapter presents key data obtained from the experimental work. Two separate stages of testing were carried out, namely, a series of tests to commission and validate the performance of the newly developed apparatus and a series of tests addressing the twin-tunnelling problem. Example data are presented to illustrate typical features of each test series. This chapter also describes the methods adopted for analysing the test data as well as discussion of how any associated difficulties were overcome. The key observations, from both the single and twin tunnel experiments, are discussed in terms of the key tunnelling parameters identified in Chapter 4. These are generally  $i$  or  $K$  (settlement trough width),  $S_{\max}$  (maximum vertical displacement) and  $V_L$  (volume loss).

### 8.1 Single Tunnel Apparatus Results

It was considered important to assess the effectiveness of the newly developed single tunnel apparatus (described in Chapter 6). The effectiveness of the apparatus and the validity of the results were assessed by comparison with results obtained from a more traditional arrangement of an air supported cavity taken to collapse. Two tests were carried out (SD2 and SD3) where the support fluid for the tunnel cavity was air and water respectively. Results from these two tests were then compared with each other and against published material. Surface settlement displacements were obtained from the LVDTs which could be correlated with displacements obtained from digital image analysis. The image analysis data also allowed measurement of the sub-surface movements. Finally, it was possible to measure the tunnel support pressure (whether air or water supported) via pressure transducers at the axis level.

#### 8.1.1 Surface settlements

Figure 8.1 shows the development of the surface settlement immediately above the tunnel crown with the reduction of pressure within the tunnel. It can be observed that the settlement generated when using the water supported cavity (SD3) develops at approximately twice the rate of the air supported test (SD2) with respect to tunnel support pressure. This was due to the speed set by the volume apparatus motor to ensure the simulated tunnel construction was

undrained. The maximum settlement in SD3 reaches a plateau and remains constant as the tunnel pressure equalises. The plateau indicates the point in the experiment where the anticipated 3% volume loss has been reached. This was different from the air test where the data was selected based on one point in time.

Figure 8.2 plots the surface settlement profile as measured by the LVDTs from tests SD2 and SD3. Settlements are plotted about the tunnel centre-line. Because of the different support fluids in these tests the methods of tunnel simulation differ significantly. In the case of air support (SD2) the tunnel pressure was reduced at a constant rate until collapse. In the case of water support (SD3) the volume loss required was extracted from the tunnel over a set period of time. As a result of this differing approach the settlement data presented were obtained using different methods. In both tests baseline readings were taken immediately prior to tunnel construction simulation (i.e. after the pore pressures have equalised on the centrifuge). In test SD3 the settlement data presented are simply the movements observed upon completion of the extraction of 3% of the volume of water in the tunnel. In the case of test SD2 the results are analysed by calculating the area of the surface settlement trough for each set of measurements using Simpson's Rule. The settlement data presented are therefore those corresponding with 3% volume loss measured at the surface. A similar calculation of the area of the surface settlement trough generated by test SD3 was also 3% and therefore the settlement data are considered comparable.

The maximum settlements measured at the tunnel centre-line varied between tests by  $50\mu\text{m}$  (a percentage difference of around 14% of the average  $S_{\text{max}}$ ). The remainder of the measurements showed closer correlation with the average difference between the tests being 1%. Figure 8.2 also shows the measurements from the second rows of LVDTs (not on the centre-line of the model) which are labelled '2D Check'. The purpose of the additional LVDTs is to ascertain whether the model is behaving in plane strain. Quantifying the comparisons between sets of data was conducted using the nonlinear regression method (similar to the method described in Jones & Clayton, 2012) varying  $V_L$ ,  $K$  and the position of  $S_{\text{max}}$  to find the minimum value of the sum of the residuals squared. This assumes that both data sets contain corresponding points

which in the case of the LVDT measurements is true. A value of zero would indicate that the two data sets were identical and therefore higher values indicate lesser agreement. The sum of the residuals squared will be referred to here as the Correlation factor.

To ascertain whether the models are behaving in plane strain the centre-line and '2D Check' displacements were compared using the nonlinear regression method. These data sets had Correlation factors of 0.07 and 0.01, respectively. The 0.01 value is due to the centre-line reading being used for both the 2D check and model centre-line data. It was decided that the maximum permissible value for the Correlation Factor was 0.1 when comparing any two data sets. Therefore, the models were behaving 2-dimensionally. This method was conducted again for the sets of discrete points across the centre-line in SD2 and SD3. The Correlation factor between these data sets was 0.07 and considered to be in good agreement. It could be assumed that the movements generated by using air or water were similar.

A Gaussian curve can be fitted to data utilising the difference squared method. The only variables are the point of inflexion and the maximum settlement and these can be changed to give mathematically the best fitting curve (i.e. variables that give a Correlation factor closest to zero). Figure 8.3 has the settlement data and the individual fitted curves normalised against tunnel diameter for clarity. Gaussian curves fitted to each test showed the points of inflexion varied by 4.8mm. This was 7.3% of the average distance to the point of inflexion. The Correlation factor between the curves and the data from SD2 and SD3 were 0.05 and 0.04 respectively. Again, these were considered well-fitting curves as the Correlation factors were less than 0.1.

The key parameters from SD2 and SD3 can be found in Table 8.1. Figure 8.4 is the surface vertical displacements in SD3 ( $S_{\max} = -341\mu\text{m}$ ,  $K = 0.542$  and a volume loss of 3%) and various estimation methods. Mair & Taylor (1997) contains a database of tunnelling induced settlement parameters. Figure 3.5 provides typical values of  $i$  or  $K$  at the surface. Tunnelling through clay typically gives values of  $K$  between 0.4 and 0.6. Prediction methods regularly take a conservative 0.5 and, therefore,  $K = 0.542$  was deemed acceptable. The Gaussian curve of SD3 data agreed most favourably with Mair *et al.* (1981) in magnitude and shape due to the lowest

Correlation factor value at 0.04. The other prediction methods were at or higher than the 0.1 benchmark (i.e. Loganathan & Poulos (1998) and Verruijt & Booker (1996) showed a 0.1 correlation but Clough & Schmidt (1981) showed a 0.13 match).

These analyses depend on the accuracy of the instrumentation used. The LVDTs signals were sent to an on-board solid state computer via an A/D card and this system used  $2^{16}$  bits to read 10V of signal. An example of an LVDT calibration shows 3.42mm of movement is equal to 1V. Hence, 1V is equal to 6553.6bits and 1bit is equal to  $5.21 \times 10^{-4}$ mm or 0.5 $\mu$ m. The accuracy of the LVDTs could be in the range of  $\pm 0.25\mu$ m. Since the smallest recorded vertical settlements are approximately 20 $\mu$ m the LVDTs are suitable for this application.

In summary, the surface settlements as a result of movements stimulated around the tunnel by the apparatus were similar to an air supported tunnel experiment taken to collapse. The settlements controlled by the volume loss apparatus were similar to those documented in published material. These have been quantified by the Correlation factors and were considered to be well represented because all are below 0.1.

### **8.1.2 Sub-surface settlement**

As previously detailed it is possible to monitor sub-surface movements using digital image analysis software. Images taken during the experiment are processed to firstly give movements in terms of pixels which are transformed using photogrammetry techniques into real space measurements. The software VisiMET was used to perform this task (Taylor *et al.*, 1998) and the resulting patterns of movements were plotted as contours using the commercial package Surfer. Comparisons are then drawn against published material.

Figure 8.5 shows a typical image taken during an experiment. The significant features are the tunnel apparatus, marker beads (embedded within the clay) and control targets etched into the window and with known-coordinates. The control targets are circled in the figure for identification. The front circular plate of the tunnel apparatus can be seen in the window recess. Once a sequence of images has been processed vector plots of pixel movement can be generated. Figure 8.6 displays the ground movements presented as vectors in SD2 and SD3 for

every marker bead at a time when the LVDTs recorded a 3% volume loss. In this figure there are two scales featured at the top of each test. The first scale is for the model. This is the distance between the starting positions of the targets (given as crosses). The second scale displayed is for displacements (shown as lines) which have been exaggerated. It may be noted that the overall pattern of movements is as expected (i.e. the soil move towards the tunnel with maximum deformations being above the tunnel centreline) but there are the occasional random or misdirected vectors. These are caused by slight fluctuations in the lighting levels or partial obscuring of the markers.

Figures 8.7 and 8.8 are contoured plots (using Surfer) of the vertical displacement data from Figure 8.6. The contours have been shown within the surrounding soil mass for clarity and at an exaggerated scale. In addition to the boundary of the soil mass the boundary for the tunnel lining is also indicated. In these figures the vector focus points described in Mair *et al.* (1993) and Grant (1998) are overlain to highlight the direction of movements or the possible position of the points of inflexion with depth. Overall the distribution of the contoured movements in SD2 and SD3 show a similar pattern. The reason for the slight differences is owing to the varied supporting fluid used. In SD2 the construction was simulated by a reduction in pressure and produced more radial ground movements towards the cavity. However, in SD3 the self-weight of the water meant that larger movements occurred at the tunnel crown (evident in Figure 8.8) and restricted the movement at the invert. In SD2 largely all the movements can be observed just within the dashed line of Mair *et al.* (1993) and larger movements within the points of inflexion dashed line from Grant (1998). Whereas, in SD3, although the larger movements are within the lines by Grant (1998) the extent of movements are much less than described those lines described by Mair *et al.* (1993). These figures show that the change in supporting fluid has still generated sub-surface ground movements of a similar shape to those documented in previous work.

The movements observed by the CCD cameras, however, were less than anticipated. Mair *et al.* (1993), illustrated by Figure 3.6, demonstrated that the Gaussian distribution curves representing horizons of soil displacement are larger and narrower with depth. The movements

by the marker beads closest to the surface (near-surface) should be marginally larger than those measured by the LVDTs. Therefore, to establish confidence in the processing capability of the image analysis system, a calibration test was devised. This test would clarify two matters; whether the introduction of the additional (tunnel supporting) Perspex window had affected the system's ability to measure settlements (due to added refraction) and whether the software was capable of accurately tracking a known displacement. The two Perspex windows were placed on the swing-bed at the correct distance from the CCD camera (i.e. in the position they would be in during the tunnelling experiments). A sheet of paper was attached to the rear of the window in order to provide contrast for the control targets. This sheet had a square hole cut into it large enough for a two by two grid of targets. These targets were printed on a smaller sheet of paper and glued to a rigid stand which rested on a micrometer controlled bed. By this arrangement it was possible to move the small group of four targets by known, precise amounts. Images were captured whilst the targets were moved from 0 to 500 $\mu$ m in 100 $\mu$ m steps. These images were analysed by VisiMET and at each step the measured average displacement of the four targets was correctly recorded to within  $\pm 5\mu$ m (Figure 8.9). By this method the accuracy of the image analysis software was verified as well as eliminating an influence of the additional thickness of Perspex. However, Figure 8.10 shows the level of noise between images of apparent no movement. This essentially was the vector plots of the marker beads from a collection of images before the start of the tunnel construction. The movements have been magnified by 500 times. The noise is spatially random with the odd row of horizontal movement due to "horizontal line jitter" which Grant (1998) states were due to the camera electronics. For the most part, the level of noise is approximately  $\pm 20\mu$ m. Assuming  $n=100$ ,  $\pm 20\mu$ m at model scale would be equal to  $\pm 2$ mm at prototype scale. This is far below 10% of the maximum settlement expected during twin-tunnelling and therefore considered acceptable. Based on this the sub-surface settlements monitored using VisiMET during the tunnelling tests were considered a relatively accurate reflection of the behaviour. Further investigation into the reasons for the apparent discrepancy between surface and sub-surface movements were required.

Grant (1998) determined that the movements measured from image analysis were less than expected because of the friction between the window and the clay/marker beads. This work noted that the image analysis displacements were, after a certain magnitude, around 100µm lower than the corresponding LVDT value due to a 'stick-slip' mechanism at the window. Analysis conducted by Grant (1998) shows that once the marker beads began to move they did so at the same rate as the LVDTs. Therefore, Grant (1998) focused on the patterns of sub-surface movement and not the magnitude of the ground movements. However, to account for the window friction Grant (1998) modified the vertical displacements recorded by the image analysis by increasing their magnitude by 100µm over a distance of  $\pm 2i$  from the tunnel centre-line and normalising the vertical settlement against the maximum settlement.

Figure 8.11 shows the vertical settlement measured by an LVDT and a near-surface marker bead above the tunnel centre-line in tests SD2 and SD3. It can be seen that for a given event (i.e. the fluid removal was completed) both the LVDT and the image analysis system show a response at the same time but the magnitudes differ. The behaviour in test SD2 shows the near-surface data acting in what might be considered as 'stick-slip' behaviour particularly at larger values of settlement. In test SD3, the displacements measured by both systems respond to the removal of fluid from inside the tunnel cavity at the same time. The test was essentially displacement controlled because this amount of fluid was requested. Therefore, the quantification of this error was considered achievable from further analysis of the data from SD3. It was assumed that similar errors would exist in each test and consequently the remaining analysis focused on the water supported test, SD3.

Figure 8.12 has used the method by Grant (1998) for quantifying the influence of the friction for SD3 sub-surface displacement data. For each LVDT reading at the surface, the near-surface movements underneath was determined. These points were plotted in the space: image analysis against LVDT settlement. If the two readings were equal they would describe a line of gradient equal to one. As the readings in tests SD2 and SD3 do not a different description was required. The 'best fit' line for this data was a squared function and the conversion between the two sets



of displacements. An equation could then be determined which corrects the sub-surface data to account for the friction and is defined as;

$$S_{z(mod)} = \frac{-0.094 + \sqrt{0.094^2 + 2.784 \cdot S_z}}{1.392} \quad (8.1)$$

where  $S_z$  is the sub-surface vertical settlement from image analysis and

$S_{z(mod)}$  is the modified sub-surface vertical settlement.

Once Equation 8.1 had been applied to the sub-surface displacement data a Gaussian curve could be fitted to the modified sub-surface data utilising the difference squared method. These curves, similar to the surface data, would mathematically be the best fitting possible. The subsequent correlation factors were calculated over the same horizontal distances from the centre-line as Grant (1998) which was  $x = \pm 2i$ . Grant (1998) also stated that without this adjustment the distances to the point of inflexion would have been much narrower than expected. Therefore, this step is needed in order for the data to be compared with published material.

Figures 8.13a, Figure 8.13b and Figure 8.13c show three depths of settlement from test SD3. Figure 8.13a shows the near-surface vertical displacement in SD3 against settlement estimation methods for a depth of 2mm. The Gaussian fit ( $S_{max} = -354\mu m$  and  $K = 0.492$ ) agrees most favourably with Mair *et al.* (1993) with a Correlation factor of 0.04 whereas Loganathan & Poulos (1998) was 0.11 matching. Figure 8.13b shows the vertical settlement for a horizon one diameter from the surface. The Gaussian fit ( $S_{max} = -430\mu m$  and  $K = 0.671$ ) to this sub-surface data again agrees more favourably with Mair *et al.* (1993) with a correlation factor of 0.1. Finally, at 1.5 diameters depth from the surface (Figure 8.13c) the Gaussian fit ( $S_{max} = -541\mu m$  and  $K = 0.799$ ) has a correlation factor of 0.09 with Mair *et al.* (1993) compared with 0.22 for Loganathan & Poulos (1998).

In summary, a description of how the overall patterns of sub-surface movement during tests SD2 and SD3 were obtained was shown. The magnitudes of the displacement were shown to be affected by friction at the window as the '2D Check' LVDTs were consistent with the row of

LVDTs at the centre-line of the model. Although the rest of this study will describe sub-surface movements in terms of relative patterns of movement, useful parameters of the settlements trough can be determined by taking into account the window friction.

### 8.1.3 Tunnel support pressure

Figure 8.14 shows the history of the tunnel pressure and pore pressure transducers during simulated tunnel excavations. SD2 and SD3 show a reduction in pressure following the simulated construction before pore-water pressures begin to equalise. This was due to the constant water supplied by the standpipe to maintain the water table at the surface level.

The values of time (on the x-axis) are set from the start of the reduction of air pressure or start of the fluid removal. The behaviour of the water pressure data (SD3) was completely different to a 'typical' air supported tunnel (SD2). This was because the pressure in an air supported cavity is controlled and thus will show a linear reduction in pressure. However, in SD3 the pressure was only measured and a result of the change in volume. The difference in pressure change has previously been directly related to the observed magnitude of movement at the face. This could be further investigated using the empirical relationship described by Macklin (1999) and substituting the parameters from test SD3. The expression featured in this work aimed to predict the volume loss around single tunnels in overconsolidated clay. As stated in Chapter 4 the relationship was formulated after collating many recorded volume losses and their corresponding load factors.

This was conducted by first calculating the stability ratio of the tunnel in SD3 and the load factor using the equations below;

$$N = \left( \frac{\sigma_s + \gamma(C + D/2) - \sigma_T}{S_u} \right) \quad (3.12)$$

The tunnel pressure used was the lowest recorded value during the fluid removal (98.2kPa) and the value of  $S_u$  was recorded post-test by shear vane (51.6kPa). The vertical stress above the tunnel was calculated using the depth to the tunnel axis level (also where the shear vane reading was taken) and the unit weight of soil (taken from Grant, 1998) equal to 17.5kN/m<sup>3</sup>.

$$N = \left( \frac{0 + 17.5(10 + 5/2) - 218.75}{51.6} \right) \quad (8.2)$$

Therefore,  $N = 2.3$ . This value is divided by  $N_c = 4$  using Equation (4.1) to obtain the load factor (LF) as shown below;

$$LF = \frac{N}{N_c} \quad (4.1)$$

$$LF = \frac{2.3}{4} \quad (8.3)$$

The load factor is therefore equal to 0.584 and satisfies the condition  $LF \geq 0.2$ . The empirical relationship by Macklin (1999) could then be used to predict a volume loss equal to 3% as shown below;

$$V_L(\%) = 0.23e^{4.4(LF)} \text{ for } LF \geq 0.2 \quad (4.2)$$

$$V_L(\%) = 0.23e^{4.4(0.584)} = 3.006\% \quad (8.4)$$

This is important for a few reasons. Firstly, that the soil model was analogous to an overconsolidated clay and therefore so will any subsequent soil movements. It is also evidence that the pressure within the tunnel is directly related to the amount of soil movement at the surface (which was also measured to have a volume loss equal to 3%) and that the construction event was undrained. Lastly, as the expression by Macklin (1999) was based on many field measurements, in addition to other centrifuge experiments using the pressured air filled rubber bag method, and therefore the removal of fluid to simulate parts of a tunnel construction could be used.

#### **8.1.4 Summary of experimental verification**

In summary, the tunnelling-induced settlements controlled by the volume loss apparatus were comparable with those documented in published material. The parameters extracted from the

curve fitting exercise are shown to be similar to those presented in the Mair & Taylor (1997) database figures. This completes the verification of the apparatus. The methodology of the analysis applied over Section 8.1 is also applied to the twin-tunnelling analysis.

## **8.2 Overall patterns from the twin-tunnelling tests**

Results presented in this section are intended to highlight overall observed patterns of displacements over various twin-tunnel arrangements outlined in Chapter 6 and 7. Tunnel A (known as Tunnel A) chosen for construction varies from test to test (i.e. left or right hand tunnel first). This verified no external effects to the displacements were evident. Therefore, in the twin-tunnel figures a centre-line label denotes whether the tunnel was bored first ( $T_A$ ) or second ( $T_B$ ).

### **8.2.1 Surface settlement from twin-tunnels**

In total eight twin-tunnel tests were conducted. A summary of the details from each test can be found in Table 7.1. The settlements between the varying volume losses and geometries have been compared by normalising vertical displacements against the maximum settlement from the construction of Tunnel A.

Figure 8.15 shows the normalised total vertical settlement from both the twin-tunnel arrangements spaced 1.5D apart (i.e. tests SD10 and SD13). Figure 8.16 shows the respective data for arrangements spaced 3D apart (i.e. SD11 and SD14). The results from tests SD12 and SD15 are shown in Figure 8.17 and are from the arrangements with a centre-to-centre spacing of 4.5D. Finally, the two offset arrangement tests 2.12D (SD18) and 2.7D (SD17) are shown on Figure 8.18 and Figure 8.19, respectively. Generally, across Figures 8.15 – 8.19 the total vertical settlements between the 3% and 5% tests show a fairly good level of consistency. In section 8.1 the settlement data chosen was after the completion of the fluid removal from within the tunnel. In the case of all the twin-tunnel tests the settlement data was taken after the completion of the fluid removal from within Tunnel B.

In addition to the discrete points there are also various curves representing the prediction methods first outlined in Chapter 4. The prediction curves for the twin-tunnel arrangements

were produced after an assessment of the settlements due to Tunnel A. Tunnel A data was taken after the completion of the fluid removal and assessed using the curve fitting exercise outlined in Section 8.1.1. This curve was duplicated and transported over the centre-line of Tunnel B for the prediction of these settlements. Dependant on the method, the Tunnel B prediction curve could be summed with the prediction curve for Tunnel A for superposition or modified and summed for the prediction method of Addenbrooke & Potts (2001) or Hunt (2004). The Twin-tunnel curves would then be eliminating any inconsistencies in soil preparation and give a fairer assessment of any prediction method's effectiveness. Moreover, settlement trough shape has been shown to remain constant with volume loss (Grant & Taylor, 2000) between volume losses of 2 - 20%. At different spacings, the settlement troughs for the twin-tunnel tests were also found to remain constant between volume losses of 3% and 5%. Therefore, the fitted normalised curves were averaged between the 3% and 5% tests for the plots.

Figure 8.15 shows the superposition and Addenbrooke & Potts (2001) prediction curves equally spaced away from the settlement data which is reflected in the Correlation factors. Superposition and Addenbrooke & Potts (2001) had Correlation factors larger than the 0.1 benchmark for SD3 at 0.14 and 0.13 respectively. Hunt (2005) was larger still at 0.19. In Figure 8.16 there is a marginal increase in the prediction curves reflected in the subsequent Correlation factors. Superposition, Addenbrooke & Potts (2001) and Hunt (2005) have values of 0.1, 0.09 and 0.16 respectively. At this spacing (3D) Addenbrooke & Potts (2001) could be used as a fairly accurate method for the prediction of twin-tunnel settlements. In the 4.5D spacing, Figure 8.17, superposition under predicts the magnitude of the settlement whereas Addenbrooke & Potts (2001) and Hunt (2005) over predict the amount of settlement. This is evident from the Correlation factor values where Addenbrooke & Potts (2001) and Hunt (2005) are as much as 0.17 and 0.18 respectively. In the offset arrangements, Figures 8.18 and 8.19, the theoretical settlement for a greenfield tunnel had to be used for Tunnel B instead of the transposed Tunnel A fitted curve. This was because the varying depths of the tunnels meant the settlement predicted settlement troughs would not have been equal for Tunnel A and Tunnel B. However, in Figure 8.18 superposition was still superior with a Correlation factor of 0.07

whereas Addenbrooke & Potts (2001) had a value of 0.26 and Hunt (2005) a value of 0.16. This trend is repeated in Figure 8.19 for the 2.7D spacing. Superposition is the closet of all the Correlation factors at a value of 0.03. Addenbrooke & Potts (2001) and Hunt (2005) had values of 0.34 and 0.16 respectively which both over predict the settlements.

It is clear that superposition does not take into account the sequential unloading of the soil and therefore, the curve does not always represent the final displacement very well. The predictions of Addenbrooke & Potts (2001) at specific tunnel spacings tend to be in fairly good agreement with the experimental data at the extremities of the settlement trough. Although, with the exception of the 2.7D spacing test, Addenbrooke & Potts (2001) showed the closest fit to the centrifuge data in the 3D test with a Correlation factor of 0.09. This was still not as well fitting as the single tunnel tests addressed in the section 8.1. Hunt (2004) had the largest errors and largest range with errors between 0.16 and 0.19. Hunt's research has shown to produce a good agreement with the centrifuge results at both the extremities. However, this method tends to over predict the magnitude of settlements. Both Addenbrooke & Potts (2001) and Hunt (2005) produced prediction methods that give fairly good correlation with the test data for different specific spacings given the proviso for the extra volume loss in the simulation of a second tunnel construction. Table 8.2 contains a summary of the Correlation factors for all the twin-tunnelling tests.

In Figures 8.20 – 8.24 the twin-tunnelling settlements were separated into those associated with Tunnel A and Tunnel B. The settlement after the construction of Tunnel A was subtracted from the total settlement to give the settlement solely due to Tunnel B. These figures were then normalised by the same method as outlined previously. Figure 8.20 shows Tunnel A and Tunnel B settlement for 1.5D spacing. The Tunnel A settlement had an average Correlation factor of 0.04. Figure 8.21, which illustrates the settlement from the 3D spacings, shows a Tunnel A Correlation factor of 0.05. The Tunnel A settlement in Figure 8.22 shows a correlation factor of 0.07 which is the largest spacing and shows the largest value. Both the offset arrangement, Figures 8.23 and 8.24 had a Correlation factor of 0.03. Therefore, across all eight tests the Tunnel A settlements were well matching with the standard tunnelling-induced

Gaussian distributions. Therefore, Tunnel A settlement was minimally effected by the presence of the other tunnel apparatus and the subsequent loss of shear strength due to the replaced soil. Furthermore, the larger values of the Correlation factor associated with the twin-tunnel prediction curves must be due to the Tunnel B settlement. In summary, from these figures it is clear the data points associated with Tunnel B are not equal to Tunnel A. The trends of the non-standard response, with spacing, of the second tunnels are explored in more detail in Chapter 9.

### **8.2.2 Sub-surface Settlements from Twin-Tunnels**

Figures 8.25 – 8.27 illustrate the distribution of unmodified vertical displacements, in the parallel arrangements, calculated using VisiMET and contoured by Surfer. The largest insert displays the twin-tunnelling contours after both tunnel constructions have been simulated. The widest spacing (Figure 8.27) shows almost symmetrical contour patterns and therefore little or no visible interaction. However, in the 3D case (Figure 8.26) there was a level of asymmetry. Around one of the tunnels there is an increase in the magnitude of settlement around the crown and at the surface directly above the crown. In the closest spacing (Figure 8.25) due to the level of interaction the amount of lean displayed in the contours has been greatly affected. The inserts show the individual tunnel settlements of Tunnel A and Tunnel B. The movements associated with Tunnel A in all these figures show a similar pattern and magnitude regardless of position. However, in Tunnel B the contours vary in their pattern. It can be seen that the closer the spacing the nearer the -0.30 to -0.35 (mm) contour gets to the surface. In the widest centre-to-centre spacing the contour remains just above the crown of the tunnel. As the spacing between the tunnels decreases, the contour bridges from the crown to the surface.

Similar to section 8.1.2 these sub-surface vertical displacements, at three depths in each model, were modified using friction equations to assess how essential prediction parameters change with depth. The individual friction equations can be found in Appendix B. The modified sub-surface settlements are shown in Figures 8.28 – 8.32. The figures show the total settlement (measured immediately after both tunnel constructions), the Tunnel A settlements (measured immediately after the first tunnel construction) and the difference of these two sets of settlements (Tunnel B). The curve fitting exercise was applied to Tunnel A settlements in order

to determine parameters for comparison with published work. Figures 8.28a, 8.28b and 8.28c show the three depths from one of the 1.5D spacing tests. Consistently,  $K$  is within that of published works and is approximately 0.5 at near-surface and is larger with depth. The Correlation factors for the three Tunnel A sets of data are approximately 0.1. Figures 8.29a, 8.29b and 8.29c are the three depths analysed from test SD11. At the 3D spacing the Tunnel A is shown to be narrower at near-surface than the surface data. However, the  $K$  values are still reasonable (between 0.4 and 0.6) and get larger with depth. The Correlation factors for these depths vary between 0.09 and 0.13. The 4.5D spacing sub-surface data is shown in Figures 8.30a, 8.30b and 8.30c. The near-surface settlement of Tunnel A has  $K$  values which follow the standard trend (increasing from 0.5 at the surface with depth), however the Correlation factors are larger than the previous arrangements at approximately 0.15. The 2.7D offset arrangement is the best fitting Tunnel A data. The Correlation factors with depth in Figures 8.32a, 8.32b and 8.32c range between 0.03 – 0.05. However, the  $K$  values are slightly narrower starting at the near-surface with a value of 0.48. In summary, the effects that can be observed at the surface are also present in the sub-surface data. Similar to the surface data, the trends in the Tunnel B data will be explored further in Chapter 9.

### **8.2.3 Tunnel support-pressure data from Twin-Tunnels**

A change in the pressure was created during this removal of fluid from inside the tunnels. Figures 8.33 – 8.37 show the significant tunnel pressure and pore-water pressure during these experiments. The behaviour resulting from the simulated construction was similar for each test. Typically the tunnel pressure reduced linearly for the first stage of the construction. In the second stage the rate reduced in a non-linear behaviour until reaching its lowest point. This was when the simulated construction has finished. The tunnel pressure then began to rise again to a new equilibrium pressure in an inverted non-linear behaviour. This final point was lower than the start of the simulated tunnel construction. The second tunnel construction always began during the stage of regaining equilibrium. The reduction of the pressure due to the construction of the second tunnel was always a greater change than that by the first. This will be discussed in greater detail in Chapter 9.



The pore-water pressure data displayed in Figure 8.34 and 8.35 is from the PPT situated between the tunnels. This data was only available for tests with sufficient space between the tunnels (i.e. not the 1.5D cases). In all cases this shows that at the start of the tunnel construction there was a rise, followed by linear decrease, during the tunnel construction, and after the tunnel construction there was a non-linear decrease. The pore-water pressure showed this same behaviour but exaggerated due to the second tunnel construction. As with the tunnel pressure, a detailed discussion of the pore-water pressure behaviour can be found in Chapter 9.

In summary, the tunnel pressure data showed similar behaviour to the single tunnel cases. However, the reductions in pressures were not identical between each of the tunnels in a test. It appears the second tunnel consistently has a greater change in pressure when compared to the first. The trends of the difference in pressure and the relationship with the settlement data will be explored in greater detail in Chapter 9.

## 9 DISCUSSION

This chapter explores the implications and application of the data presented in the previous chapter. The patterns across all the various tunnel spacings were combined to give new insight into tunnelling-induced settlements which may be useful for future design.

It was shown in the previous chapter that in these experiments the settlements generated upon construction of the first tunnel (Tunnel A) agreed well with established prediction methods. This is expected as Tunnel A is effectively constructed under greenfield conditions. It therefore follows that any improvements in prediction methods for twin tunnelling projects must focus solely on the settlements induced by the second tunnel (Tunnel B). The relative differences in settlement have been addressed in terms of the parameters needed to predict displacements due to twin-tunnel construction. These are volume loss ( $V_L$ ), maximum settlement ( $S_{max}$ ) and trough width parameter ( $K$ ).

### 9.1 Increase in volume loss caused by second tunnel construction

This section addresses the magnitude of the differences in volume loss associated with construction of the second tunnel. Across the tests performed the measured volume loss created by Tunnel B consistently increased when compared with the volume loss observed upon construction of Tunnel A settlement. Figures 8.20 – 8.24 and Figures 8.28 – 8.32 show the surface and sub-surface vertical settlements from Tunnel A and Tunnel B in each test. The figures have the distance from the centre of the model normalised against the diameter (x-axis) and the settlement normalised against the maximum settlement measured in Tunnel A (y-axis). The normalisation allowed the 3% and 5% volume loss tests, for a particular spacing, to be shown on the same figure. The vertical settlements due to Tunnel B were separated into those towards Tunnel A and those away from Tunnel A. In order to extract parameters for comparison Gaussian curves were fitted to the vertical settlement measurements on each side of the settlement trough in this way. The volume loss was determined by the addition of the area on each side of the settlement trough. In Chapter 7 it was shown that the magnitude of settlement due to Tunnel B was larger than Tunnel A. This could be better described as an

increase in volume loss. An increase was determined by calculating the difference in volume loss between Tunnel B and Tunnel A in each model. This was converted into a percentage increase by dividing this difference by the volume loss from Tunnel A. Using the Tunnel A volume loss as the greenfield volume loss ( $V_{Lg}$  or  $V_{L \text{ greenfield}}$ ) from each test would minimise any inconsistencies in model making. Table 9.1 summarises the percentage increases from these analyses.

Figure 9.1 presents the relative percentage increases in the volume loss from Table 9.1 in terms of centre-to-centre spacing. This shows at 1.5D spacing the maximum percentage increase in volume loss caused by the second tunnel was 29%. The maximum spacing tested (4.5D) shows only an 8% increase in volume loss. The offset arrangements were incorporated into Figure 9.1 by using the distance from the centre points of the tunnels.

Also included in this figure is a trend from a numerical study by Addenbrooke & Potts (2001) and two case studies. Lafayette Park measurements were taken at the surface with twin-tunnels bored at 1.7D spacing which resulted in a 32% increase (Cording & Hansmire, 1975). The Heathrow Express tunnel measurements, however, were taken at a depth of 1.44D and a spacing of 2.6D with a 19% increase in volume loss (Cooper *et al.*, 2002). These published measurements lay between the trend of Addenbrooke & Potts (2001) and the 5% volume loss tests from the current work. The overall trend shows that the centrifuge study demonstrates lower increases in volume loss when compared with the numerical study and case histories. The reason for this could be because often numerical studies model the soil as a continuum and therefore the movements tend to be larger. In addition, Stallebrass & Taylor (1997) stated that often centrifuge data is preferred because it is possible to avoid uncertainties such as soil variability, scarcity of instrumentation and the uniqueness of the data which may be reflected in the position of the field monitoring data points on the figures.

As well as surface settlement analysis there was analysis conducted on the sub-surface settlement. Although an attempt was made to modify the sub-surface vertical settlements by taking into account the window-soil friction (discussed in Chapter 8) for some of the tests the correlation between surface and modified sub-surface data was unclear. Therefore, any tests

that were affected in this way were omitted which resulted in one test per spacing being used. Table 9.2 summarises the sub-surface vertical movement data extracted at three different depths below the surface of the models. The three depths were near-surface (9mm), 1D below surface (39mm) and 1.5D below the surface (59mm). Figure 9.2 presents all the volume loss percentage increase for sub-surface data and surface data from Table 9.2. The near-surface and surface data show similar levels of increase with the near-surface sitting slightly higher. Largely, at the 1D depth the magnitude of percentage volume loss increase was higher than the surface and conversely the 1.5D depth had lower values although the reason for this remains unclear.

Figure 9.3 is a simplified version of Figure 9.2 and could be used for design. An average of all the percentage increases from surface and all the levels of sub-surface is shown on Figure 9.3 and the equation from this line. However, an error banding of this data was also carried out. The upper and lower bounding lines were the best fit lines generated from the 1D and 1.5D depth sub-surface data. These two lines which make up the band are at a maximum  $\pm 7\%$  from the design line. Also displayed on Figure 9.3 is the trend of Addenbrooke & Potts (2001) and data points which represent the two aforementioned field studies. It should be noted that both the measurements from Lafayette Park and the Heathrow Express Tunnels fall within this range as does the Addenbrooke & Potts (2001) curve below a spacing of 3D. However, the larger spacings by Addenbrooke & Potts (2001) show a larger percentage increase in volume loss than the centrifuge data possibly caused by this being a numerical study as opposed to field observations or physical test data.

## **9.2 Trough width parameter**

This section addresses the extent of the settlements associated with the construction of Tunnel B. At closer tunnel spacings there was a tendency for the settlement trough induced by Tunnel B to become asymmetric. This asymmetry was characterised by the relative differences in the K values between each half of the settlement trough. These are referred to as K towards Tunnel A and away from Tunnel A.

In both the 1.5D spacing tests (SD10 and SD13) the K value away from Tunnel A changed minimally compared with the K value towards Tunnel A. In SD10 this was 0.55 to a narrower 0.54 and in SD13 the value was 0.56 which increased to 0.57. These are all within the 0.4 – 0.6 accepted range for clay suggested by Mair *et al.* (1993) and, therefore, fit well with field measurements for clay. However, on the opposite side of the settlement trough (towards Tunnel A) the values of K increased. In SD10 K increased from 0.54 to a wider 0.70 and in SD13 K increased from 0.55 to 0.71. This trend was not apparent in the other parallel spacings which were largely symmetrical, however, in the offset geometries a similar effect can be observed. The settlement troughs observed with the offset arrangements were for the first (deeper) tunnels within the accepted range for K values. However, in the 2.12D spacing (SD18) the K value towards Tunnel A increased from 0.46 to 1.09 and in the 2.7D spacing (SD17) the K value increased from 0.47 to 0.85.

Figure 9.4 shows the K values with depth given in Table 9.1 and Table 9.2 This figure is presented in the same format as that given in Mair *et al.* (1993). This gives the trough with parameters towards and away from Tunnel A for all tests. The trough width parameters away from Tunnel A and towards Tunnel A for spacings above 3D agree with the published values of K in Mair *et al.* (1993). However, for the spacings below 3D the trough width parameter towards Tunnel A are shown in Figure 9.4 to form a different line. This new line is similar in shape to the published single tunnel line by Mair *et al.* (1993) but offset to the right. Instead of starting at a value of  $K = 0.5$  at the surface, the new line starts at 0.7 and increases with depth.

### **9.3 Support pressure associated with Tunnel B construction**

In Section 8.3 the results from the tunnel support pressure and PPT data were presented during the two constructions. In this section the support pressure data and PPT data will be analysed further in order to provide some insight into the relative differences in Tunnel B behaviour.

The arrangements where the tunnel depths were equal should imply that the initial supporting pressure would be equal. However, before the simulations of the tunnel constructions, the tunnel support pressures were varied. This was assumed to be owing to the interaction between

the soil and tunnel membranes during pore-water pressure equalisation. To account for the tunnel support pressures not being equal at the start of the simulated constructions the data was plotted in terms of the change in pressure. Figures 9.5 – 9.7 show the differences in Tunnel pressure and pore-water pressures for the parallel arrangements. The difference in tunnel pressure for Tunnel B was always larger than that for Tunnel A.

In Chapter 4 the relationships between tunnel stability (N) and tunnel support pressure were outlined. Macklin (1999) and Mair (1979) related movement (or volume loss) to tunnel stability and therefore tunnel support pressure. It was shown in these studies that a reduction in support pressure would result in movement and therefore a greater reduction in pressure would result in greater volume loss. This is perhaps the reason for the additional second tunnelling-induced settlement. This relationship between tunnel stresses and tunnel settlements were investigated in more detailed by Mair & Taylor (1993). This study produced closed-form plasticity solutions for an unloading cylindrical cavity. In order to relate stability (or tunnel pressure) to displacements and changes in pore-water pressure a number of equations were derived. These equations assumed undrained behaviour, an initial isotropic stress state and geometrical axisymmetry.

For a linear elastic perfectly plastic continuum;

$$\frac{U_r}{r} = \frac{3 S_u R_p^2}{2 E r^2} \quad (9.1)$$

$$\Delta u = S_u \frac{R_p^2}{b^2} \quad (9.2)$$

$$\frac{R_p}{a} = \exp\left(\frac{N-1}{2}\right) \quad (9.3)$$

where  $U_r$  is radial movement at radius  $r$ ,

$a$  is radius of tunnel cavity,

$b$  is radius of far field measurement i.e. distance to surface,

N is the stability ratio given in Chapter 3,

$S_u$  is the undrained shear strength at tunnel axis level,

E is the Young's Modulus,

$\Delta u$  is the change in pore-water pressure,

$R_p$  is the radius, r, of plastic zone, and

$\Delta u$  is predicted as equalling zero in the elastic region, where  $r > R_p$

However, using the non-linear function (for the Boom clay in Mair & Taylor, 1993);

$$G = G_0 \left( \frac{r}{x} \right) \quad (9.4)$$

The secant stiffness, G, increases linearly with radius.  $G_0$  is an arbitrary reference stiffness at r equals x.

$$\frac{U_r}{r} = \frac{3}{2} \frac{r}{E} \frac{S_u}{r} \frac{R_p}{r} \quad (9.5)$$

$$\Delta u = S_u \left( -\frac{R_{pnl}}{r} \right) \quad (9.6)$$

$$\frac{R_{pnl}}{a} = \exp \left( \frac{N}{2} - 1 \right) \quad (9.7)$$

$\Delta u$  in the plastic region is still as given by Equation (9.2) but the radius, r, of the plastic zone is  $R_{pnl}$  and  $\Delta u$  in the elastic region is given by Equation (9.6) and Equation (9.7).

Predictions from these relationships were compared with pore pressure data obtained from the 3D and 4.5D spacing tests. Due to the limited space available between the tunnels for installation of PPTs, data only exists for the tests with wider spacings. As a direct result of the change in volume during a tunnel construction the PPT readings show a change pressure. In these arrangements a PPT was set at the tunnel axis level half way between the two tunnels. In

the 4.5D tests (SD12 and SD15) this was 60mm from each tunnel's centre point and therefore in the elastic region as defined above.

The radial displacement,  $U_r$ , for the 3D spacing case, was calculated using a linear-elastic perfectly plastic approach. This used values of Tunnel pressure during the experiment and the undrained shear strength after the experiment. If this value of displacement was assumed to act uniformly around the circumference of the tunnel the volume loss would be 2.4%. It is also assumed at this distance from the tunnel boundary that no overall change in pore-water pressure has occurred. During SD11 the volume loss measured at the surface was 2.6% and therefore this method gave a reasonable estimation of the displacements. When using the non-linear elastic approach the prediction is much lower for volume loss at only 0.9%. However, this method estimates a reduction in pore-water pressure of 16kPa. This compares well with the 12kPa reduction measured by the PPT in the centrifuge test SD11.

The linear-elastic perfectly plastic approach was then applied to the data obtained from simulation of Tunnel B. The volume loss calculated was equal to 2.6% and had no change in pore-water pressure. This shows an increased volume loss compared to Tunnel A, although the magnitude is not as significant as the 2.9% measured at the surface during SD11. The non-linear elasticity approach was also undertaken for Tunnel B data and predicted the volume loss was 0.5% and the change in pore-water pressure was -17.5kPa. However, in SD11 the change in pore-water pressure measured by the PPT during Tunnel B was less than 1kPa.

This behaviour was repeated in the 4.5D tests for both the volume losses tested. The analysis described in Mair & Taylor (1993) produces pressure changes and Volume loss values that agree well with the data obtained for construction of Tunnel A. This is expected because Tunnel A was constructed in a greenfield scenario. However, this analysis approach cannot be used to predict changes in pore-water pressure due to Tunnel B. The detailed analyses of these linear-elastic perfectly plastic calculations are given in Appendix C.



## 9.4 Application of the design charts

A set of procedures are described in this section to be used for the prediction of twin tunnelling-induced settlements in the plane transverse to the advancing tunnels. These procedures are a modification to the superposition method first outlined by O'Reilly & New (1982) in which the settlements due to Tunnel A and Tunnel B constructions are summed to predict the twin-tunnel settlement. Tunnel A settlements can be calculated by the methods outlined in Chapter 4 using the equations by Peck (1969), O'Reilly & New (1982) and Mair *et al.* (1993). Tunnel B settlements can be estimated using the expressions, featured in these texts, but with specific parameters changed according to Figure 9.3 and Figure 9.4. The specific modifications are detailed in the following sections which have been separated into those associated with surface and sub-surface settlements in overconsolidated clay.

### 9.4.1 Surface settlements

Tunnel A surface settlement profiles were well described by the established Gaussian curve distribution where the volume loss is usually calculated by the area under a curve fit through these settlements. Twin-tunnel surface settlement predictions could be improved by considering the relative differences between Tunnel A and Tunnel B surface settlements. Previously, it has been shown that the relative differences between Tunnel A and Tunnel B settlements can be quantified by relative increases in volume loss and a difference in  $K$ . The method for predicting surface Tunnel B settlements is described herein.

Predictions of Tunnel B settlements are similar to Equation (4.3), Equation (4.4) and Equation (4.5) for centre-to-centre spacings larger than  $3D$  where a  $K$  value of 0.5 for both sides of the settlement trough would be appropriate. However, Figure 9.3 could be used to quantify the amount of increase in volume loss used in these expressions. Once a volume loss is known or one has been assumed for Tunnel A, a modified value, obtained using Figure 9.3, can be used as the basis of a prediction for Tunnel B volume loss. Subsequently, Tunnel B settlement can be estimated by using Equation (9.1), Equation (9.2) and Equation (4.5) for centre-to-centre spacings larger than  $3D$ ;

$$S_{\max T_B} = 0.313 \frac{V_{LT_B} D^2}{i} \quad (9.8)$$

$$i = K \cdot z_0 \quad (4.5)$$

$$S_{vT_B} = S_{\max T_B} \exp\left(-\frac{x_B^2}{2i^2}\right) \quad (9.9)$$

where  $S_v$  is the vertical settlement, at a defined horizontal point, in the x-z plane,

$S_{\max}$  is the theoretical maximum settlement at the tunnel centre-line,

$x_B$  is the lateral distance from Tunnel B centre-line,

$i$  is the lateral distance from the tunnel centre-line to the point of inflection in the Gaussian distribution curve,

$V_L$  is volume loss expressed as a ratio,

$D$  is the bored tunnel diameter,

$z_0$  is the vertical distance from the un-deformed surface to Tunnel B axis level,

$K$  is a dimensionless trough width parameter and

The suffix  $T_B$  infers the modified value related to Tunnel B settlements using Figure 9.3.

However, the estimation of Tunnel B surface settlement for centre-to-centre spacings below  $3D$  must use a similar procedure to that above. It is suggested here that a value of  $K$  equal to 0.7 appears more appropriate for the side of the settlement trough towards Tunnel A. Therefore, the determination of the settlement due to the construction of Tunnel B would be in two parts, firstly, towards Tunnel A and secondly, away from Tunnel A. Settlement away from Tunnel A can be estimated using the procedure outlined above. The settlement towards the tunnel must change Equation (4.5) to give a modified the value for  $i$  towards the tunnel. Equation (4.5)

should use a value of K equal to 0.7 instead of 0.5. The increased in volume loss and subsequent  $S_{\max}$  remain the same as the side away from Tunnel A but  $S_v$  towards Tunnel A will be calculated using the new value for K and subsequently i.

Similar to the superposition method of O'Reilly & New (1982) the two individual tunnelling-induced settlements, positioned over the tunnels respective centre-lines, can be summed to give the total predicted twin-tunnel surface settlement.

#### 9.4.2 Sub-surface settlements

Tunnel A sub-surface settlements were reasonably approximated by the Gaussian distribution described by Mair *et al.* (1993). A similar pattern in the relative differences of settlements was apparent in the sub-surface data for Tunnel B as at the surface. Therefore, a similar procedure to the prediction Tunnel B surface settlement could be used for the prediction of Tunnel B sub-surface settlements. Centre-to-centre spacings larger then 3D could use an increased volume loss from Figure 9.3 and K values predicted by using Equations (4.11) and Equation (4.12) from Mair *et al.* (1993). However, as with the surface prediction procedure, a different procedure would be needed for sub-surface settlements towards Tunnel.

$$S_z = S_{z,\max} \exp\left(-\frac{x^2}{2K_{TB}^2(z_0 - z)^2}\right) \quad (9.10)$$

where  $z$  is the vertical distance from the un-deformed surface to the horizon analysed,  
 $S_z$  is the subsurface settlement in the x-z plane, and  
 $S_{z,\max}$  is the maximum subsurface settlement (above the tunnel centre-line) at depth,  $z$ .

Figure 9.4 can be used to estimate the trough width parameter,  $K_{TB}$ , at a specific depth ( $z_0 - z$ ). The new value of K can be entered into Equation (9.10) with the modified  $S_{\max}$  value resulting from the increased volume loss (Figure 9.3). Similar to the surface superposition method the sub-surface twin-tunnelling settlement can be estimated by summing Tunnel A and Tunnel B settlement for a given depth.

## 9.5 Summary

The data obtained in the previous chapter has been compiled to give new insight into tunnelling-induced settlements which may be useful for future design. Improvements in the prediction methods for twin tunnelling projects were shown to be possible when considering the settlements induced by a closely constructed second tunnel (Tunnel B). Tunnel B settlements were shown to be larger in magnitude compared with Tunnel A at the surface and with depth. This phenomenon was characterised as an increase in volume loss. In addition the side of the settlement trough towards Tunnel A was wider than predicted by published values of  $K$  indicating an asymmetry of settlements generated by Tunnel B.

A possible synthesis for these observations would be an increased stiffness within parts of the soil mass. During both tunnel constructions the Pore Pressure Transducer between the tunnels measured the increase in excess pore pressure (shown in Figures 9.6 and 9.7). In both cases the magnitude of excess pore pressure was greater for the second simulated tunnel construction compared with the first.

The amount of fluid removed from both tunnelling systems remains the same and therefore the tests are displacement controlled. In order to achieve the observed PPT readings the stress change must be different between the two simulated tunnel constructions. Hence, a greater change in excess pore pressure could result from an increase in stiffness. Different stress changes within the soil mass will lead to different displacements as was observed in Figures 8.15-8.24 and Figures 8.28-8.32. In order to fully understand these possible stiffness changes either a numerical model could be developed or a comprehensive series of triaxial tests carried out to investigate the stress paths associated with twin tunnel construction. Such detailed numerical analysis is outside the scope of this current research.

## 10 CONCLUSIONS

Within this final chapter the findings of the thesis will be drawn together to give a summary and a series of conclusions. The limitations of the current research and recommendations for possible further work are made based on these conclusions.

### 10.1 Summary of work undertaken

This thesis contains an extensive literature review into the prediction of ground movements generated from twin-tunnelling in urban environments analogous to London (i.e. built in moderately stiff overconsolidated clay). Current practices are largely based on empirical prediction methods, concerned with single tunnel greenfield arrangements (i.e. Peck, 1969; Cording & Hansmire, 1975; Clough & Schmidt, 1981; O'Reilly & New, 1982; Attewell & Yates, 1984; Cording, 1991; Mair *et al.*, 1993 and Mair & Taylor, 1997). A number of case studies have shown a relative difference in the settlements due to each tunnel construction (e.g. Cooper *et al.*, 2002; Cording & Hansmire, 1975 and Nyren, 1998). These were further investigated by numerical studies which support these observations (e.g. Addenbrooke & Potts, 2001 and Hunt, 2005). It was clear that significant insight could be gained from a physical modelling investigation, at prototype scale, into sequential twin bored tunnel construction.

Therefore, apparatus was designed and fabricated to be used in a series of plane strain centrifuge tests investigating twin tunnelling-induced settlements in overconsolidated clay. The apparatus necessary to perform these tasks required a significant amount of time to develop and was relatively complex. The novel apparatus was designed during the research to enable the simulation of the construction processes related to volume loss in separate tunnels, sequentially. A total of eighteen tests were performed. These included two single tunnel tests in order to validate the apparatus before the main series of tests began. During the twin-tunnel tests the main variables were the spacing between the tunnels, horizontally and vertically, in addition to the magnitude of volume loss (3% and 5%). The tests were conducted at 100g where the cavities represented two 4m diameter tunnels usually at a depth of 10m at prototype scale. The vertical settlement results were obtained by LVDTs at the surface and using a close range

photogrammetry system at sub-surface levels. These were shown to give reasonably consistent results which have been presented in order to provide greater insight during twin-tunnel construction.

## 10.2 Conclusions

The main findings from the physical model tests can be summarised in the following points: -

1. Replacing air support with a water support within two cavities in an overconsolidated clay model still resulted in single tunnel surface and sub-surface settlement troughs that were well represented by Gaussian distributions.
2. The twin-tunnelling settlement predictions can be improved by modifying the settlements solely due to the second tunnel construction. The second tunnel settlements can be predicted using equations by Peck (1969), O'Reilly & New (1982) and Mair *et al.* (1993) but with modifications. These modifications, if required, involve increasing the magnitude of the superimposed greenfield settlement and increasing the trough width towards the existing tunnel.
3. The relative increase in settlements due to the second tunnel compared with the first tunnel was best described by an increase in the volume loss (given as a percentage). This effect was lessened by larger spacings between the tunnels.
4. The increase in volume loss could be observed at the surface and at depths within the models.
5. At the surface the trough width parameter towards the first tunnel was observed to be wider than a single tunnel ( $K$  increased from 0.5 to a wider 0.70).
6. The case studies Cooper *et al.* (2002) and Cording & Hansmire (1975) also described an increase in volume loss and were found to fit within the findings. The numerical investigation by Addenbrooke & Potts (2001) was found to fit the findings but only below a spacing of  $3D$ .
7. Linear-elastic perfectly plastic solutions using linear and non-linear stiffnesses by Mair & Taylor (1993) are unable to predict the displacements or distribution of pore pressures as a result of the second tunnel construction.

### 10.3 Limitations of the results

The results are limited by the capabilities of the apparatus. The obvious flaw in the apparatus is the loss of shear strength due to replacing the cavities with water. In the single tunnel tests the 'lost soil' is below the area of interest and the soil movements being investigated are minimally effected. The soil directly at either side of a tunnel greatly affects the stability of tunnel and the subsequent movements as a result of a simulated construction. This was shown by Xu *et al.* (2013) in the case where the resin tubes either side of the cavity improved the tunnel stability. Moreover, in the case of the side-by-side twin-tunnel tests the soil missing from one side of the cavity will cause the settlement to shift towards the other tunnel.

This effect can be measured by the change in the position of the maximum surface settlement ( $S_{\max}$ ) away from the tunnel centre-line. Tunnel A settlements were well matched with greenfield published values in magnitude and distribution, however, the position of  $S_{\max}$  was not over the centre-line of the tunnel in the closest spaced tests. In the tests with a spacing of 1.5D (or  $\pm 30\text{mm}$  from the model centre-line) the position of  $S_{\max}$  was 10.77mm from the centre-line of the model. This effect was not evident in the 3D or 4.5D tests. However, the position of  $S_{\max}$  in the Tunnel B settlement data shows a pattern. At 1.5D the eccentricity of  $S_{\max}$  was 22.6mm from the centre-line of Tunnel B, at 3D the eccentricity was 7.8mm and at 4.5D the eccentricity was 4.05mm. Essentially, the effect reduced the further away the cavities were.

### 10.4 Recommendations for further research

The results presented within this thesis were limited by the relatively few number of tunnel arrangements tested. The arrangements were carefully chosen to maximise the significant amount of data from the tests. However, increasing the number of arrangements tested would add significantly more information about the relative increases in settlement due to spacing between the tunnels. The cover, to at least one tunnel, was kept equal to twice the diameter. Further investigations which also varied the depths would add significant information to the behaviour during twin-tunnel construction. The time between the tunnel constructions was fixed in all the tests.

Further work should therefore be undertaken to determine the influence of varying the time between the tunnel constructions. Once a significant range of geometries and arrangements have been investigated a series of tests should be conducted using different stress histories of soils and soil types. The centrifuge tests carried out in this research only used kaolin clay and had an overconsolidation ratio equal to 2 with an average measured undrained shear strength of 42kPa.

The amount of pore-water pressure data around the tunnels was minimal and it was shown that the dissipation of pore pressure resulting from the second tunnel construction was not typical. Therefore, any further work should utilise more instrumentation around the second tunnel to characterise the differences in excess pore pressures compared with the greenfield scenario. The amount of surface data was restricted to the number of LVDTs and assumptions were made about the topography. The use of laser displacement transducers for continuous readings or surface photogrammetry techniques would lead to a better understanding of the shape and volume of the settlement troughs.

In addition to a continued physical model testing series there should be a series of numerical analysis conducted which also model twin-tunnel construction in overconsolidated clay. A numerical model of the physical model investigating the effective stress paths around the second tunnel will provide additional data on any increase in stiffness and therefore an understanding of the displacements.



## REFERENCES

- Al-Tabbaa, A. (1987). Permeability and stress-strain response of Speswhite kaolin. Ph.D. Thesis, University of Cambridge.
- Addenbrooke, T. I. and Potts, D. M. (2001). Twin tunnel interaction - surface and subsurface effects. *International Journal of Geomechanics*, Vol. 1, pp. 249-271.
- Atkinson, J. H. (1993). *Introduction to the Mechanics of Soils and Foundations: through critical state soil mechanics*. 3<sup>rd</sup> ed. McGraw Hill International series in Civil Engineering.
- Atkinson, J. H. and Potts, D. M. (1977). Subsidence above shallow tunnels in soft ground. *Journal of the Geotechnical Engineering Division*, Vol. 103, No. 4, pp. 307-325.
- Atkinson, J. H., Brown, E. T. and Potts, D. M. (1975). Collapse of shallow unlined tunnels in dense sand. *Tunnels and Tunnelling*, Vol. 3, pp. 81-87.
- Attewell, P. B. (1978). Ground movements caused by tunnelling in soil. *Proceedings of the International Conference on Large Movements and Structures* (ed. J.D. Geddes), London, pp. 812-948, Pentech Press.
- Attewell, P. B. and Yeates, J. (1984). *Ground movements and their effects on structures*. Blackie and Son Ltd, Attewell, P.B. and Taylor, R.K.
- Barlett, J. V. and Bubbers, B. L. (1970). Surface movements caused by bored tunnelling. *Conference on Subway Construction*, Budapest, pp. 513-53.
- Begaj-Qerimi, L. (2009). Re-use of pile foundations in urban environments. Ph.D. Thesis, City University London.

Boscardin, M. D. and Cording, E. J. (1989). Building response to excavation-induced settlement. ASCE, Journal of Geotechnical Engineering, Vol. 115, No. 1, pp. 1-21.

Broms, B. B. and Bennermark, H. (1967). Stability of clay at vertical openings. ASCE Journal of Soil Mechanics and Foundation Engineering Division SM1, Vol. 93, pp. 71-94.

Burland, J. (2001). Assessment methods used in design. In: Burland, J., Standing, J. and Jardine, F. ed. (2001). Building Response to Tunnelling - Case Studies from Construction of the Jubilee Line Extension, London, Vol. 1, Thomas Telford, Ch. 3, pp. 23-43.

Chambon, P., Corte, J. F. and Garnier, J. (1991). Face stability of shallow tunnels in granular soils. Proceedings of an International conference on Centrifuge, A.A. Balkema, Rotterdam, pp. 99-105.

Chapman, D. N., Ahn, S. K., Hunt, D. V. L. and Chan, A. H. C. (2006). The use of model tests to investigate the ground displacements associated with multiple tunnel construction in soil. Tunnelling and Underground Space Technology, Vol. 21, No. 3-4, pp. 413-413.

Clough, G. W. and Schmidt, B. (1981). Design and performance of excavations and tunnels in soft clay. Soft clay engineering, Elsevier, pp. 569-634.

Cooper, M. L. and Chapman, D. N. (1998). Movement of the Piccadilly Line Tunnels caused by the new Heathrow Express Tunnels. Proceedings of the World Tunnel Congress '98 on Tunnels and Metropolises, Sao Paulo, Brazil, pp. 294-254. Balkema.

Cooper, M. L., Chapman, D. N. and Rogers, C. D. F. (2002). Prediction of Settlement in Existing Tunnel Caused by the Second of Twin Tunnels. Transportation Research Record 1814, Paper No. 2-2729, pp. 103-112.

Cording, E. I and Hansmire, W. H. (1975). Displacement around soft ground tunnels. Proceedings of the 5th Pan-Am Conference on Soil Mechanics and Foundation Engineering, Buenos Aires, Vol. 4, pp. 571-633.

Cording, E. I. (1991). Control of ground movements around a tunnel. General report, Proceedings of the 9<sup>th</sup> Pan-Am Conference on Soil Mechanics and Foundation Engineering, Buenos Aires, Vol. 4, pp. 571-633.

Davis, E. H., Gunn, M. J., Mair, R. J. and Seneviratne, H. N. (1980). The stability of shallow tunnels and underground openings in cohesive material. *Géotechnique*, Vol. 30, No. 4, pp. 397-416.

Divall, S., Goodey, R. J., & Taylor, R. N. (2012). Ground movements generated by sequential Twin-tunnelling in over-consolidated clay. Proceedings of the 2<sup>nd</sup> European Conference on Physical Modelling in Geotechnics, Delft – online publication by TU Delft Library.

Fang, Y. S., Lin, L. S. and Su, C. S. (1994). An estimation of ground settlement due to shield tunnelling by the Peck-Fujita method. *Canadian Geotechnical Journal*, Vol. 31, No. 3, pp. 431-443.

Gasparre, A., Nishimura, S., Minh, N., Coop, M. R. and Jardine, R. J. (2007). The stiffness of natural London Clay. *Géotechnique*, Vol. 57, No. 1, pp. 33-47.

Grant, R. J. (1998). Movements around a tunnel in two-layer ground. Ph.D. Thesis, City University London.

Grant, R. J. and Taylor, R. N. (2000). Tunnelling-induced ground movements in clay. Proceedings of the Institution of Civil Engineers, Geotechnical Engineering, London, England, Vol.143, pp. 43-55.

Grammatikopoulou, A., Zdravkovic, L. and Potts, D. M. (2008). The influence of previous stress history and stress path direction on the settlement trough induced by tunnelling. *Géotechnique*, Vol. 58, No. 4, pp. 269-281.

Hergarden, H. J. A. M., Van der Poel, J. T. and Van der Schrier, J. S. (1996). Geotechnical aspects of underground construction in soft ground. Proceedings of the International Symposium on Geotechnical Aspects of Underground Construction in Soft Ground, City University London, pp. 519-524.

Hoyaux, B. and Ladanyi, B. (1970). Gravitational stress field around a tunnel in soft ground. Canadian Geotechnical Journal, Vol. 7 pp. 54-61.

Hunt, D. V. L. (2005). Predicting the ground movements above twin tunnels constructed in London Clay. Ph.D. Thesis, University of Birmingham.

Imamura, S., Hagiwara, T., Kenji, N. and Nomoto, T. (1998). Settlement trough above a model shield observed in a centrifuge. Proceedings of the International Conference Centrifuge '98, Vol.1, pp. 713-719.

Jacobsz, S. W. (2002). The effects of tunnelling on piled foundations. Ph.D. Thesis, Cambridge University.

Jones, B. D. and Clayton, C. R. I. (2012). Surface settlements due to deep tunnels in clay, London: ICE Research and Development Enabling Fund Grant 1021, Funder's Report, Document No. 1021 03.

Kimura, T and Mair, R. J. (1981). Centrifugal testing of model tunnels in soft clay. Proc. 10<sup>th</sup> Int. Conf. ISSMFE, Stockholm, Vol.1, pp. 319-322.

Ladanyi, B. and Hoyaux, B. (1969). A study of the trap door problem in a granular mass. Canadian Geotechnical Journal, Vol. 6, No. 1, pp. 1-14.

Lee, C. J., Wu, B. R., Chen, H. T. and Chiang, K. H. (1996). Tunnel stability and arching effects during tunnelling in soft clayey soil. Tunnelling and Underground Space Technology, Vol. 21, No. 2, pp. 119-132.

Lee, Y. and Yoo, C. (2006). Behaviour of a bored tunnel adjacent to a line of load piles. Tunnelling and Underground Space Technology, Vol. 21, No. 3 pp. 370.

Lo, K. Y., Ng, M. C. and Rowe, R. L. (1984). Predicting settlement due to tunnelling in clays. ASCE – Proceedings of Two Sessions at GEOTECH '84, Atlanta, Georgia, pp. 47-76.

Lognathon, N. & Poulos. H. G. (1998). Pile response caused by tunnelling. *Journal of Geotechnical and Geoenvironmental Engineering*, Vol. 124, No. 9, pp. 846-856.

Love, J. P. (1984). Model testing of geogrid in unpaved roads. D.Phil. Thesis, Oxford University, UK.

Macklin, S. R. (1999). The prediction of volume loss due to tunnelling in overconsolidated clay based on heading geometry and stability number. *Ground Engineering*, Vol. 32, No. 4, pp. 30-34.

Mair, R. J. (1979). Centrifugal Modelling of Tunnel Construction in Soft Clay. Ph.D. Thesis, Cambridge University.

Mair, R. J. and Taylor, R. N. (1993). Predictions of clay behaviour around tunnels using plasticity solutions. *Predictive soil mechanics, Proceedings of the Wroth memorial symposium*, Oxford, pp. 449-463.

Mair, R. J. and Taylor, R. N. (1997). Bored tunnelling in the urban environment. *Proceedings of the 14<sup>th</sup> International Conference on Soil Mechanics and Foundation Engineering*, Vol. 4, pp. 2353-2385.

Mair, R. J., Gunn, M. J. and O'Reilly, M. P. (1981). Centrifugal testing of model tunnels in soft clay. *Proceedings of the 10<sup>th</sup> International Conference on Soil Mechanics and Foundation Engineering*, Vol.1, pp. 323-328.

Mair, R. J., Taylor, R. N. and Bracegirdle, A. (1993). Subsurface settlement profiles above tunnels in clays. *Géotechnique*, Vol.43, No.2, pp. 315-320.

Mair, R. J., Taylor, R. N. and Burland, J. B. (1996). Prediction of ground movements and assessment of risk of building damage due to bored tunnelling. *Proceedings of the International Symposium on Geotechnical Aspects of Underground Construction in Soft Ground*, City University London, pp. 713-718.

Marshall, A. (2009). Tunnelling in sand and its effects on pipelines and piles. Ph.D. Thesis, Cambridge University.

McNamara, A. M. (2001). Influence of heave reducing piles on ground movements around excavations. Ph.D. Thesis, City University London.

Meguid, M. A., Saada, O., Nunes, M. A. and Mattar, J. (2008). Physical modeling of tunnels in soft ground: A review. *Tunnelling and Underground Space Technology incorporating Trenchless Technology Research*, Vol. 23, No. 2, pp. 185-198.

Moh, Z. C., Ju, D. H. and Hwang, R. N. (1996). Ground movements around tunnels in soft ground. *Proceedings of the International Symposium on Geotechnical Aspects of Underground Construction in Soft Ground*, City University London, pp. 725-730.

Ng, C. W. W., Hu, L. and Peng, S. Y. (2012). Three-dimensional centrifuge modelling of twin tunnelling effects on an existing pile. *Tunnelling and Underground Space Technology*. - Accepted.

Nomoto, T., Imamura, S., Hagiwara, T., Kusakabe, O. and Fujii, N. (1999). Shield tunnel construction in a centrifuge. *Journal of Geotechnical and Environmental Engineering*, Vol. 125, No. 4, pp. 289-300.

Nyren, R. (1998). Field measurements above twin tunnels in London Clay. Ph.D. Thesis, Imperial College.

O'Reilly, M. P. and New, B. M. (1982). Settlements above tunnels in the United Kingdom - their magnitude and prediction. *Tunnelling '82, Papers Presented at the 3<sup>rd</sup> International Symposium*, Institute of Mining and Metallurgy, London, England, pp. 173-181.

Oteo, C. S. and Sagaseta, C., (1982). Prediction of settlements due to underground openings. *Proceedings of the 7<sup>th</sup> International Symposium on Numerical Methods in Geomechanics*, Zurich, pp. 653-659.

Panet, M. and Guenot, A. (1982). Analysis of convergence behind the face of a tunnel. Tunnelling '82, Papers Presented at the 3<sup>rd</sup> International Symposium, Institute of Mining and Metallurgy, London, England, pp. 197-204

Peck, R. B. (1969). Deep excavation and tunnelling in soft ground. Proceedings of the 7<sup>th</sup> International Conference on Soil Mechanics and Foundation Engineering, Mexico City, Vol.3, pp. 225-290.

Phillips, R. (1995). Centrifuge modelling: practical considerations. Geotechnical Centrifuge Technology, Blackie Academic & Professional, Taylor, R.N., pp. 34-60.

Rose, A. V. (2012). Behaviour and efficiency of perimeter pile groups. Ph.D. Thesis, City University London.

Rowe, R. K., Lo, K. Y. and Kack, C. A. (1983). A method of estimating surface settlement above tunnels constructed in soft ground. Canadian Geotechnical Journal, Vol. 20, No. 8, pp. 11-22.

Sagaseta, C. (1987). Analysis of undrained soil deformation due to ground loss. Géotechnique, Vol.37, No.3, pp. 301-320.

Schmidt, B. (1989). Consolidation settlements due to soft ground tunnelling. 12<sup>th</sup> International Conference on Soil Mechanics and Foundation Engineering, Rio, Vol. 2, pp. 797-800

Schofield, A. N. (1980). Cambridge University geotechnical centrifuge operations - Rankine lecture. Géotechnique, Vol. 30, No. 3, pp. 227-268.

Sharma, J. S., Bolton, M. D. and Boyle, R. E. (2001). A new technique for simulation of tunnel excavation in a centrifuge. Geotechnical Testing Journal, Vol. 24, No. 4, pp. 343-349.

Skempton A. W. and Chrimes, M. M. (1994). Thames Tunnel: geology, site investigation and geotechnical problems. Géotechnique, Vol. 44, No. 2, pp. 191-216.

Stewart, D. I. (1989). Groundwater effects on in-situ walls in stiff clay. Ph.D. Thesis, Cambridge University.

Sugiyama, T., Hagiwar, T., Nomoto, T., Nomoto M., Ano, Y., Mair, R. J., Bolton, M. D. and Soga, K. (1999). Observations of ground movements during tunnel construction by slurry shield method at the Docklands Light Railway Lewisham Extension – East London. *Soils and Foundations*, Vol. 39, No. 3, pp. 99-112.

Stallebrass, S. E. (1990). Modelling the effect of recent stress history on the deformation of overconsolidated soils. Ph.D. Thesis, City University London.

Stallebrass, S. E. and Taylor, R. N. (1997). The development and evaluation of a constitutive model for the prediction of ground movements in overconsolidated clay. *Géotechnique*, Vol. 47, No. 2, pp. 235-253.

Taylor, R. N. (1984). Ground movements associate with tunnels and trenches. Ph.D. Thesis, Cambridge University.

Taylor, R. N. (1995). Centrifuges in modelling: principles and scale effects. *Geotechnical Centrifuge Technology*, Blackie Academic & Professional, Taylor, R. N., pp. 19-33.

Taylor, R. N., Grant, R. J., Robson, S. and Kuwano, J. (1998). An image analysis system for determining plane and 3-D displacements in soil models. *Centrifuge 98*, Kimura, Kusakabe and Takemura (Eds), Balkema, Rotterdam.

Verruijt, A. and Booker, J. R. (1996). Surface settlements due to deformation of a tunnel in an elastic half plane. *Géotechnique*, Vol. 46, No. 4, pp. 753-756.

Viggiani, G. and Atkinson, J. H. (1995). Stiffness of fine-grained soil at very small strains. *Géotechnique*, Vol. 45, No. 2, pp. 249-265.



White, D. and Take, A. (2002). GeoPIV: Particle Image Velocimetry (PIV) Software for use in Geotechnical Testing. CUED/D-SOILS/TR322, University of Cambridge, UK.

Withers, A. D., Page, D. P. and Linney, L. R. (2001) Geology and geotechnical properties. In: Burland, J., Jardine, F. and Standing, J., ed. (2001). Building Response to Tunnelling - Case Studies from Construction of the Jubilee Line Extension, London, Vol. 1, Thomas Telford, Ch. 5, pp. 57-82.

Wongsaroj, J. (2005). Three-dimensional finite element analysis of short and long-term ground response to open-face tunnelling in stiff clay. Ph.D. Thesis, Cambridge University.

Wu, B. R., Chiou, S. Y., Lee, C. J. and Chen, H. T. (1998). Soil Movements around Parallel Tunnels in Soft Ground. Proceedings of the International Conference Centrifuge '98, Vol. 1, pp. 739-744.

Xu, M., Divall, S. and Taylor, R. N. (2013). Centrifuge modelling of tunnelling with embedded forepoles. International Journal of Physical Modelling in Geotechnics - in preparation.

## TABLES

<i>Category of damage</i>	<i>Normal degree of severity</i>	<i>Limiting tensile strain (<math>\epsilon_{lim}</math>) (%)</i>
0	Negligible	0 – 0.05
1	Very Slight	0.05 – 0.075
2	Slight	0.075 – 0.15
3	Moderate*	0.15 – 0.3
4 to 5	Severe to Very Severe	> 0.3

\* Note: Boscardin & Cording (1989) describes the damage corresponding to  $\epsilon_{lim}$  in the range 0.15 – 0.3% as “Moderate to Severe”. However, none of the cases quoted by them exhibit severe damage for this range of strains. There is therefore no evidence to suggest that tensile strains up to 0.3% will result in severe damage (from Mair *et al.*, 1996).

**Table 2.1:** Relationship between category of damage and limiting tensile strain,  $\epsilon_{lim}$  (after Boscardin & Cording, 1989)

<i>Reference</i>	<i>Range of Values for <math>V_L</math></i>	<i>Type of Tunnelling</i>
O'Reilly & New (1982)	1.0 - 1.4 %	Open Face
New & Bowers (1994)	1.0 - 1.3 %	Heathrow Trail Tunnels
Barakat (1996)	0.7 - 1.6 %	Open Face
Broms & Shirlaw (1989)	<1.0 %	Closed Face (EPBM)
Mair & Taylor (1997)	1.0 - 2.0 %	Open Face
Mair & Taylor (1997)	0.5 – 1.5 %	NATM
Mair & Taylor (1997)	1.0 – 2.0 %	EPBM or slurry shields

**Table 3.1:** Typical Values for Volume Losses (Hunt, 2005)

<i>Reference</i>	<i>Expression</i>	<i>Comments</i>
Clough and Schmidt (1981)	$V_L = me^{(N-1)}$ (for $N \geq 1$ ) $V_L = mN$ (for $N < 1$ )	Equations calculated assuming $E_u/S_u$ = 500-1500, with $m = 0.002-0.006$
Mitchell (1983)	$V_L = (S_u/E_u)e^{(N/2)}$	An $E_u/S_u$ ratio of between 200-700 is generally used for “poor workmanship” $V_L$ should be increased by factor of 3
Attewell, Yeates and Selby (1986)	$V_L = 1.33N - 1.4$	Applicable for $1.5 < N < 4$ . An alternative plot after Leach (1985) gives a design range of $V_L$ verses $N$ within which 75% of cases may be expected to lie.

**Table 4.1:** Volume loss prediction formulae (Macklin, 1999)

<i>Parameter</i>	<i>Metric Unit</i>	<i>Scaling Law (model/prototype)</i>
Gravity	m/s <sup>2</sup>	N
Length	m	$\frac{1}{N}$
Area	m <sup>2</sup>	$\frac{1}{N^2}$
Volume	m <sup>3</sup>	$\frac{1}{N^3}$
Weight, Force	N = kg m/s <sup>2</sup>	$\frac{1}{N^2}$
Density	kg/m <sup>3</sup>	1
Unit weight	N/m <sup>3</sup>	N
Stress and Pressure	Pa = N/m <sup>2</sup>	1
Strain	-	1
Bending stiffness, EI	Nm <sup>2</sup>	$\frac{1}{N^4}$
Axial stiffness, EA	N	$\frac{1}{N^2}$

**Table 5.1:** Centrifuge Scaling Laws (Marshall, 2009)

<i>References</i>	<i>Method</i>	<i>Advantages and applications</i>	<i>Disadvantages</i>
Ladanyi & Hoyaux (1969)	Trap Door	Used to evaluate surface settlement and pressure on the trap door simulating tunnelling induced movement and lining stresses	Does not simulate the actual tunnelling process
		Both 2D and 3D ground movement resulting from tunnel excavation can be evaluated under 1g and centrifuge conditions	Only appropriate estimate of the surface settlement and lining stresses can be obtained
Chambon <i>et al.</i> (1991)	Rigid tube with flexible face	Used to study failure mechanisms, face stability of shallow tunnels	Does not provide information on the surface settlements behind the tunnel face
		Tests can be conducted under 1g and centrifuge conditions	
Atkinson <i>et al.</i> (1975)	Pressurised Air Bag	2D and 3D tests that can be conducted under 1g and centrifuge conditions	Used mostly for unlined tunnels
		Used to study tunnel stability and induced ground movements around tunnels	Does not simulate the tunnel face advance
Sharma <i>et al.</i> (2001)	Polystyrene foam and organic solvent	Can be conducted in a centrifuge	Results were less satisfactory when excavation was simulated underwater
		Simulates the tunnel advance process	

<i>References</i>	<i>Method</i>	<i>Advantages and applications</i>	<i>Disadvantages</i>
Love (1984)	Soil Auguring	Simulates the tunnel advance process	Used mostly for cohesive soils
		Easy to operate	Insertion of a shield usually required
			1g only, not easily mechanised for a centrifuge
Nomoto <i>et al.</i> (1999)	Miniature TBM	Conducted in a centrifuge	Expensive
		Simulates the complete tunnelling process	Limited gravitational acceleration (up to 25g) may be applied in centrifuge
Lee & Yoo (2006)	Mechanically adjustable tunnel diameter	Simulates the 2D tunnel excavation process	Manually controlled
		Simple to operate	Limited to 2D models under 1g conditions

**Table 6.1:** Summary of Tunnel Experimentation, (Meguid *et al.*, 2008)

<i>Symbol</i>	<i>Parameter</i>	<i>Value</i>
A	coefficient in relationship for $G'_{\max(nc)}$	1964
N	exponent in relationship for $G'_{\max(nc)}$	0.65
M	exponent in relationship for $G'_{\max(oc)}$	0.2
$\kappa$	average gradient of swelling line in $v:\ln p'$ space	0.035
$\lambda$	gradient of compression line in $v:\ln p'$ space	0.18
M	stress ratio at critical state ( $q':p'$ )	0.89
$\Gamma$	specific volume at critical state when $p'=1\text{kPa}$	2.994
N	specific volume on INCL when $p'=1\text{kPa}$	3.05
$\phi'_c$	critical state angle of shearing resistance	$23^\circ$
$\gamma$	unit weight of soil (saturated for clay)	$17.5 \text{ (kN/m}^3\text{)}$
$\gamma_w$	unit weight of water	$9.81 \text{ (kN/m}^3\text{)}$

**Table 6.2:** Speswhite kaolin clay properties (Grant, 1998)



<i>Date</i>	<i>Test ID</i>	<i>Fluid</i>	<i>Volume extracted (%)</i>	<i>C/D</i>	<i>Spacing (D)</i>	<i>Consolidation stress (kPa)</i>	<i>First tunnel?</i>	<i>Notes</i>
31/03/2010	SD1	Air	to collapse	3	/	500	/	ok
05/05/2010	SD2	Air	to collapse	2	/	500	/	ok
02/09/2010		Water	3	2	/	500	/	LVDTs not responding - TEST FAILED
05/10/2010	SD3	Water	3	2	/	500	/	ok
18/03/2011	SD4	Water	/	3	/	500	/	TEST FAILED
05/04/2011		Water	/	2	1.5	500	/	Centrifuge vibrating - TEST FAILED
10/05/2011	SD5	Water	3	2	1.5	500	LHT	Tunnels not filled pre-spin up - TEST FAILED
24/05/2011	SD6	Water	3	2	1.5	500	RHT	RHT transducer not plugged in
31/05/2011	SD7	Water	3	2	1.5	350	LHT	Solenoid 3 not working correctly - TEST FAILED
07/06/2011	SD8	Water	3	2	1.5	350	RHT	Solenoid 3 not working correctly, extracted water from both tunnels first - TEST FAILED
12/07/2011	SD9	Water	3	2	1.5	500	LHT	ok - slightly weaker soil measured after testing then expected

<i>Date</i>	<i>Test ID</i>	<i>Fluid</i>	<i>Volume extracted (%)</i>	<i>C/D</i>	<i>Spacing (D)</i>	<i>Consolidation stress (kPa)</i>	<i>First tunnel?</i>	<i>Notes</i>
28/07/2011	SD10	Water	3	2	1.5	500	RHT	ok
16/08/2011	SD11	Water	3	2	3	500	LHT	ok - poor quality of Image Analysis data
31/08/2011	SD12	Water	3	2	4.5	500	RHT	ok
20/09/2011	SD13	Water	5	2	1.5	500	LHT	ok
04/10/2011	SD14	Water	5	2	3	500	RHT	ok
09/10/2011	SD15	Water	5	2	4.5	500	RHT	LHT transducer not working
30/11/2011		Water	/	2/3.5	1.5 OFFSET	500	/	Data logger stopped working - TEST FAILED
17/07/2012	SD16	Water	3	2/3.5	1.5 OFFSET	500	UPPER	Solenoid stopped working at 100g - TEST PERFORMED AT 50g
31/07/2012	SD17	Water	3	2/3.5	3D OFFSET	500	LOWER	Ok but data logger fan malfunctioned
17/08/2012	SD18	Water	3	2/3.5	1.5 OFFSET	500	LOWER	Solenoid stopped working at 100g

**Table 7.1:** Summary of Tests undertaken

<i>Test ID</i>	<i>Z<sub>0</sub> (mm)</i>	<i>i (mm)</i>	<i>K</i>	<i>S<sub>max</sub> (μm)</i>	<i>V<sub>L</sub> (%)</i>
SD2	100.00	62.95	0.50	-370.73	2.98
SD3	100.00	67.81	0.54	-354.05	3.06

**Table 8.1:** Summary of parameters from single tunnel tests

<i>Test ID</i>	<i>Correlation Factors</i>		
	<i>First Tunnel</i>	<i>Second Tunnel</i>	<i>Twin Tunnel</i>
SD2	0.055	NA	NA
SD3	0.041	NA	NA
SD10	0.025	0.080	0.070
SD11	0.030	0.082	0.082
SD12	0.048	0.065	0.087
SD13	0.060	0.112	0.208
SD14	0.079	0.086	0.126
SD15	0.084	0.085	0.144
SD17	0.031	0.090	0.100
SD18	0.030	0.069	0.074

**Table 8.2:** Summary of correlation factors

1.5D								
3% (Test10Wt) RHT 1st					5% (Test13Wt) LHT 1st			
	<i>Tunnel A</i>		<i>Tunnel B</i>		<i>Tunnel A</i>		<i>Tunnel B</i>	
			Towards*	Away**			Towards*	Away**
<b>S<sub>max</sub> (μm) =</b>	-259.625	-263.029	-271.953	-274.984	-386.025	-388.063	-429.947	-440.996
<b>K =</b>	0.55	0.54	0.70	0.54	0.56	0.55	0.71	0.57
<b>V<sub>L</sub> (%) =</b>	2.80	2.80	3.80	3.00	4.31	4.31	6.10	5.00
	2.80		<b>3.40</b>		4.31		<b>5.56</b>	

3D								
3% (Test11Wt) RHT 1st					5% (Test14Wt) LHT 1st			
	<i>Tunnel A</i>		<i>Tunnel B</i>		<i>Tunnel A</i>		<i>Tunnel B</i>	
			Towards*	Away**			Towards*	Away**
<b>S<sub>max</sub> (μm) =</b>	-217.415	-219.722	-282.178	-272.374	-408.029	-404.662	-426.595	-479.894
<b>K =</b>	0.59	0.60	0.58	0.60	0.60	0.60	0.59	0.66
<b>V<sub>L</sub> (%) =</b>	2.60	2.61	3.30	3.30	4.90	4.90	5.1	6.3
	2.61		<b>2.86</b>		4.86		<b>5.62</b>	

4.5D								
3% (Test12Wt) RHT 1st					5% (Test15Wt) RHT 1st			
	<i>Tunnel A</i>		<i>Tunnel B</i>		<i>Tunnel A</i>		<i>Tunnel B</i>	
			Towards*	Away**			Towards*	Away**
<b>S<sub>max</sub> (μm) =</b>	-244.531	-239.660	-245.576	-251.899	-455.002	-460.789	-497.961	-489.804
<b>K =</b>	0.55	0.51	0.55	0.56	0.57	0.55	0.55	0.59
<b>V<sub>L</sub> (%) =</b>	2.70	2.40	2.70	2.80	5.10	5.20	5.70	5.50
	2.55		<b>2.75</b>		5.15		<b>5.70</b>	

OFFSET								
2.12D (Test18Wt) LOWER 1st					2.7D (Test17Wt) LOWER 1st			
	<i>Tunnel A</i>		<i>Tunnel B</i>		<i>Tunnel A</i>		<i>Tunnel B</i>	
			Towards*	Away**			Towards*	Away**
$S_{\max} (\mu\text{m}) =$	-188.193	-188.193	-303.965	-261.663	-203.229	-203.316	-316.028	-297.286
$K =$	0.46	0.46	1.09	0.54	0.47	0.47	0.85	0.55
$V_L (\%) =$	2.74	2.74	6.60	2.80	3.07	3.07	5.40	3.30
	2.74		3.21		3.07		3.51	

**Table 9.1:** Summary of surface parameters from twin-tunnel tests

\*parameters from fitting curves to the settlements towards the existing tunnel (Tunnel A)

\*\*parameters from fitting curves to the settlements away from the existing tunnel (Tunnel A)

	<b>Test13Wt - 1.5D (5%)</b>							
	<i>Tunnel A</i>				<i>Tunnel B</i>			
	$S_{\max}$	$K_{(TO)}$	$K_{(AW)}$	$V_L$ (%)	$S_{\max}$	$K_{(TO)}$	$K_{(AW)}$	$V_L$ (%)
<b>Near-surface</b>	-370.290	0.50	0.50	<b>3.44</b>	-485.615	0.50	0.50	<b>4.58</b>
<b>1D Surface</b>	-392.206	0.58	0.58	<b>2.73</b>	-485.483	0.67	0.67	<b>3.91</b>
<b>1.5D Surface</b>	-435.904	0.88	0.88	<b>3.04</b>	-542.803	0.90	0.90	<b>3.86</b>

	<b>Test11Wt - 3D (3%)</b>							
	<i>Tunnel A</i>				<i>Tunnel B</i>			
	$S_{\max}$	$K_{(TO)}$	$K_{(AW)}$	$V_L$ (%)	$S_{\max}$	$K_{(TO)}$	$K_{(AW)}$	$V_L$ (%)
<b>Near-surface</b>	-230.355	0.58	0.58	<b>2.42</b>	-289.851	0.51	0.51	<b>2.71</b>
<b>1D Surface</b>	-262.629	0.54	0.54	<b>1.70</b>	-328.702	0.48	0.48	<b>1.90</b>
<b>1.5D Surface</b>	-424.665	0.59	0.59	<b>2.03</b>	-426.601	0.68	0.68	<b>2.34</b>

	<b>Test15Wt - 4.5D (5%)</b>							
	<i>Tunnel A</i>				<i>Tunnel B</i>			
	$S_{\max}$	$K_{(TO)}$	$K_{(AW)}$	$V_L$ (%)	$S_{\max}$	$K_{(TO)}$	$K_{(AW)}$	$V_L$ (%)
<b>Near-surface</b>	-477.064	0.50	0.50	<b>4.39</b>	-515.823	0.51	0.51	<b>4.80</b>
<b>1D Surface</b>	-541.084	0.58	0.58	<b>3.79</b>	-604.285	0.59	0.59	<b>4.35</b>
<b>1.5D Surface</b>	-625.891	0.72	0.72	<b>3.64</b>	-636.958	0.74	0.74	<b>3.80</b>

	<b>Test18Wt - 2.12D (3%)</b>							
	<i>Tunnel A</i>				<i>Tunnel B</i>			
	$S_{\max}$	$K_{(TO)}$	$K_{(AW)}$	$V_L$ (%)	$S_{\max}$	$K_{(TO)}$	$K_{(AW)}$	$V_L$ (%)
<b>Near-surface</b>	-237.360	0.42	0.42	<b>3.01</b>	-313.937	0.79	0.62	<b>3.70</b>
<b>1D Surface</b>	-231.713	0.50	0.50	<b>2.80</b>	-337.080	0.86	0.70	<b>2.76</b>
<b>1.5D Surface</b>	-291.151	0.47	0.47	<b>2.74</b>	-416.213	1.24	0.86	<b>3.01</b>

	<b>Test17Wt - 2.7D (3%)</b>							
	<i>Tunnel A</i>				<i>Tunnel B</i>			
	$S_{\max}$	$K_{(TO)}$	$K_{(AW)}$	$V_L$ (%)	$S_{\max}$	$K_{(TO)}$	$K_{(AW)}$	$V_L$ (%)
<b>Near-surface</b>	-198.408	0.48	0.48	<b>2.9</b>	-313.455	0.74	0.54	<b>3.47</b>
<b>1D Surface</b>	-215.206	0.55	0.55	<b>2.91</b>	-352.881	0.94	0.67	<b>3.55</b>
<b>1.5D Surface</b>	-228.610	0.63	0.63	<b>2.92</b>	-416.687	1.28	0.81	<b>3.21</b>

**Table 9.2:** Summary of sub-surface parameters from twin-tunnel tests

$_{(TO)}$  - parameters from fitting curves to the settlements towards the existing tunnel (Tunnel A)

$_{(AW)}$  - parameters from fitting curves to the settlements away from the existing tunnel (Tunnel A)

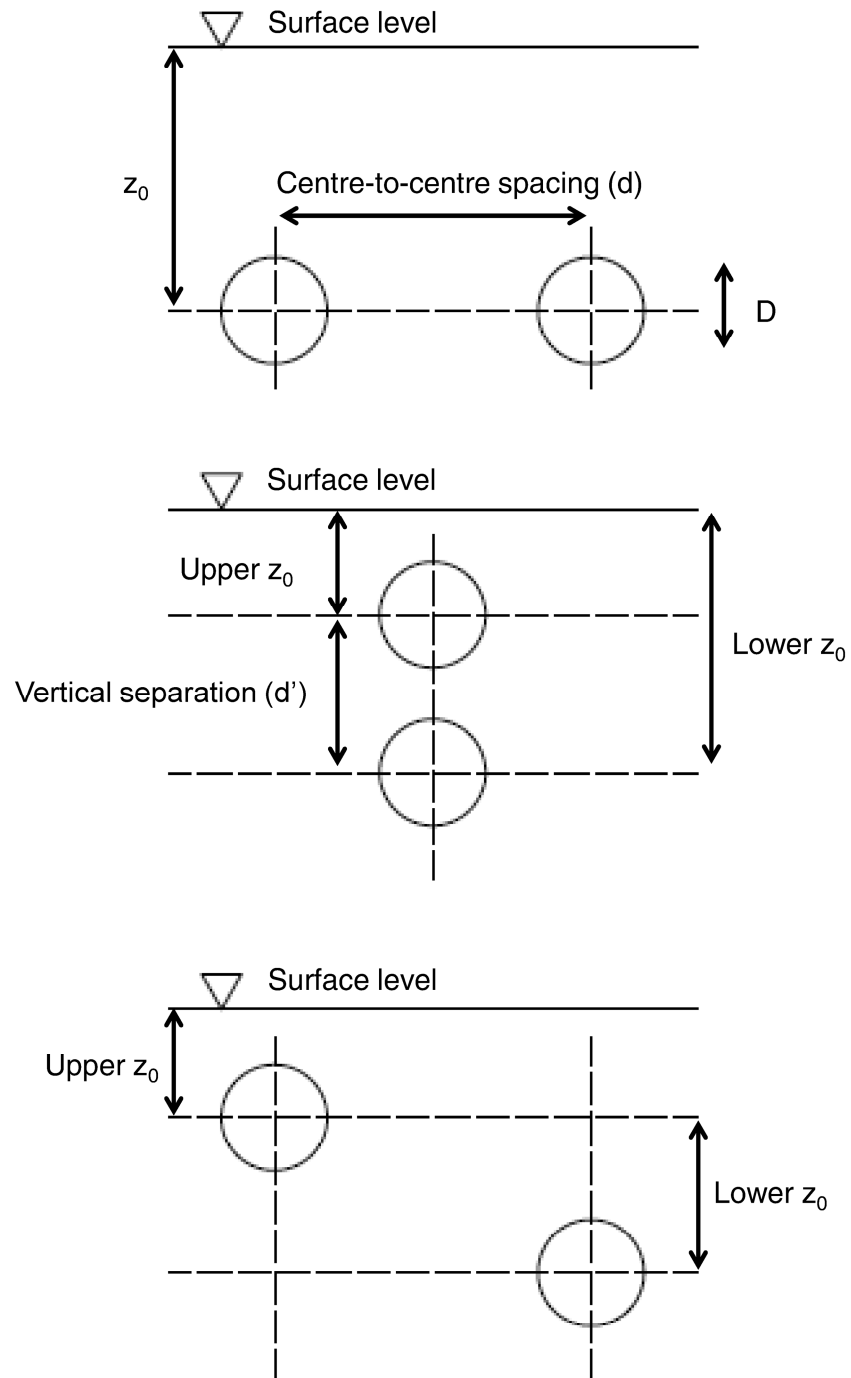
## FIGURES



**Figure 1.1:** Géotechnique artist impression of sub-surface congestion

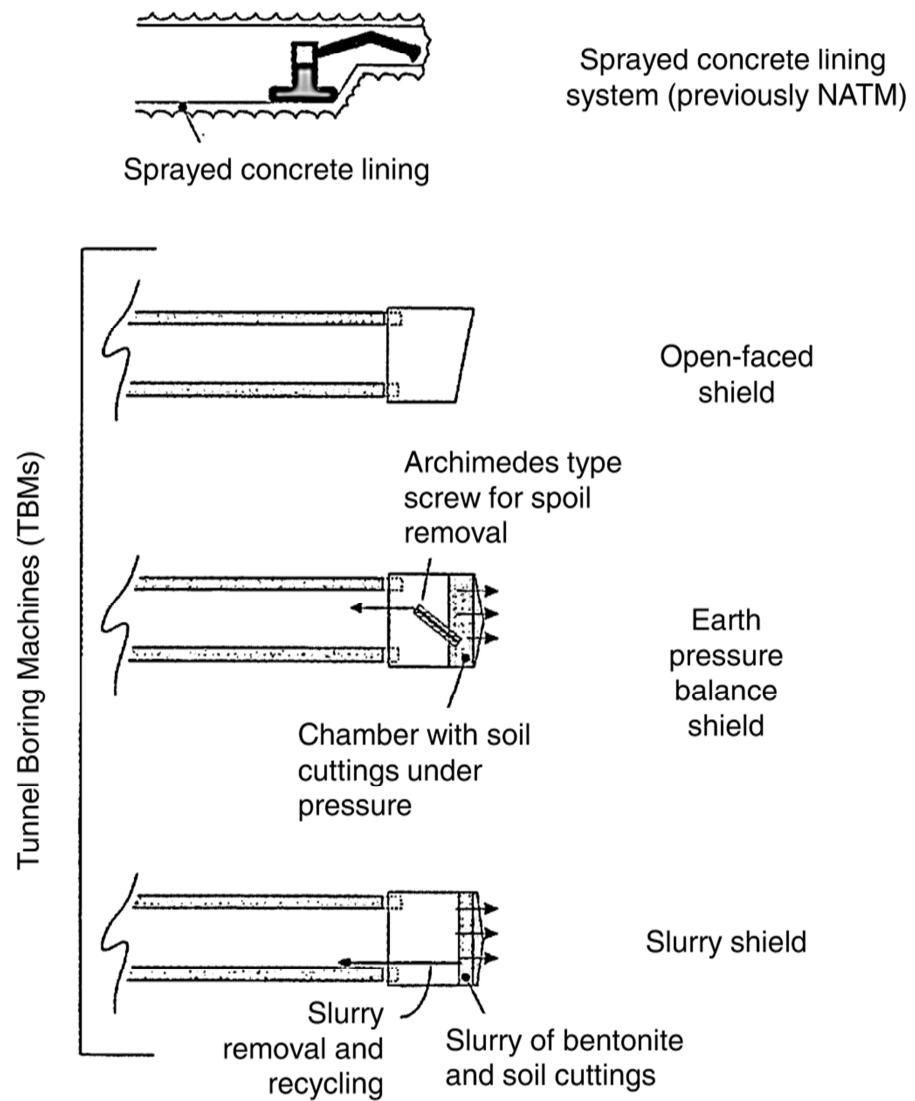
[http://www.eng.cam.ac.uk/news/stories/2009/Royal\\_Society\\_Lecture/](http://www.eng.cam.ac.uk/news/stories/2009/Royal_Society_Lecture/)



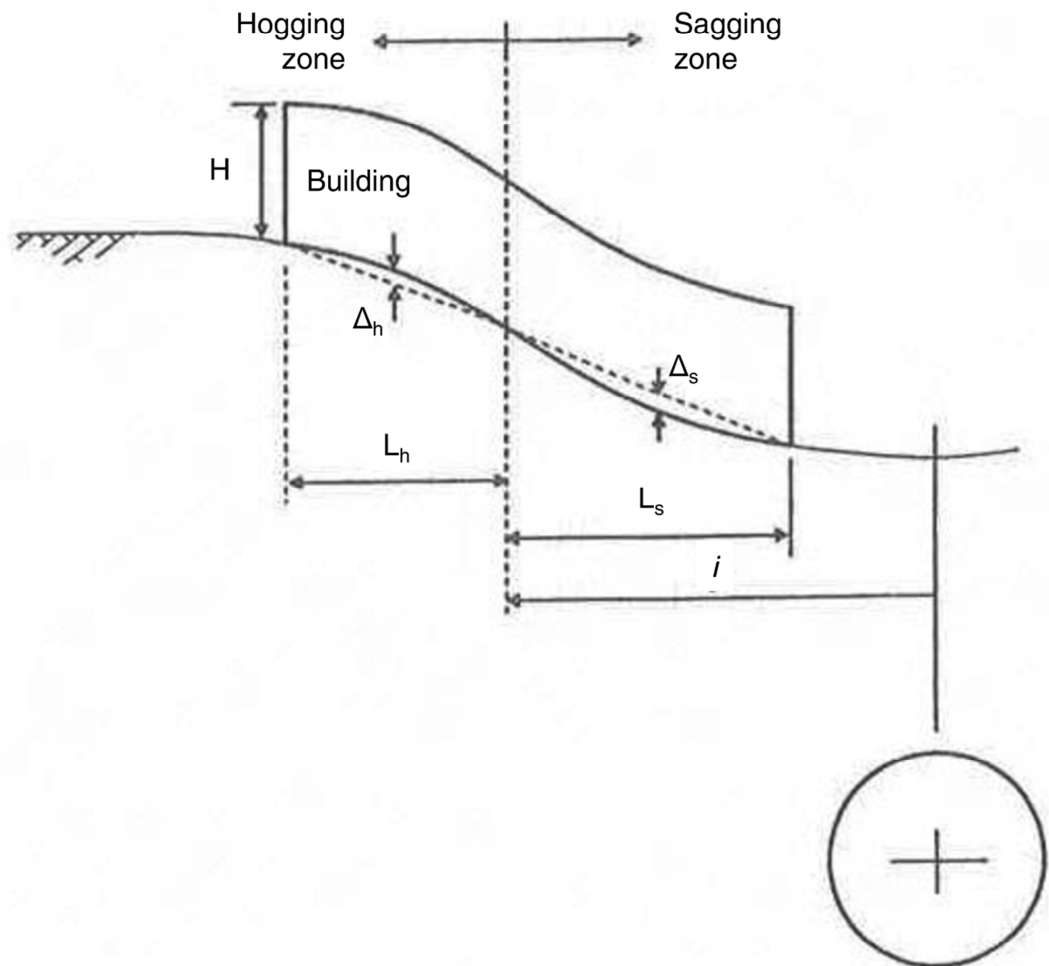


**Figure 1.2:** Idealisations of the three twin-tunnelling scenarios in the y-z plane

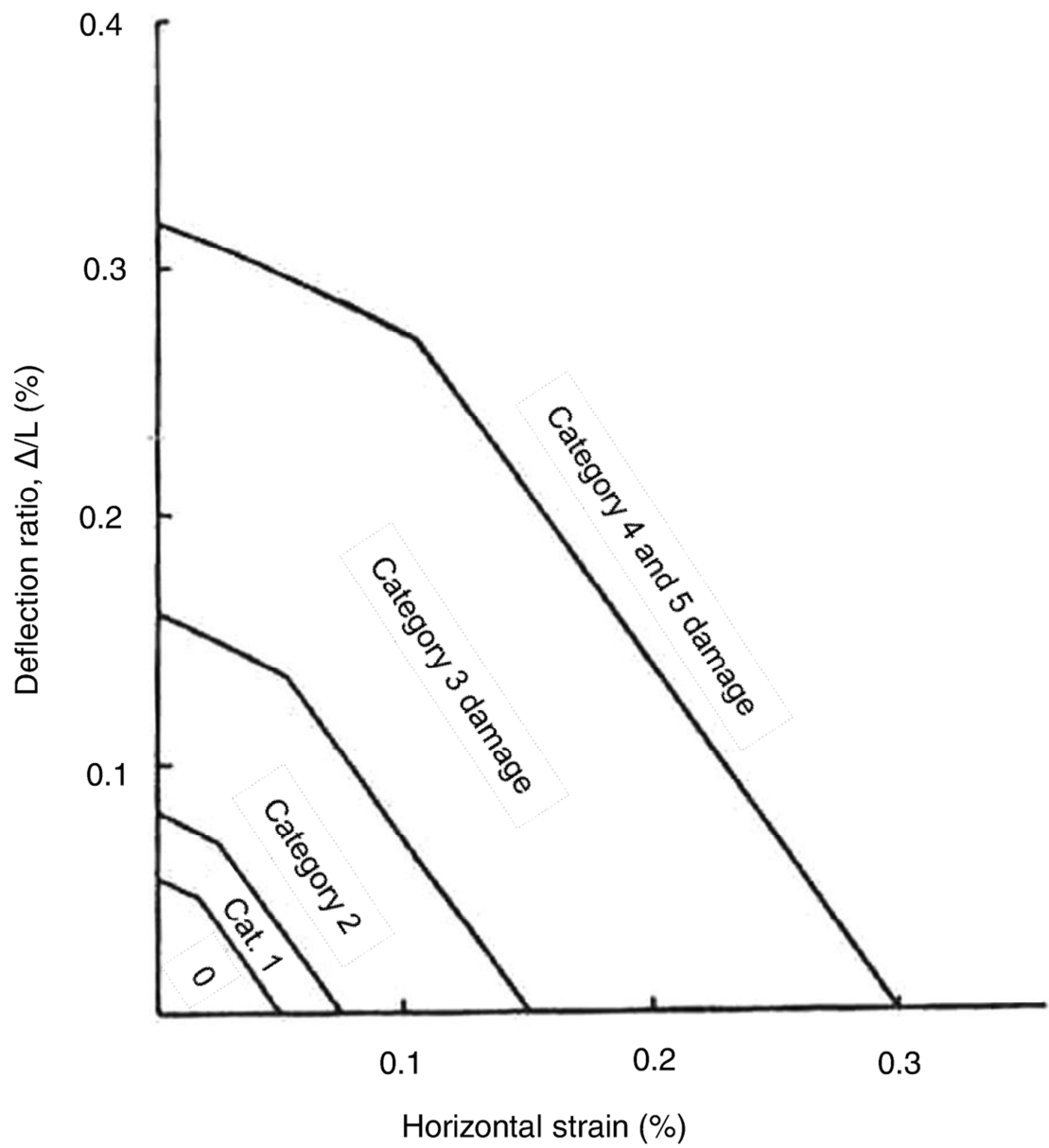
- a) Side-by-side
- b) Stacked or piggy back
- c) Offset



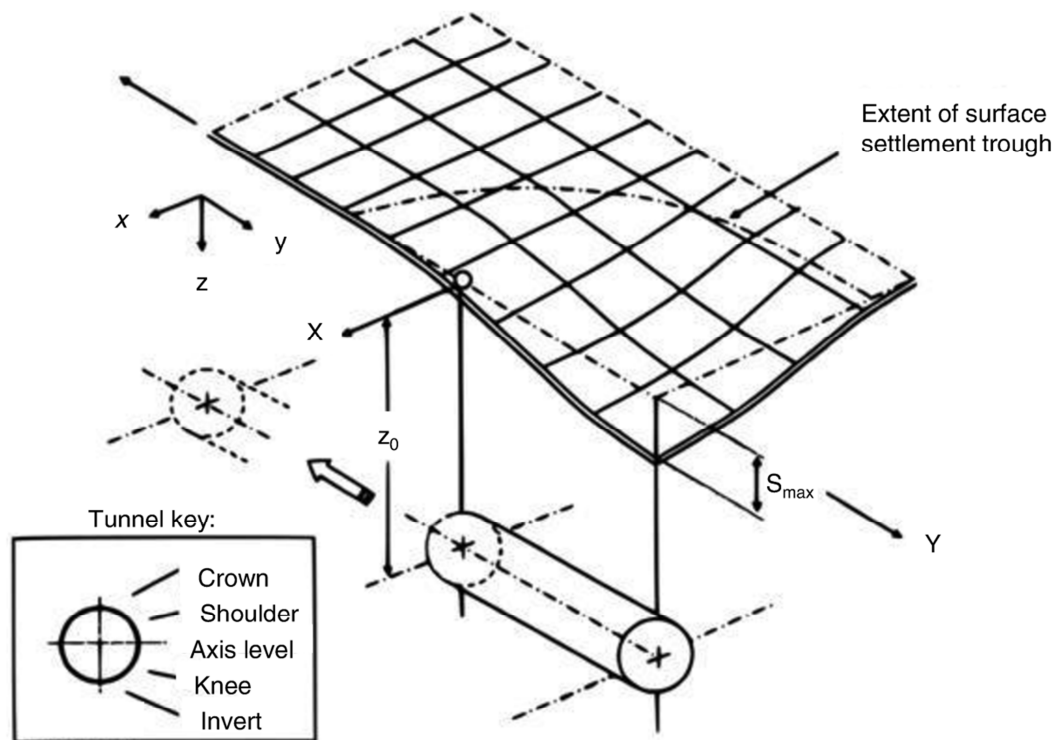
**Figure 2.1:** Schematic diagrams of sprayed concrete lining tunnelling system, conventional shield and tunnel boring machines (Nyren, 1998).



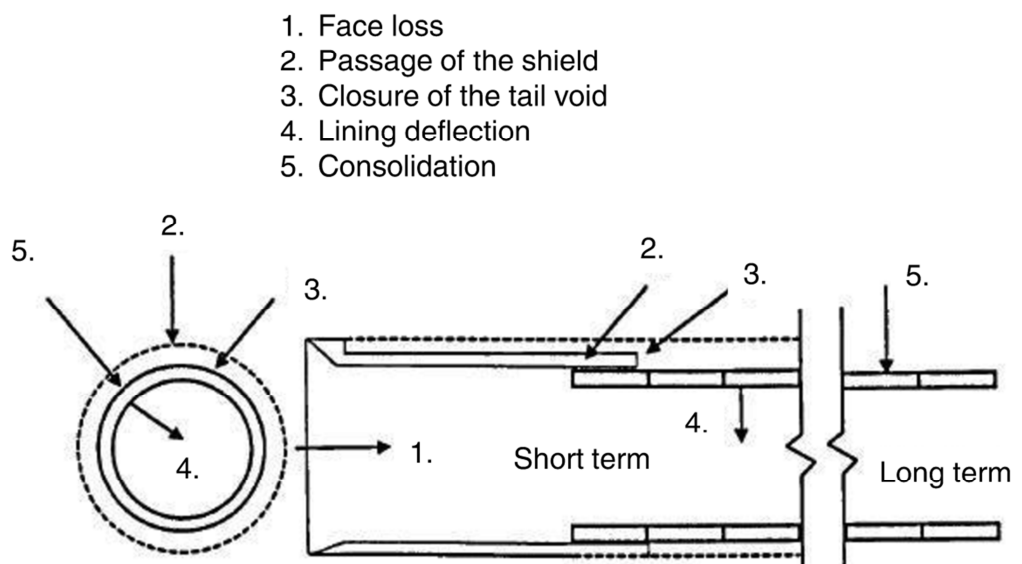
**Figure 2.2:** Hogging or sagging zone and limited by a point of inflexion or extent of settlement trough (Mair *et al.*, 1996)



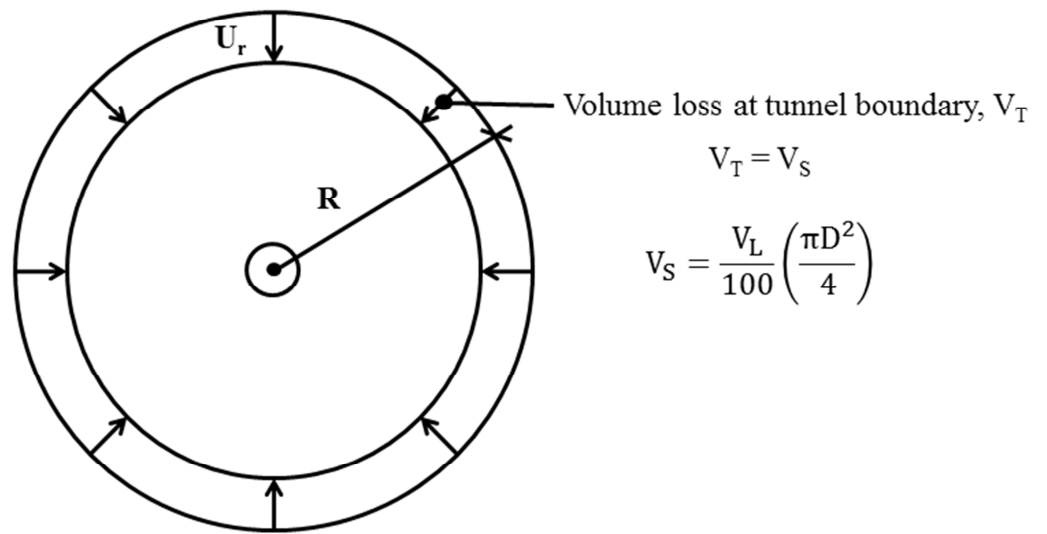
**Figure 2.3:** Damage category chart for  $L/H = 1$ , hogging mode (Mair *et al.*, 1996)



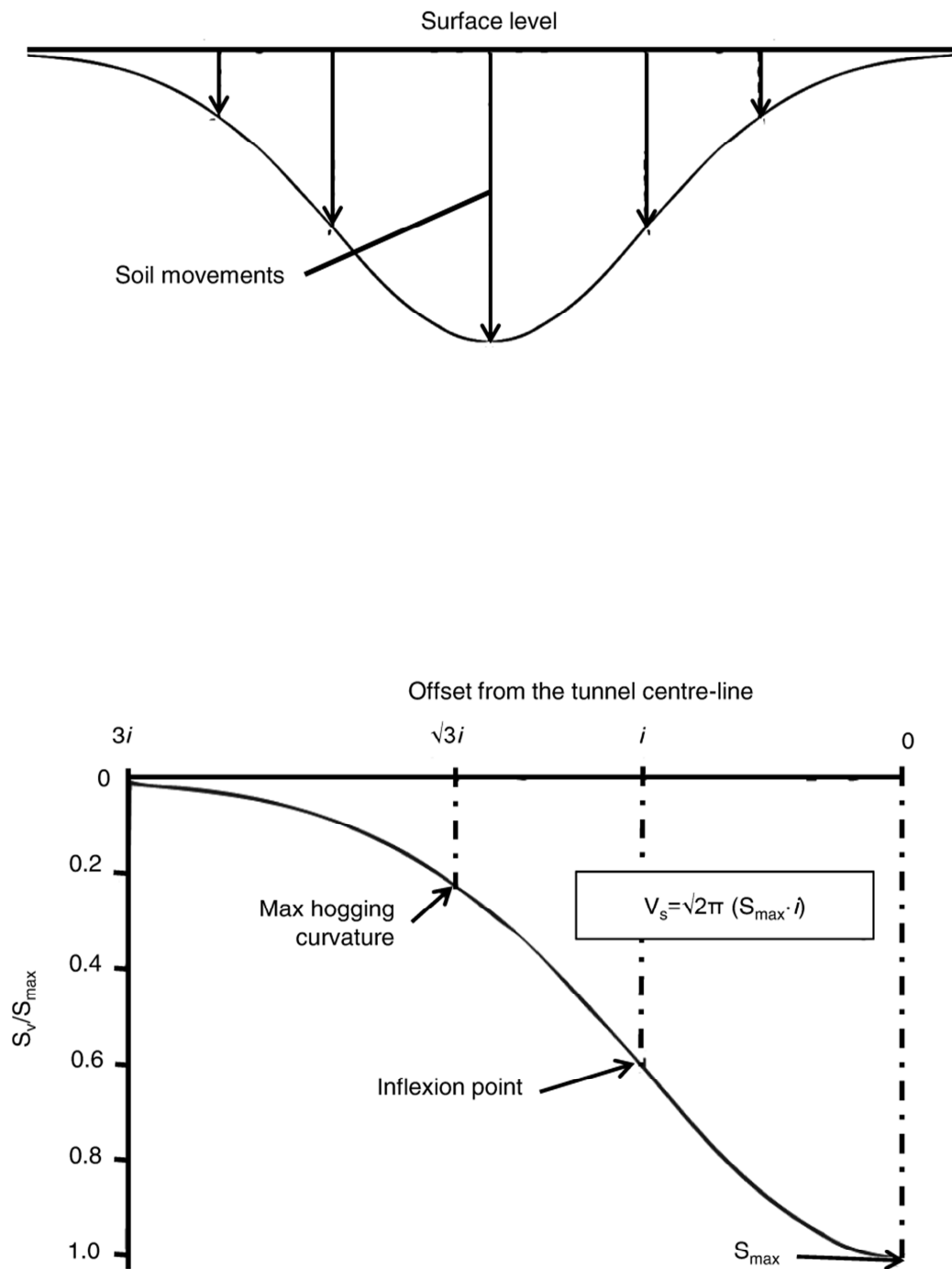
**Figure 3.1:** Settlement above an advancing tunnel heading (Attewell & Yeates, 1984)



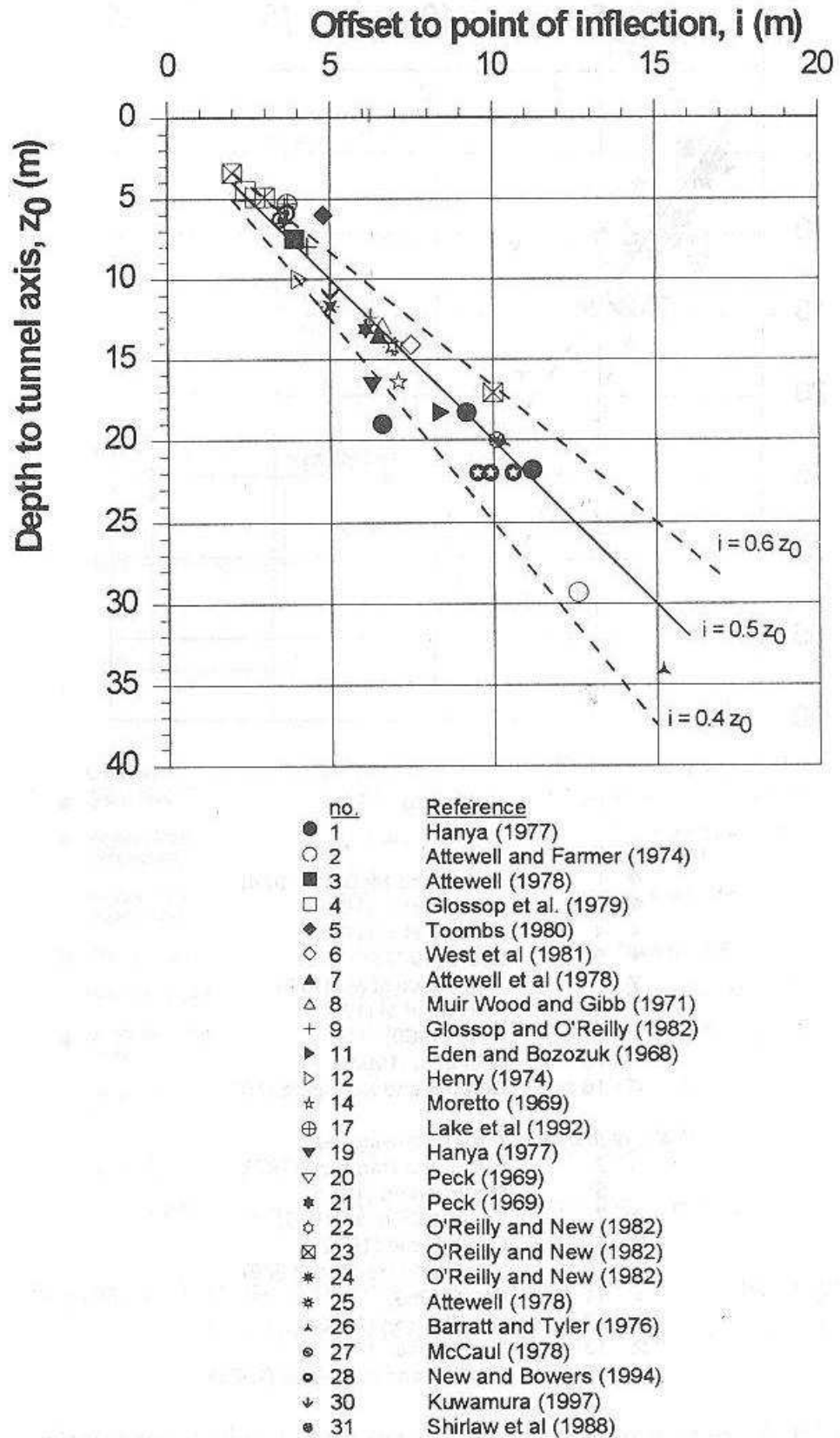
**Figure 3.2:** Sources of tunnelling deformation for a shield driven tunnel (Cording, 1991)



**Figure 3.3:** Volume loss around a circular cavity (after Peck, 1969)

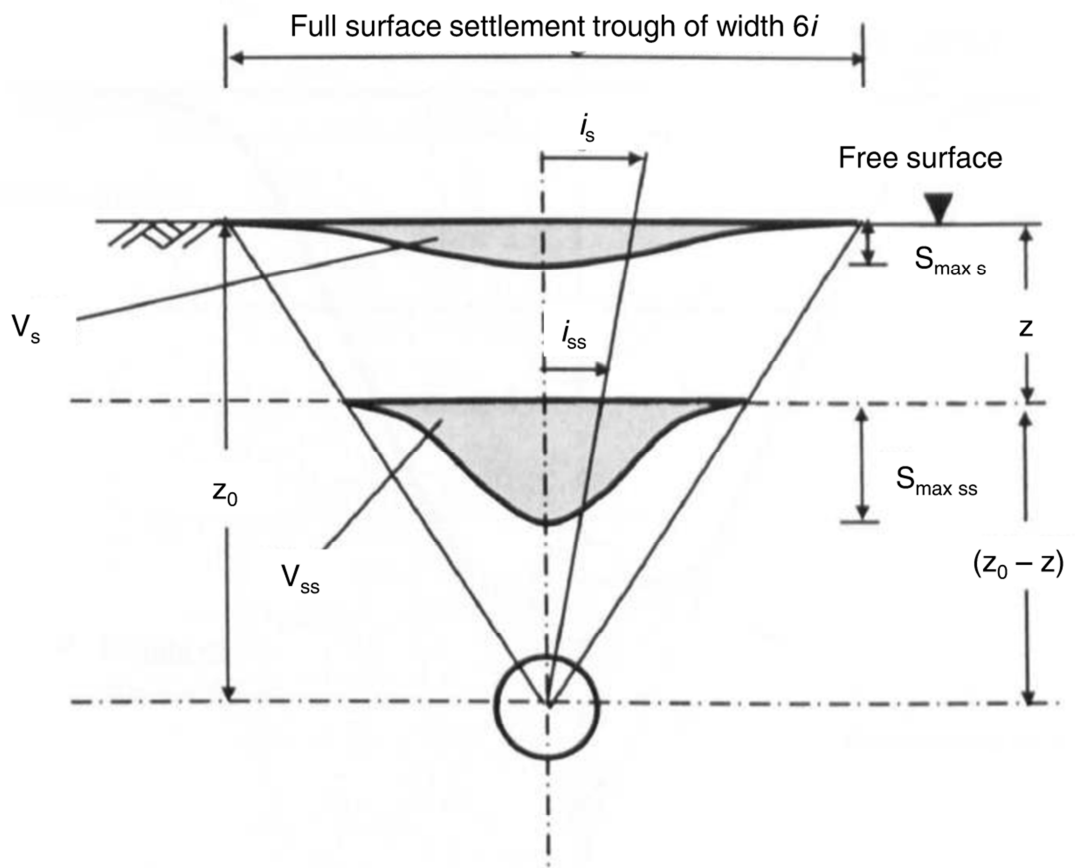


**Figure 3.4:** a) settlement trough (after Peck, 1969) and  
b) Gaussian fit to trough (after O'Reilly & New, 1982)

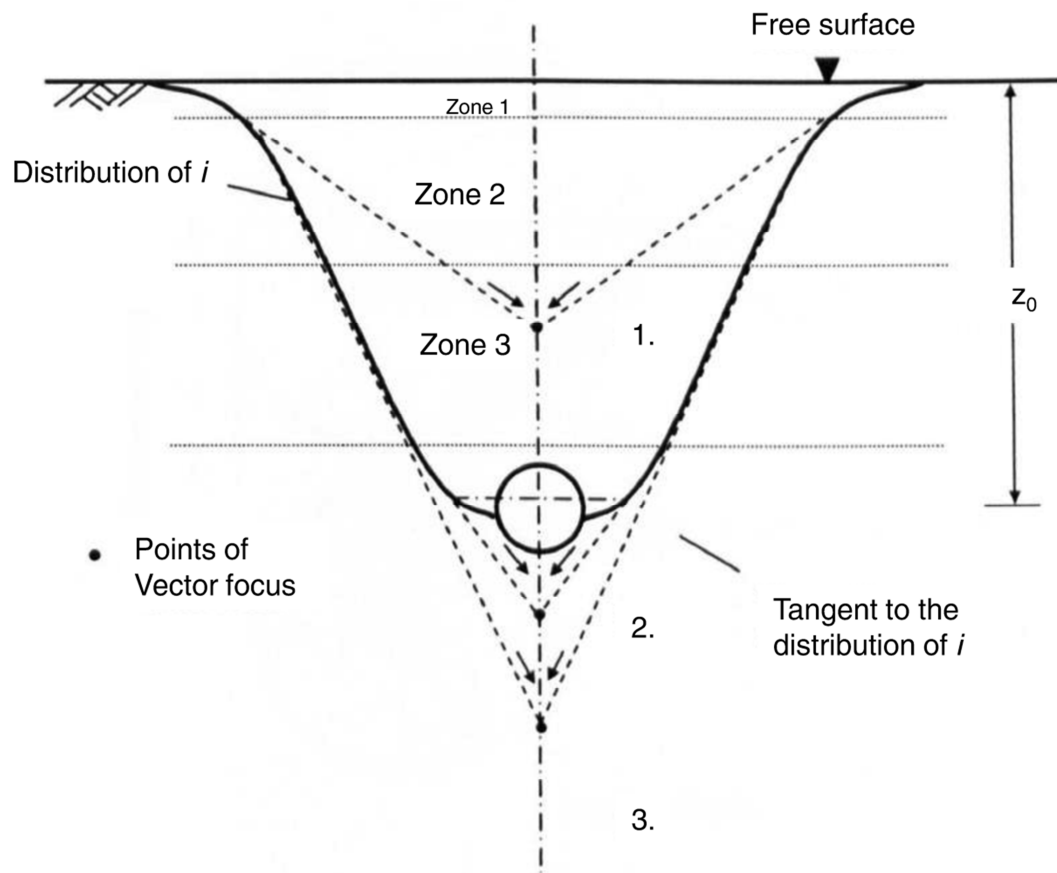


**Figure 3.5:** Variation in surface settlement trough width parameter with tunnels in clay (Mair & Taylor, 1997)

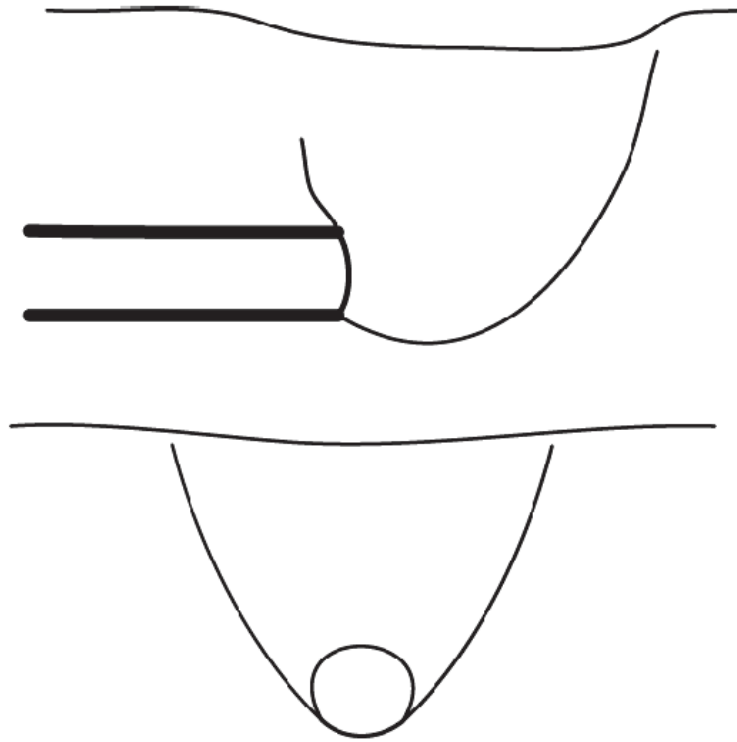




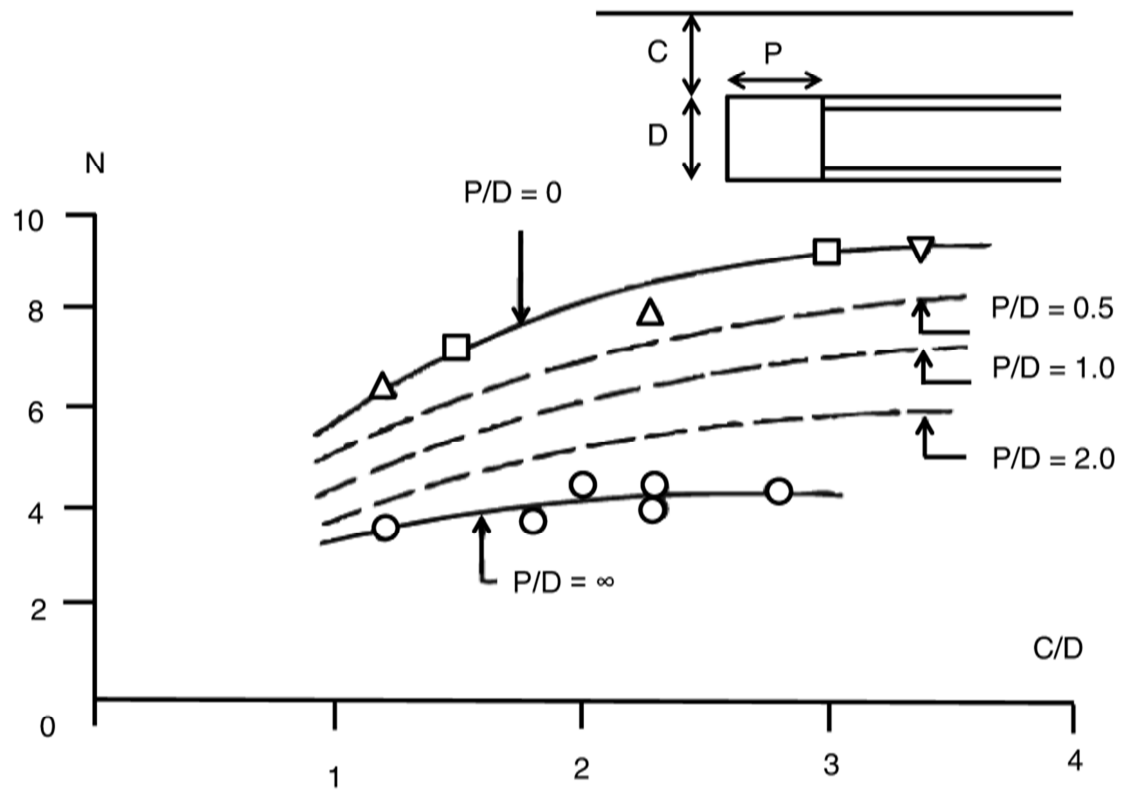
**Figure 3.6:** Settlement troughs with depth (Hunt, 2005 after Mair *et al.*, 1993)



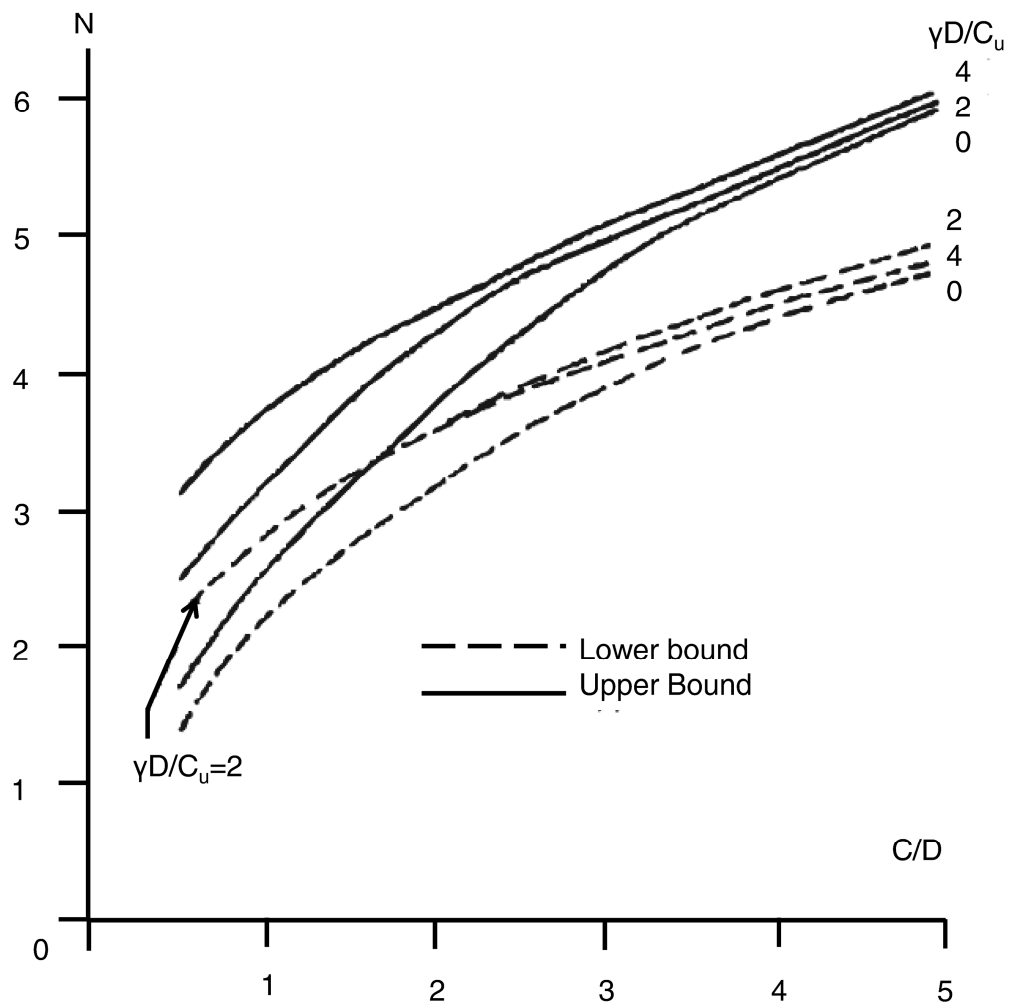
**Figure 3.7:** Vector focus (Grant, 1998)



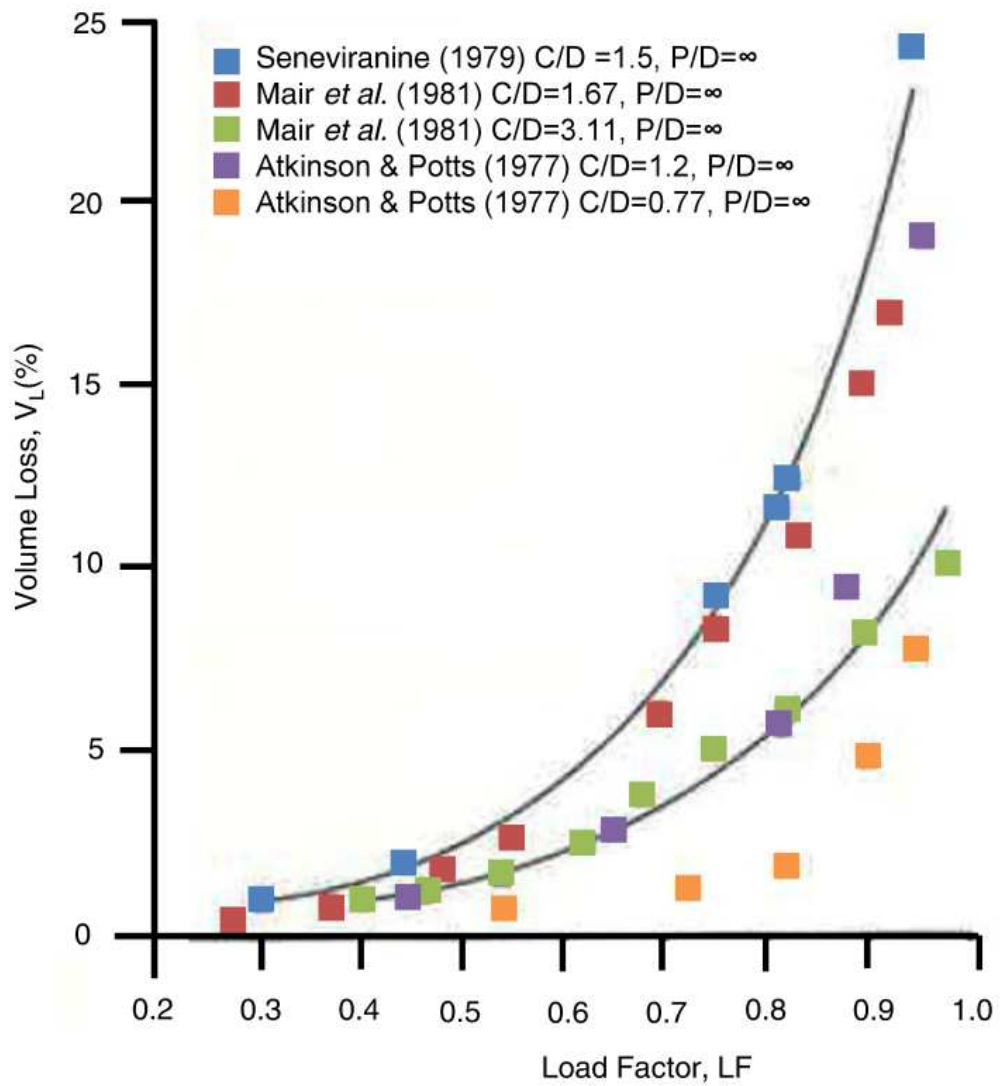
**Figure 3.8:** Observed failure mechanisms based on centrifuge model tests (Mair & Taylor, 1997)



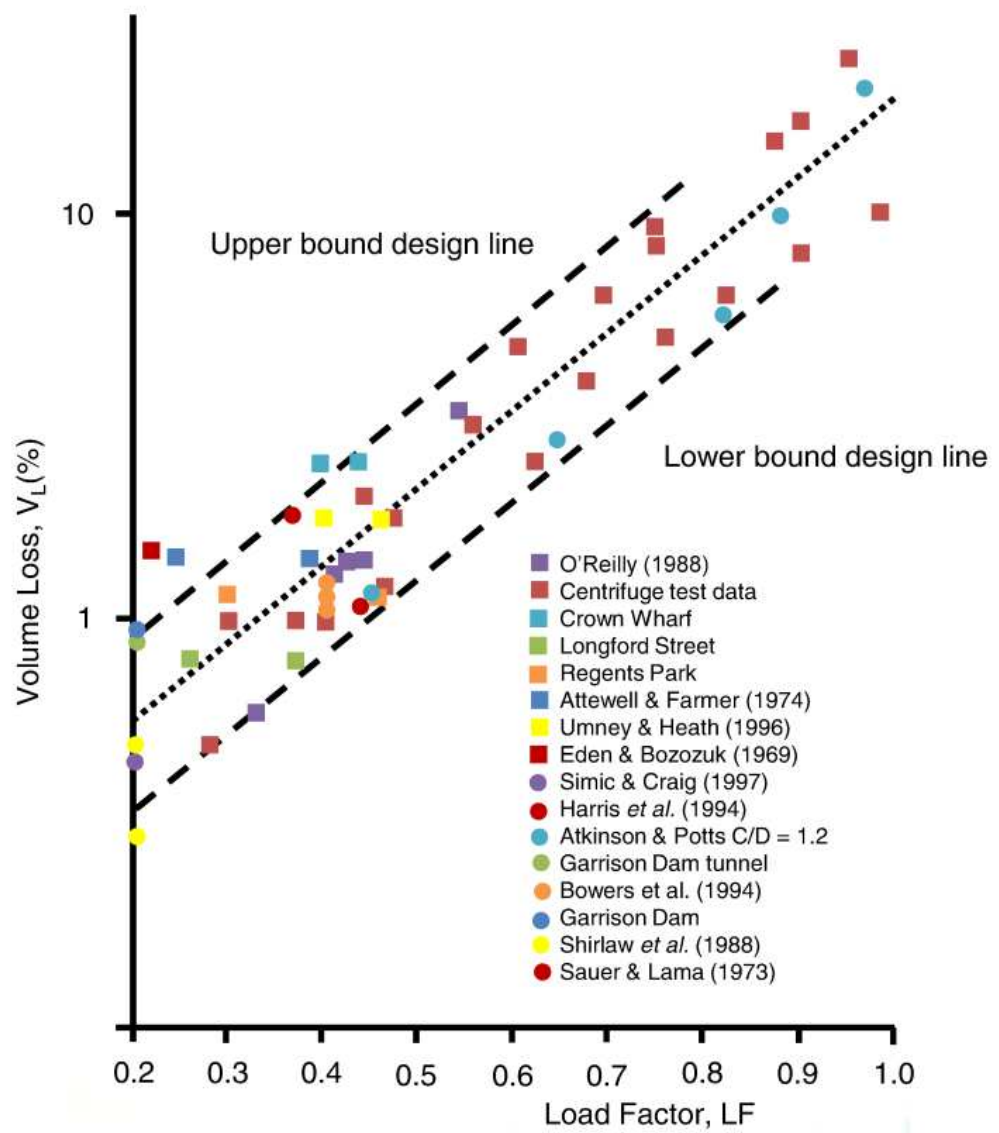
**Figure 3.9:** Dependence of critical stability ratio on tunnel heading geometry (after Mair & Taylor, 1997; Mair, 1979 and Kimura & Mair, 1981)



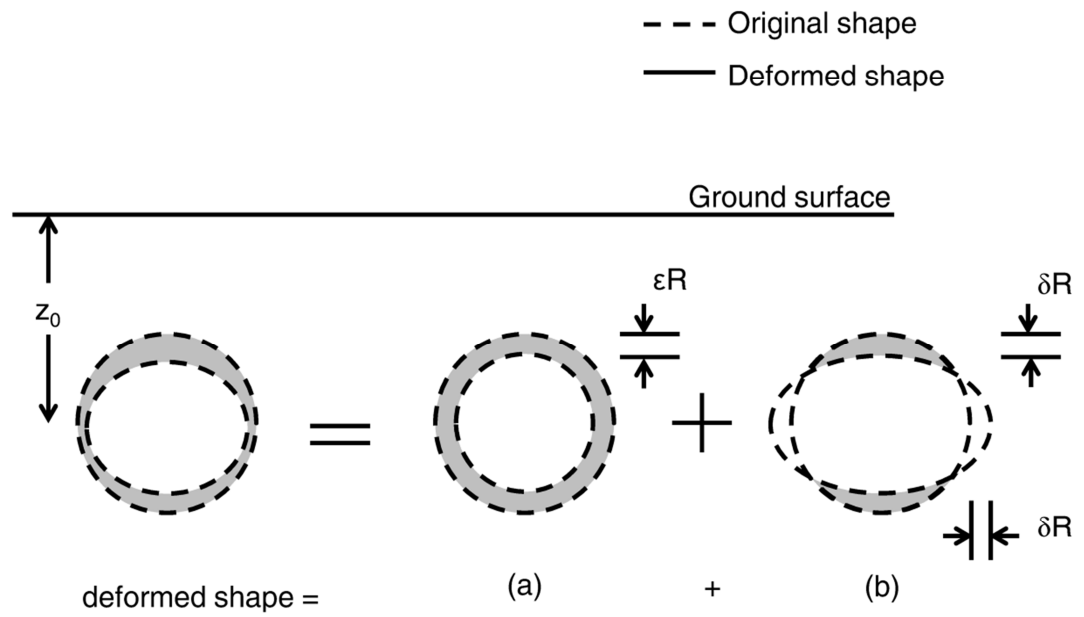
**Figure 3.10:** Upper and lower bound stability ratios for plane strain circular tunnels (after Davis *et al.*, 1980)



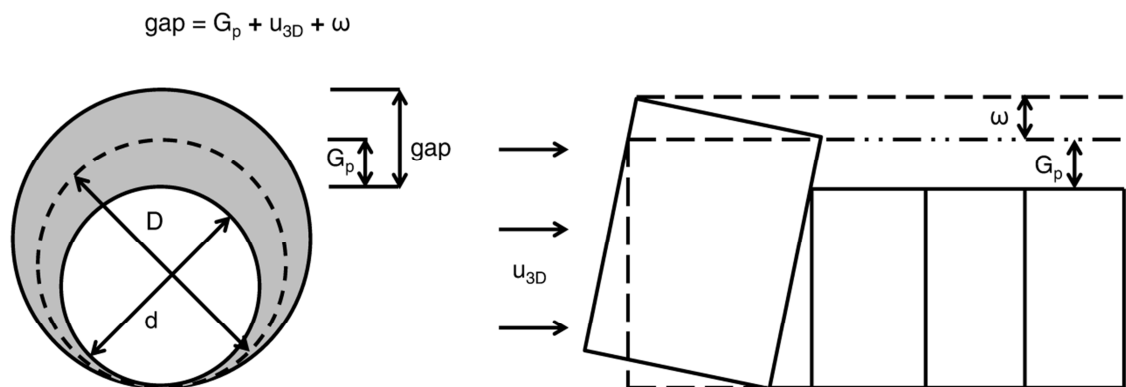
**Figure 4.1:** a) Relationship between volume loss, tunnel heading geometry and stability number within  $C/D$  between 0.77 and 3.11 (after Macklin, 1999)



**Figure 4.1:** b) Upper and lower bound design lines for a relationship between volume loss and load factor for field monitoring data from overconsolidated clay sites (after Macklin, 1999)

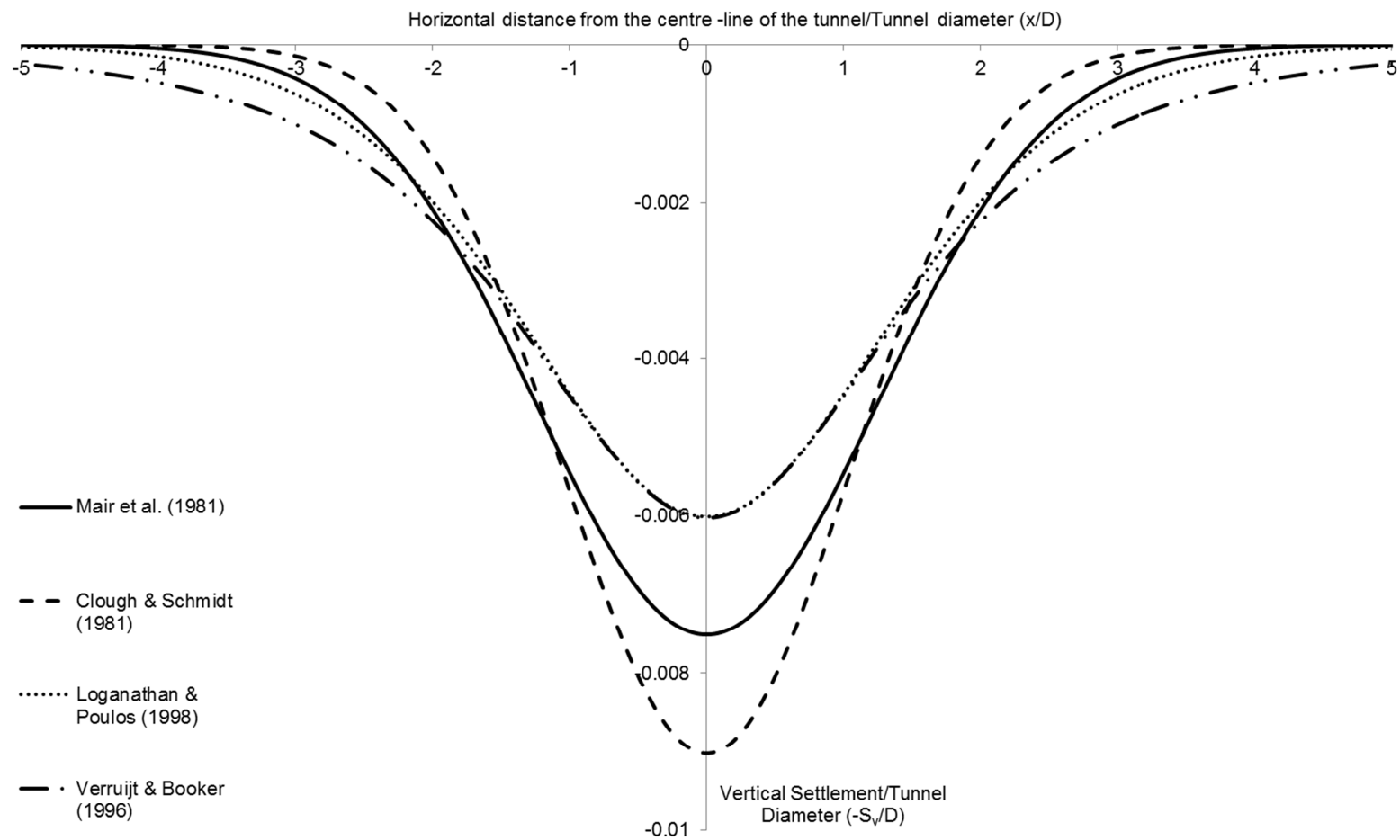


**Figure 4.2:** Deformed tunnel shape given by (a) ground loss and (b) ovalisation (after Verruijt & Booker, 1996)

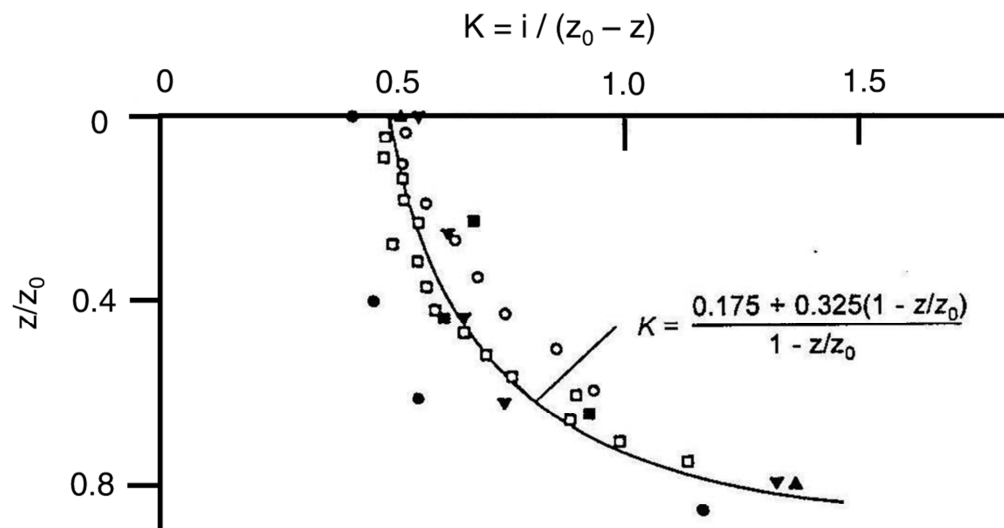


**Figure 4.3:** Definition of Gap parameter (after Rowe *et al.*, 1983)

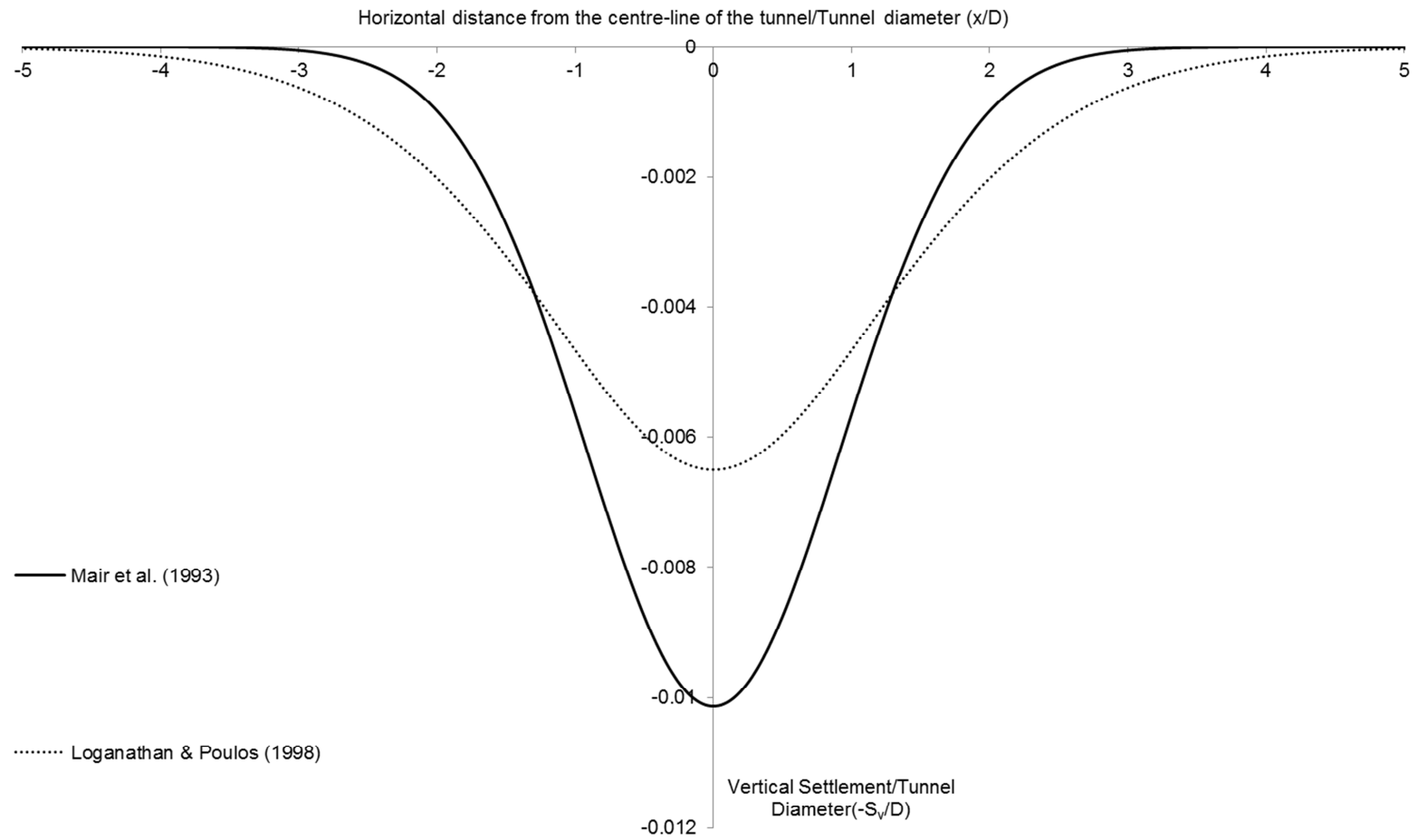




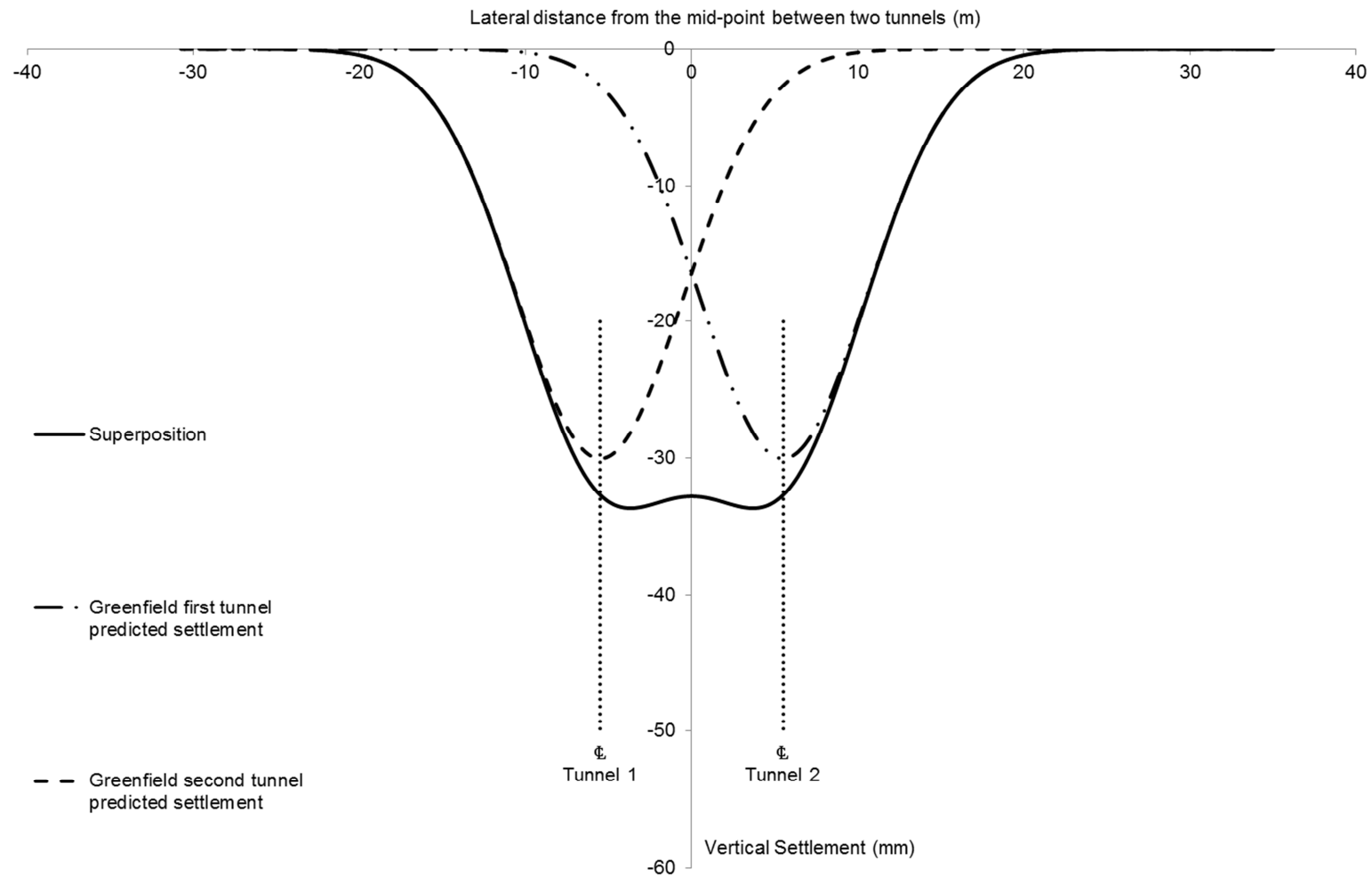
**Figure 4.4:** Comparison of different methods for estimating surface settlement above an unlined shallow tunnel in moderately stiff clay



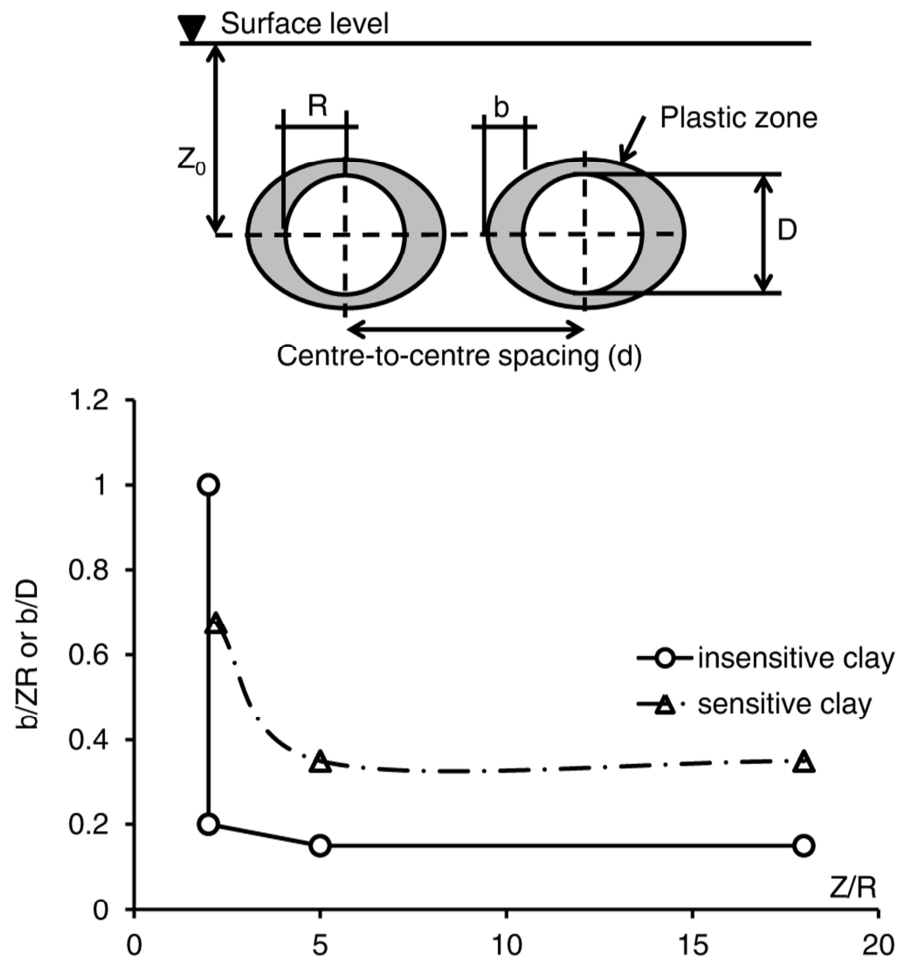
**Figure 4.5:** Variation of  $K$  with depth for sub-surface settlement profiles above tunnels in clay (after Mair *et al.*, 1993)



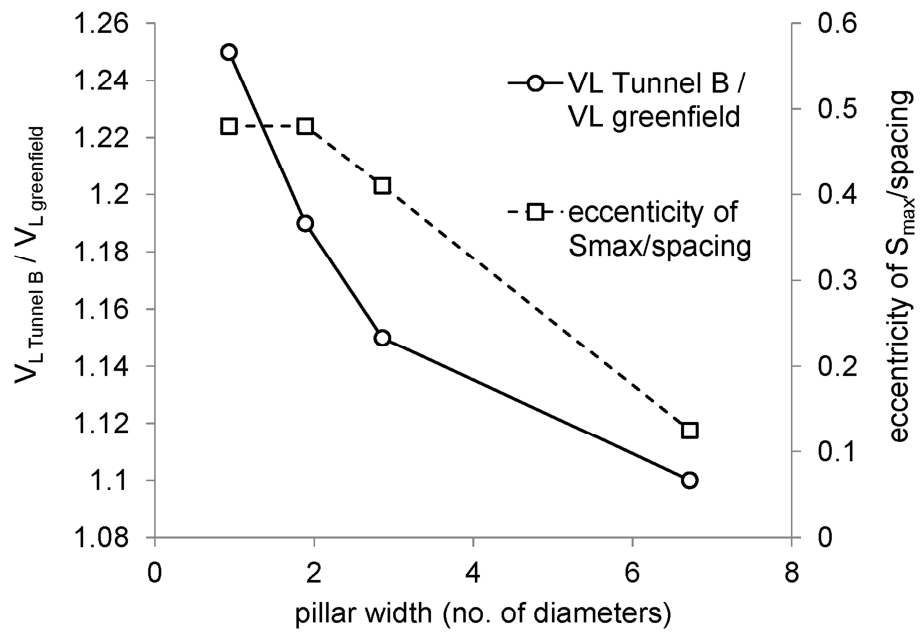
**Figure 4.6:** Comparison of different methods for estimating sub-surface settlement above an unlined shallow tunnel in moderately stiff clay



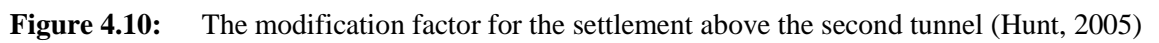
**Figure 4.7:** Example of Superposition method used to predict the surface settlement of two, 4m diameter, tunnels with a cover of 8m



**Figure 4.8:** Plastic zones induced by shield tunnelling in soft ground (after Fang *et al.*, 1994)



**Figure 4.9:** Design charts to find the increase in volume loss of the second tunnel's settlement profile (left) and an eccentricity of the maximum settlement (right). (Divall *et al.*, 2012 after Addenbrooke & Potts, 2001)



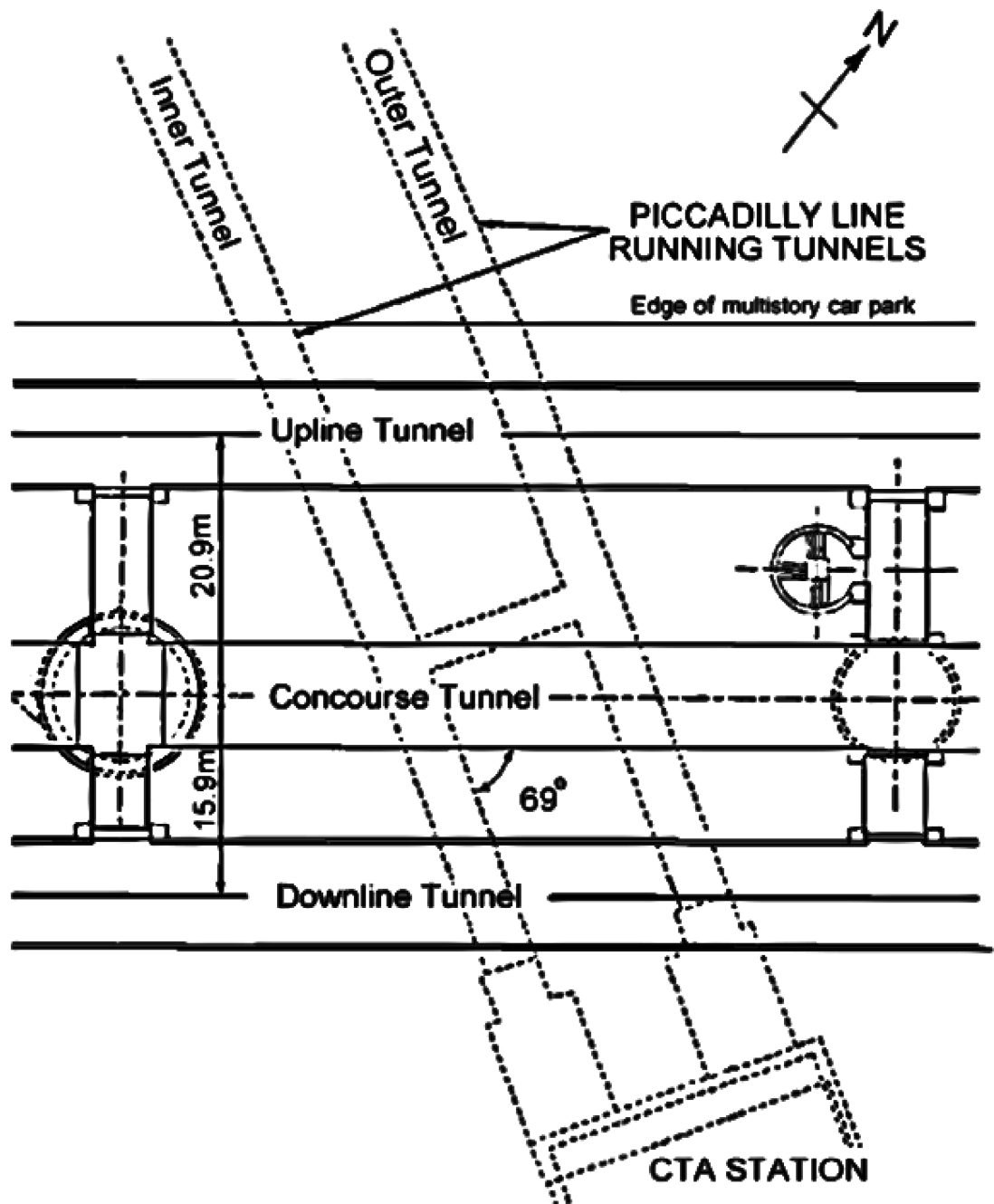


**Figure 4.11:** a) Plan schematic of the Piccadilly Line and Heathrow Express Tunnels



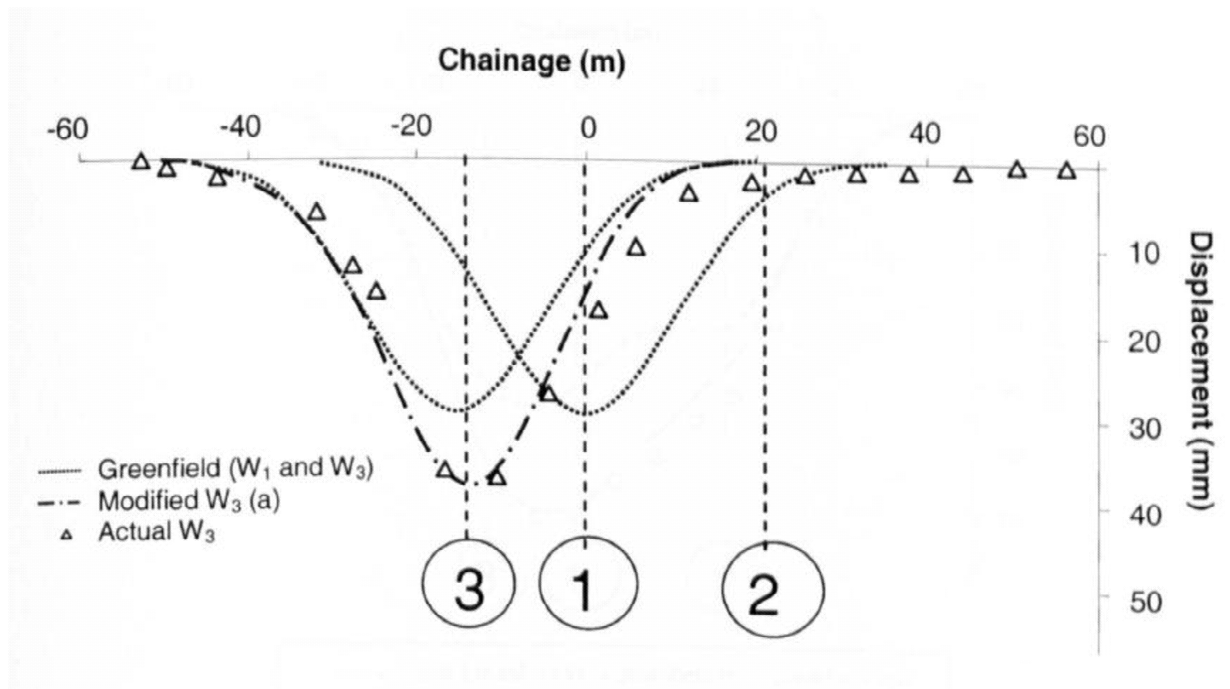


**Figure 4.11:** b) Sub-surface settlement prediction for Tunnel A (1) and Tunnel B (3) of the Heathrow Express tunnels U.K. (Hunt, 2005)

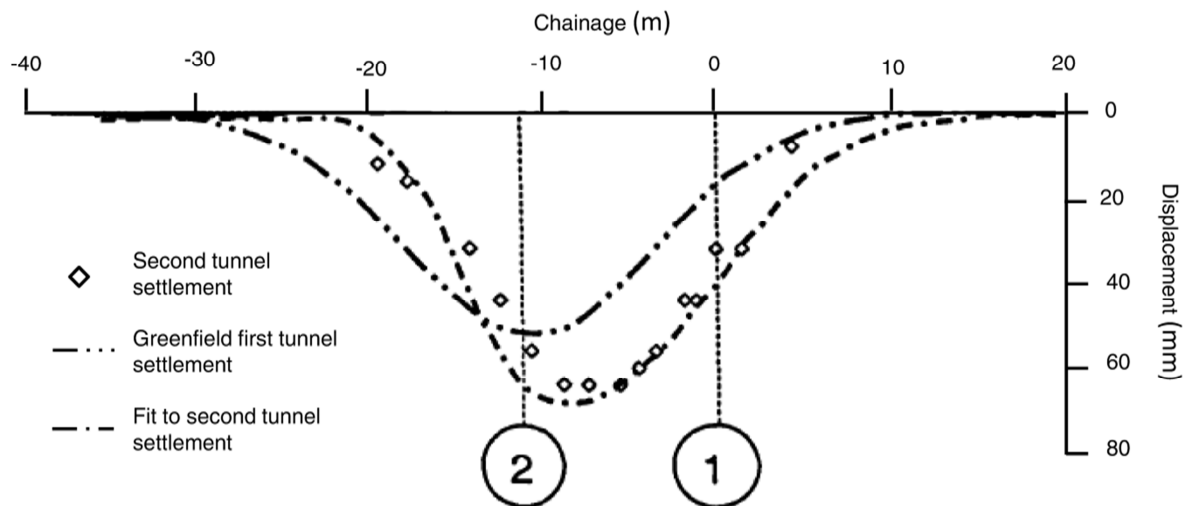


**Figure 4.11:** c) Surface vertical ground displacement predictions for Lafayette Park, U.S.A. (after Cording & Hansmire, 1975)

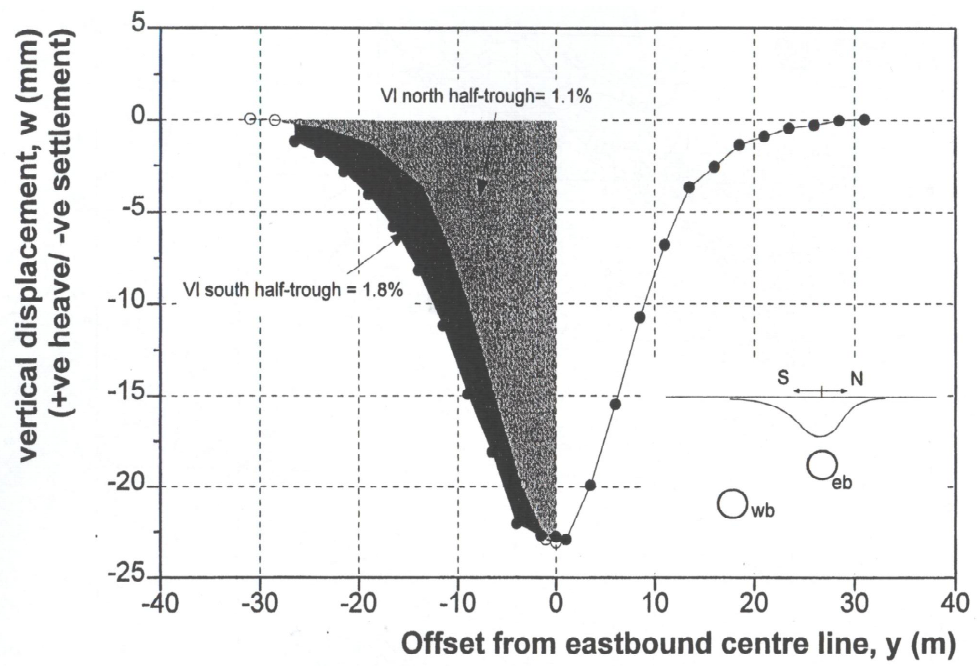


**Figure 4.11:** d) Surface vertical and horizontal ground displacements for St. James Park, U.K. (Nyren, 1998)

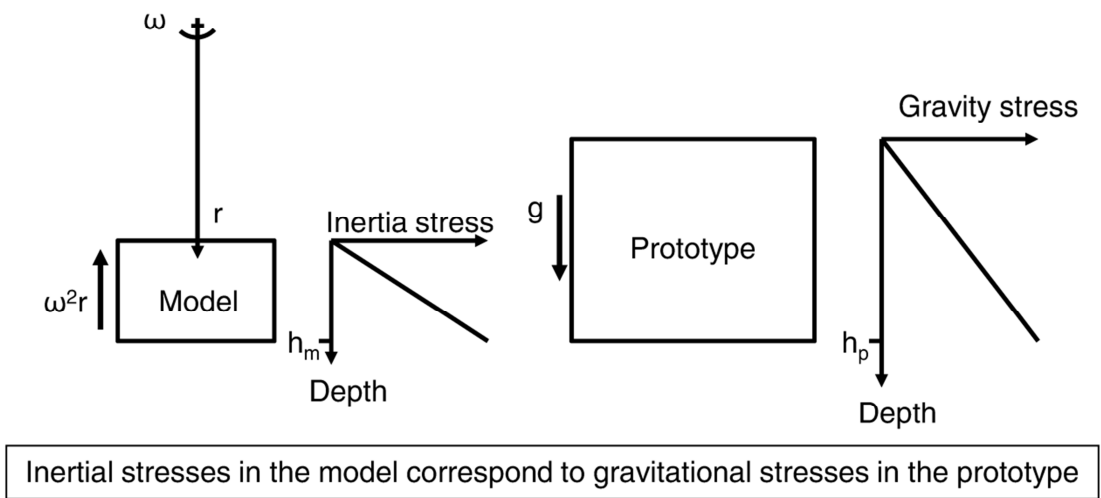


**Figure 5.1:** Principles of centrifuge modelling (after Taylor, 1995)

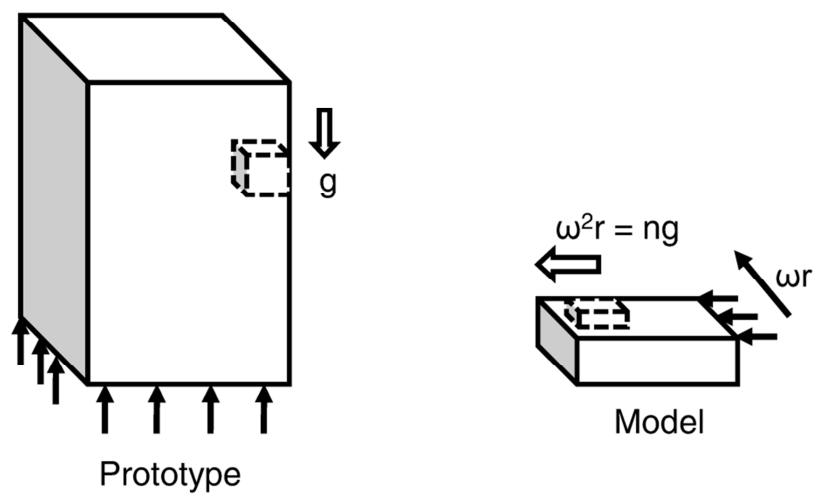


**Figure 5.2:** Stress distribution in a centrifuge sample (after Schofield, 1980)

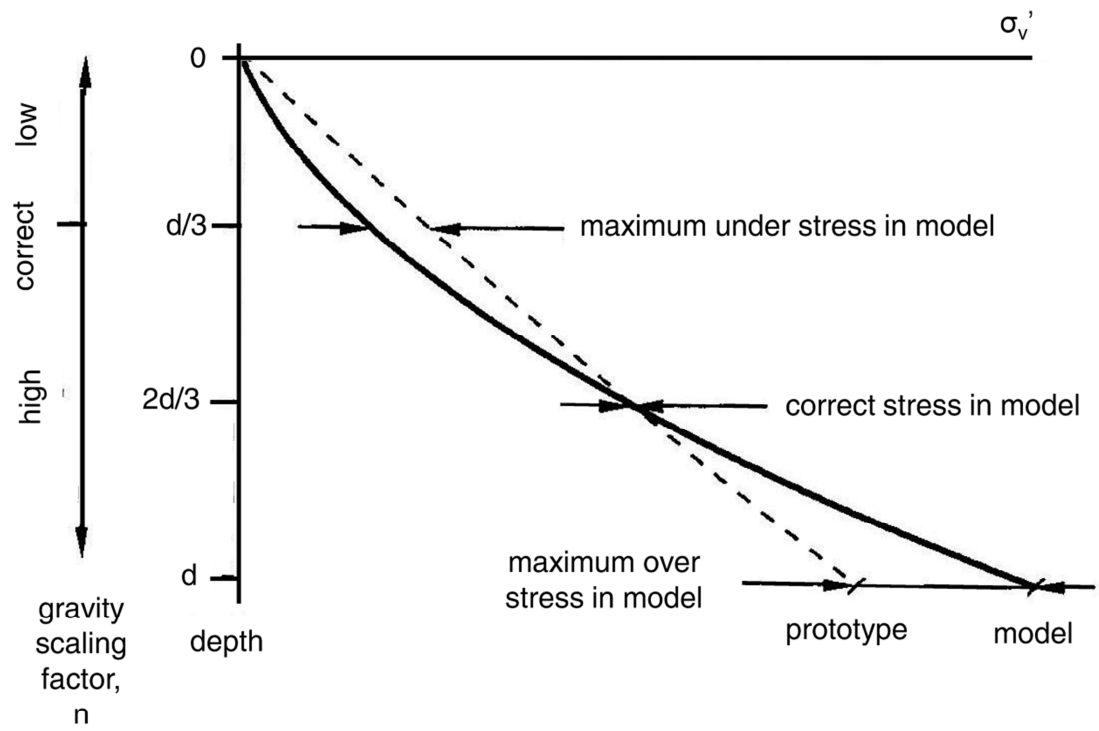


**Figure 5.3:** Stress variation with depth in a centrifuge model, exaggerated (after Taylor, 1995)

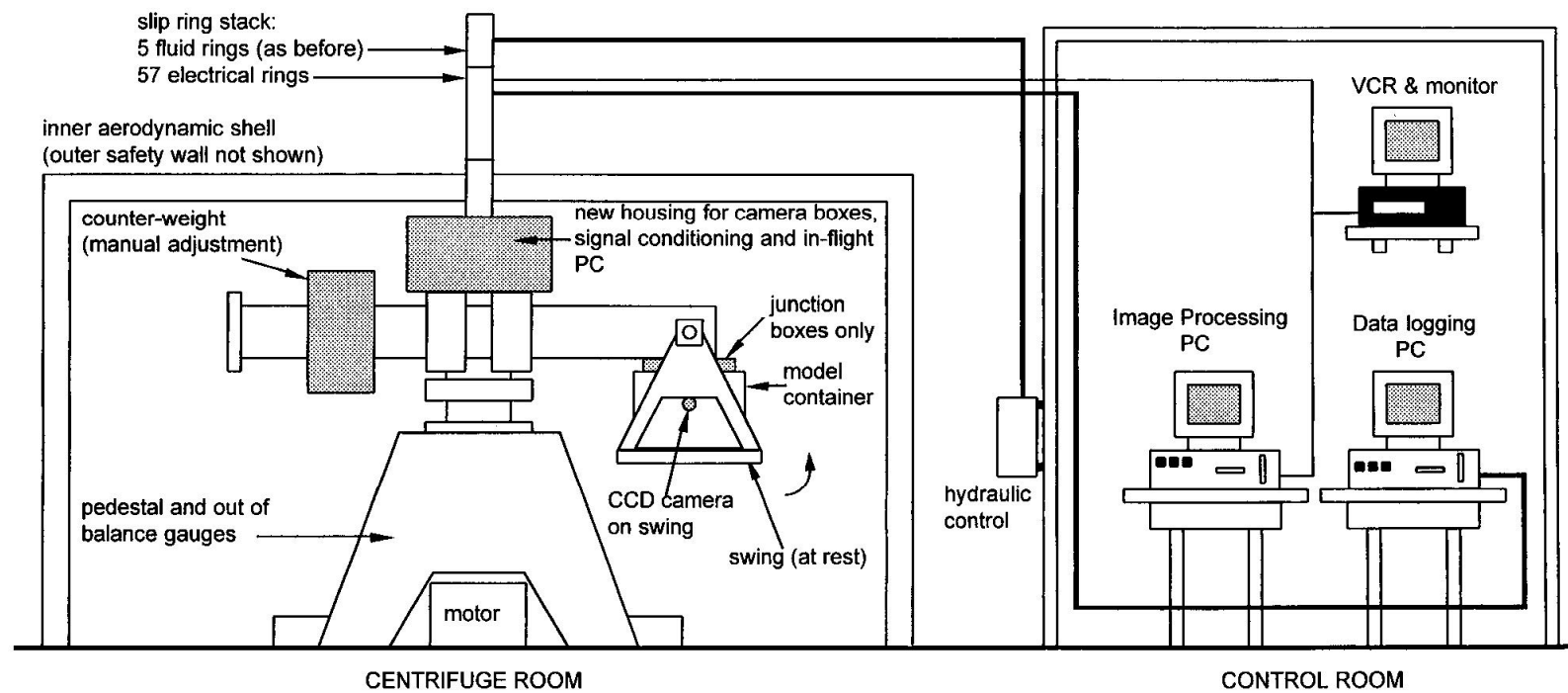


**Figure 5.4:** Schematic diagram of the Acutronic 661 at City University London (Grant, 1998)

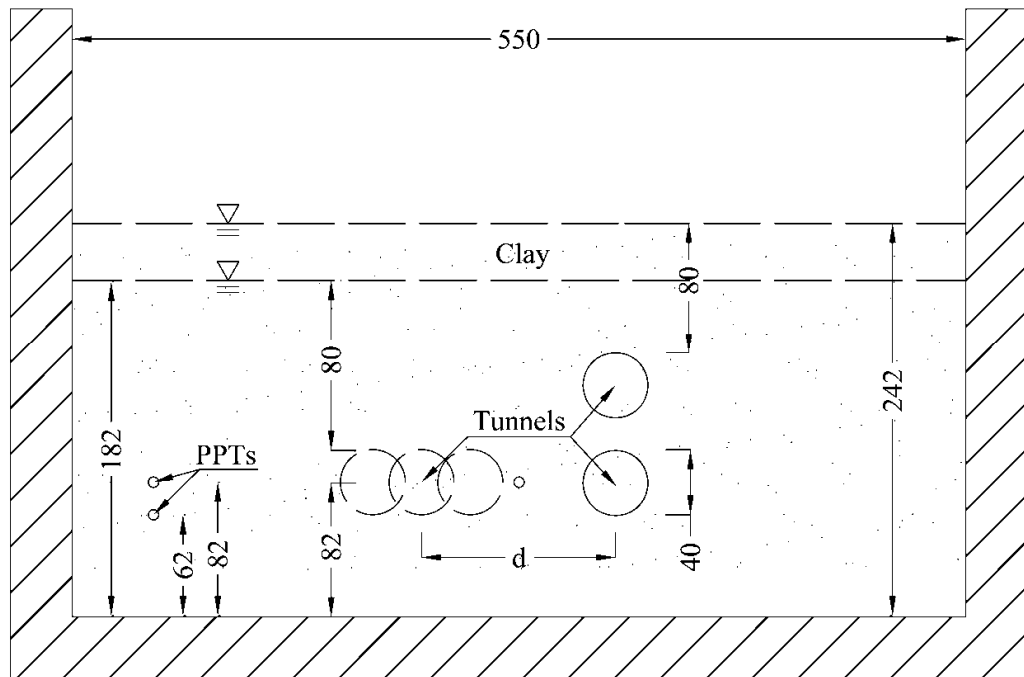


**Figure 6.1:** Schematic diagram of the centrifuge model layouts

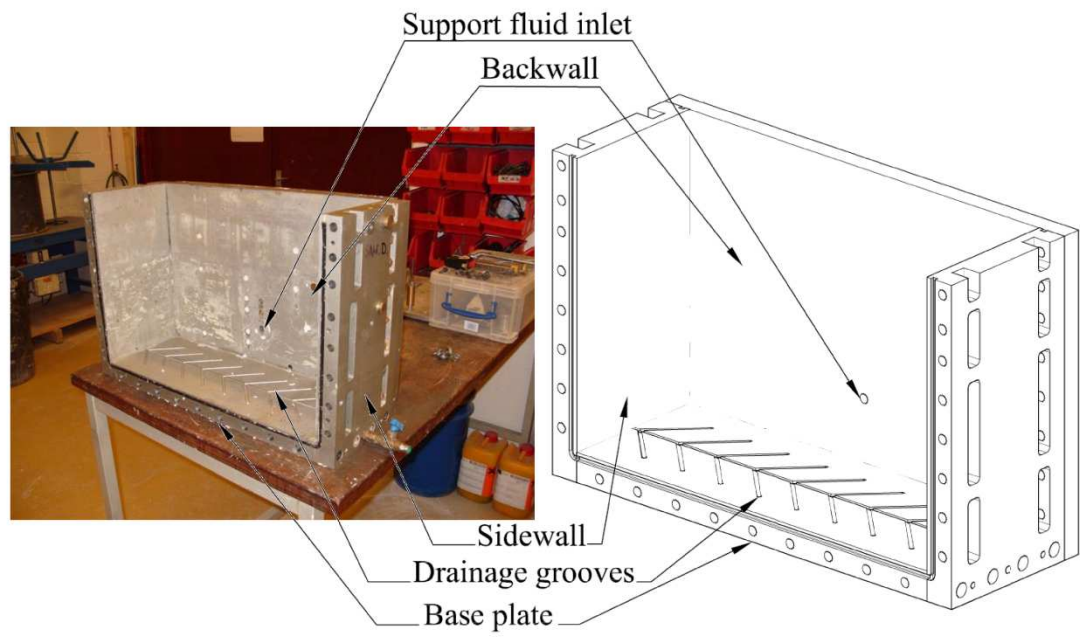
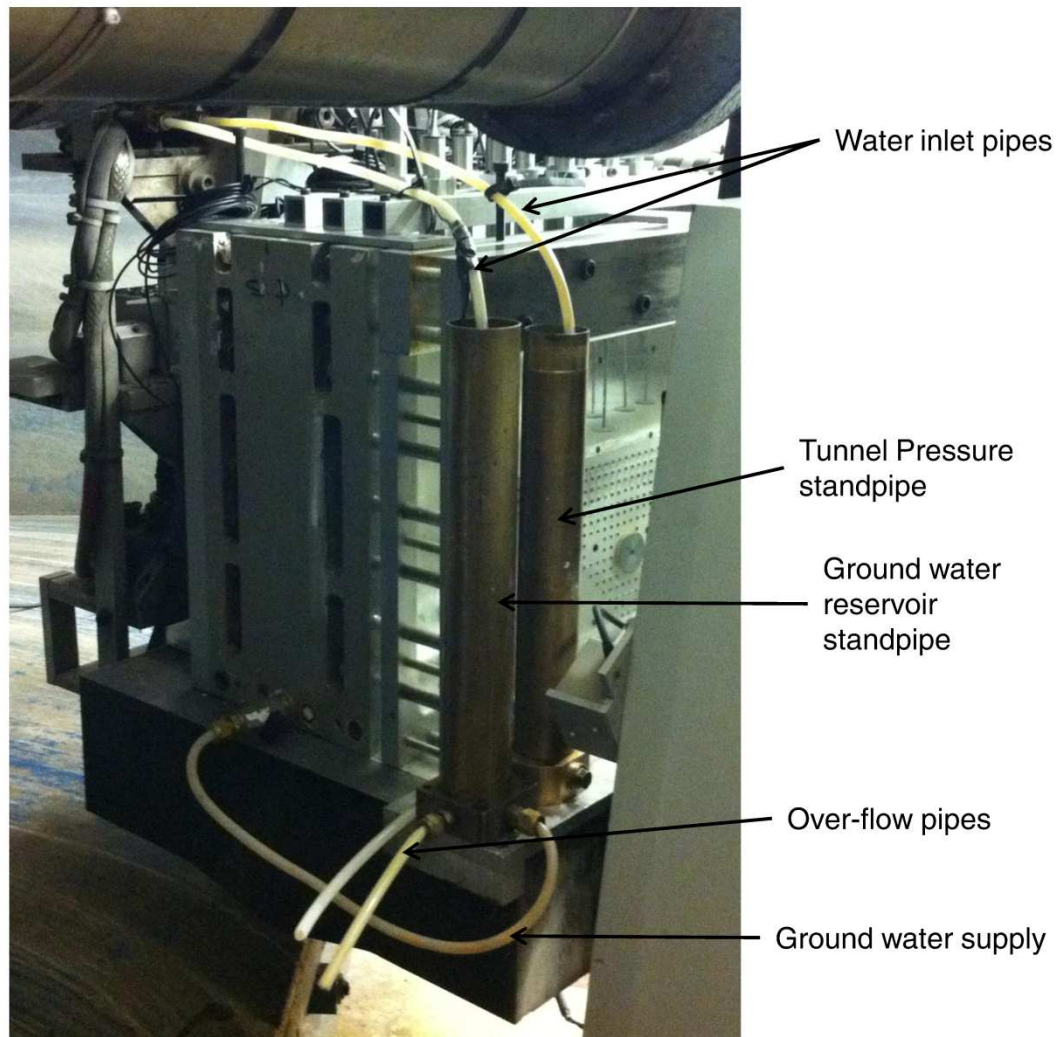


**Figure 6.2:** Photograph and schematic of strong box container for single tunnel experiments

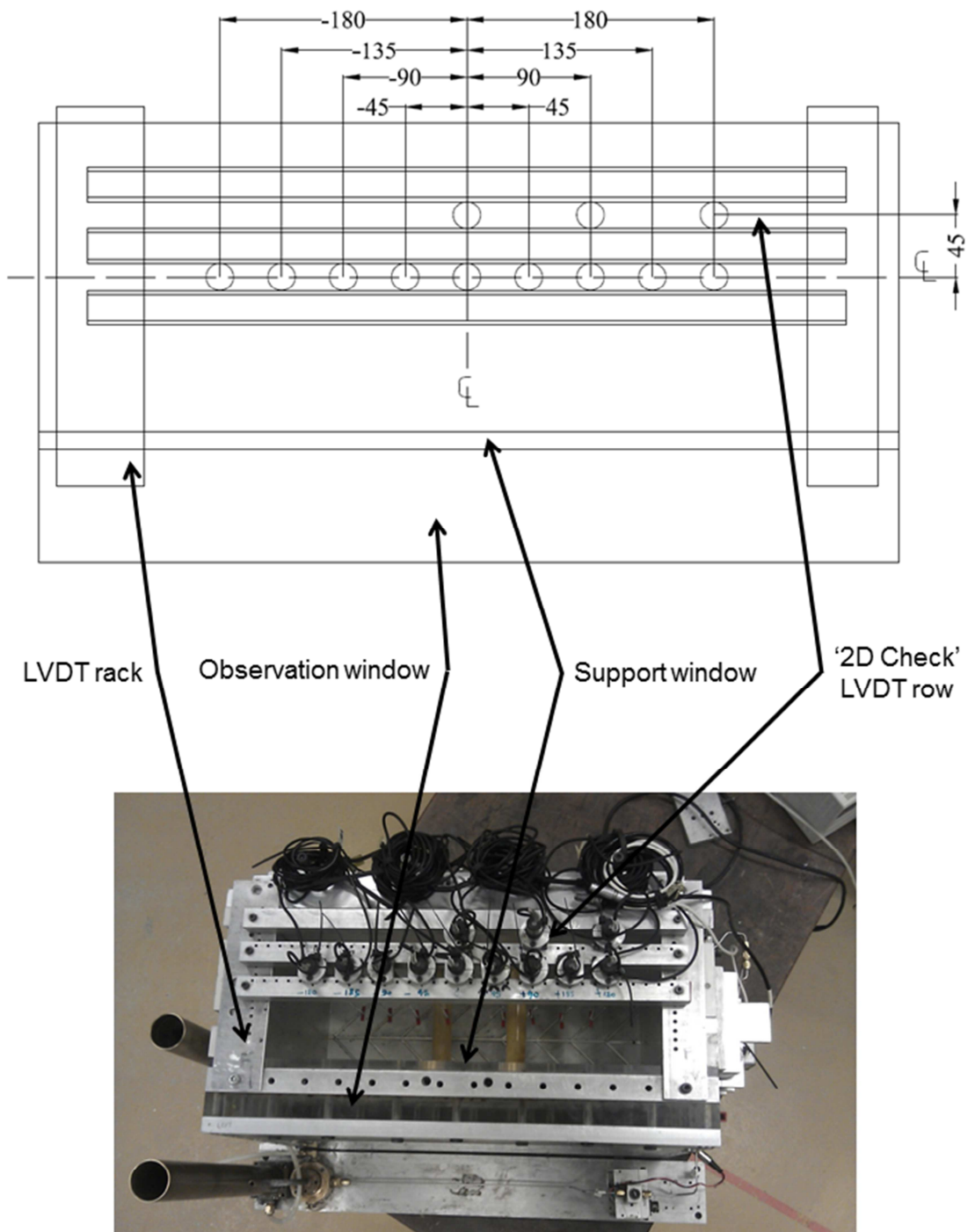


**Figure 6.3:** Photograph of consolidometer used for consolidation of slurry

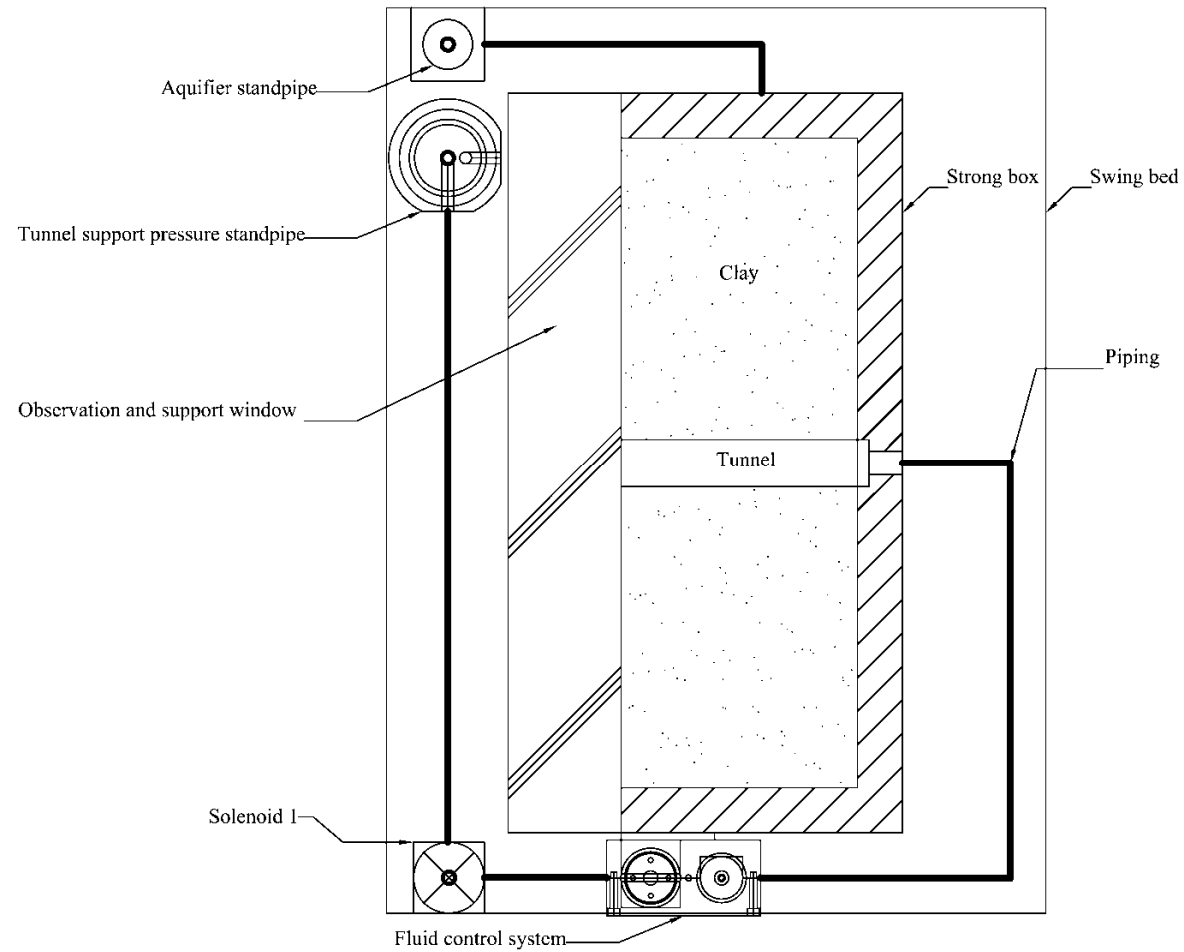




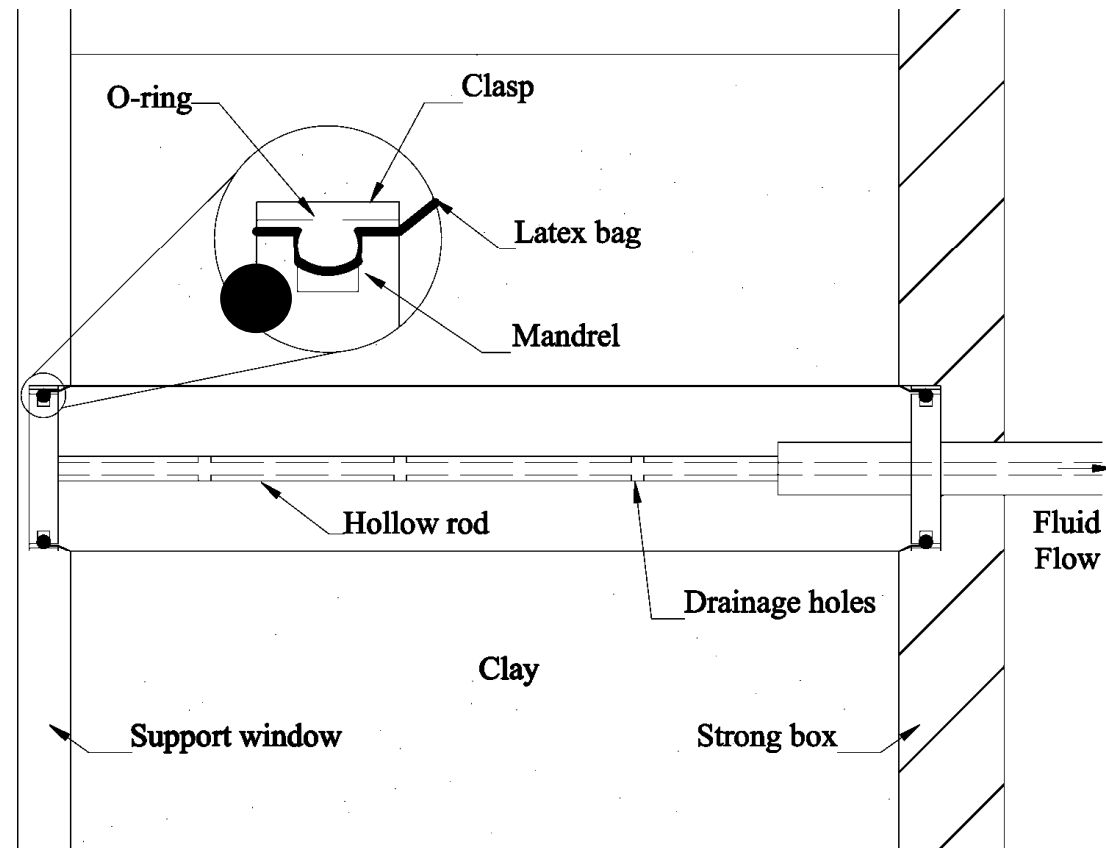
**Figure 6.4:** Photograph of the ground water reservoir standpipe and tunnel pressure standpipe on the centrifuge swing bed



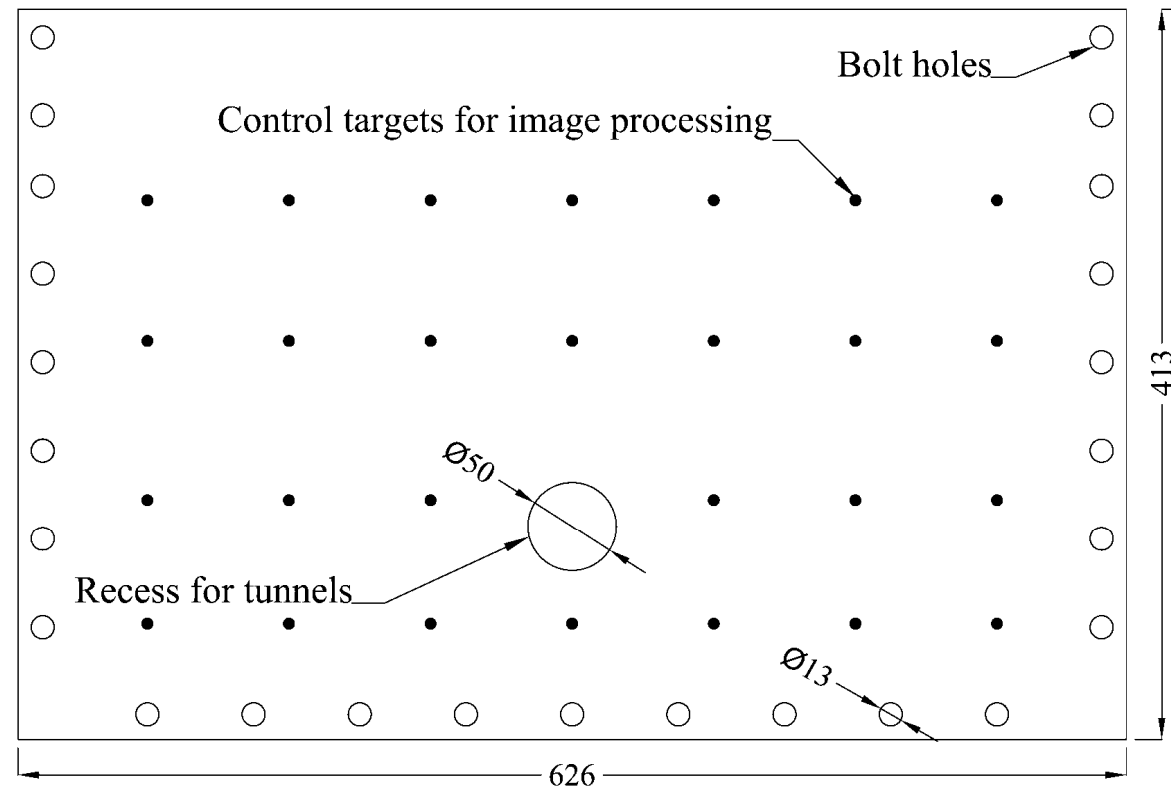
**Figure 6.5:** Schematic diagram of the LVDT gantry and spacing



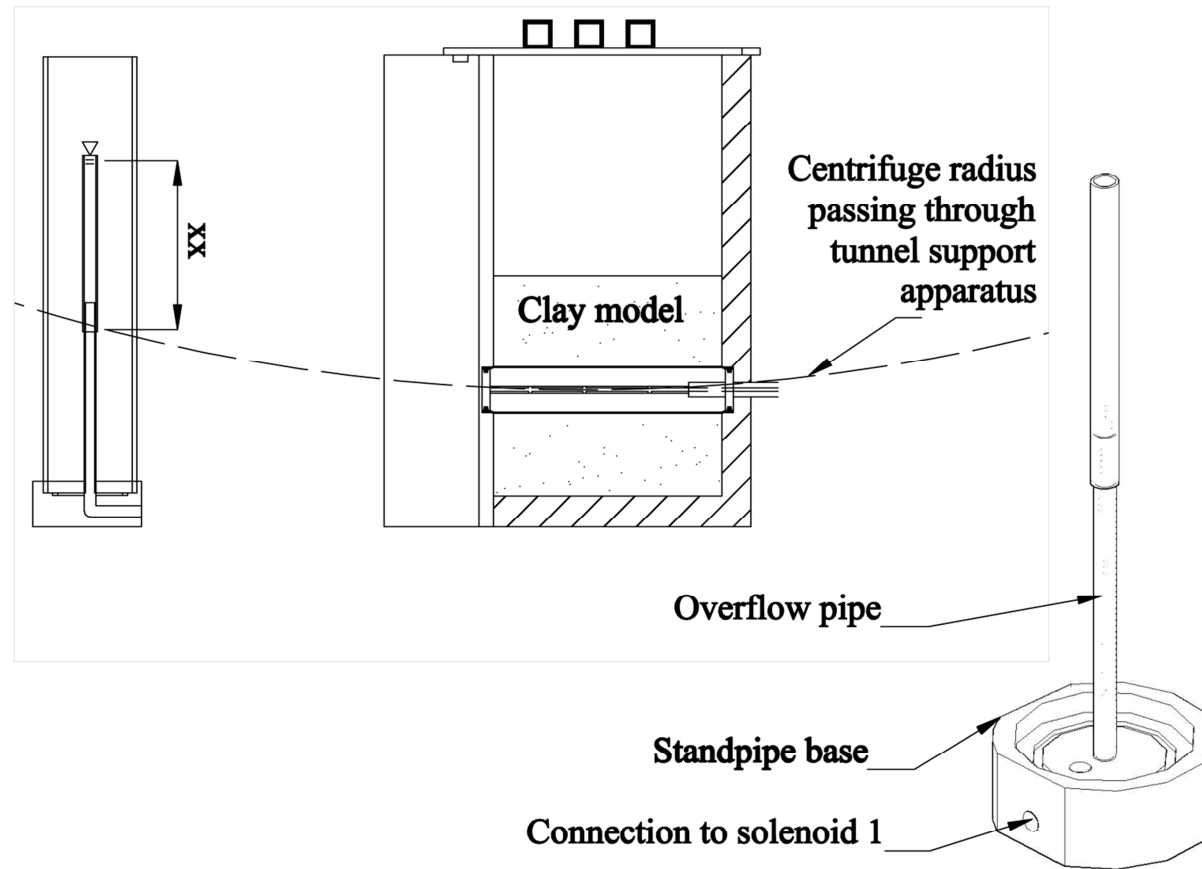
**Figure 6.6:** Plan arrangement of apparatus on the swing bed for single tunnel testing



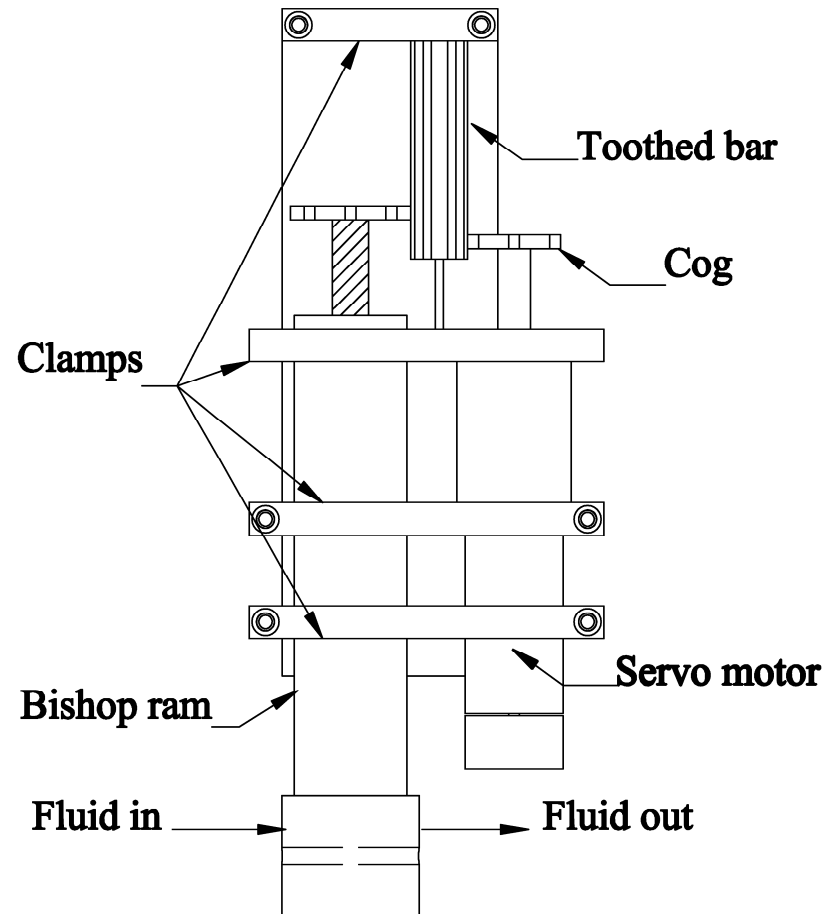
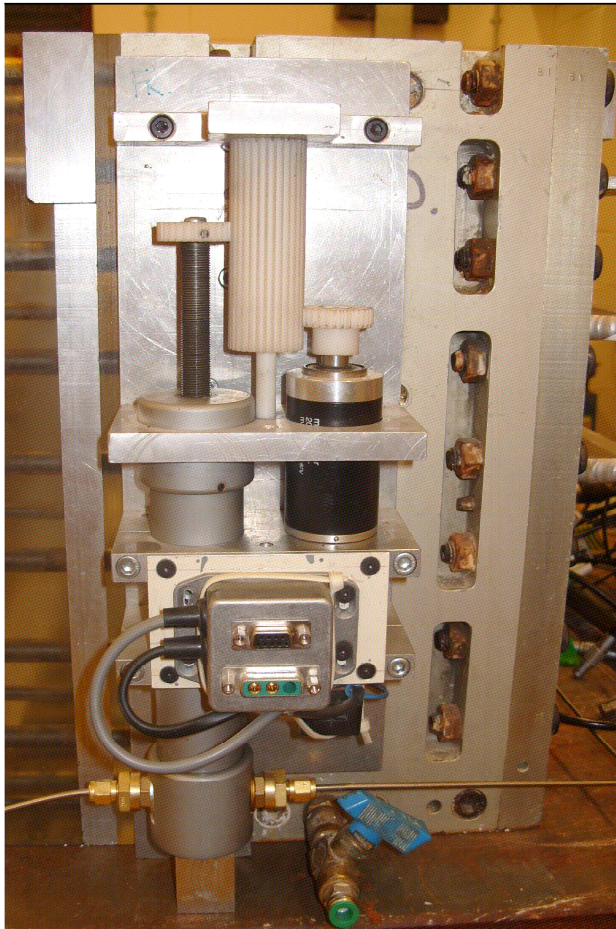
**Figure 6.7:** Cross-section through tunnel support apparatus



**Figure 6.8:** Schematic of single tunnel support window system

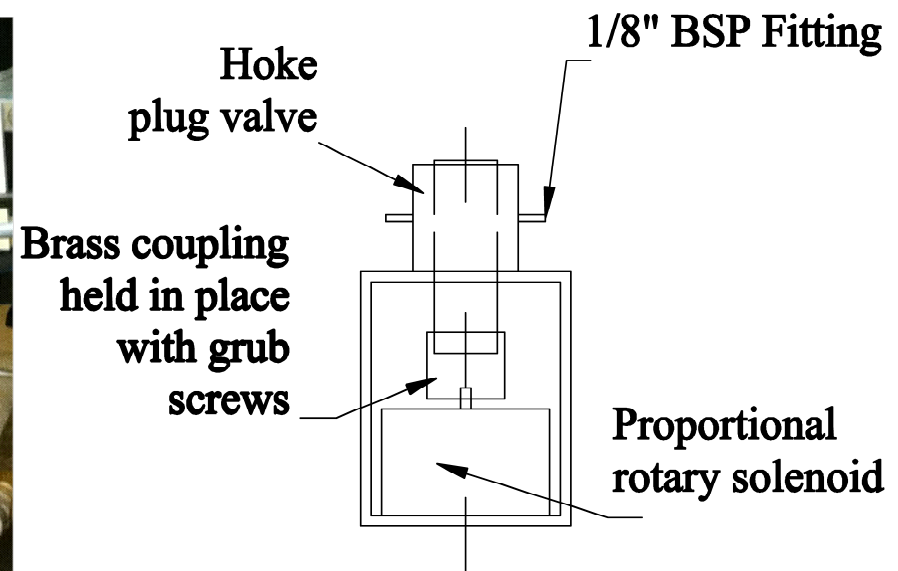
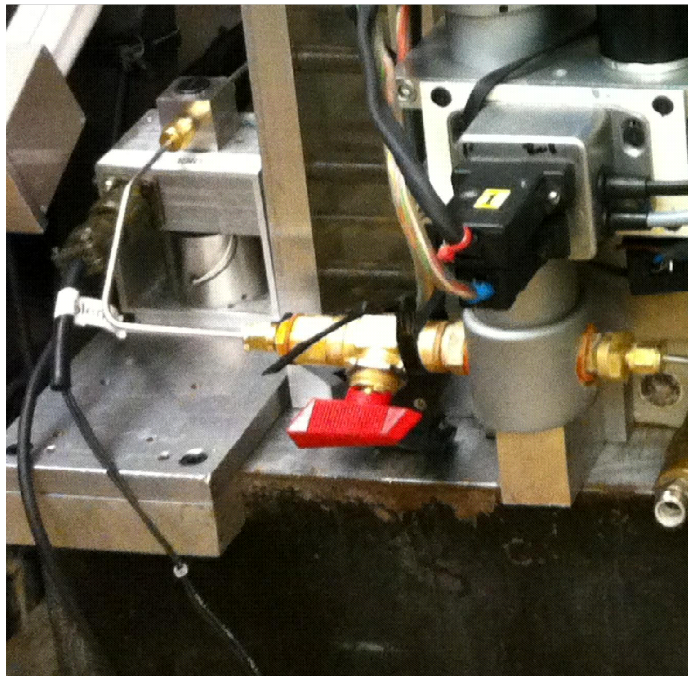


**Figure 6.9:** Details of the standpipe used to control the pressure in the tunnels



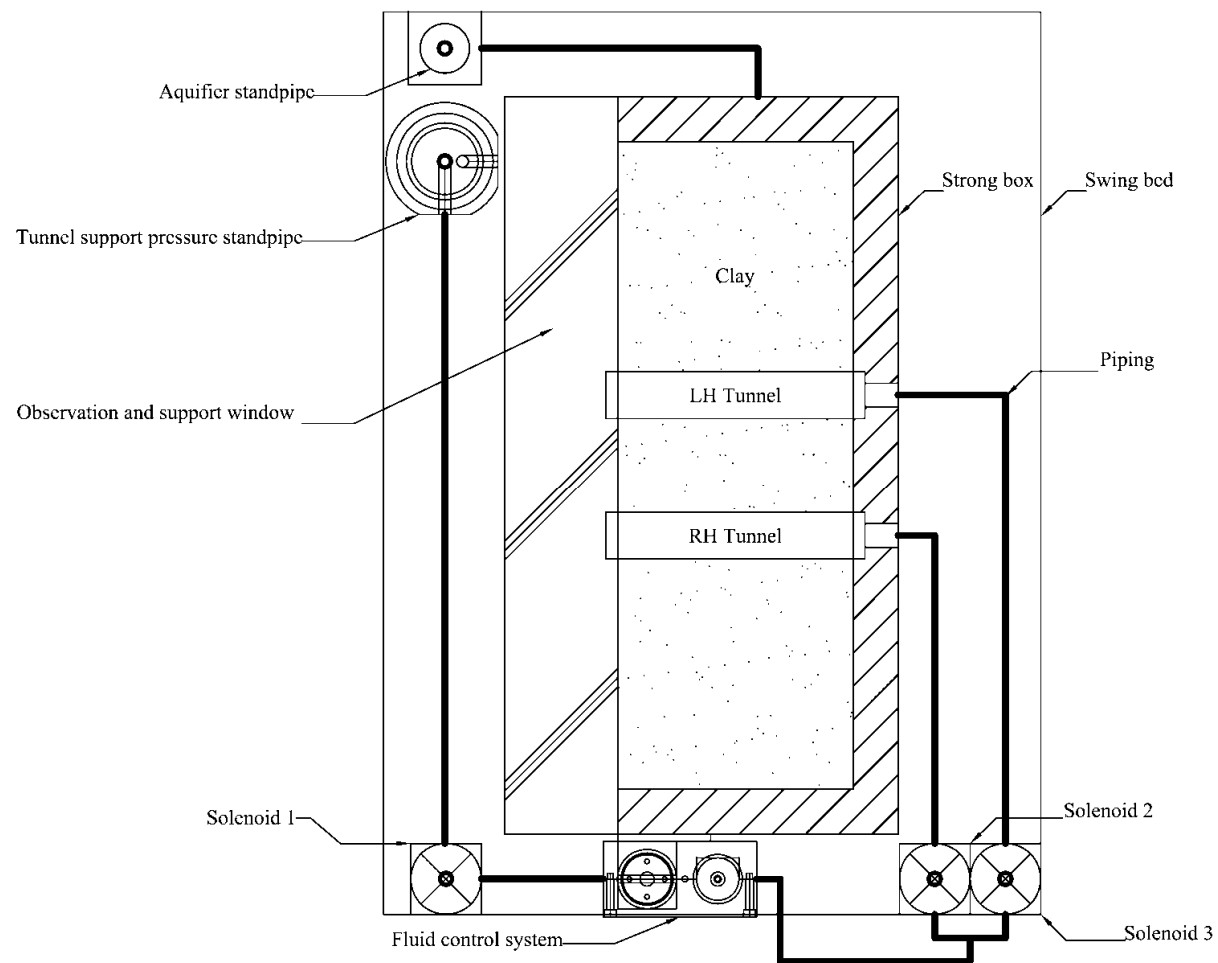
**Figure 6.10:** Photograph and schematic of fluid control apparatus



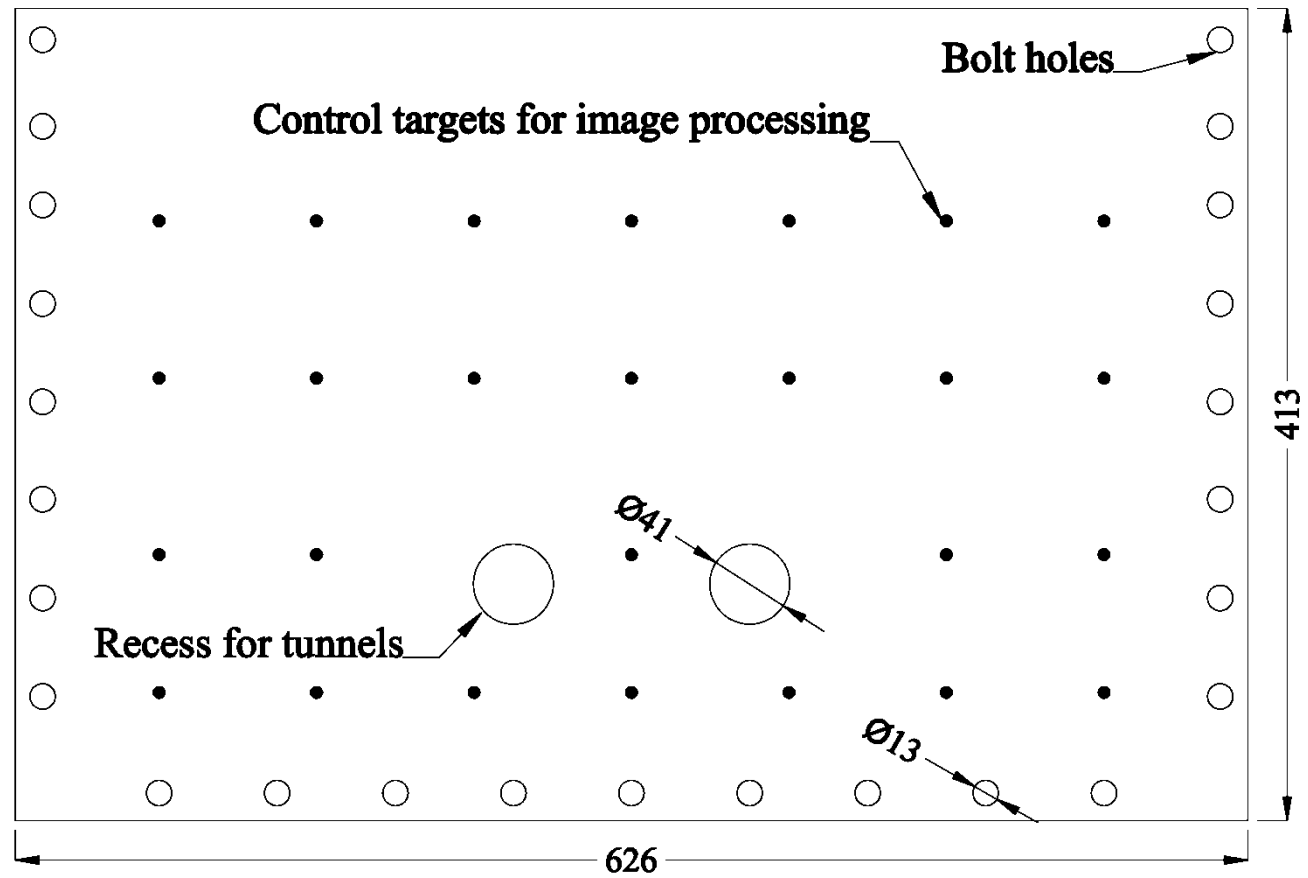


**Figure 6.11:** Photograph of solenoid and plug valve system and schematic (after McNamara, 2001)

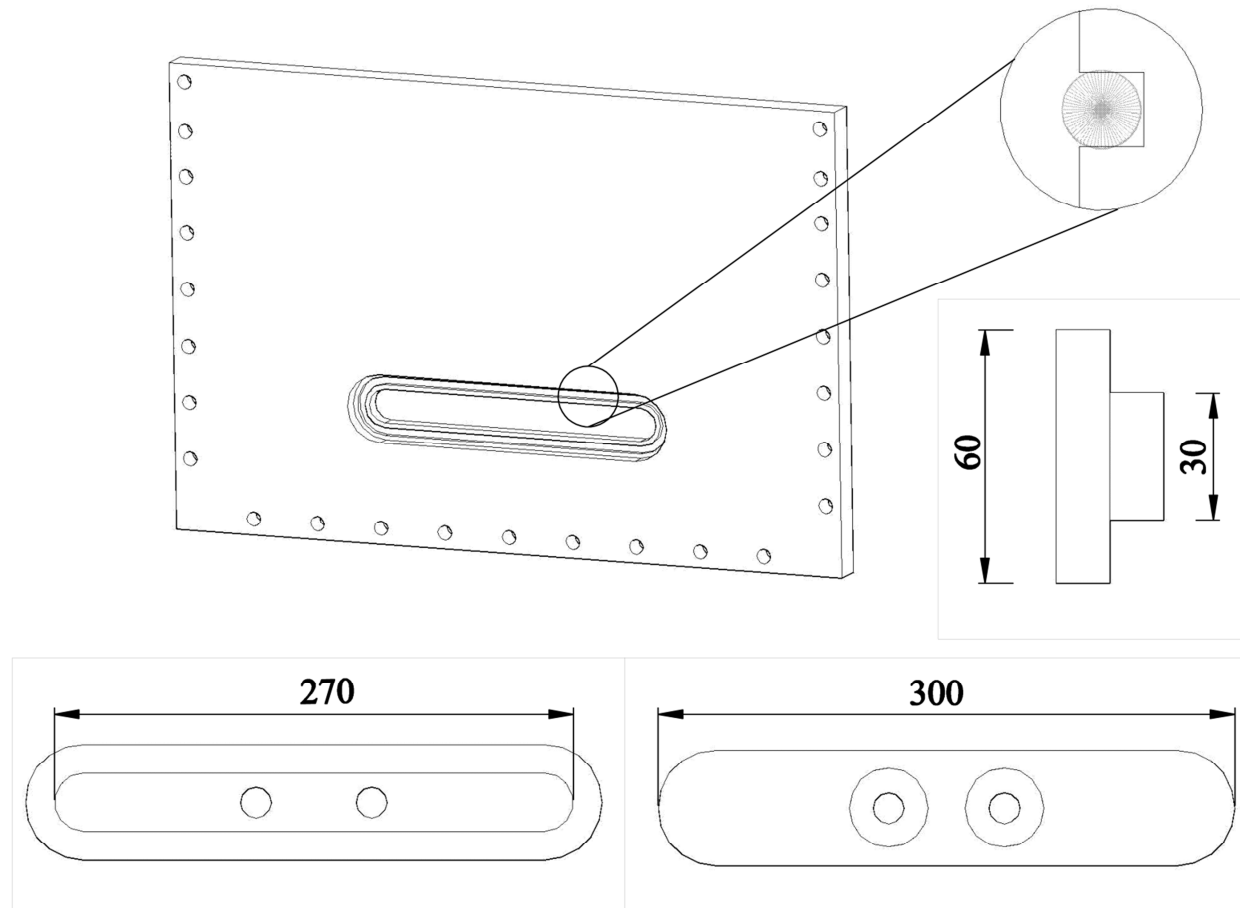




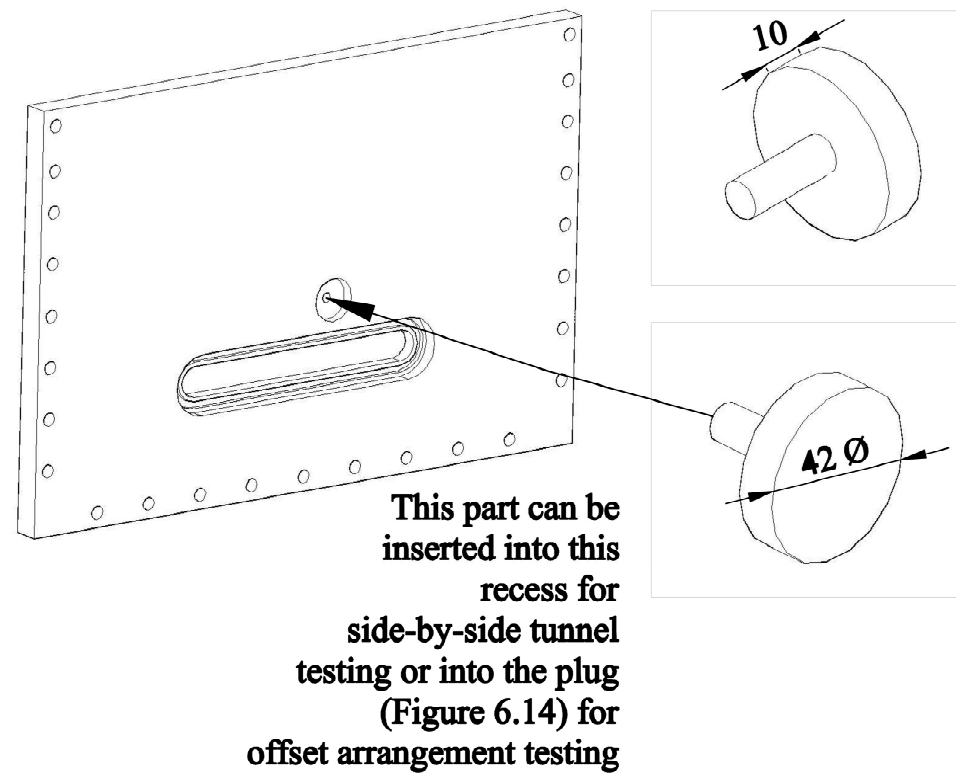
**Figure 6.12:** Plan arrangement of apparatus on the swing bed for twin tunnel testing



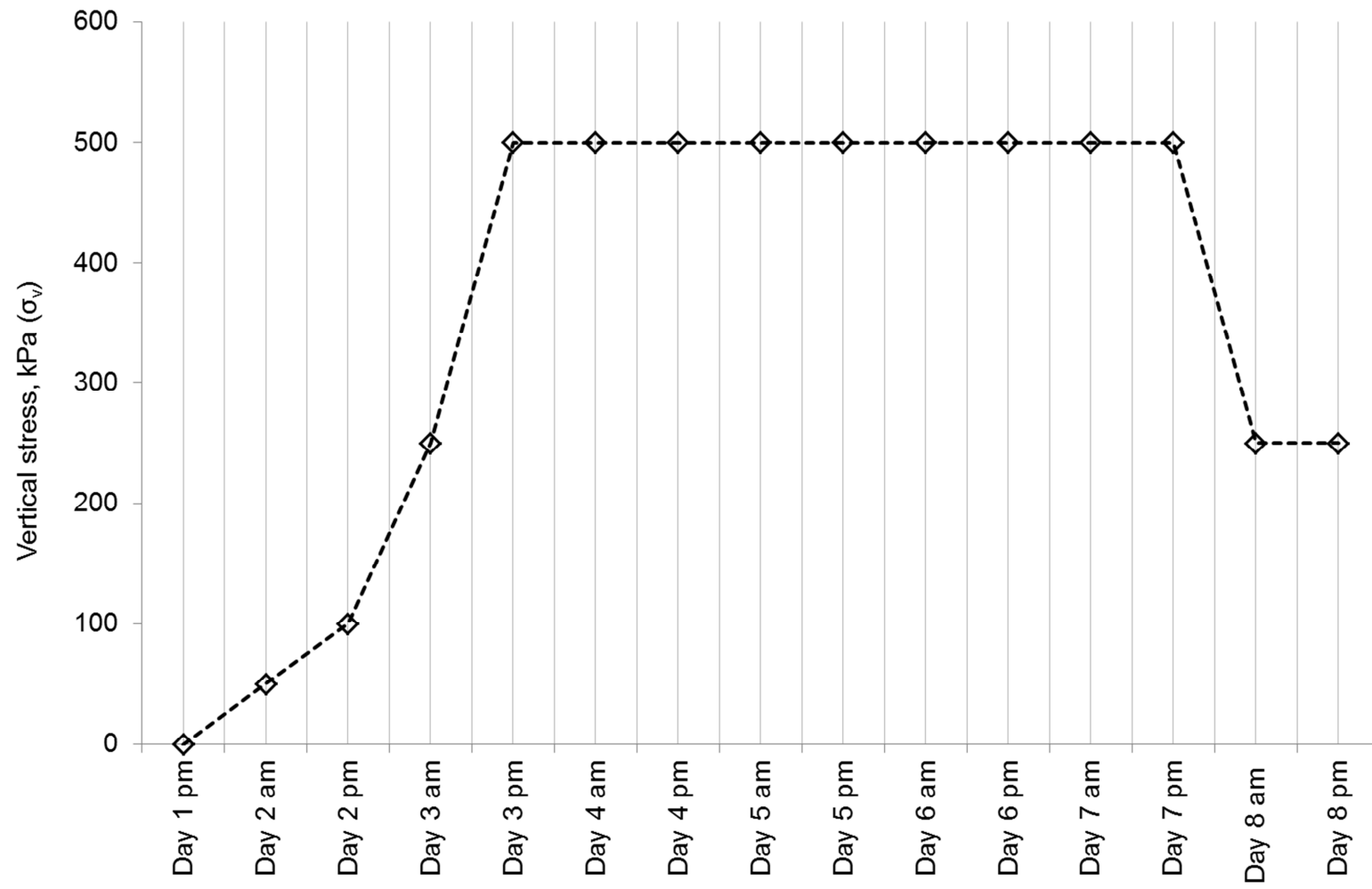
**Figure 6.13:** Schematic of supporting window system (3D twin-tunnelling case)



**Figure 6.14:** Details of strong-box back wall and interchangeable inserts with variable spacing



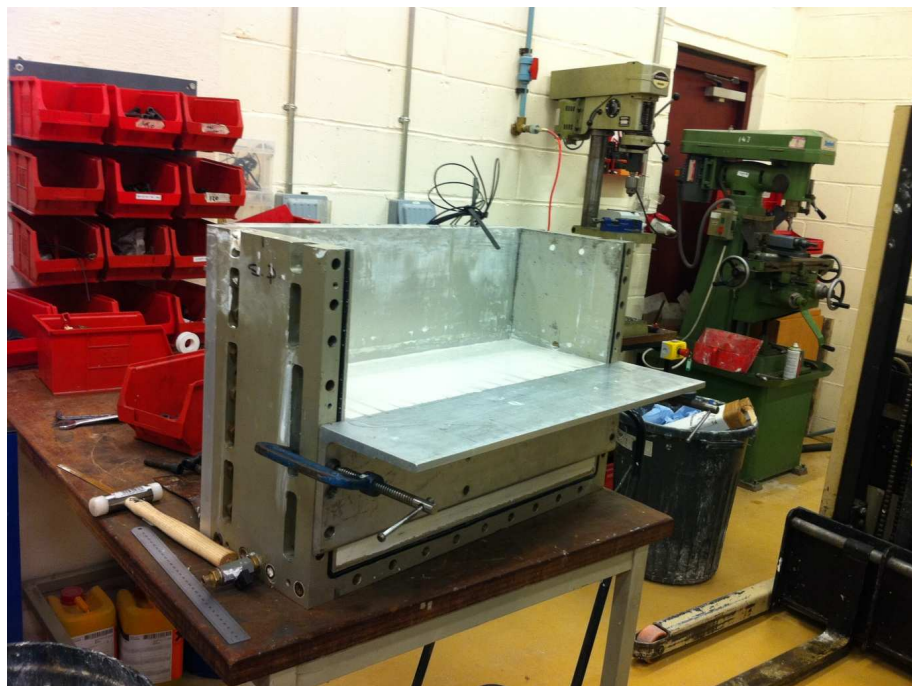
**Figure 6.15:** Alterations to strong-box back wall to accommodate offset arrangements



**Figure 7.1:** Stress history of the model from slurry to moderately stiff clay



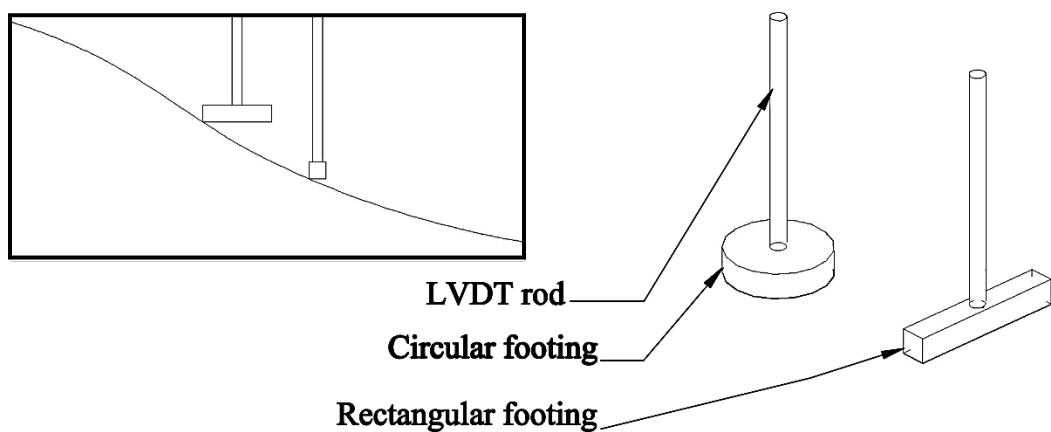
**Figure 7.2:** Jig for the creation of the twin-tunnel cavities on the bench during the model making stages of centrifuge modelling



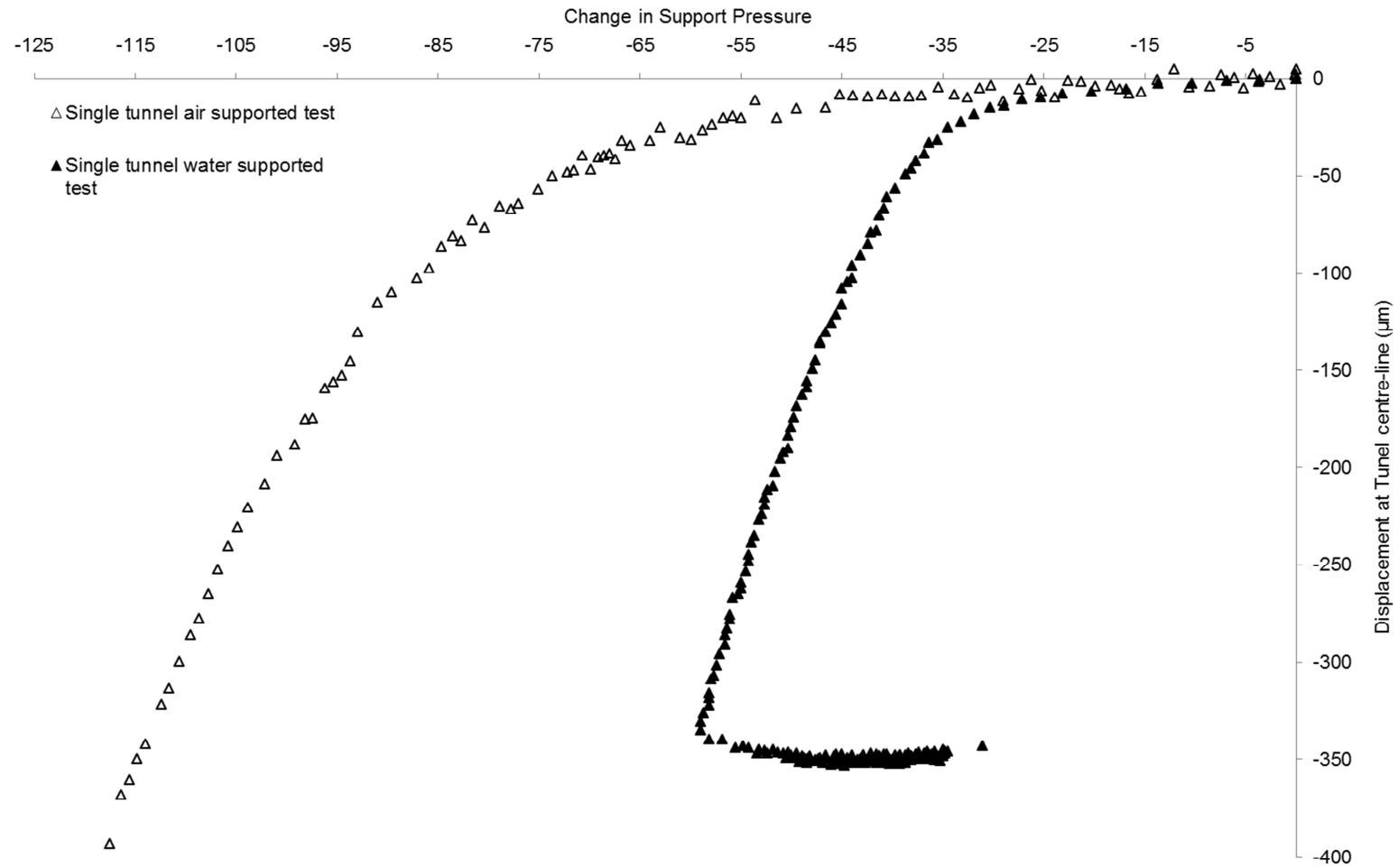
**Figure 7.3:** Shelf for trimming the model to the correct height on the bench during the model making stages of centrifuge modelling



**Figure 7.4:** Holding nut for securing the tunnelling supporting system in place and the manifold for the tunnel pressure transducer

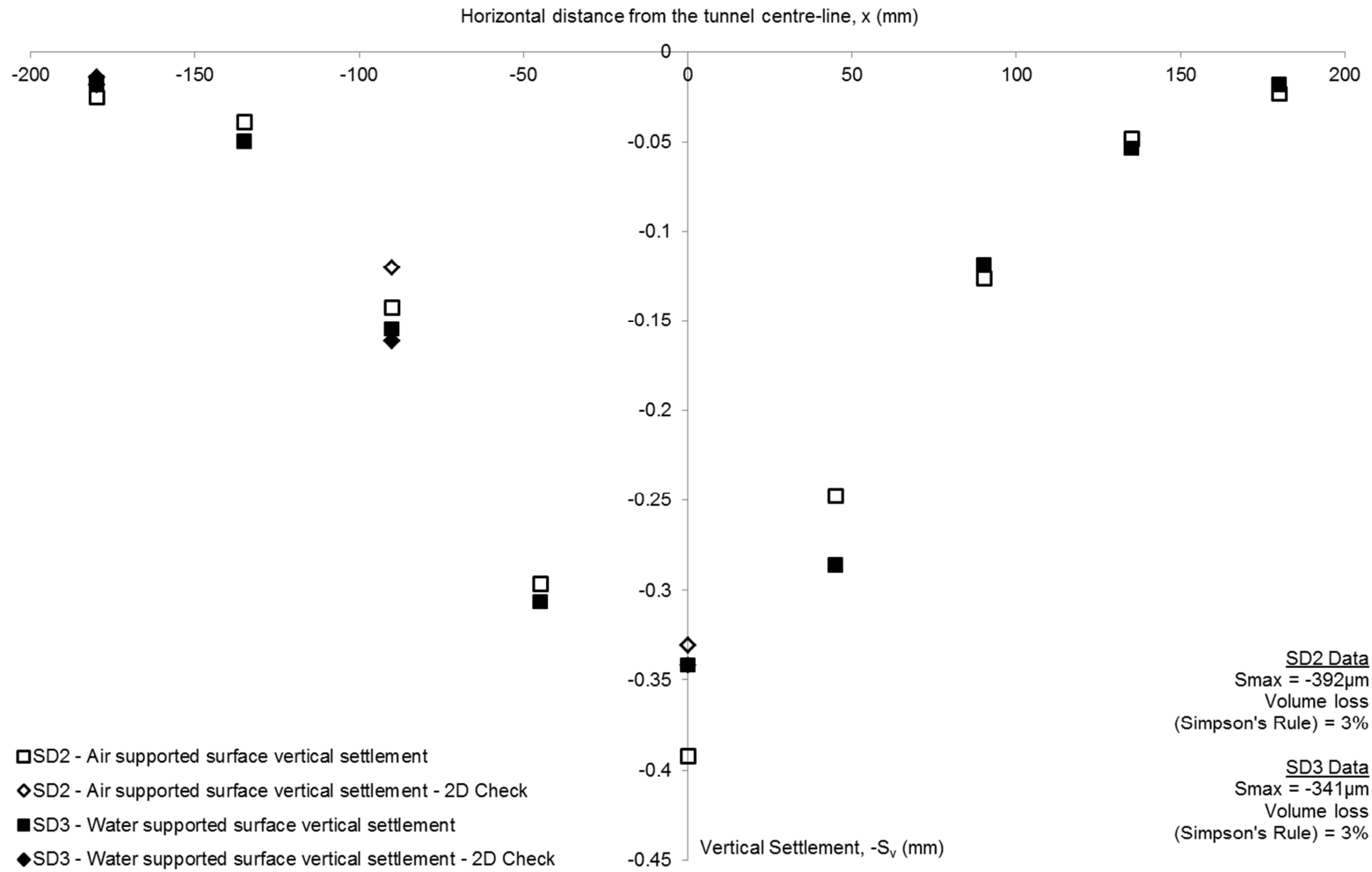


**Figure 7.5:** Comparison between circular footing and square footing on LVDTs with insert of clay surface slope

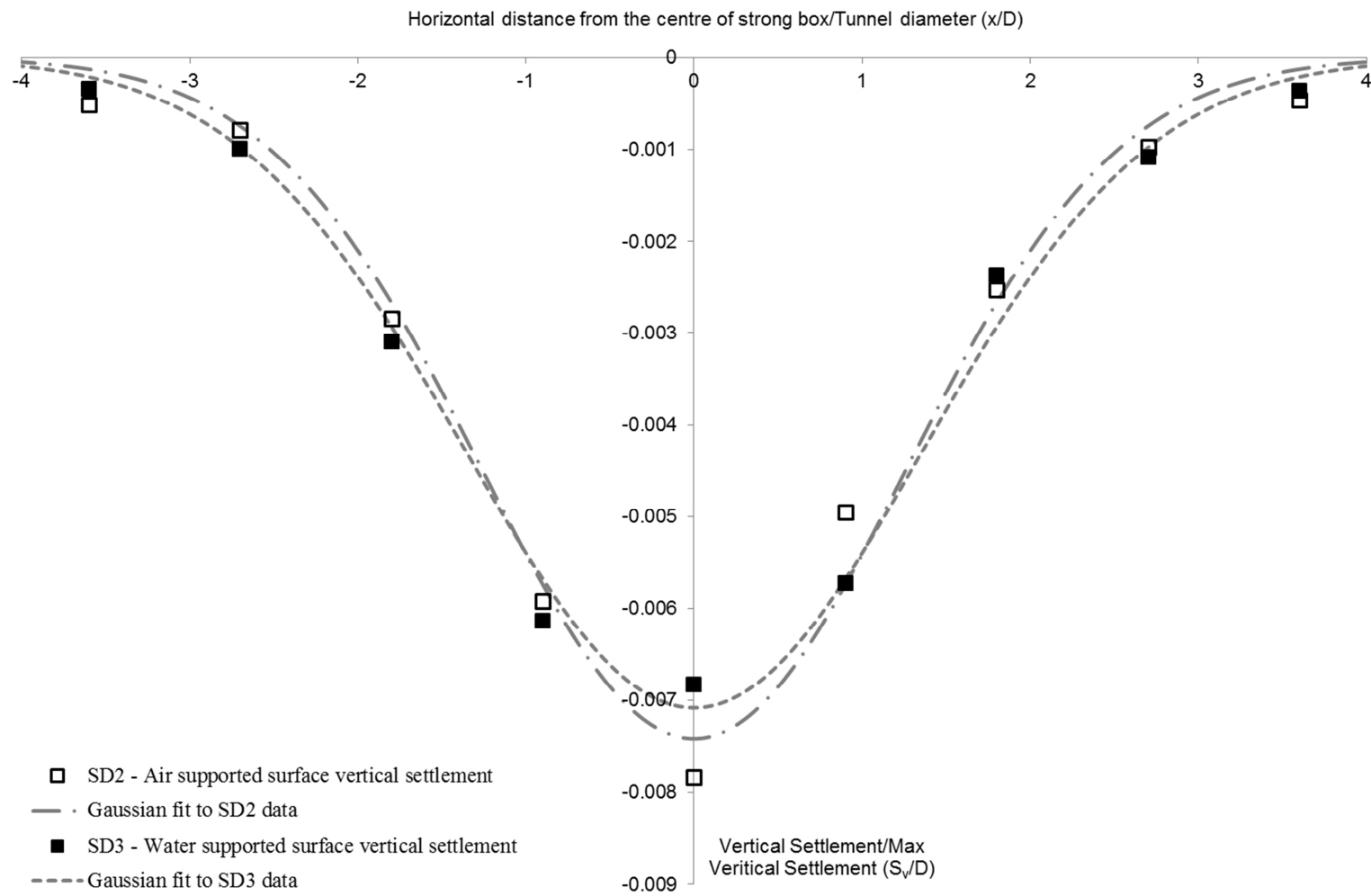


**Figure 8.1:** Comparison of centre-line vertical displacements in simulated single tunnel constructions with different support fluids

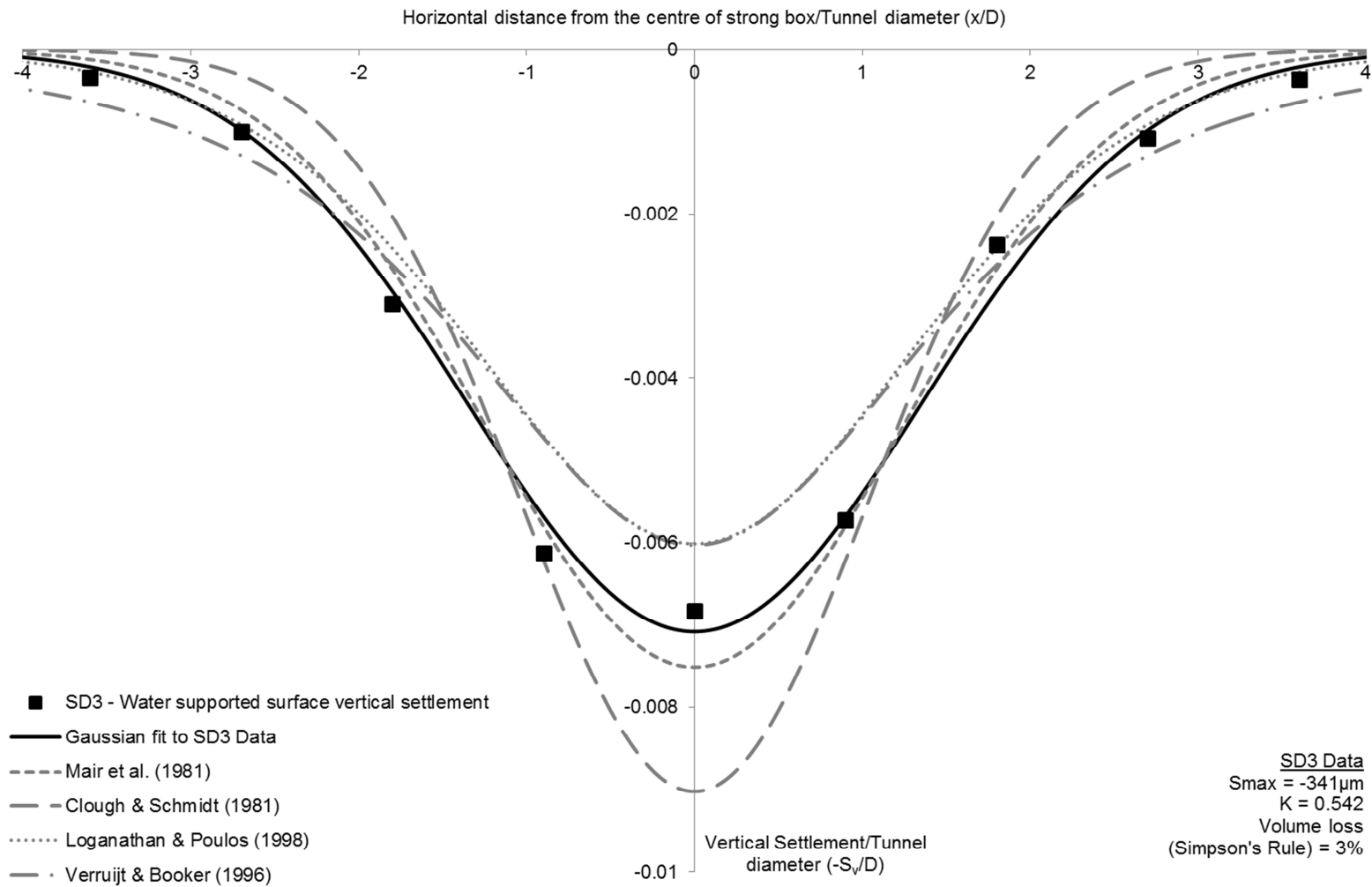




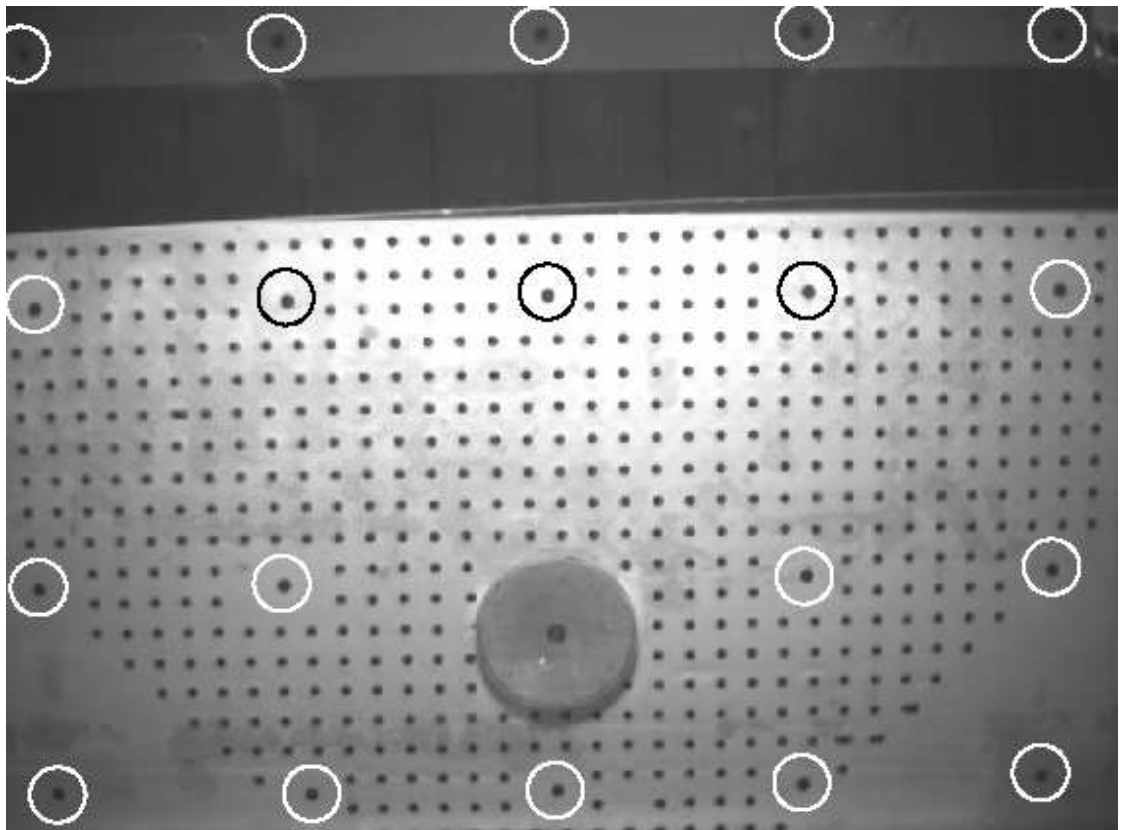
**Figure 8.2:** Raw settlement data from LVDTs (centre-line and '2D Check') after 3% volume loss in single tunnel tests of different support fluids



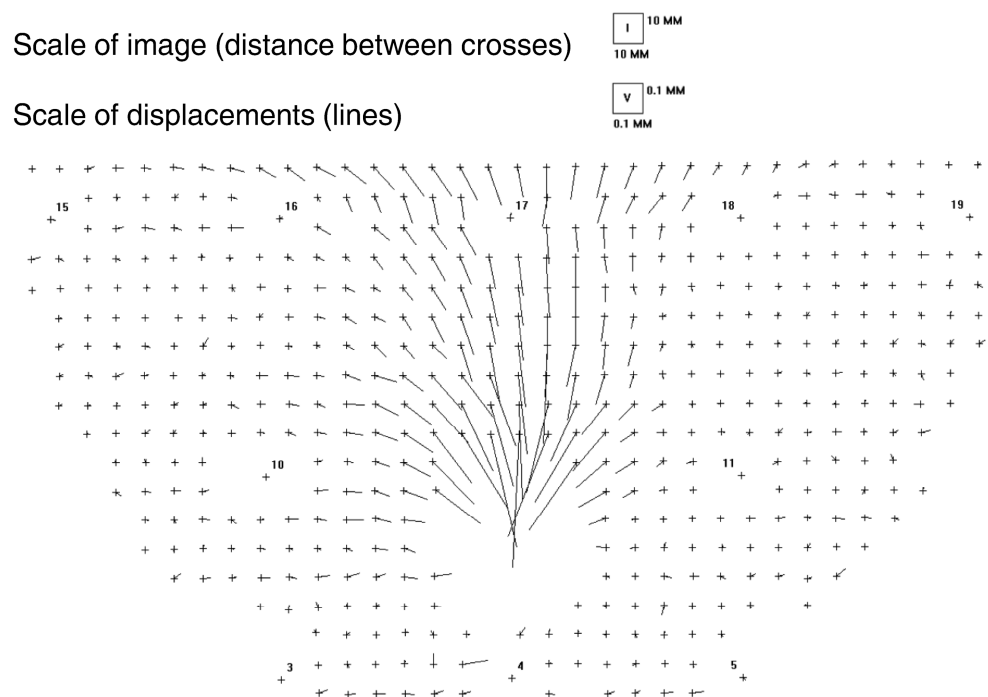
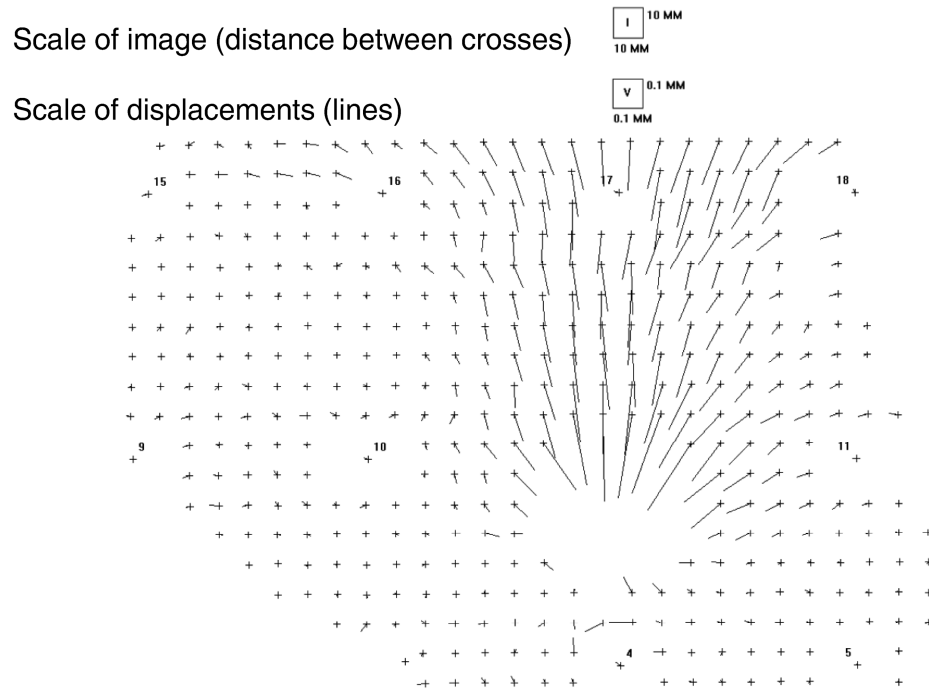
**Figure 8.3:** Gaussian curves fitted to the normalised settlement data from the single tunnel tests



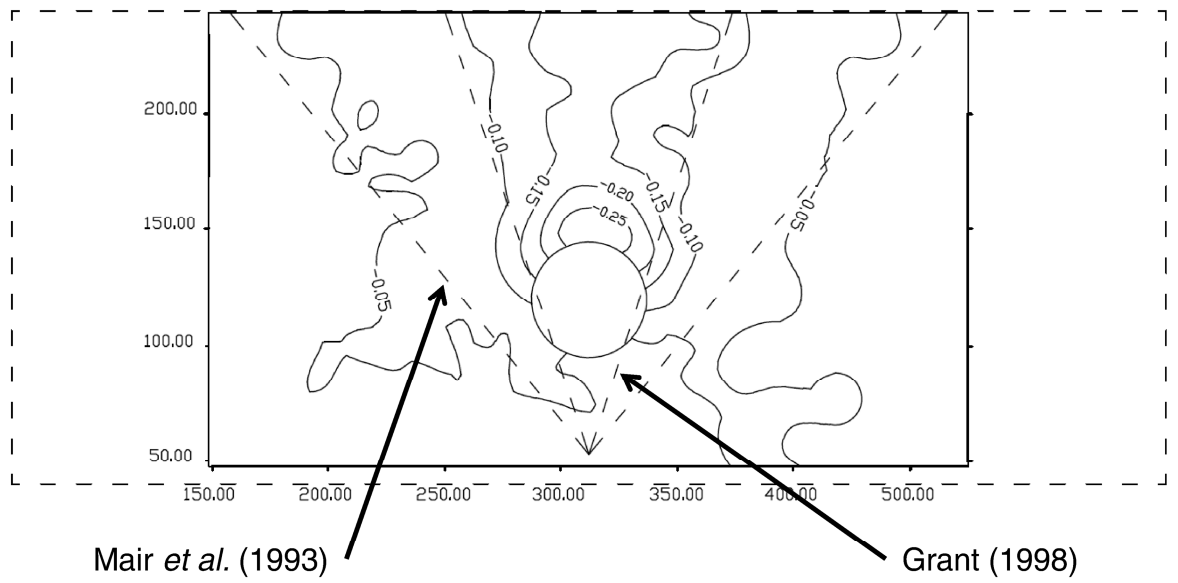
**Figure 8.4:** Comparison of the water supported single tunnel settlement data (SD3) and various prediction methods for 3% volume loss



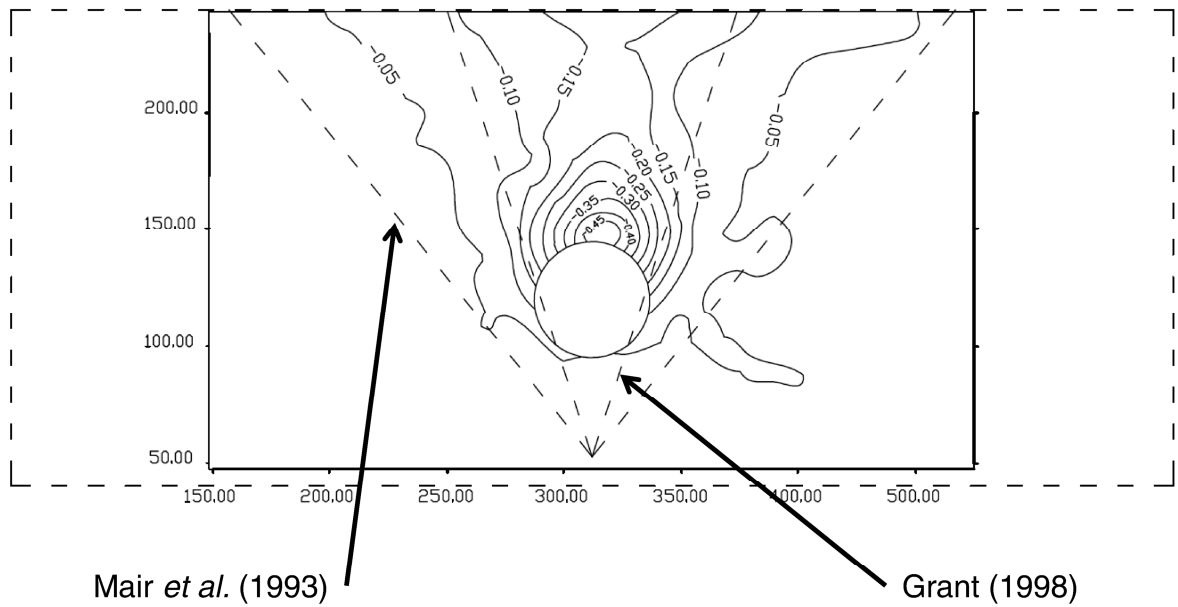
**Figure 8.5:** Typical CCD camera image taken during a test with known-coordinate markers circled



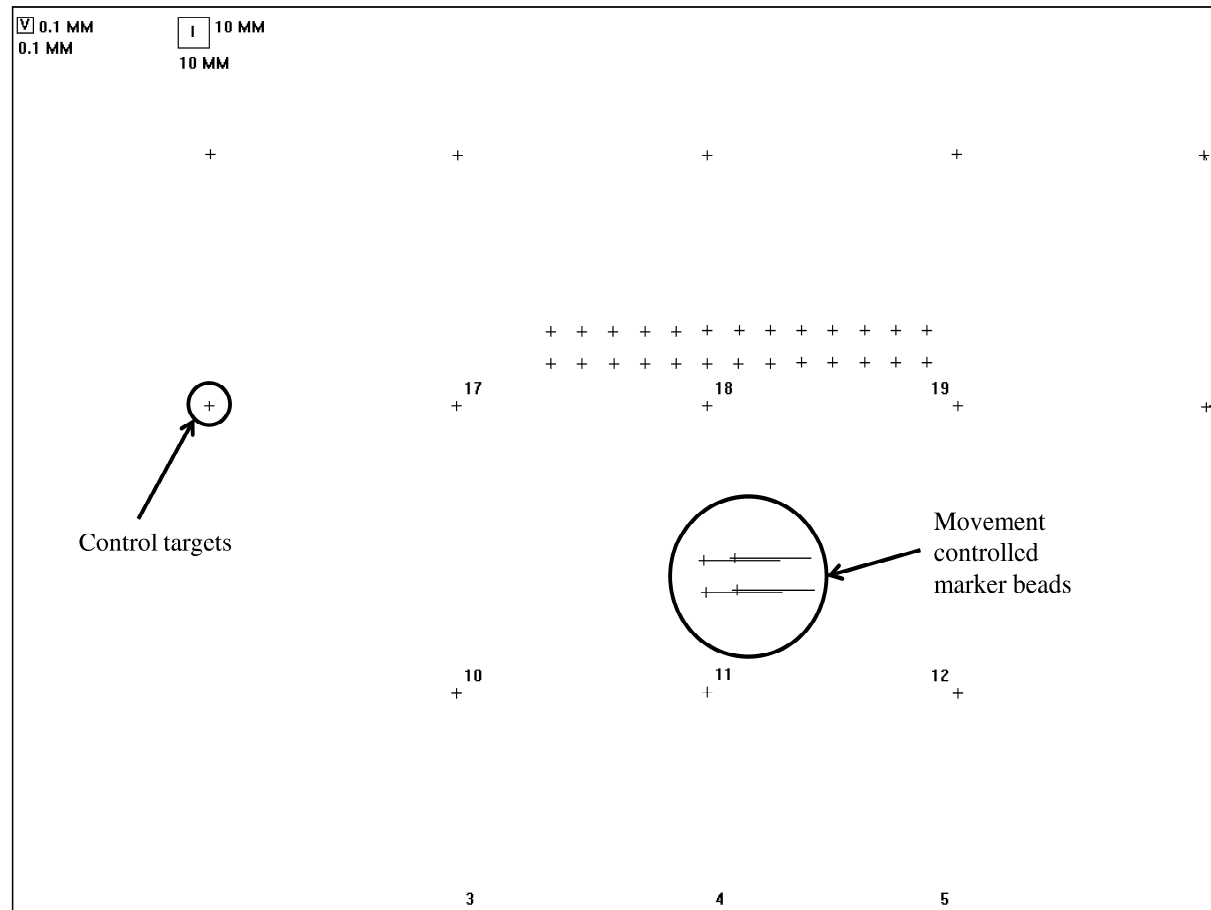
**Figure 8.6:** Sub-surface displacements displayed as vectors from air (top) and water (bottom) supported simulated single tunnel constructions for 3% volume loss




**Figure 8.7:** Sub-surface contours of SD2

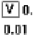


**Figure 8.8:** Sub-surface contours of SD3



**Figure 8.9:** Calibration test investigating CCD camera vector movements for 5mm horizontal movement

Scale of image (distance between crosses)  10 MM  
10 MM

Scale of displacements (lines)  0.01 MM  
0.01 MM

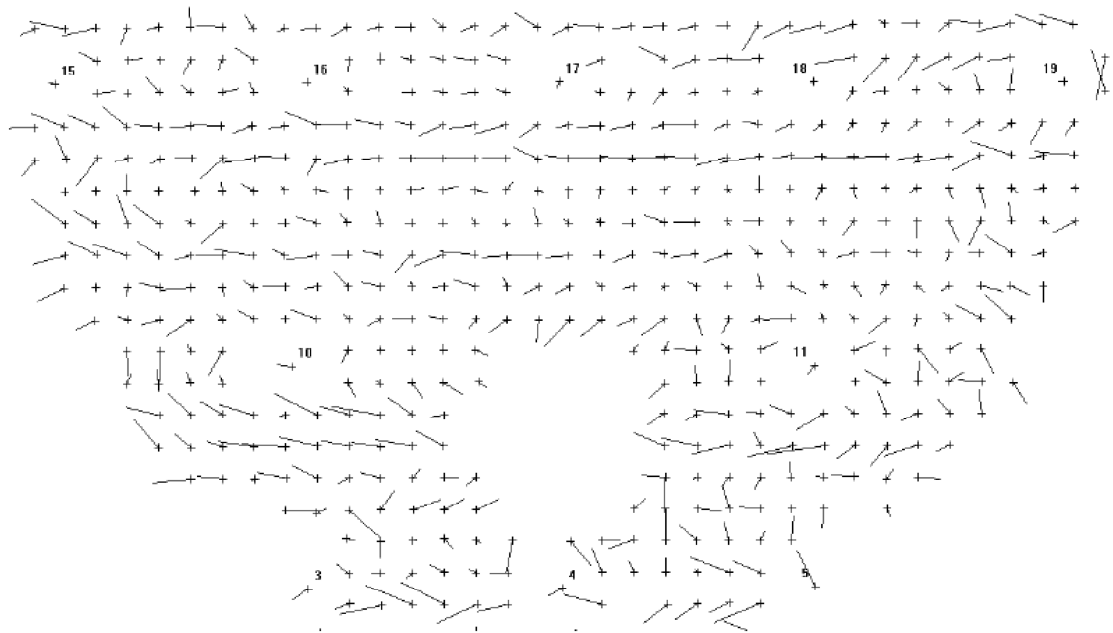


**Figure 8.10:** Noise levels during apparent no movement during a centrifuge test



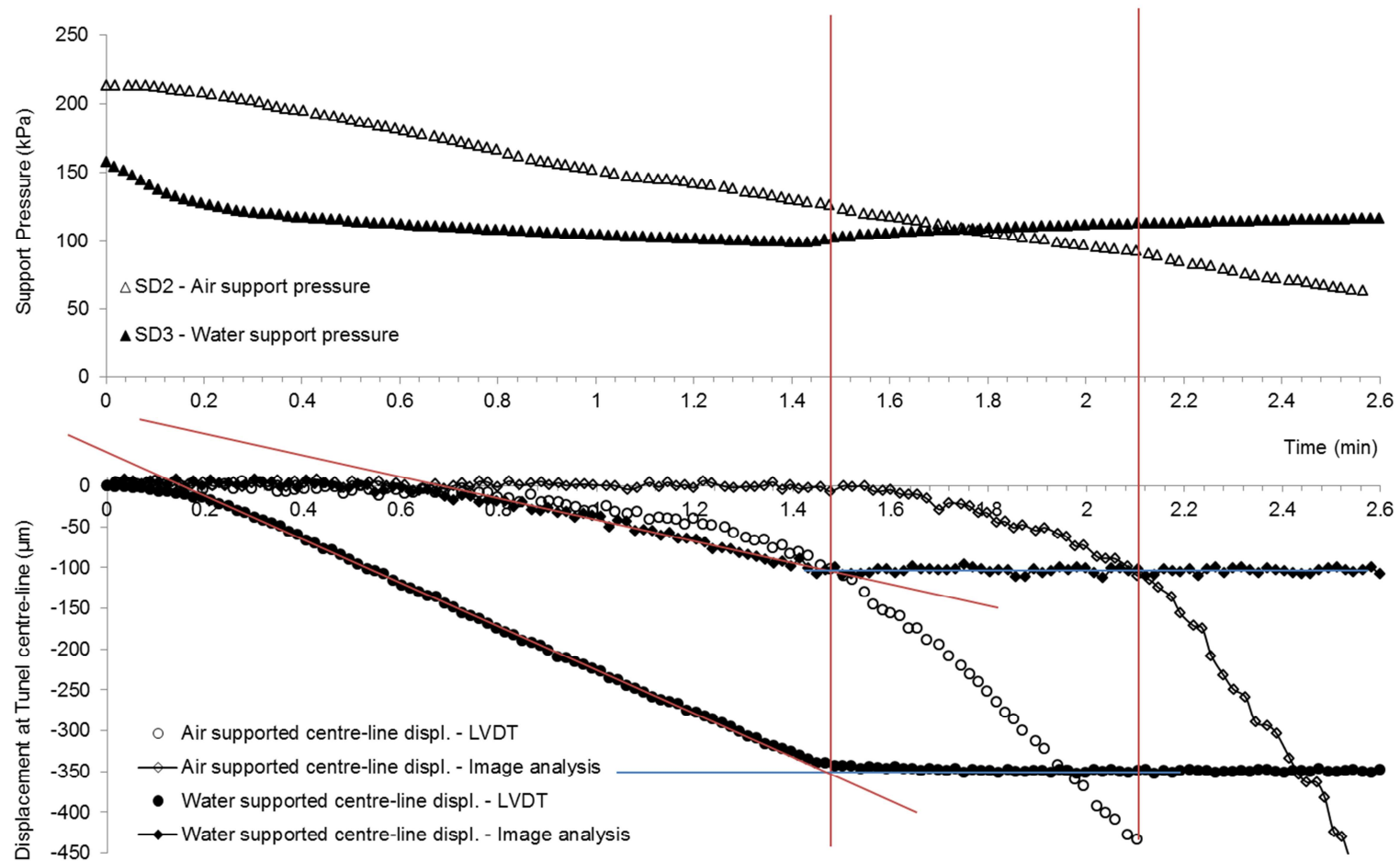


**Figure 8.11:** Movement at the tunnel centre-line measured by LVDT and Image Analysis for single tunnel air supported and water supported

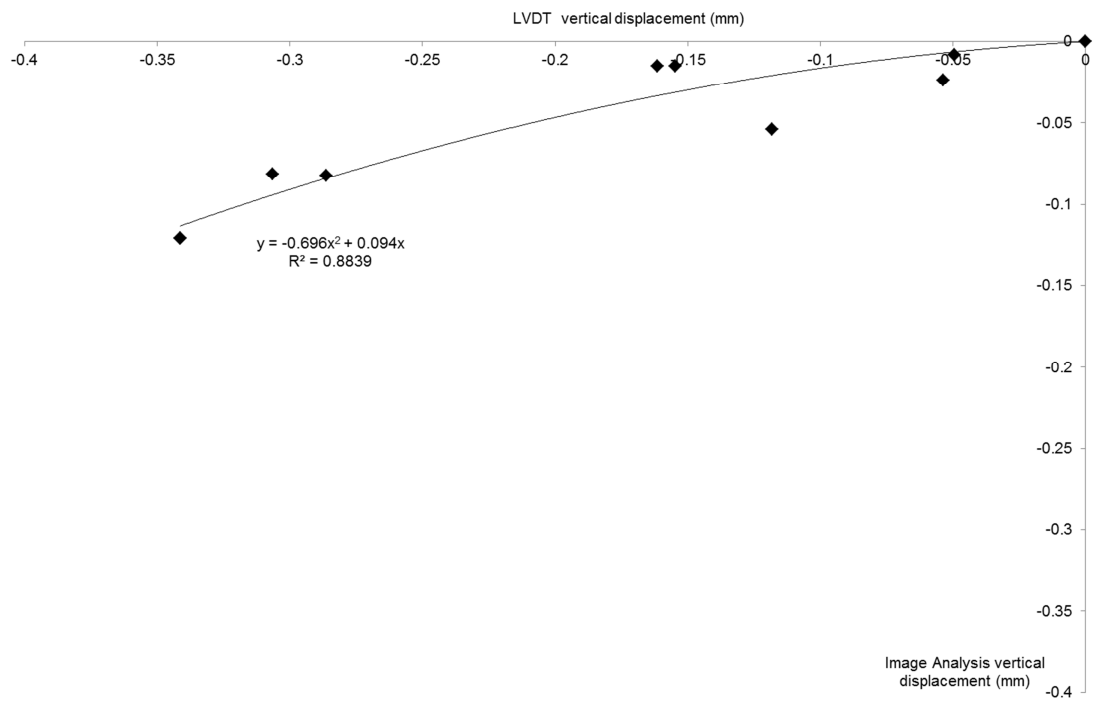


**Figure 8.12:** Relationship between vertical displacement recorded by CCD Camera and LVDT (at known distances from the centre-line of the tunnel) for a water supported single tunnel simulated construction

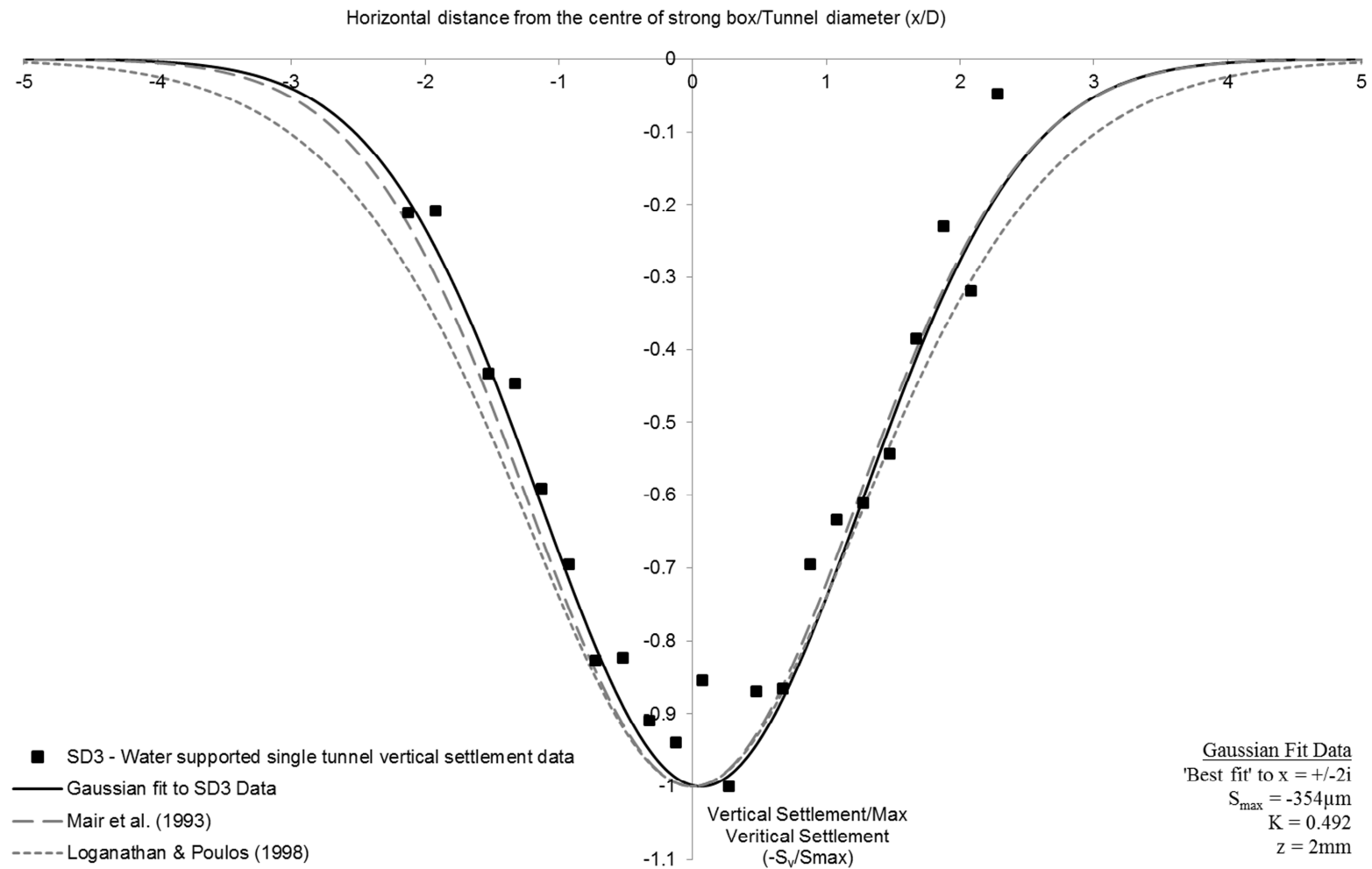


**Figure 8.13:** a) Vertical Settlement at a depth of 2mm in a simulated single tunnel construction with water support, SD3

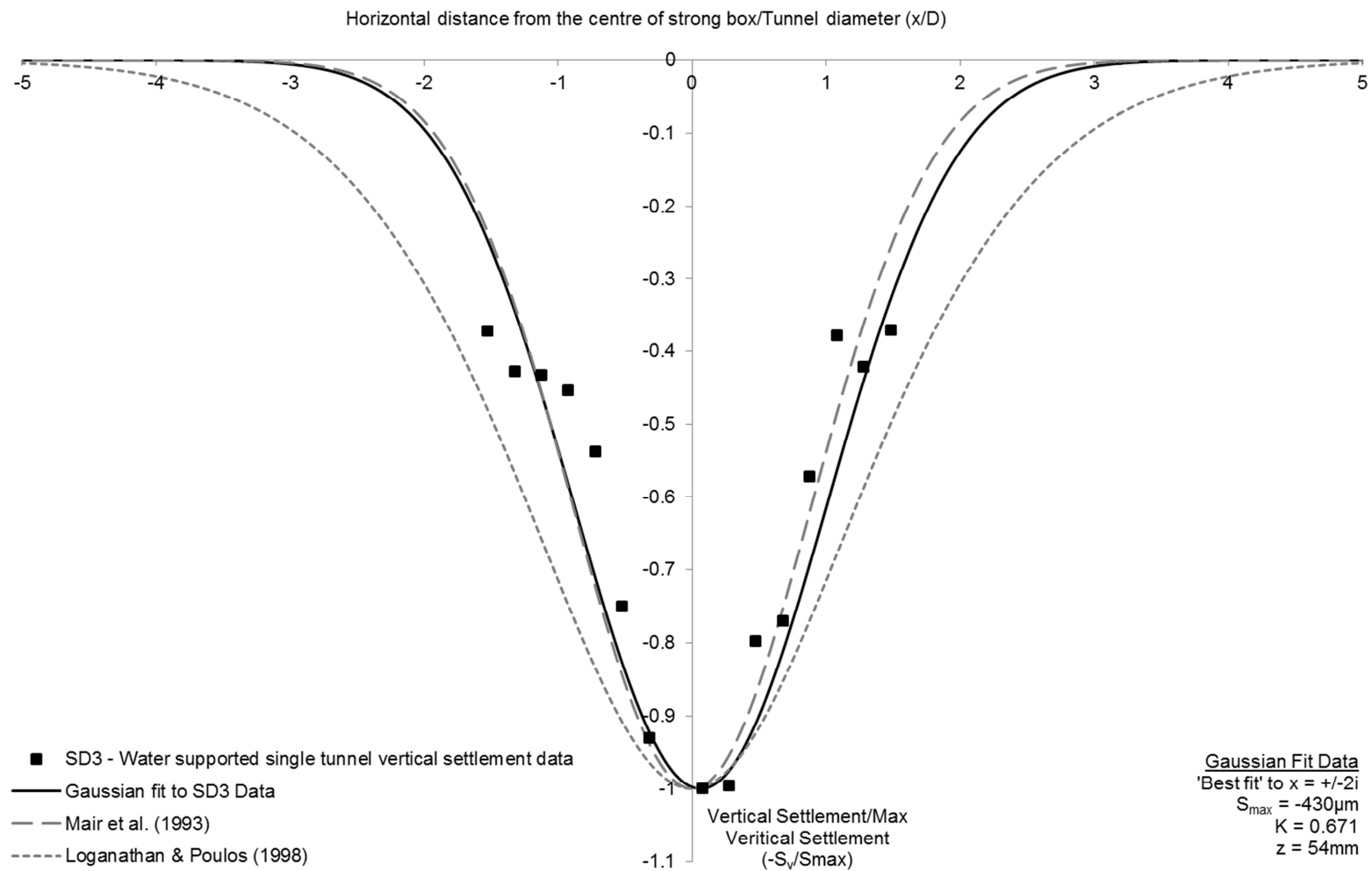


**Figure 8.13:** b) Vertical Settlement at a depth of 54mm in a simulated single tunnel construction with water support, SD3

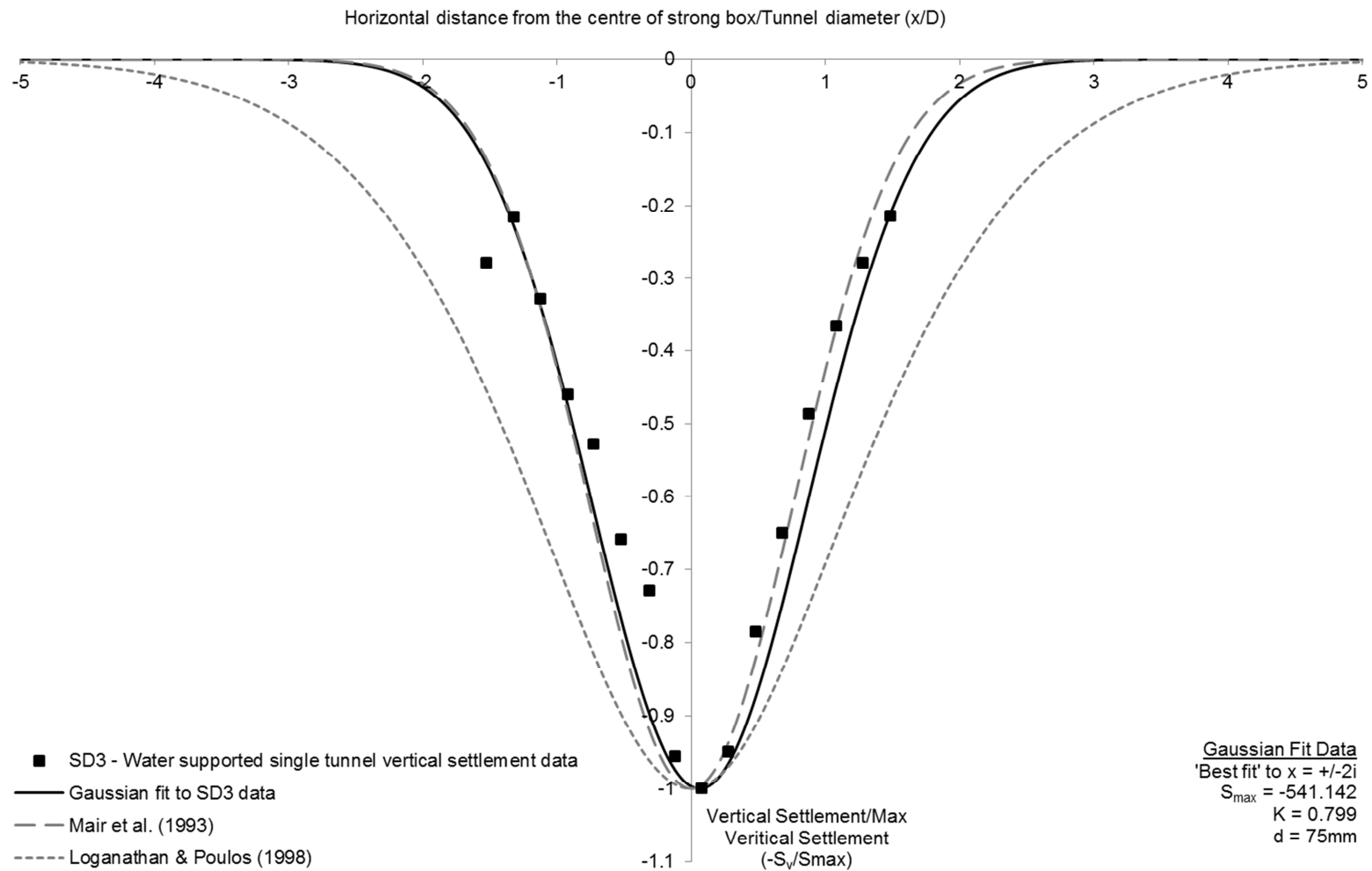


**Figure 8.13:** c) Vertical Settlement at a depth of 75mm in in a simulated single tunnel construction with water support, SD3

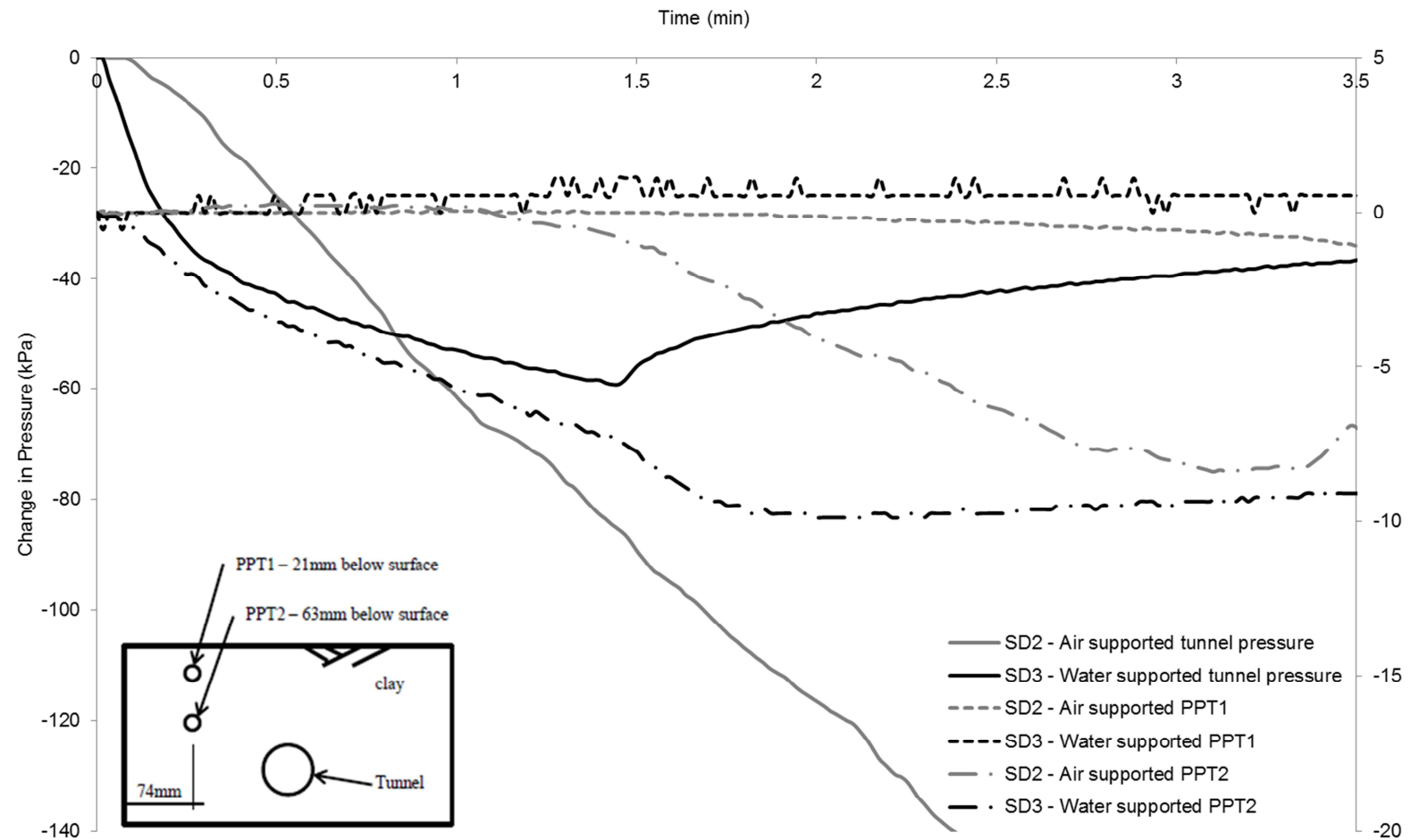


**Figure 8.14:** Comparison of changes in pore-water pressure during tests SD2 and SD3

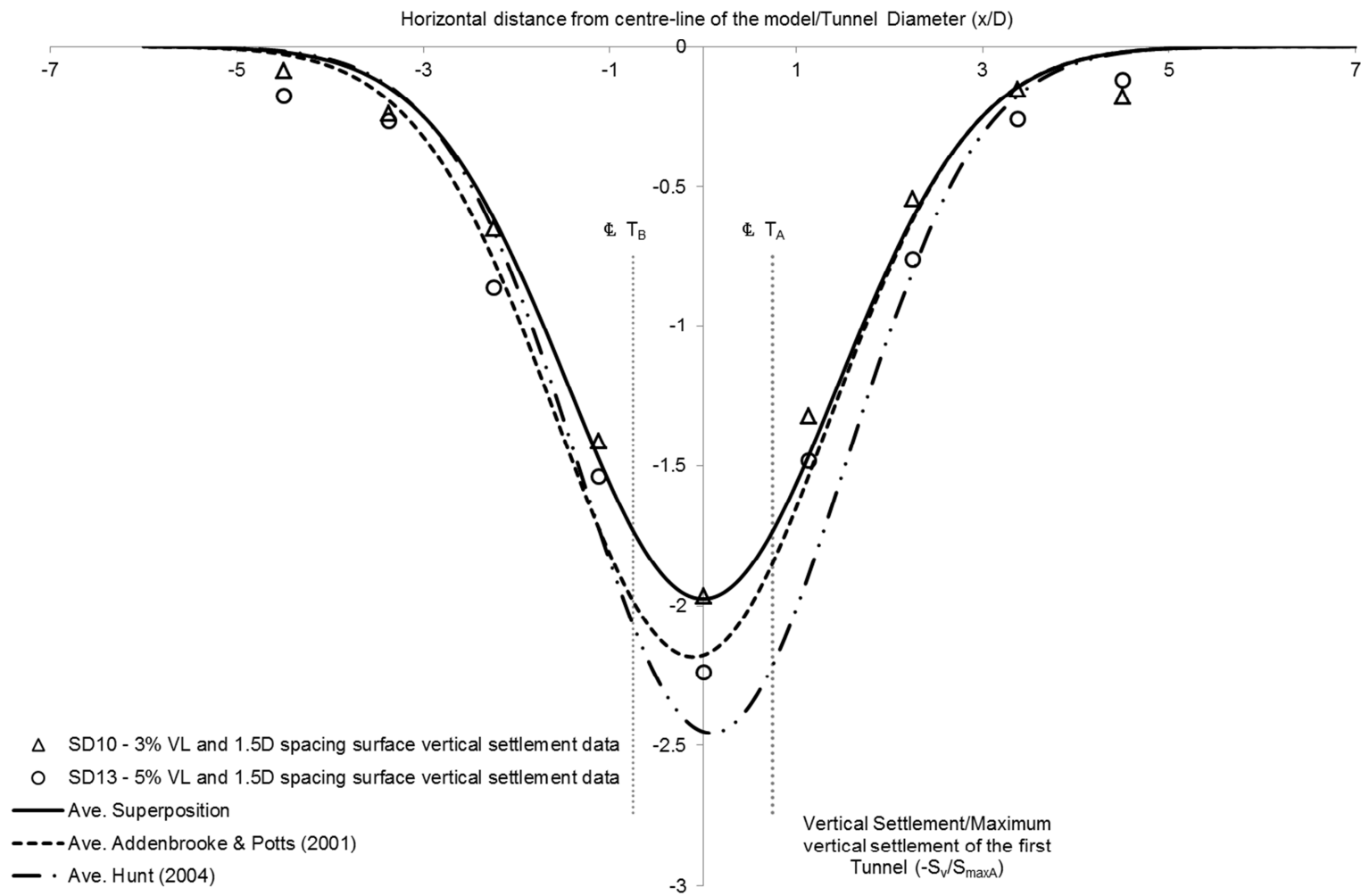


**Figure 8.15:** Twin-Tunnel vertical surface settlement from 1.5D spacing tests

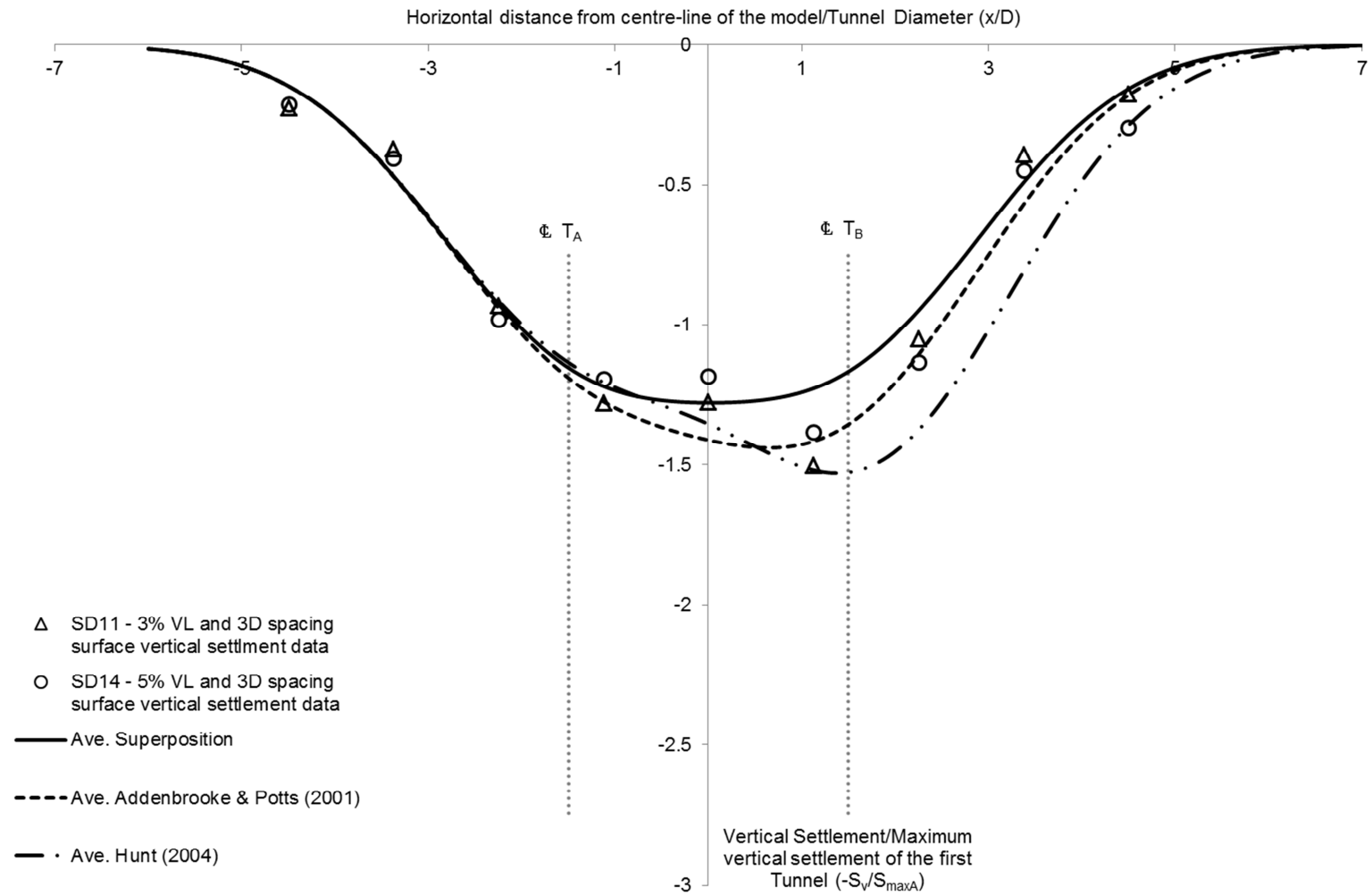


**Figure 8.16:** Twin-Tunnel vertical surface settlement from 3D spacing tests



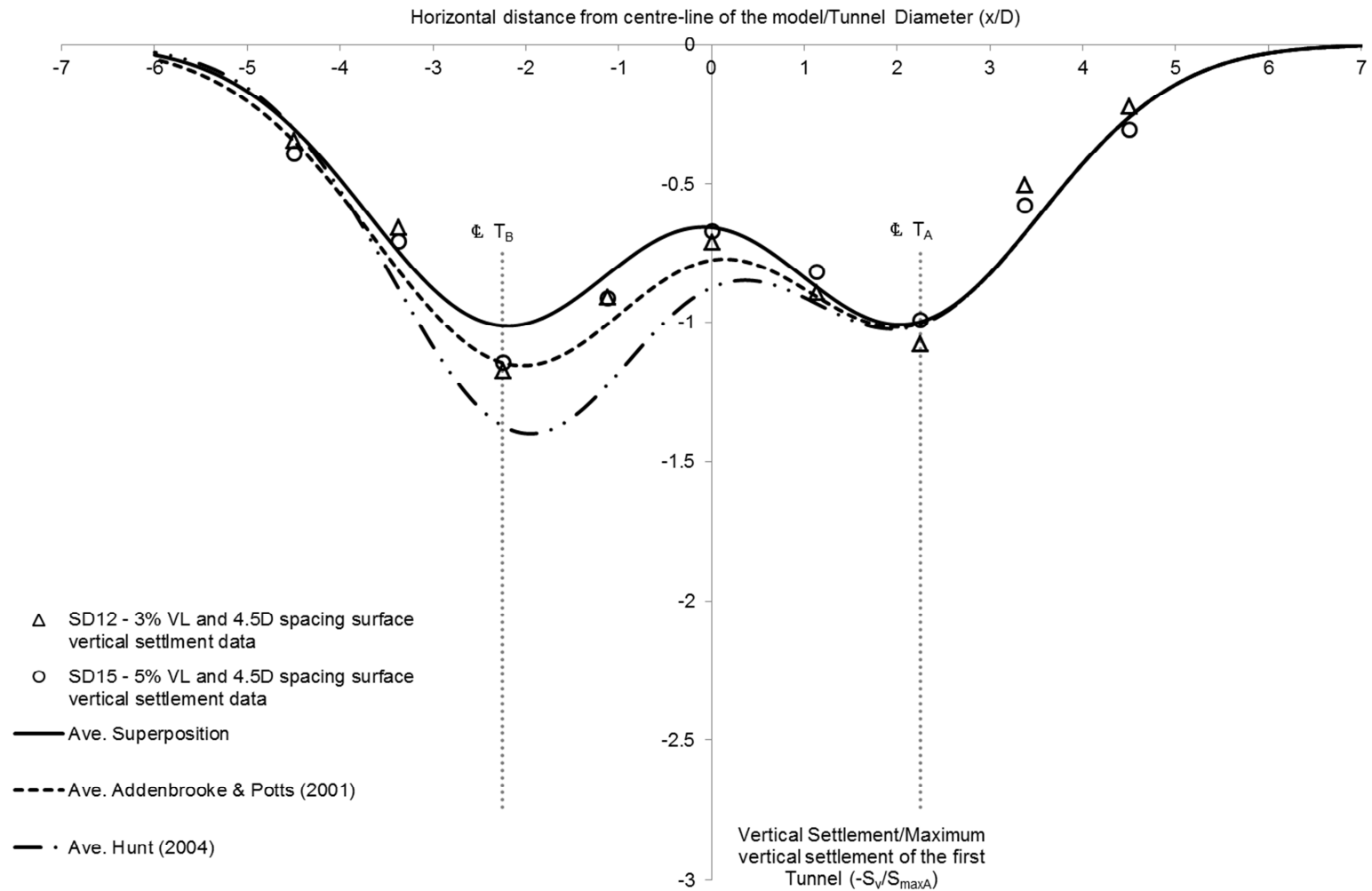


**Figure 8.17:** Twin-Tunnel vertical surface settlement from 4.5D spacing tests

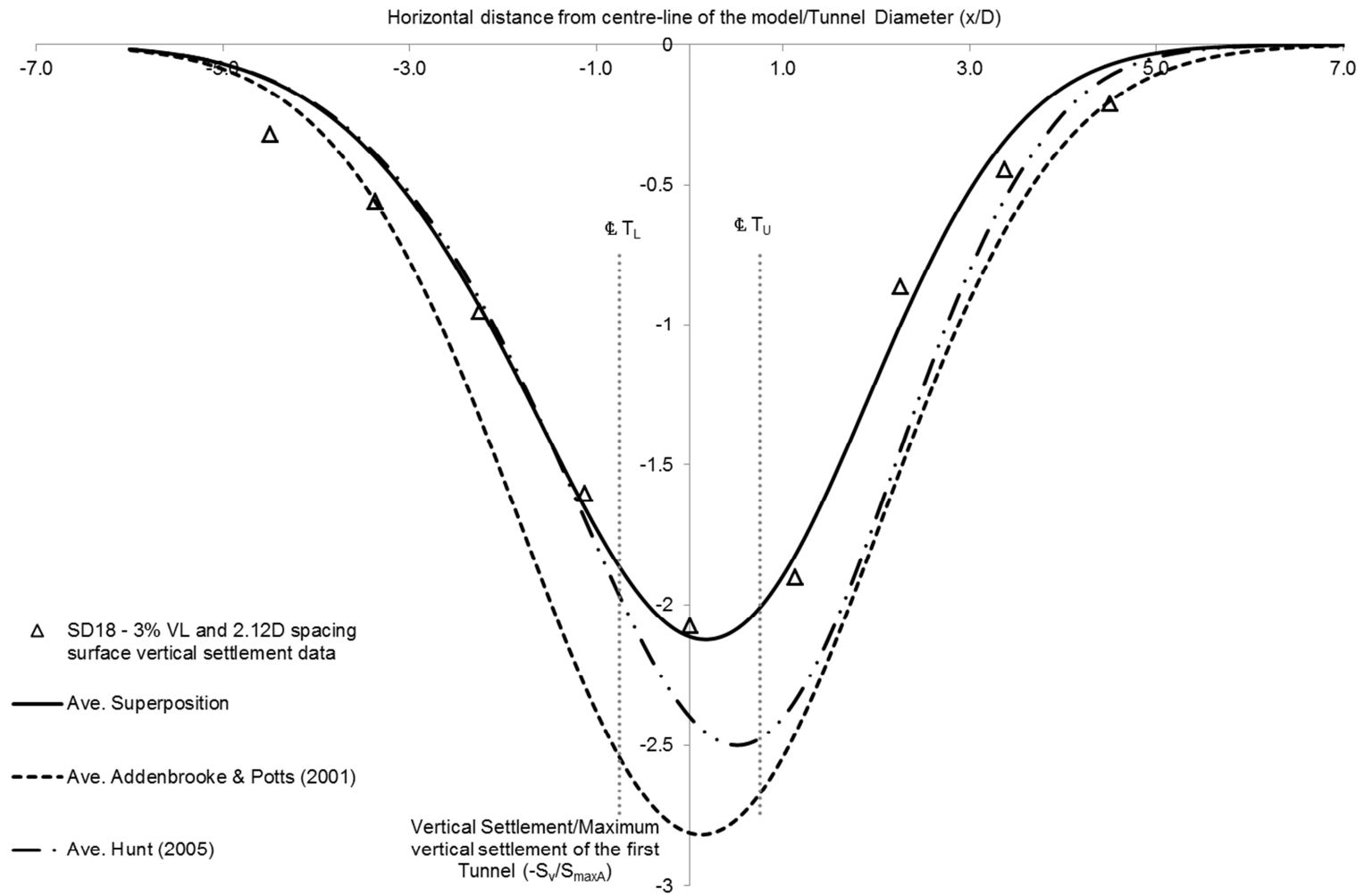


**Figure 8.18:** Twin-Tunnel vertical surface settlement from 2.12D spacing test

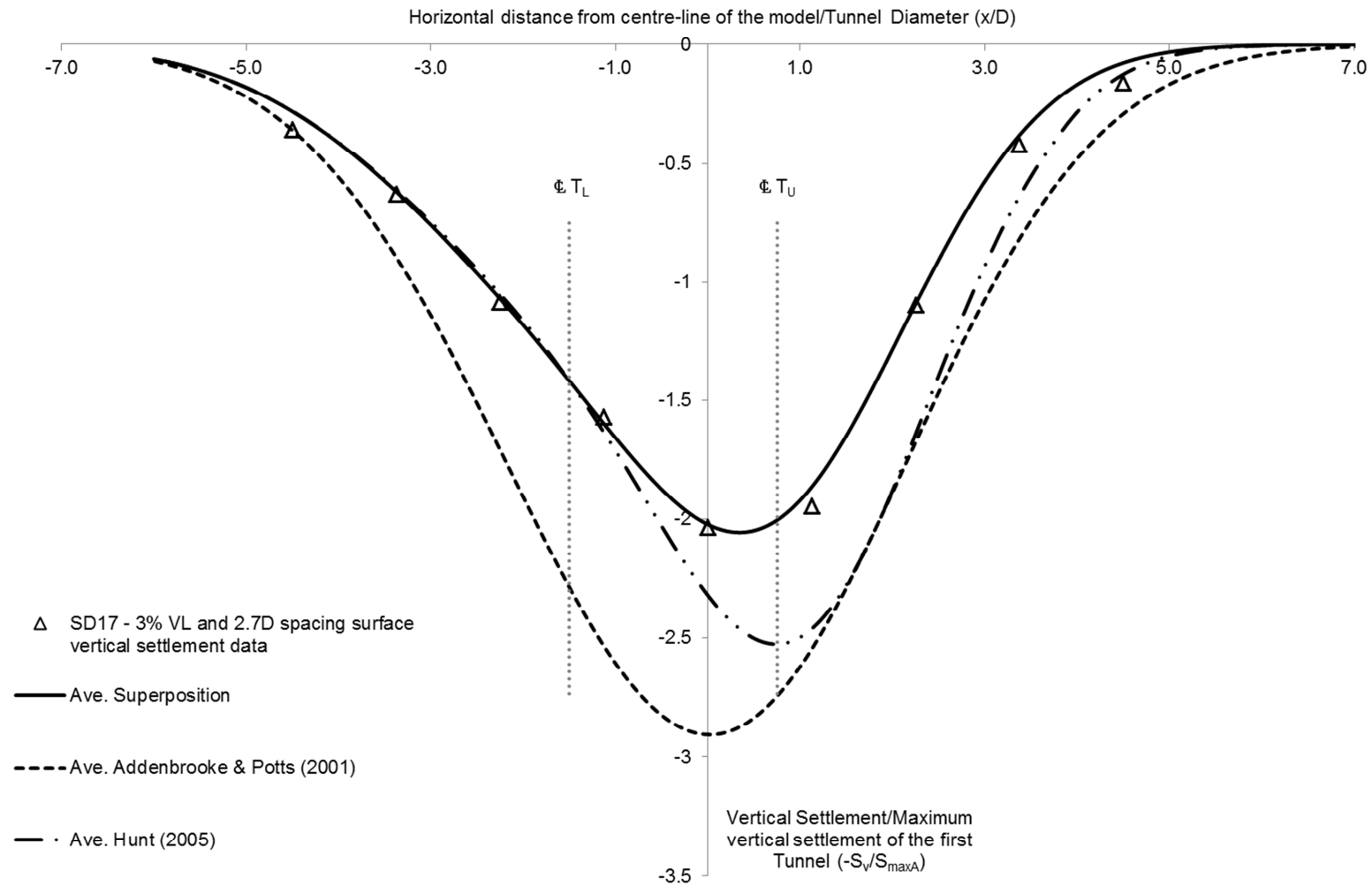


**Figure 8.19:** Twin-Tunnel vertical surface settlement from 2.7D spacing test

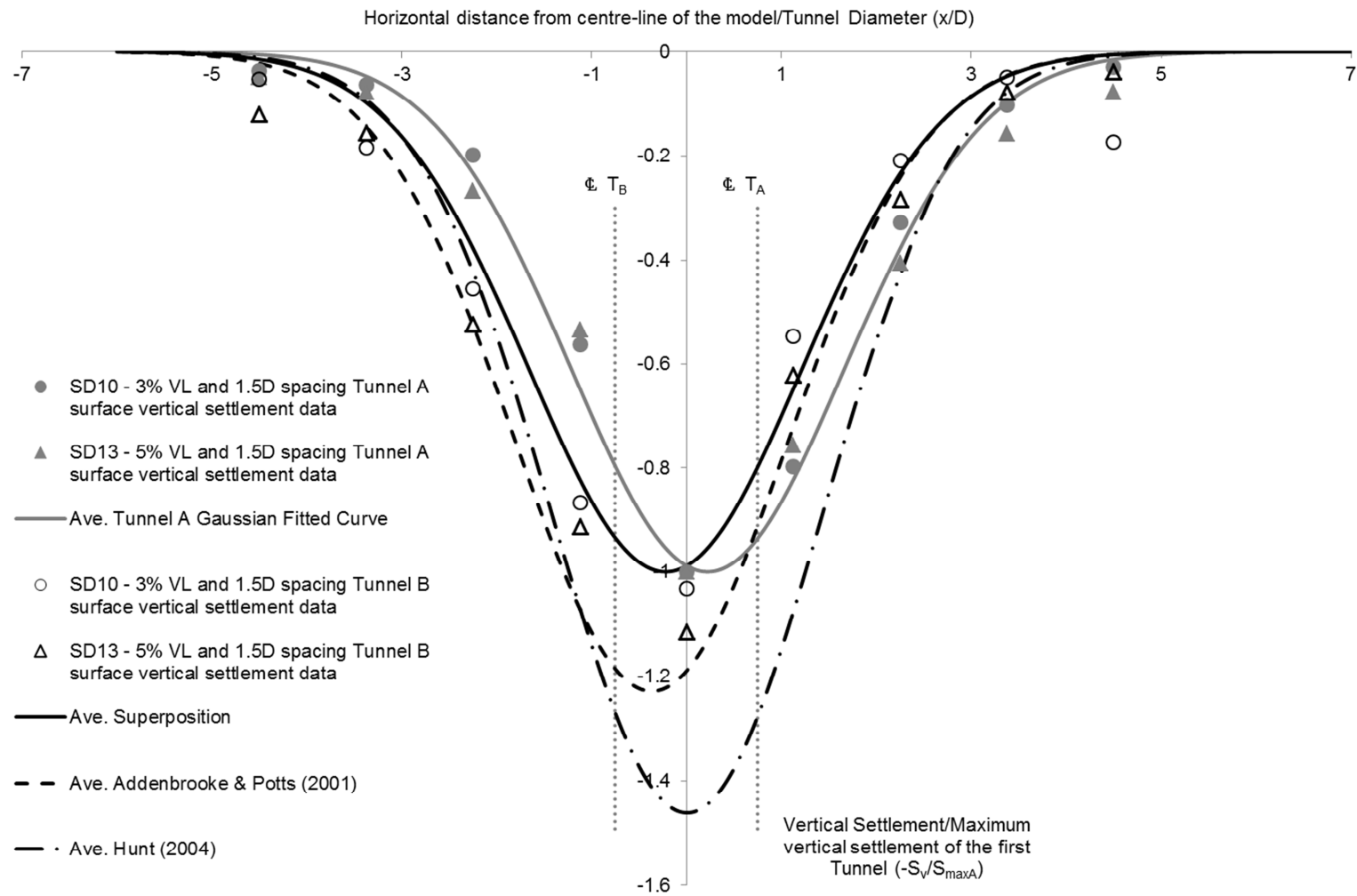


**Figure 8.20:** Tunnel A and Tunnel B vertical surface settlement from 1.5D spacing tests

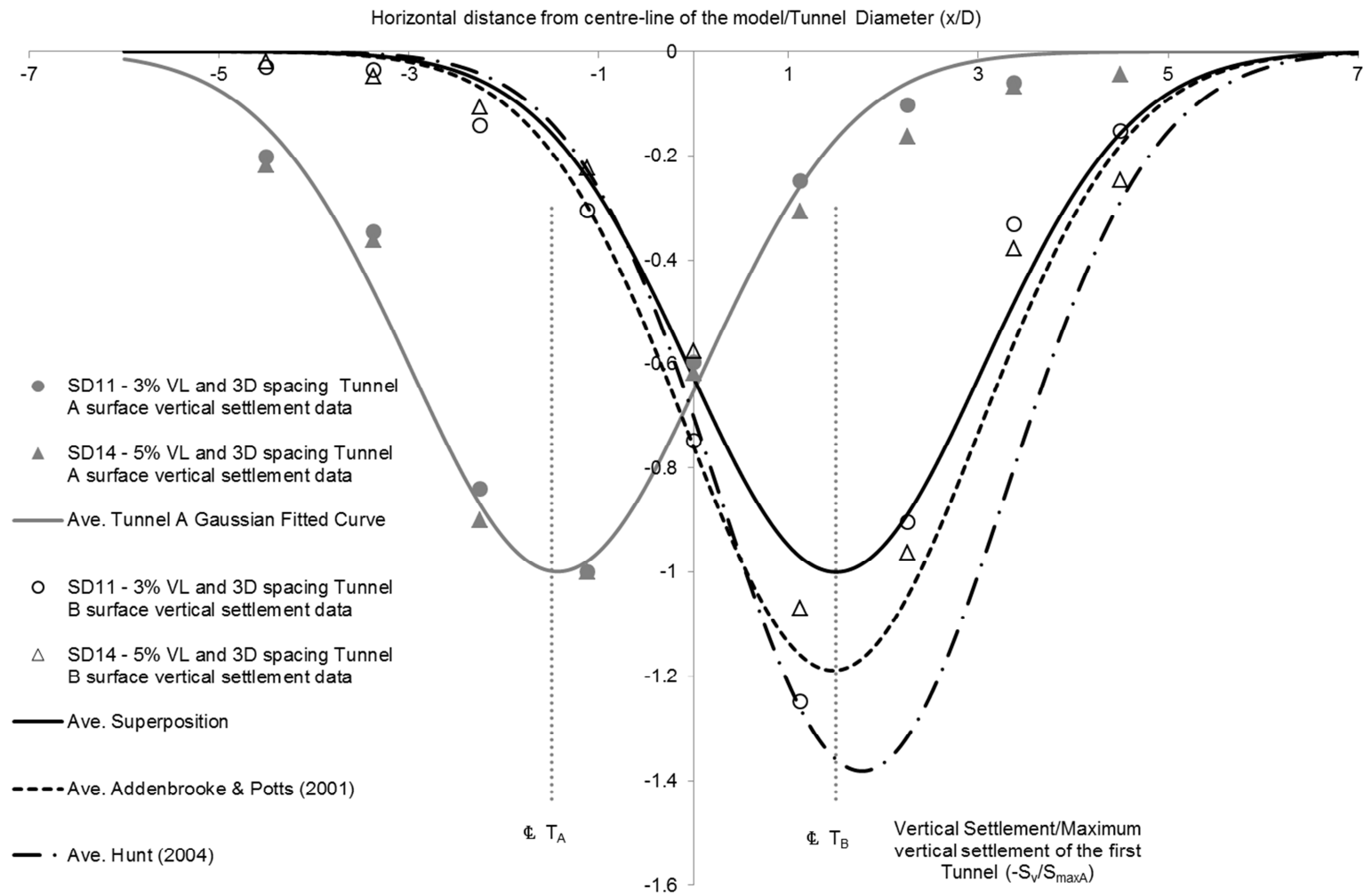


**Figure 8.21:** Tunnel A and Tunnel B vertical surface settlement from 3D spacing tests

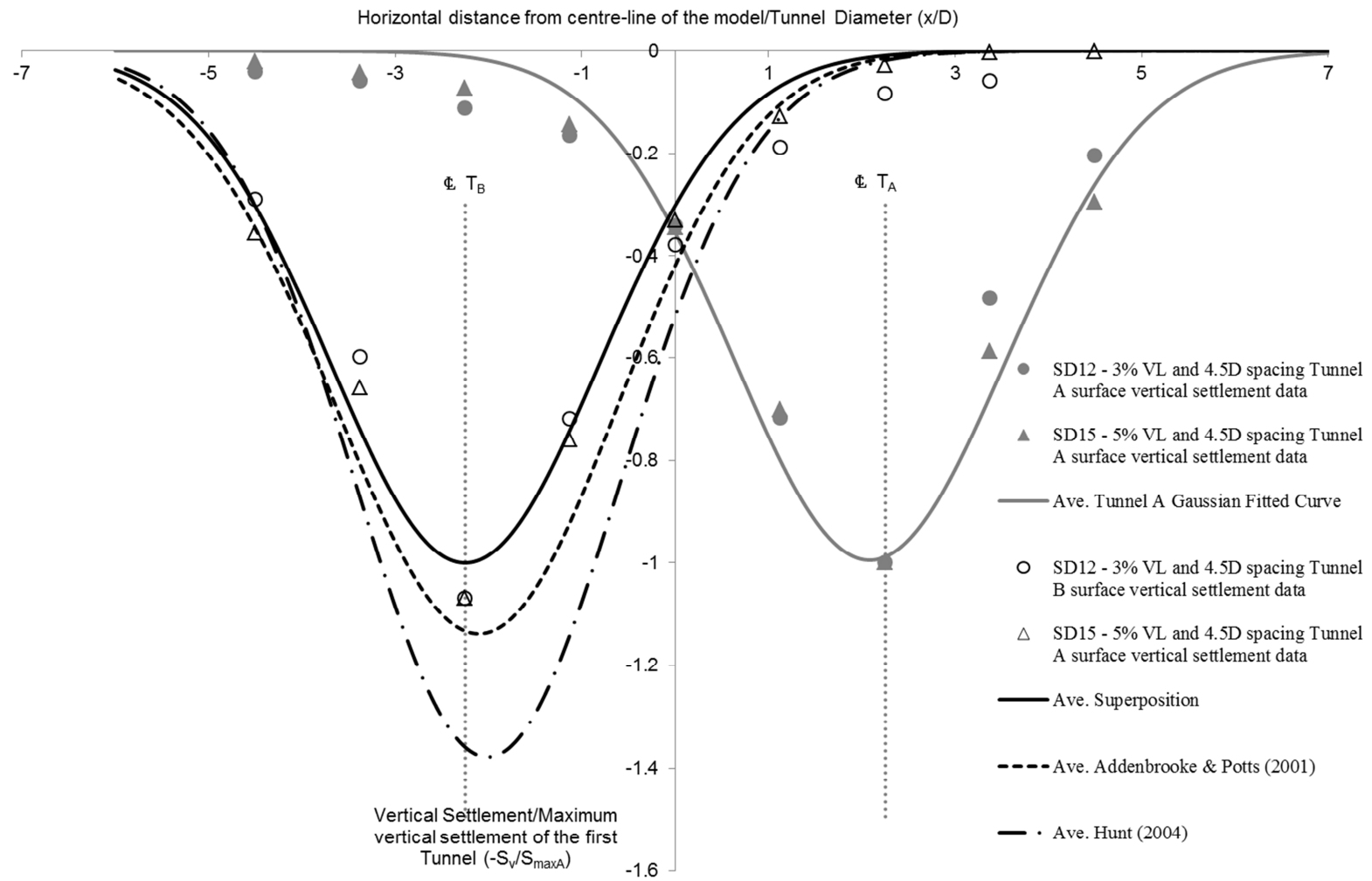


**Figure 8.22:** Tunnel A and Tunnel B vertical surface settlement from 4.5D spacing tests

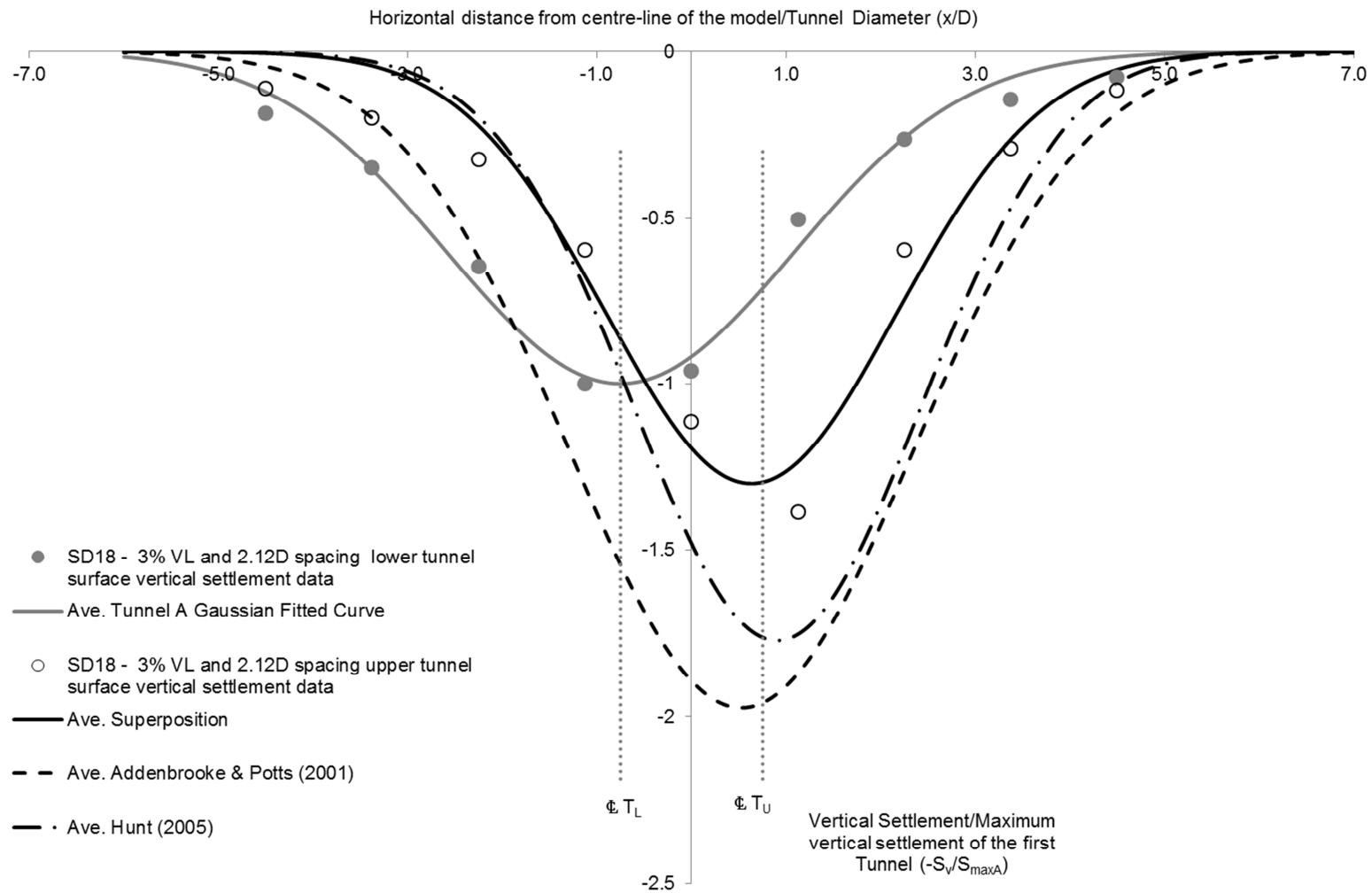


**Figure 8.23:** Tunnel A and Tunnel B vertical surface settlement from 2.12D spacing tests

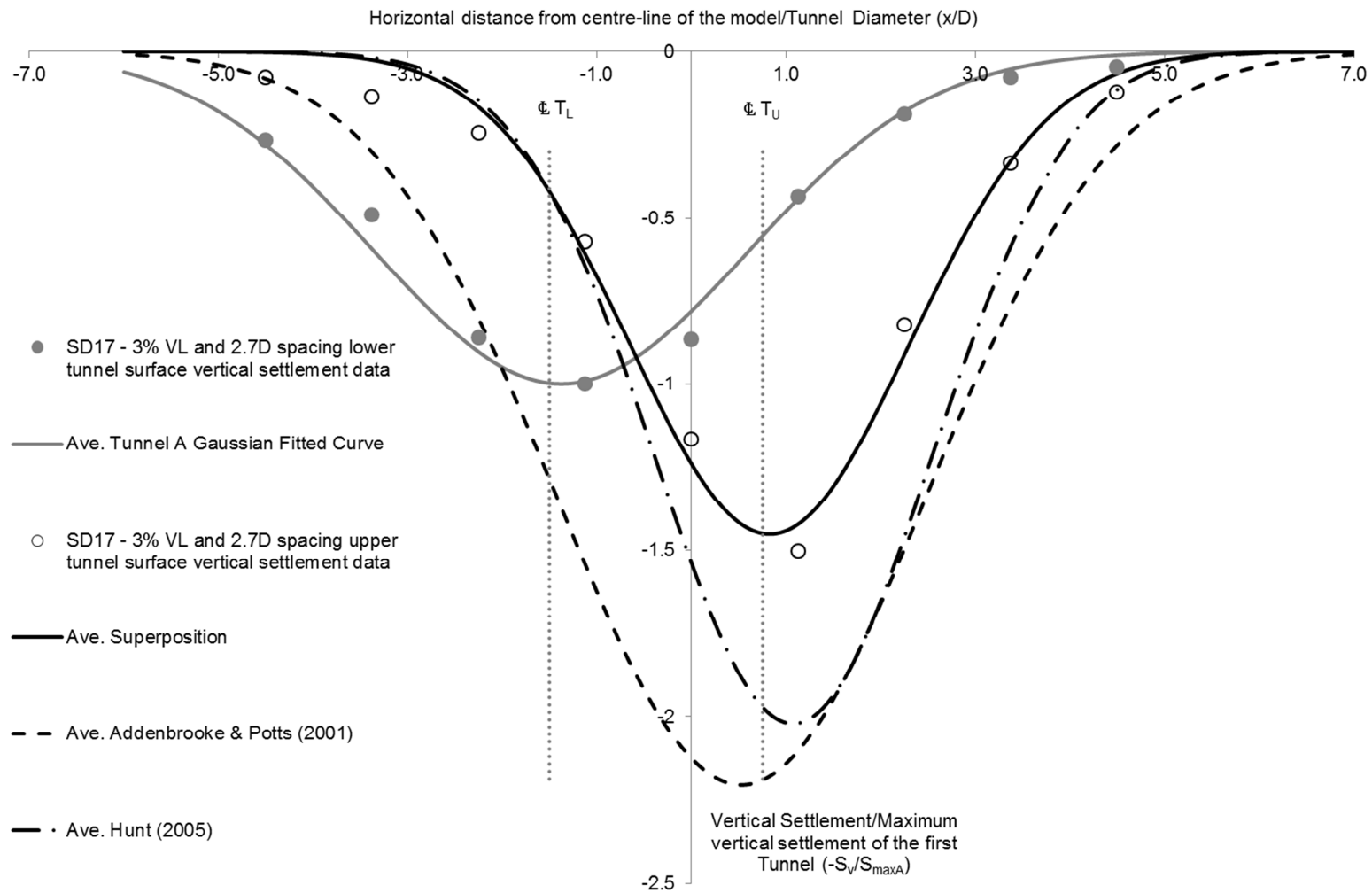
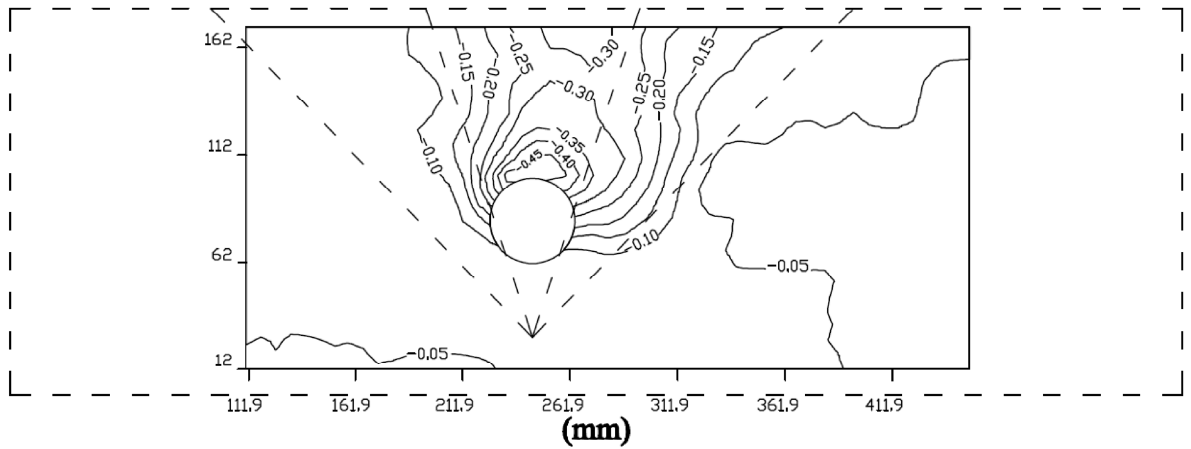


**Figure 8.24:** Tunnel A and Tunnel B vertical surface settlement from 2.7D spacing tests

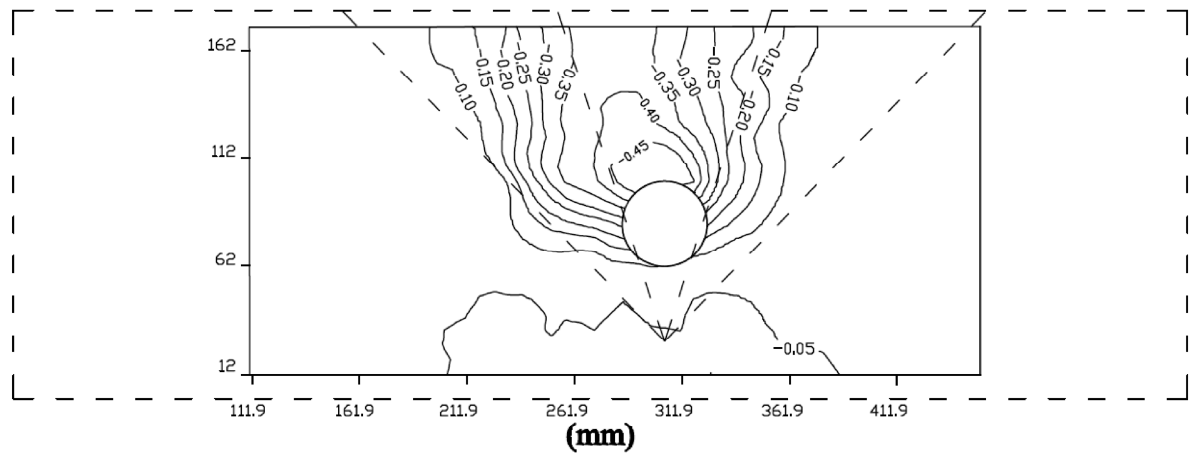


# SD13 - 5% volume loss test at 1.5D spacing

Vertical settlement solely from the simulated first tunnel construction



Vertical settlement solely from the simulated second tunnel construction



Vertical settlement from the simulated twin-tunnel construction

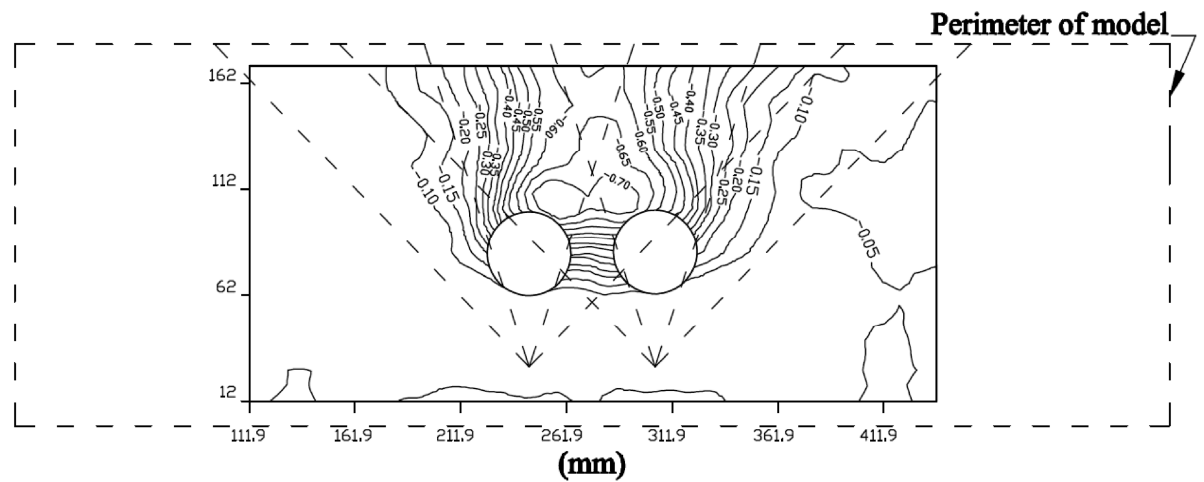
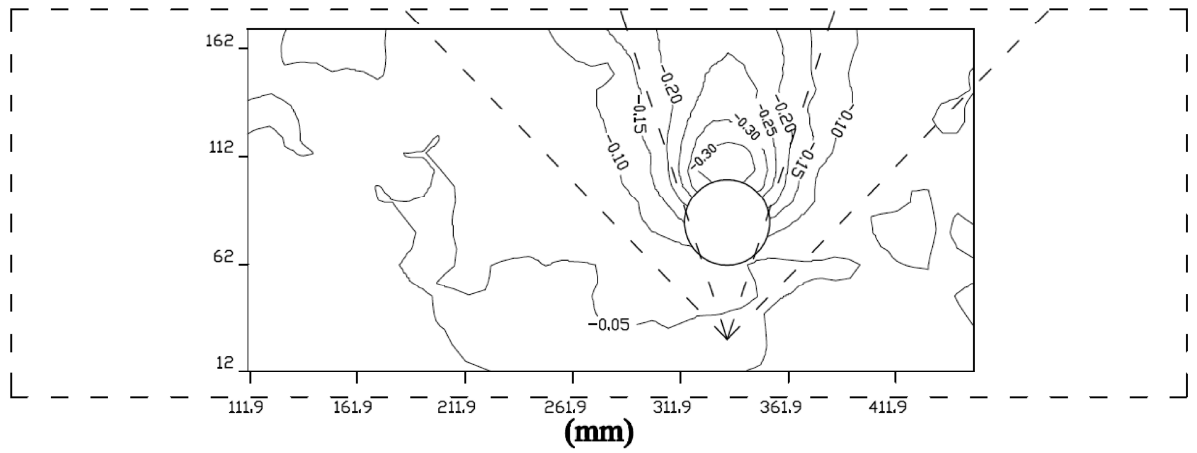


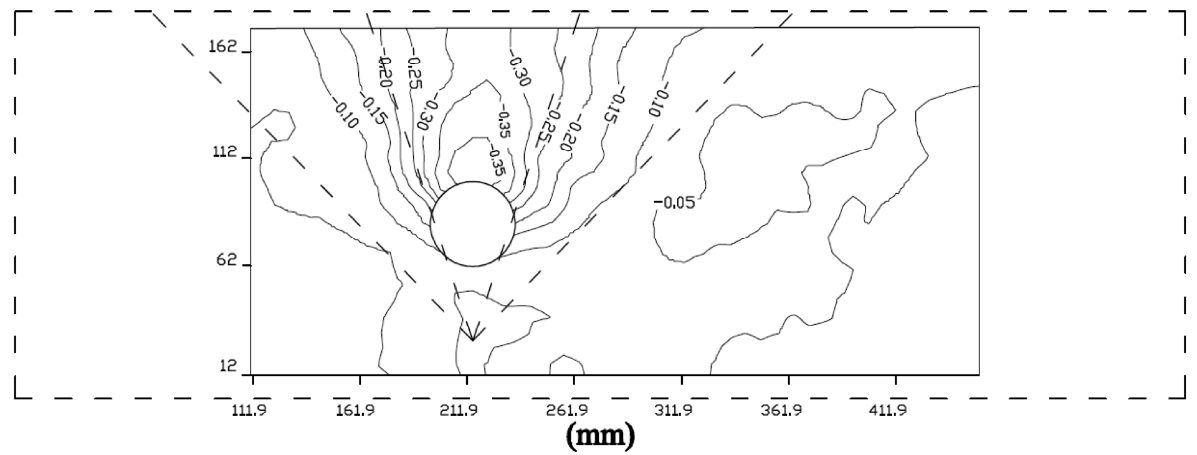
**Figure 8.25:** Sub-surface vertical displacement vectors presented as contours from tests SD13

# SD14 - 5% volume loss test at 3D spacing

Vertical settlement solely from the simulated first tunnel construction



Vertical settlement solely from the simulated second tunnel construction



Vertical settlement from the simulated twin-tunnel construction

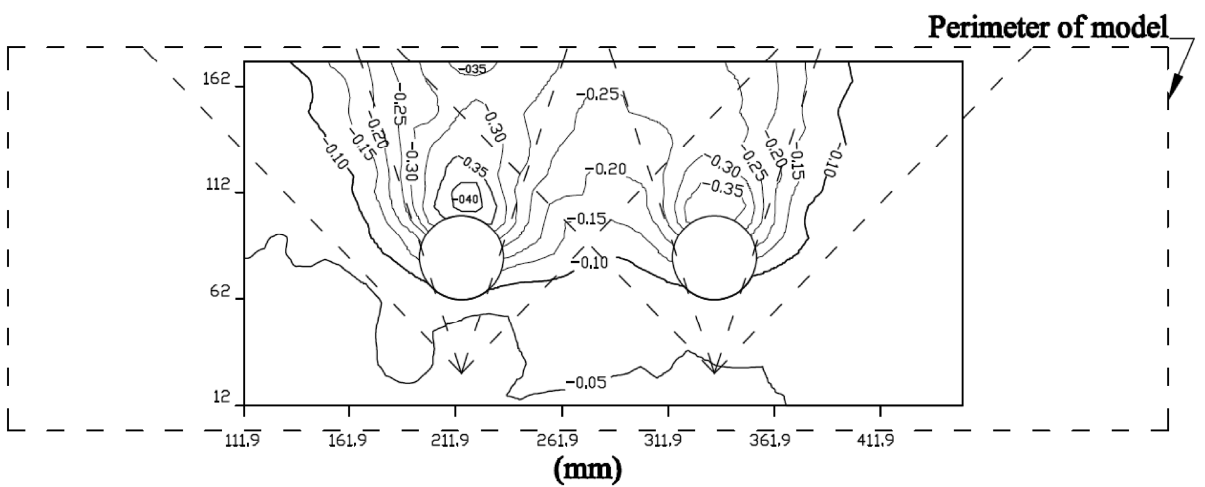


**Figure 8.26:** Sub-surface vertical displacement vectors presented as contours from tests SD14



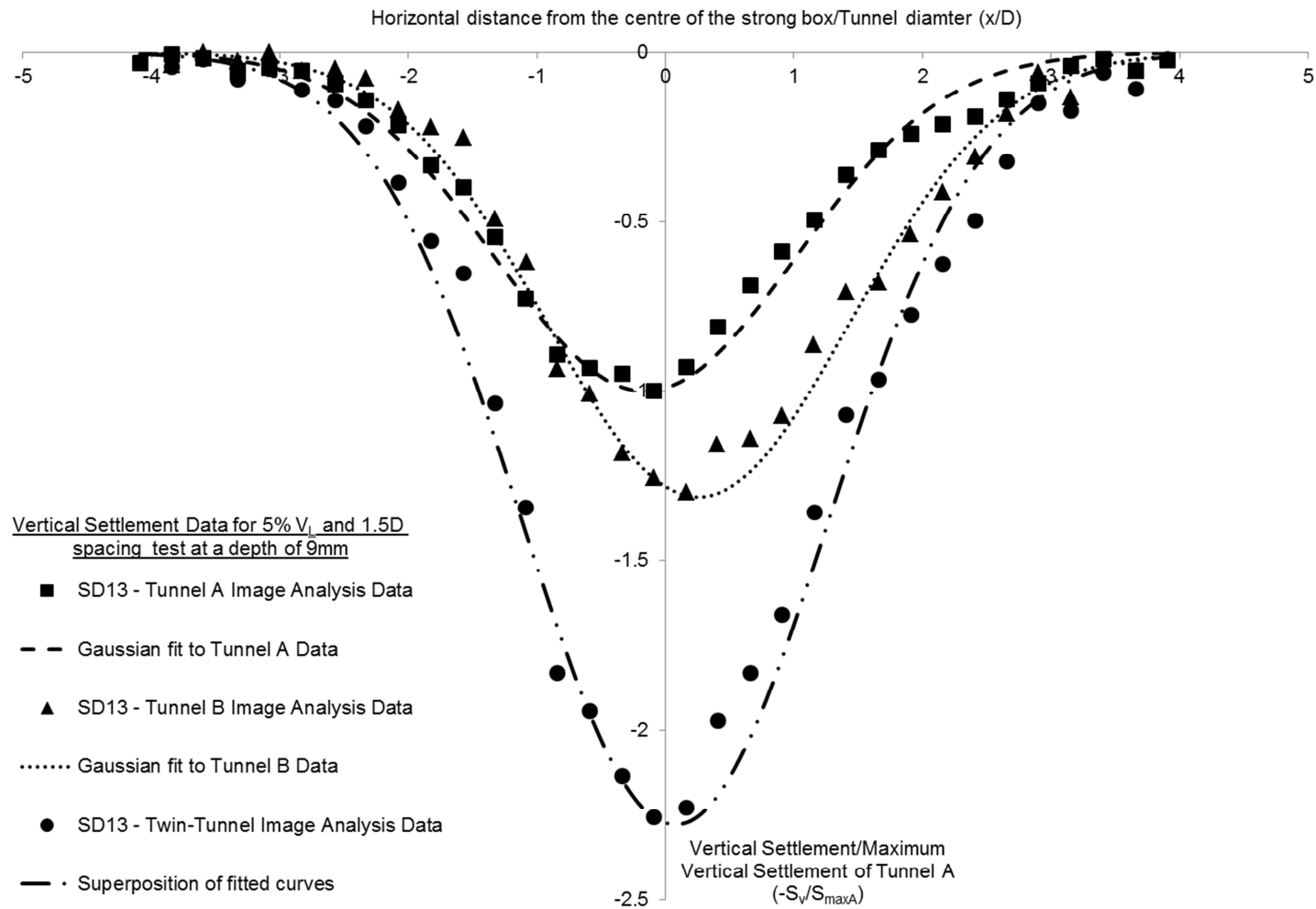


**Figure 8.28:** a) Vertical Settlement at a depth of 9mm in SD13

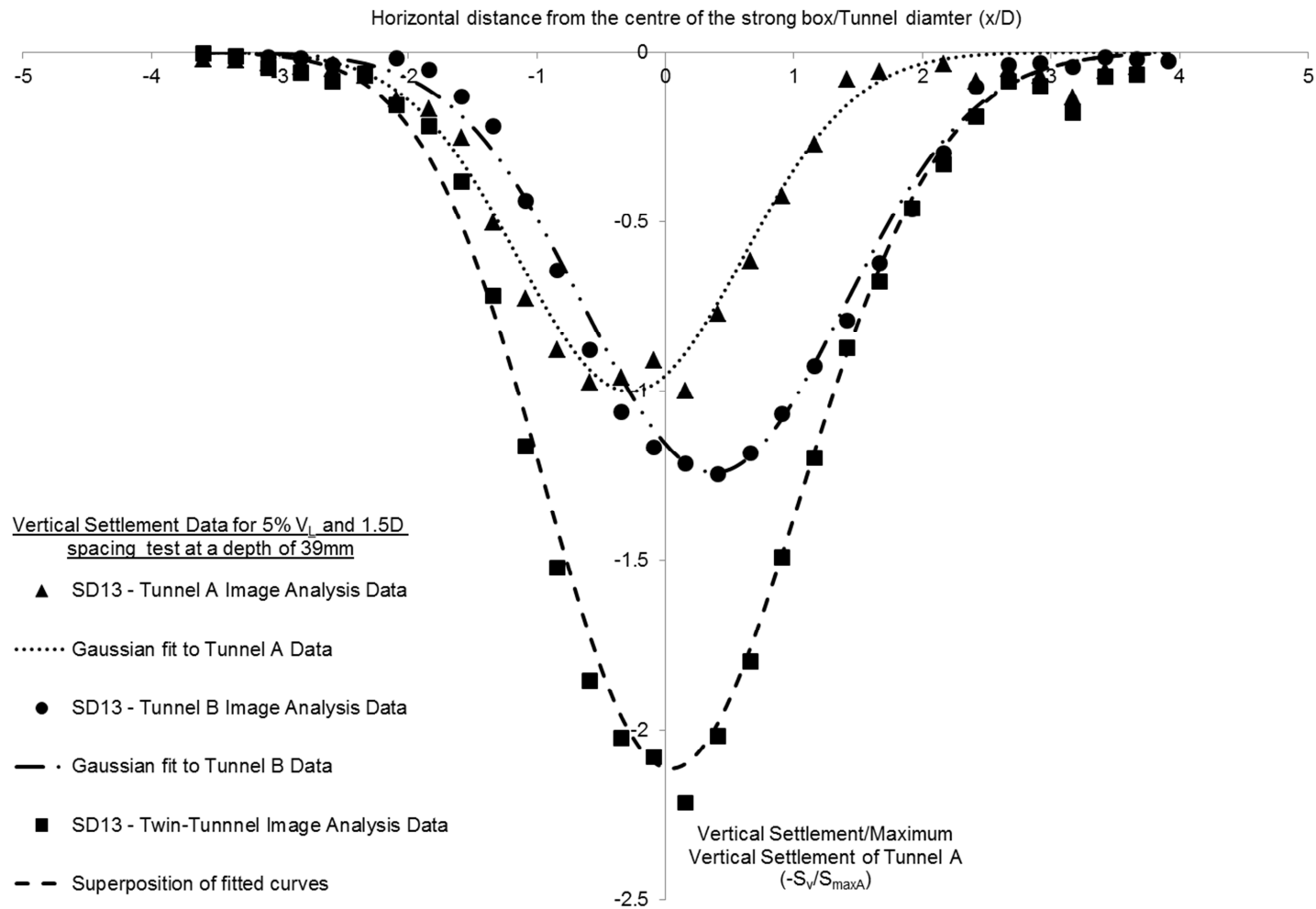


**Figure 8.28:** b) Vertical Settlement at a depth of 39mm in SD13

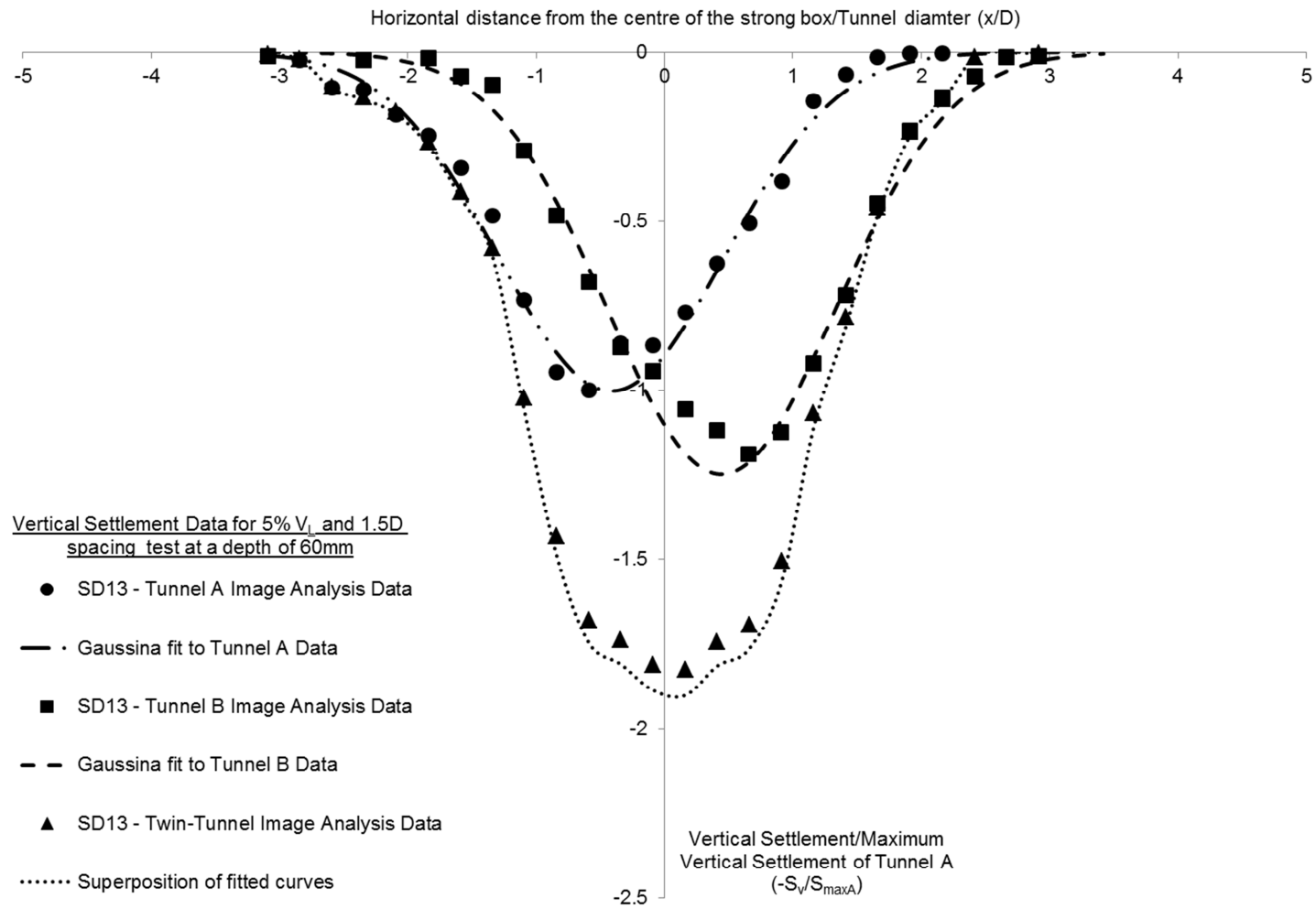


**Figure 8.28:** c) Vertical Settlement at a depth of 60mm in SD13

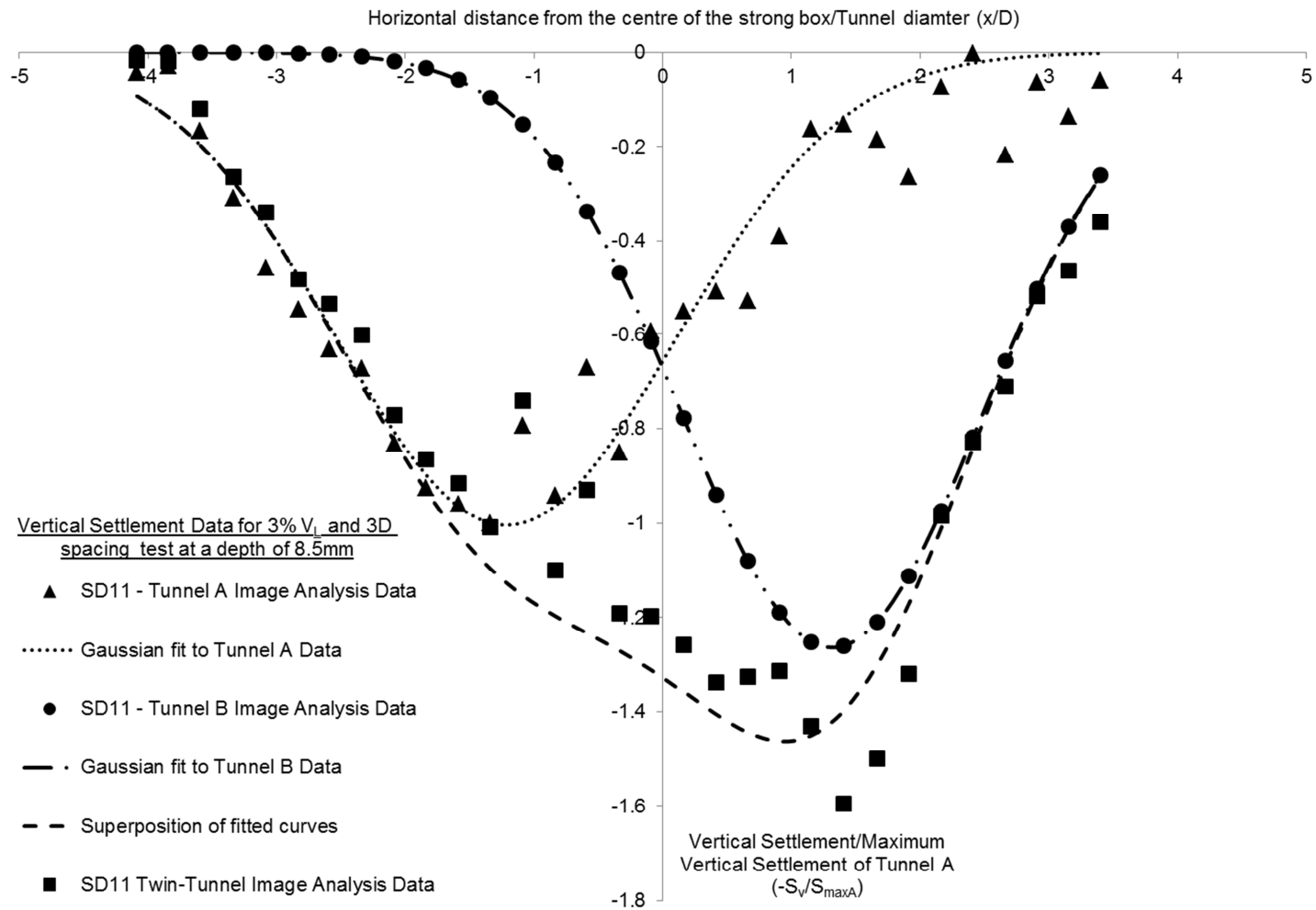


**Figure 8 29:** a) Vertical Settlement at a depth of 8.5mm in SD11

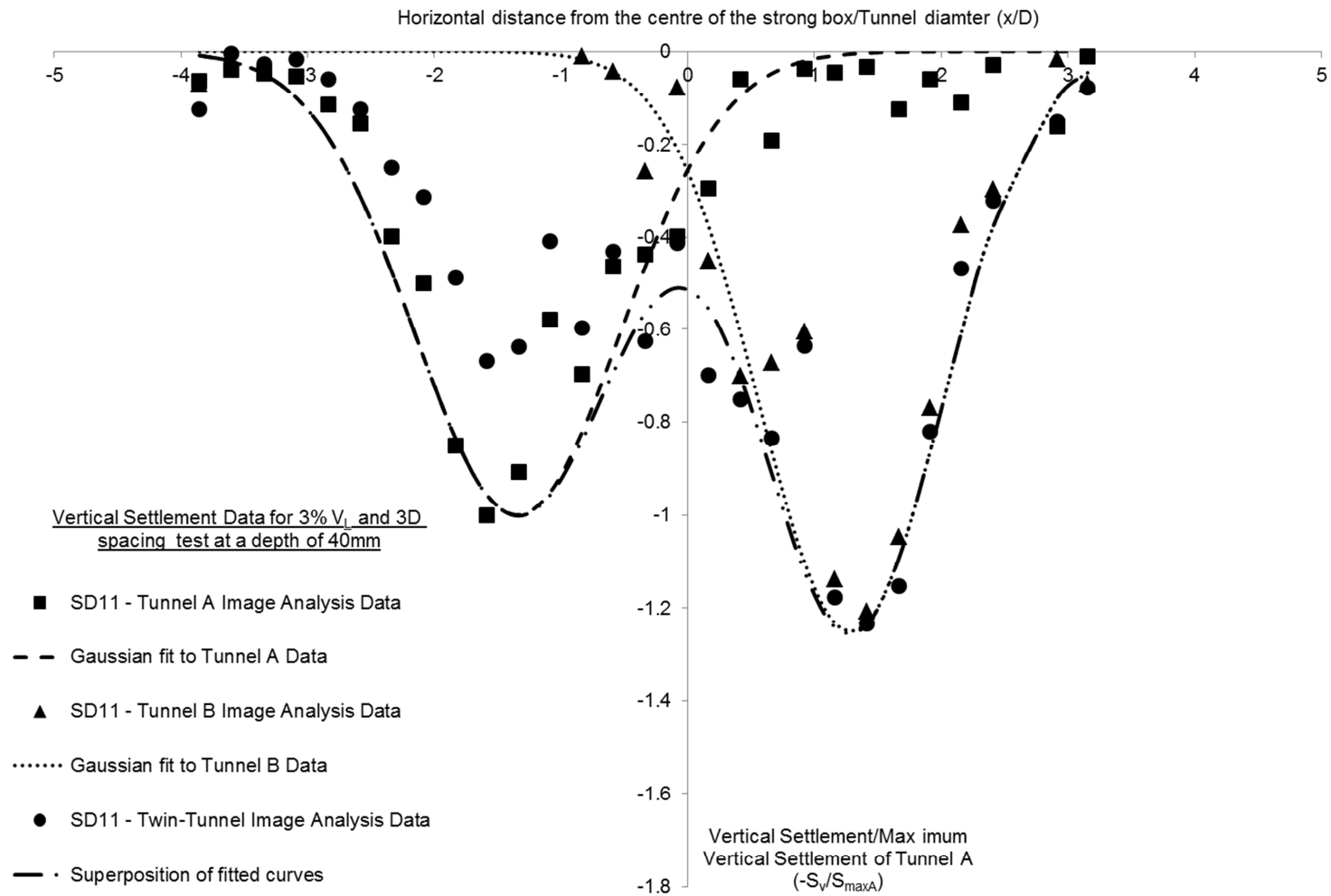


**Figure 8.29:** b) Vertical Settlement at a depth of 40mm in SD11



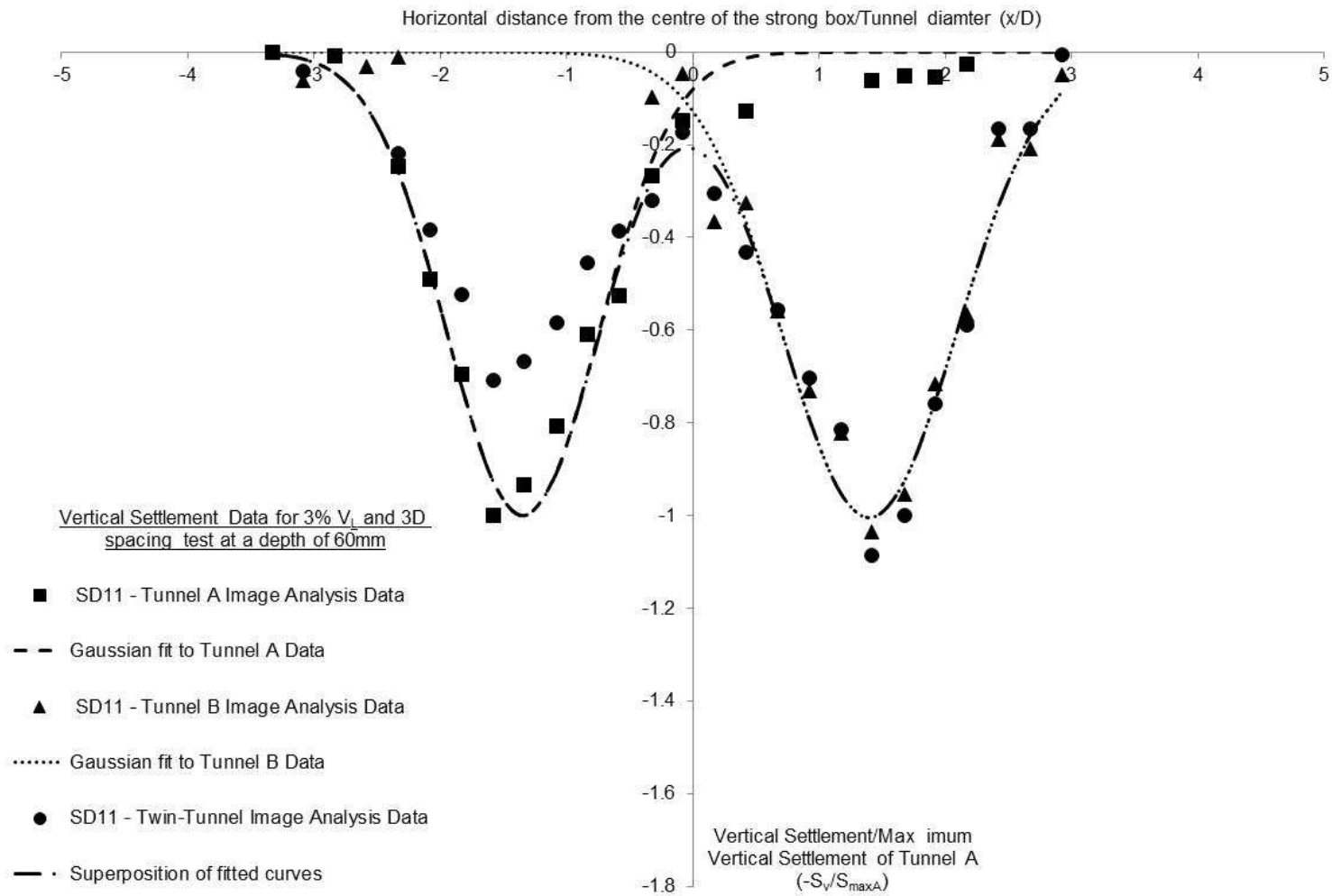


**Figure 8.29:** c) Vertical Settlement at a depth of 60mm in SD11

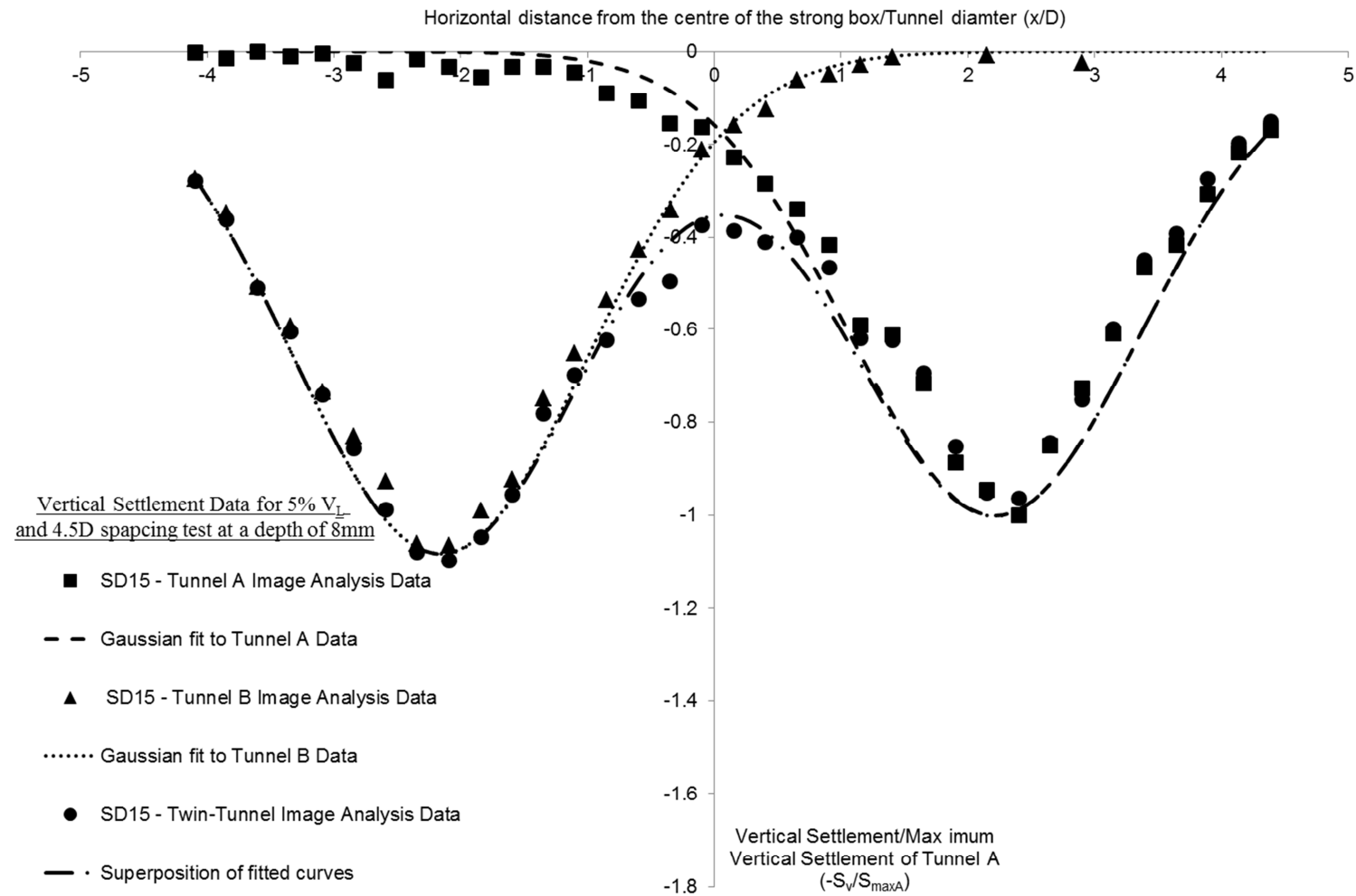


**Figure 8.30:** a) Vertical Settlement at a depth of 8mm in SD15

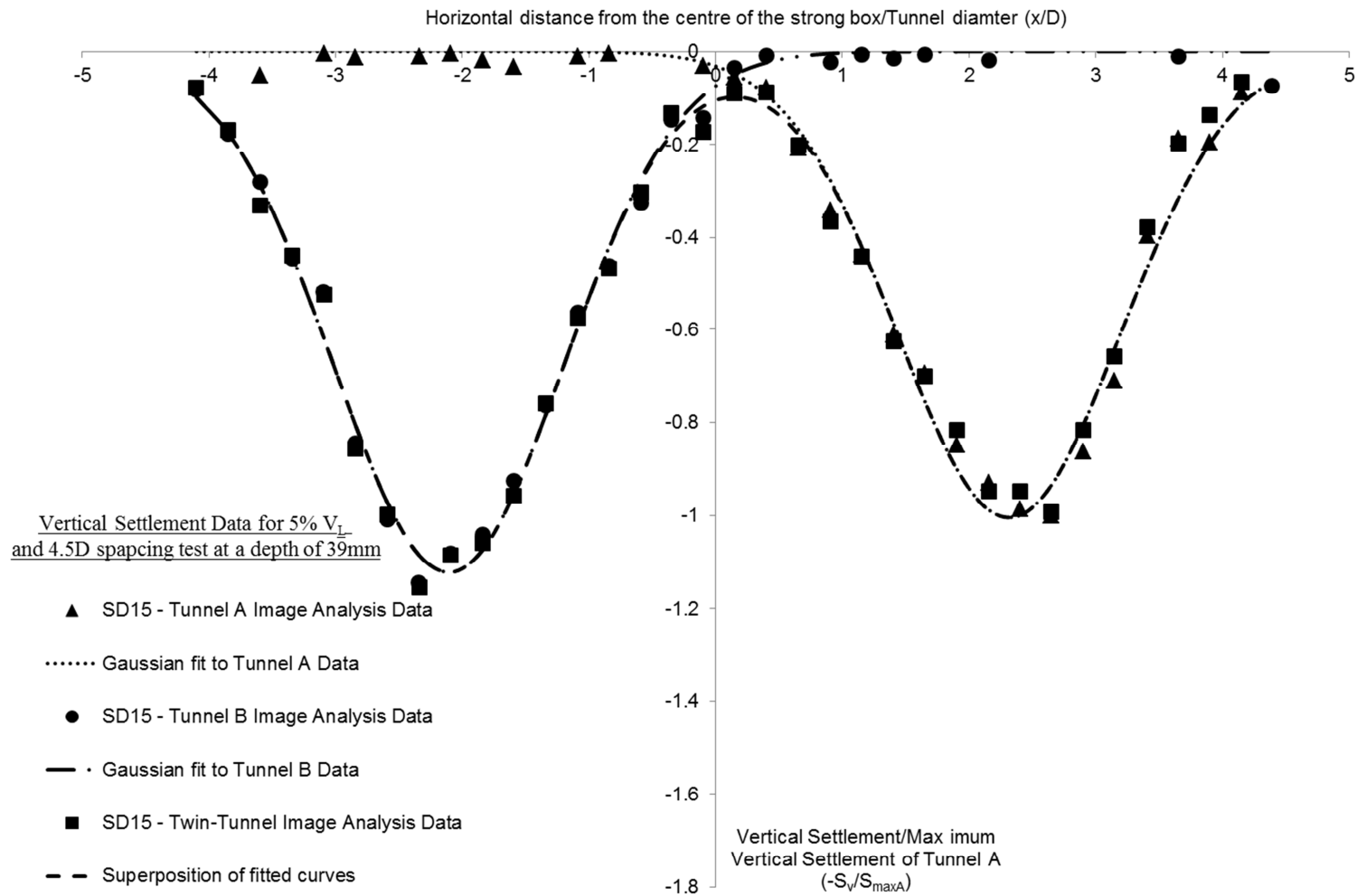


**Figure 8.30:** b) Vertical Settlement at a depth of 39mm in SD15

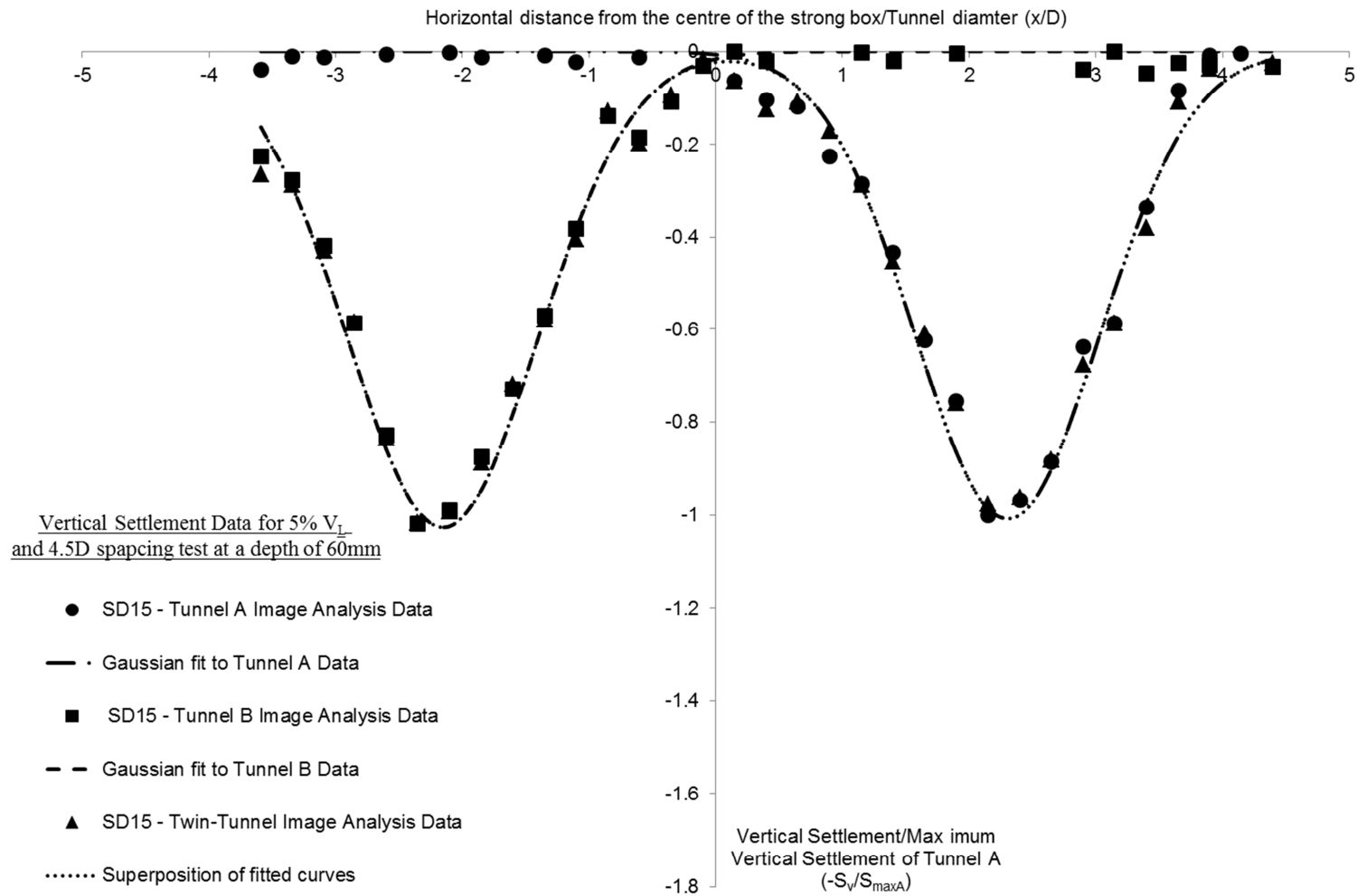


**Figure 8.30:** c) Vertical Settlement at a depth of 60mm in SD15

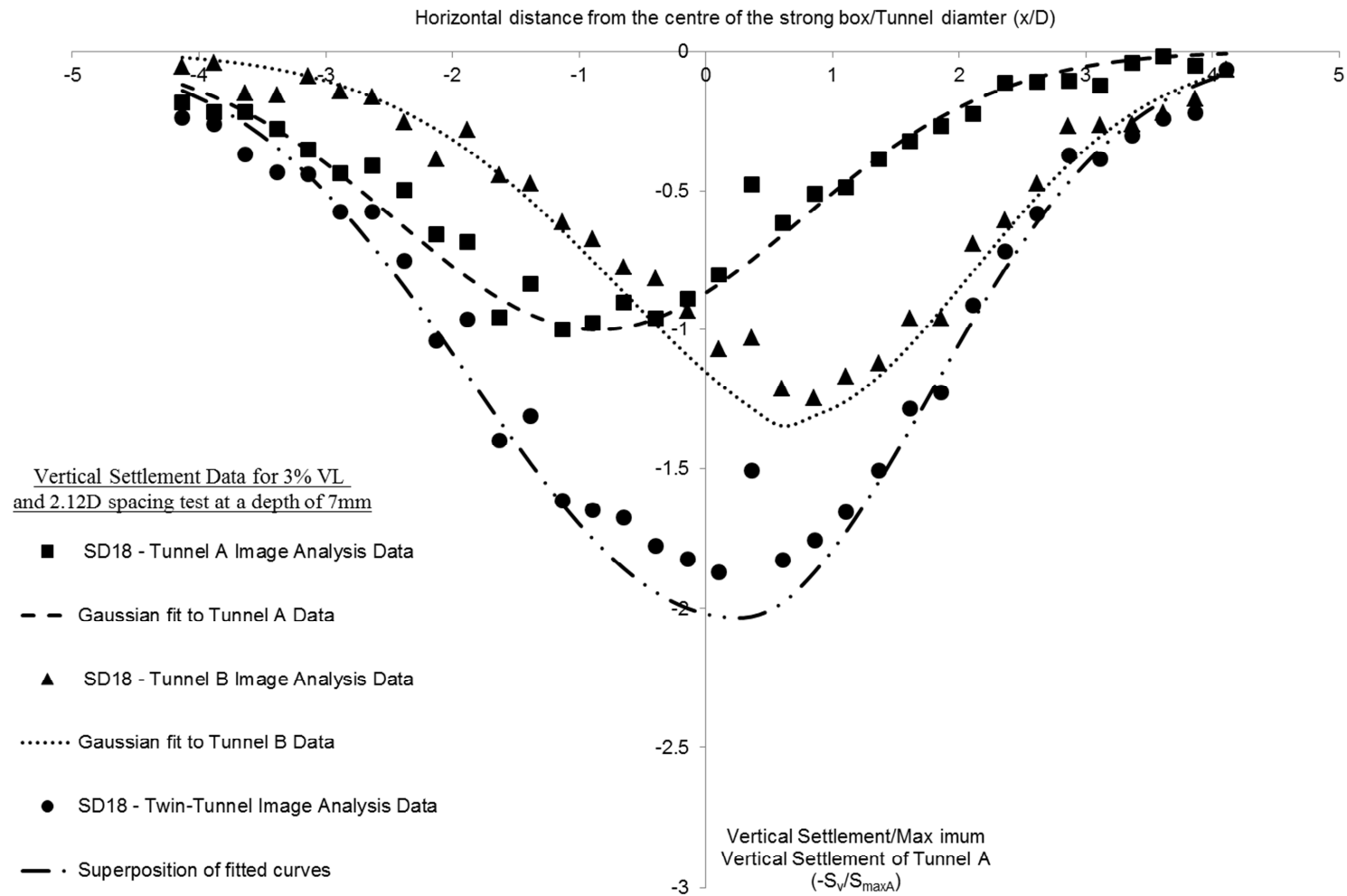


**Figure 8.31:** a) Vertical Settlement at a depth of 7mm in SD18

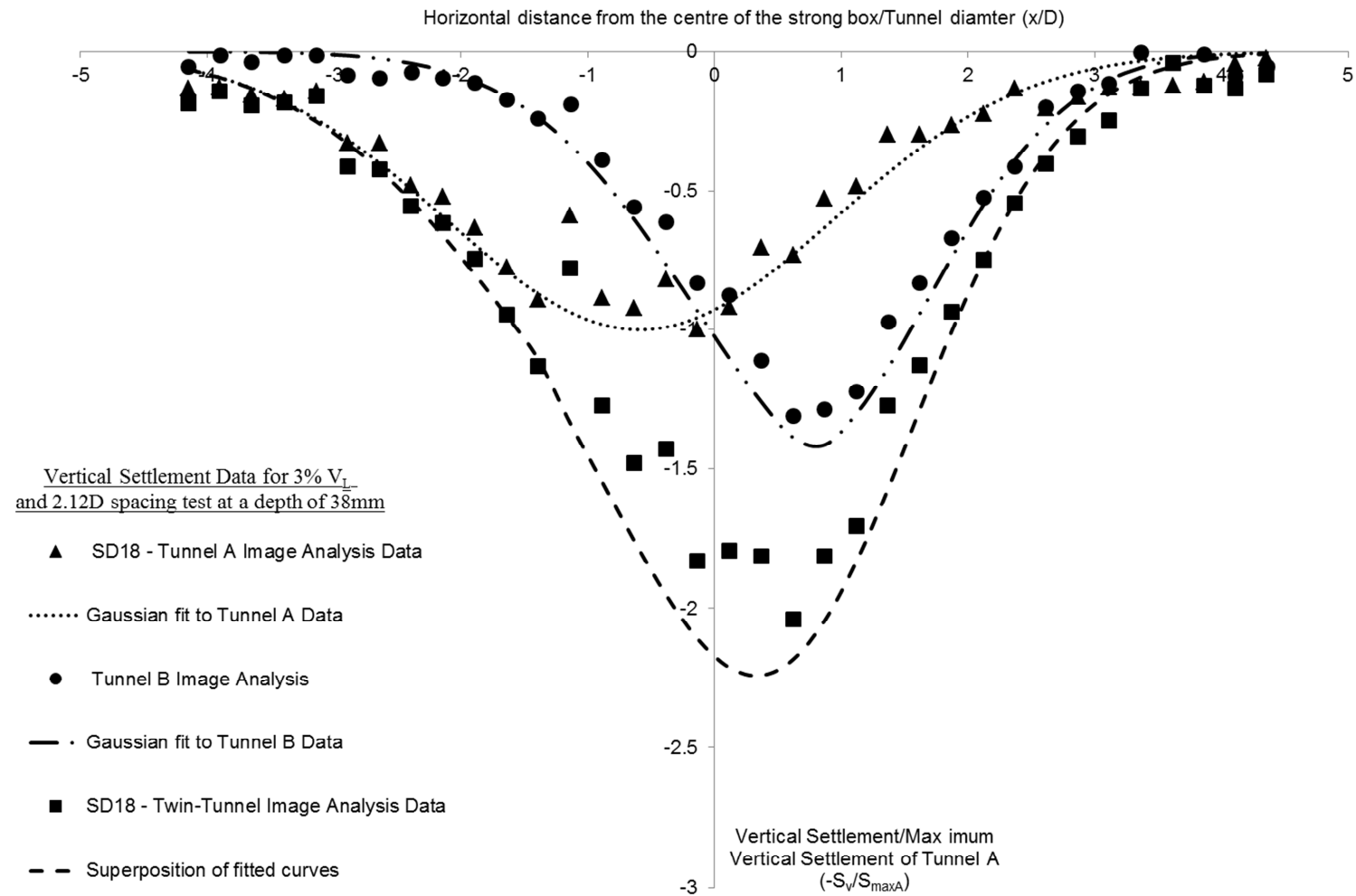


**Figure 8.31:** b) Vertical Settlement at a depth of 38mm in SD18

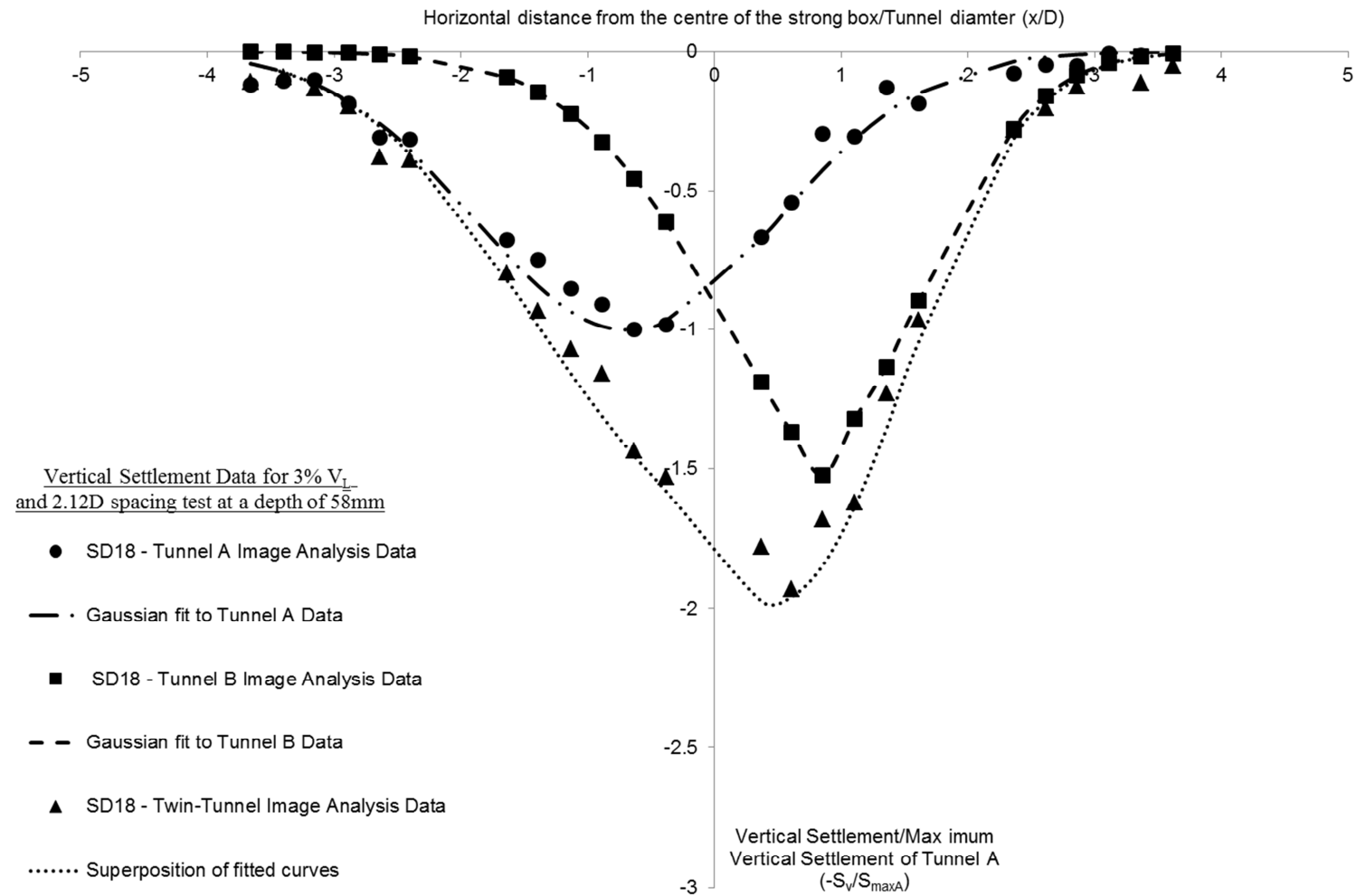


**Figure 8.31:** c) Vertical Settlement at a depth of 58mm in SD18

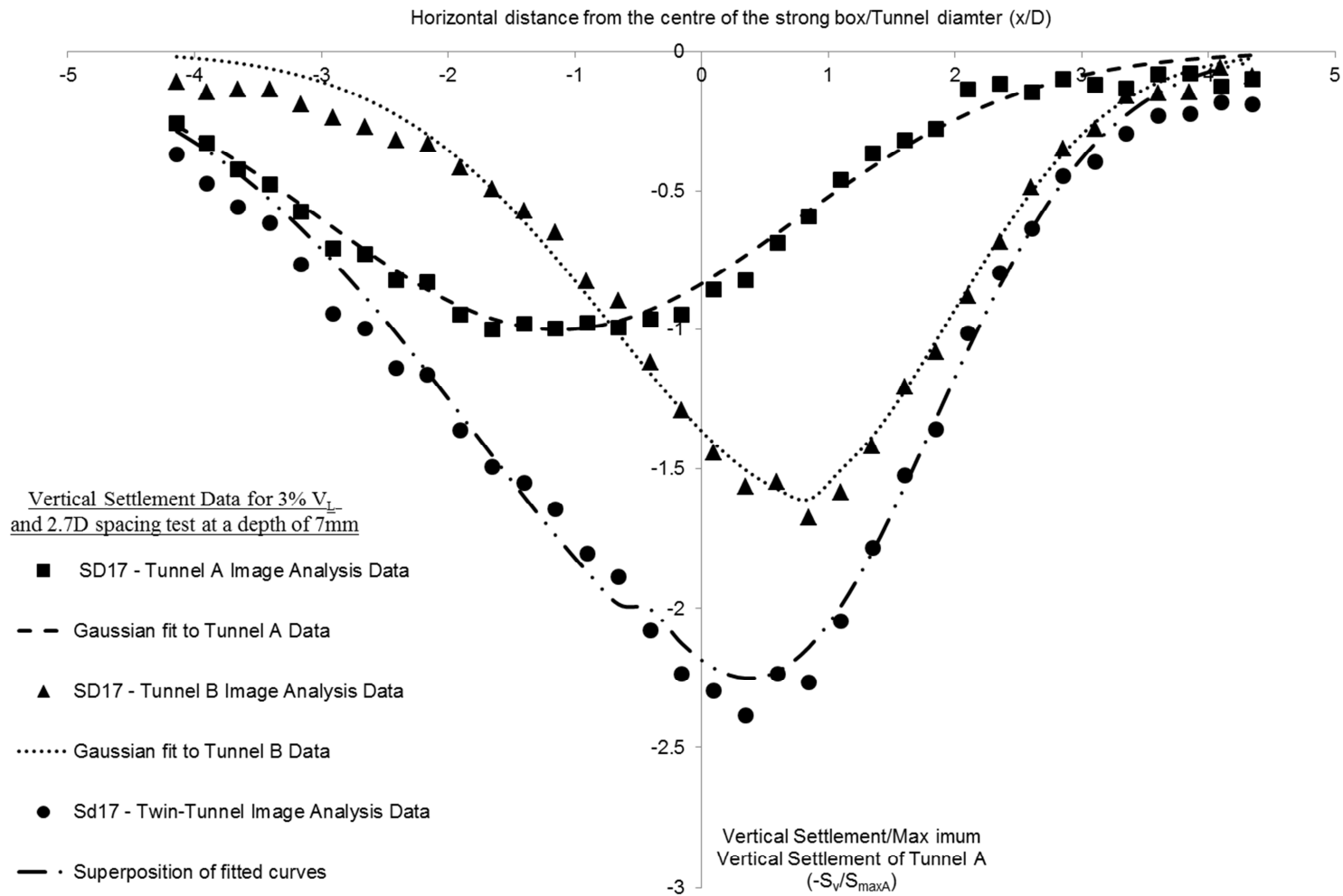


**Figure 8.32:** a) Vertical Settlement at a depth of 7mm in SD17



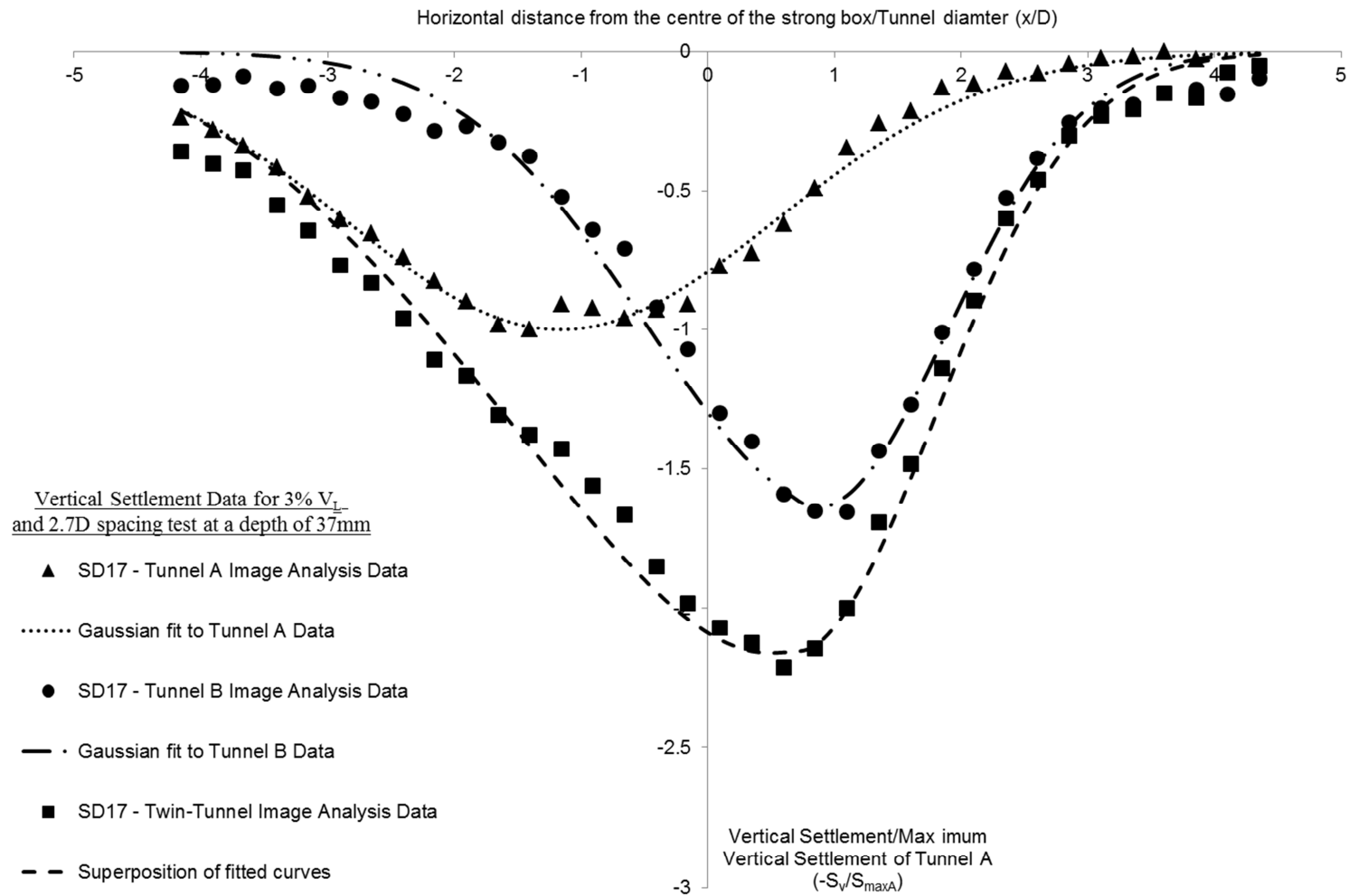


**Figure 8.32:** b) Vertical Settlement at a depth of 37mm in SD17

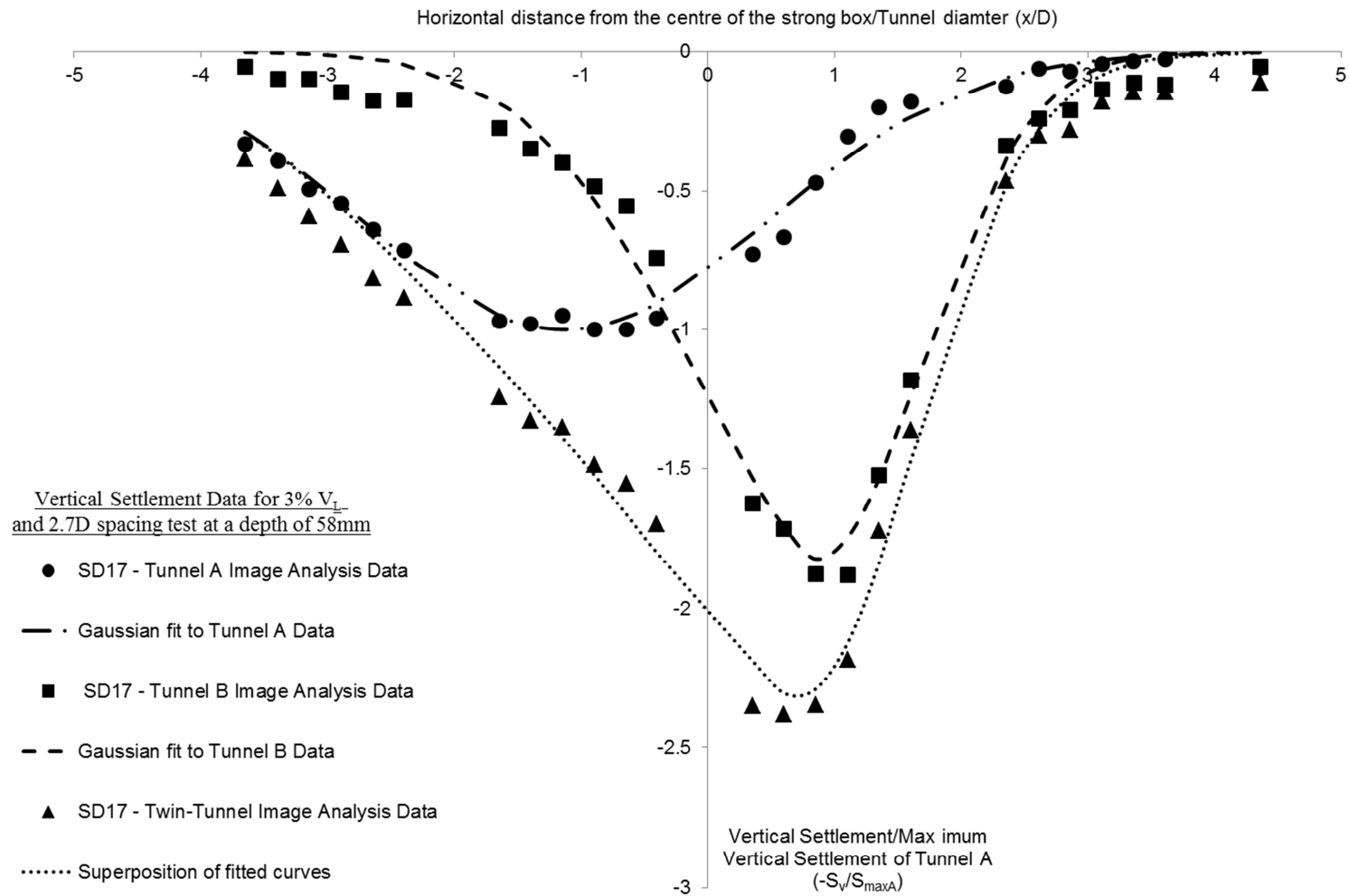


**Figure 8.32:** c) Vertical Settlement at a depth of 58mm in SD17

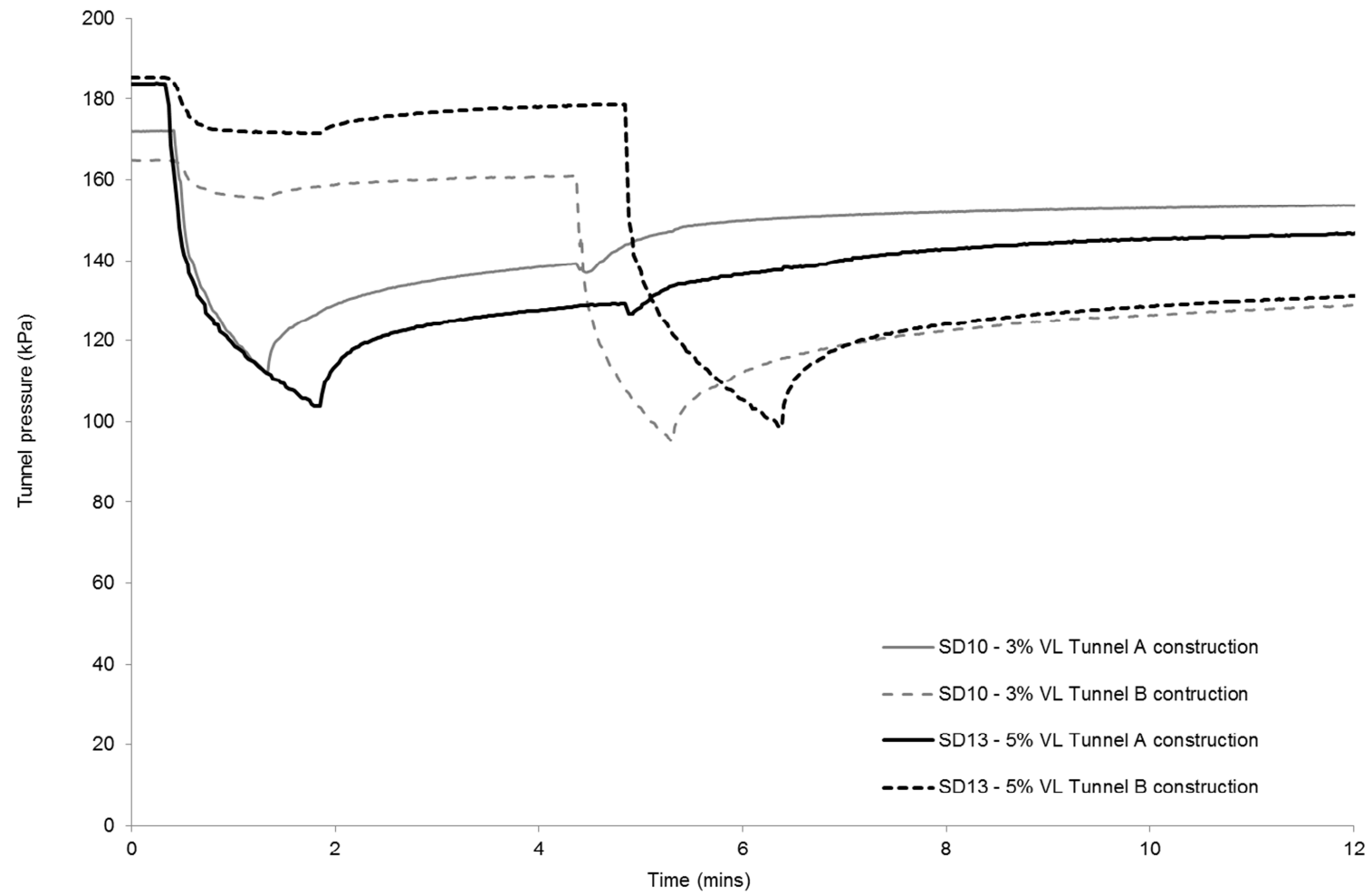


**Figure 8.33:** Tunnel Pressures measured during 1.5D spacing tests

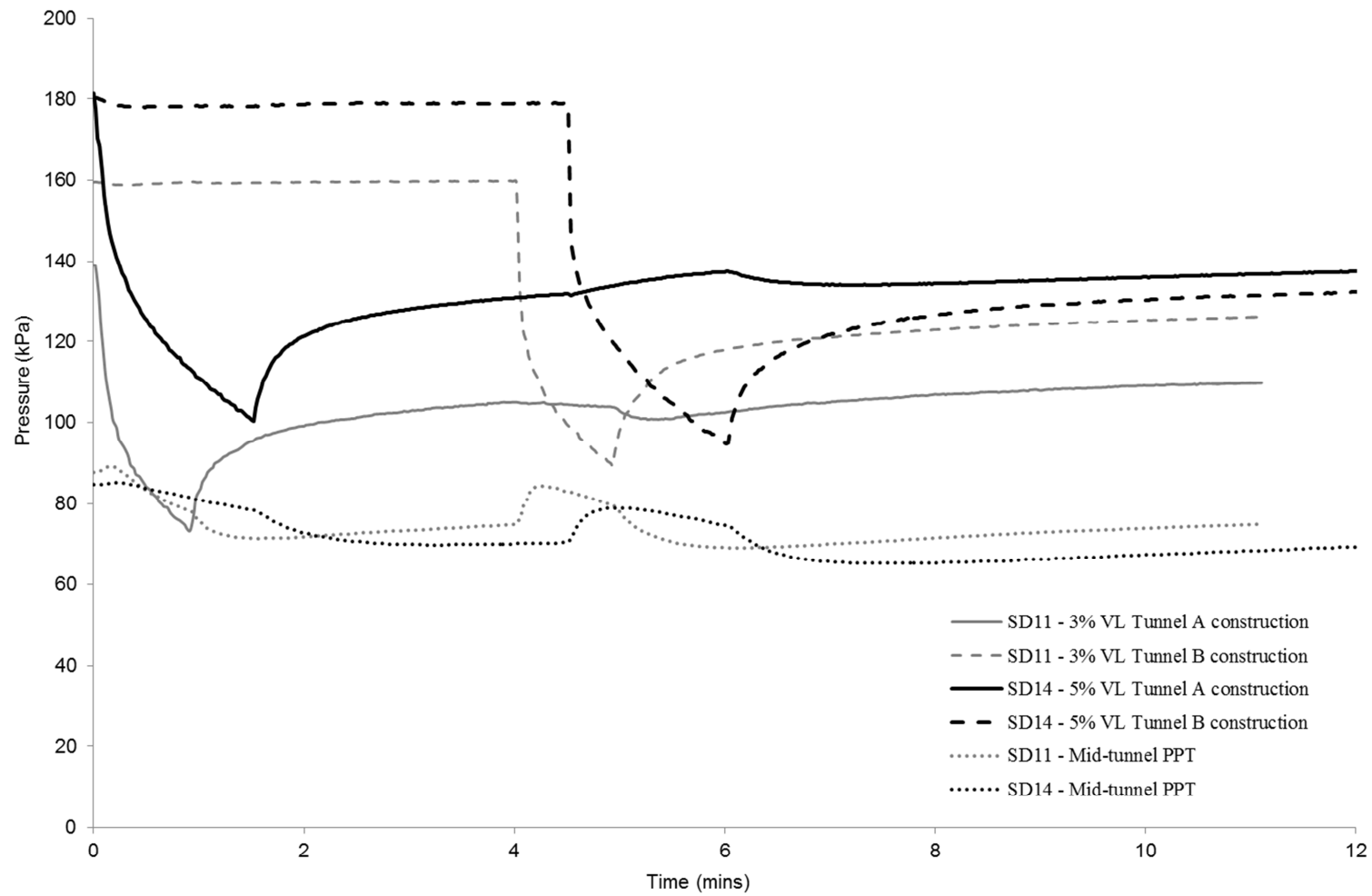


**Figure 8.34:** Tunnel Pressures and pore-water pressures measured during 3D spacing tests

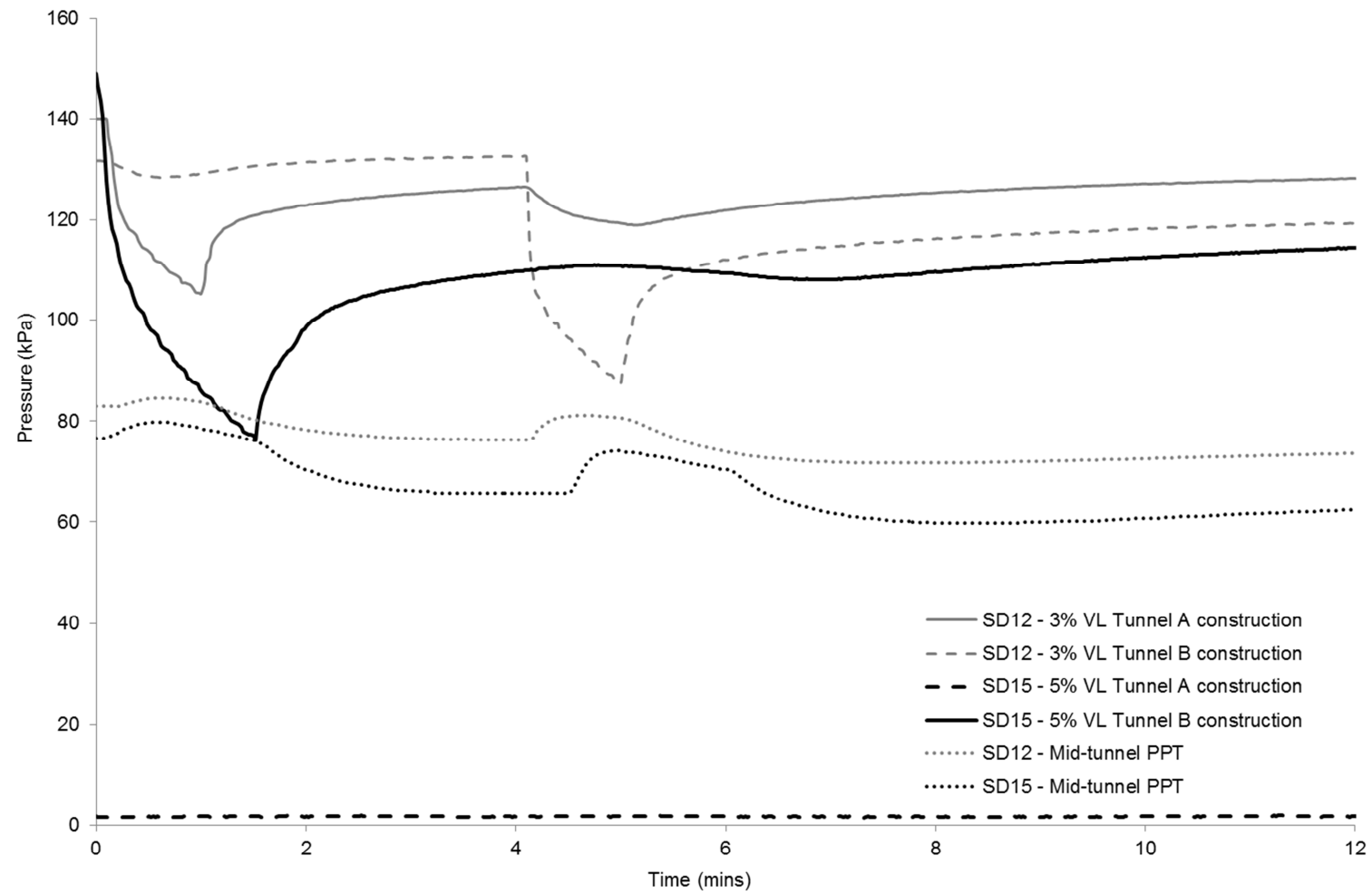


**Figure 8.35:** Tunnel Pressures and pore-water pressures measured during 4.5D spacing tests

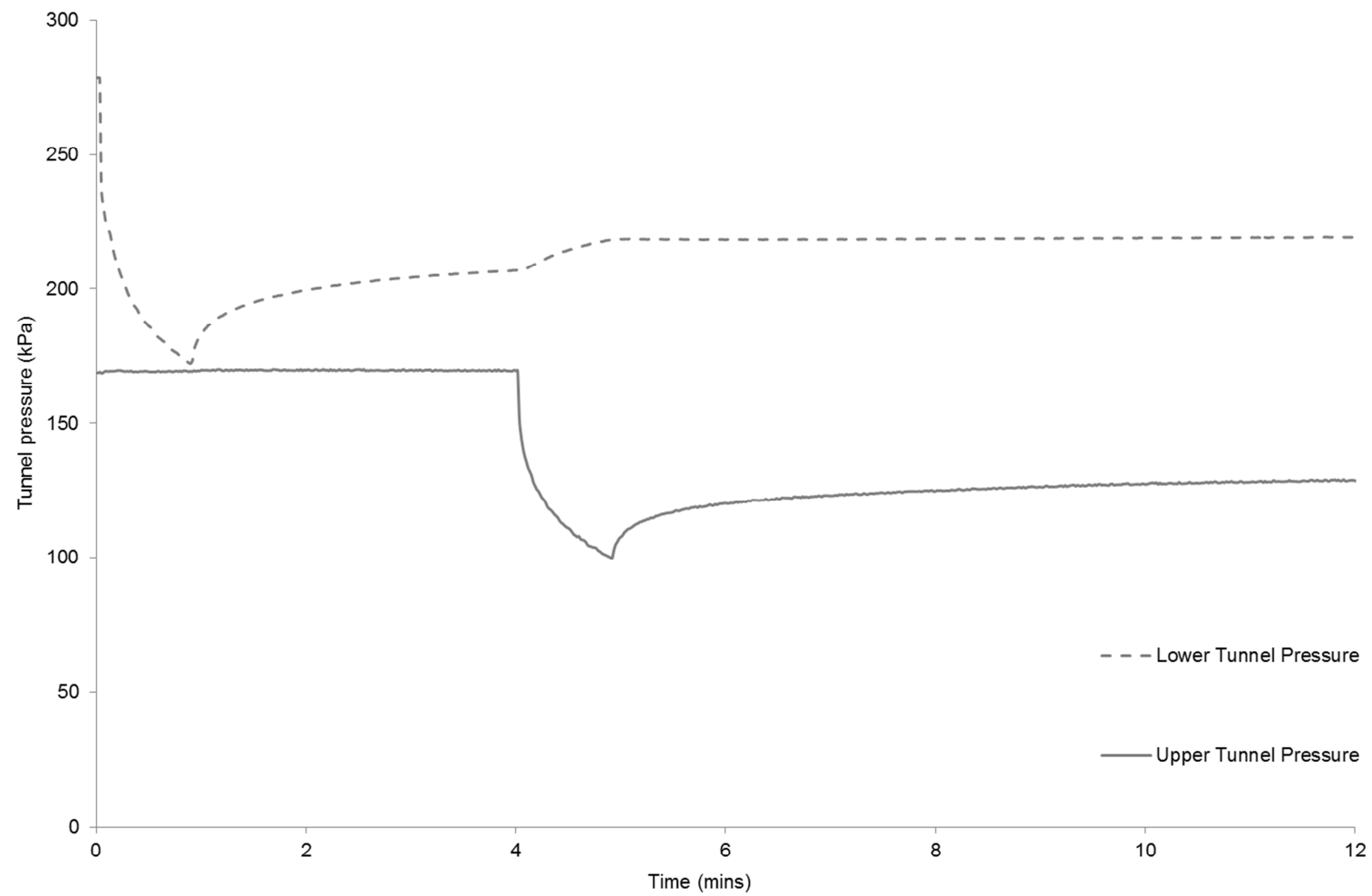


**Figure 8.36:** Tunnel Pressures measured during SD18 (2.12D spacing)

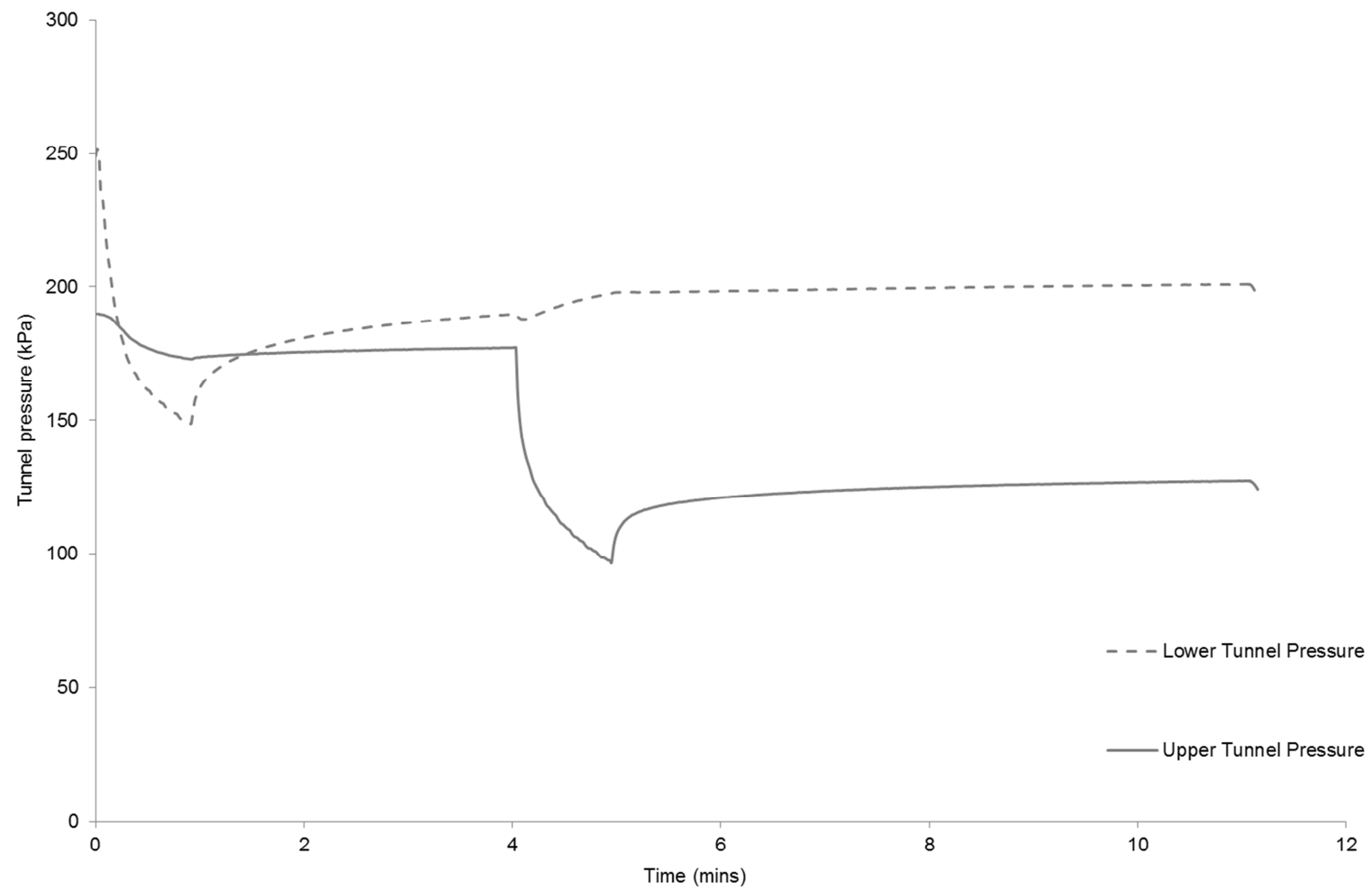


**Figure 8.37:** Tunnel Pressures measured during SD17 (2.7D spacing)

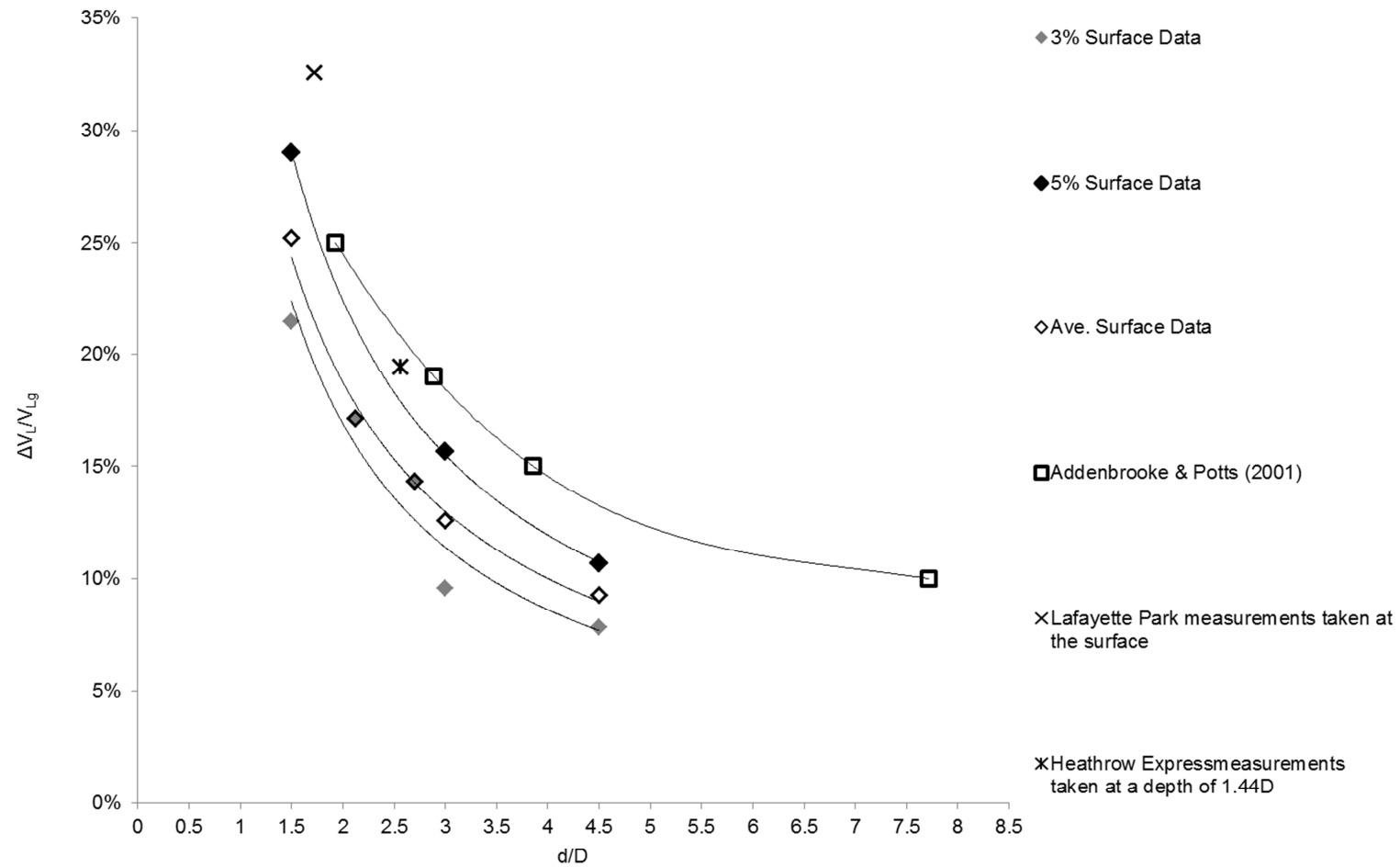


**Figure 9.1:** Volume loss of the second tunnel in respect to distance from the first (surface)



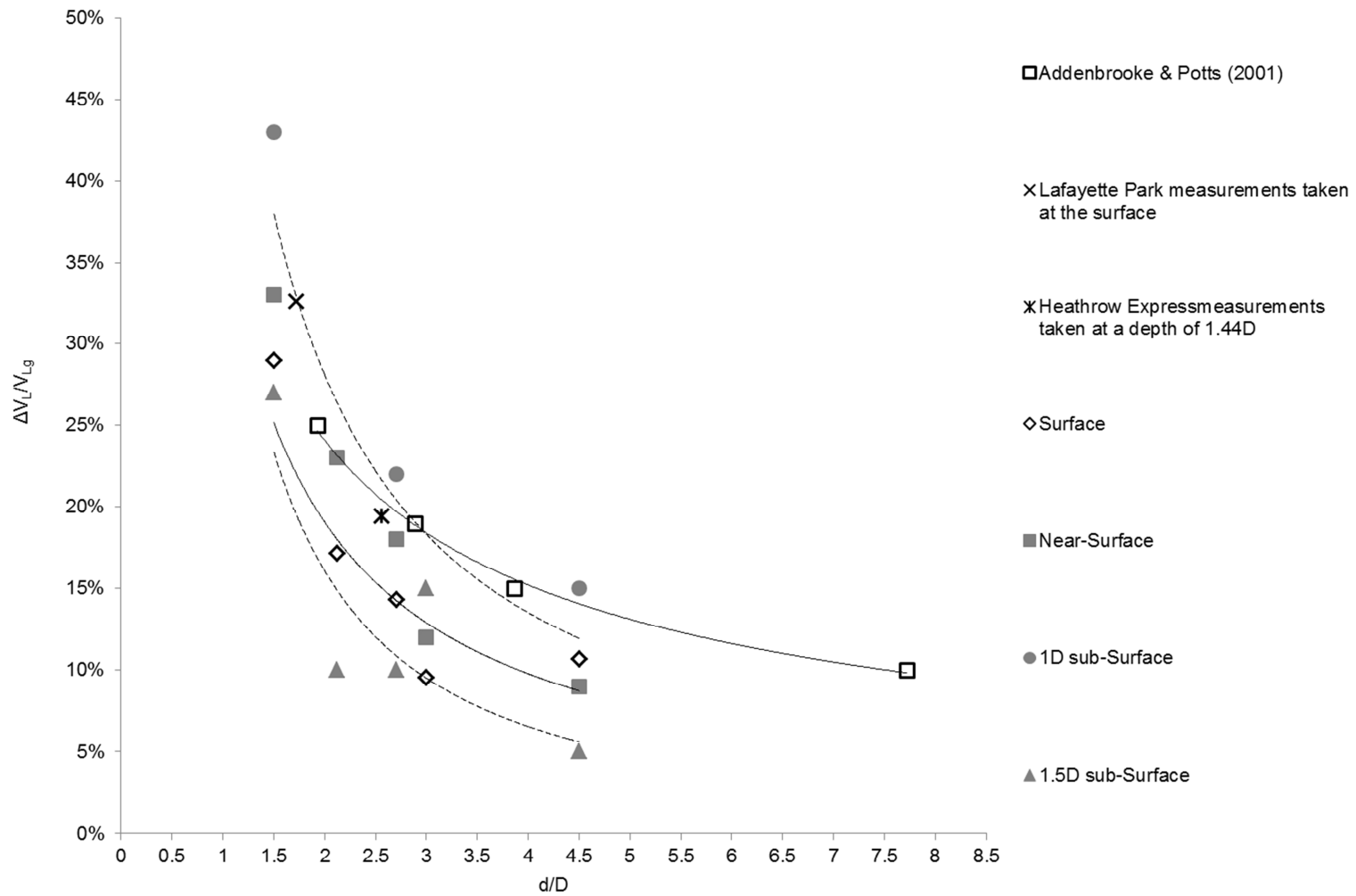


**Figure 9.2:** Volume loss of the second tunnel in regards to distance from the first (surface and sub-surface)

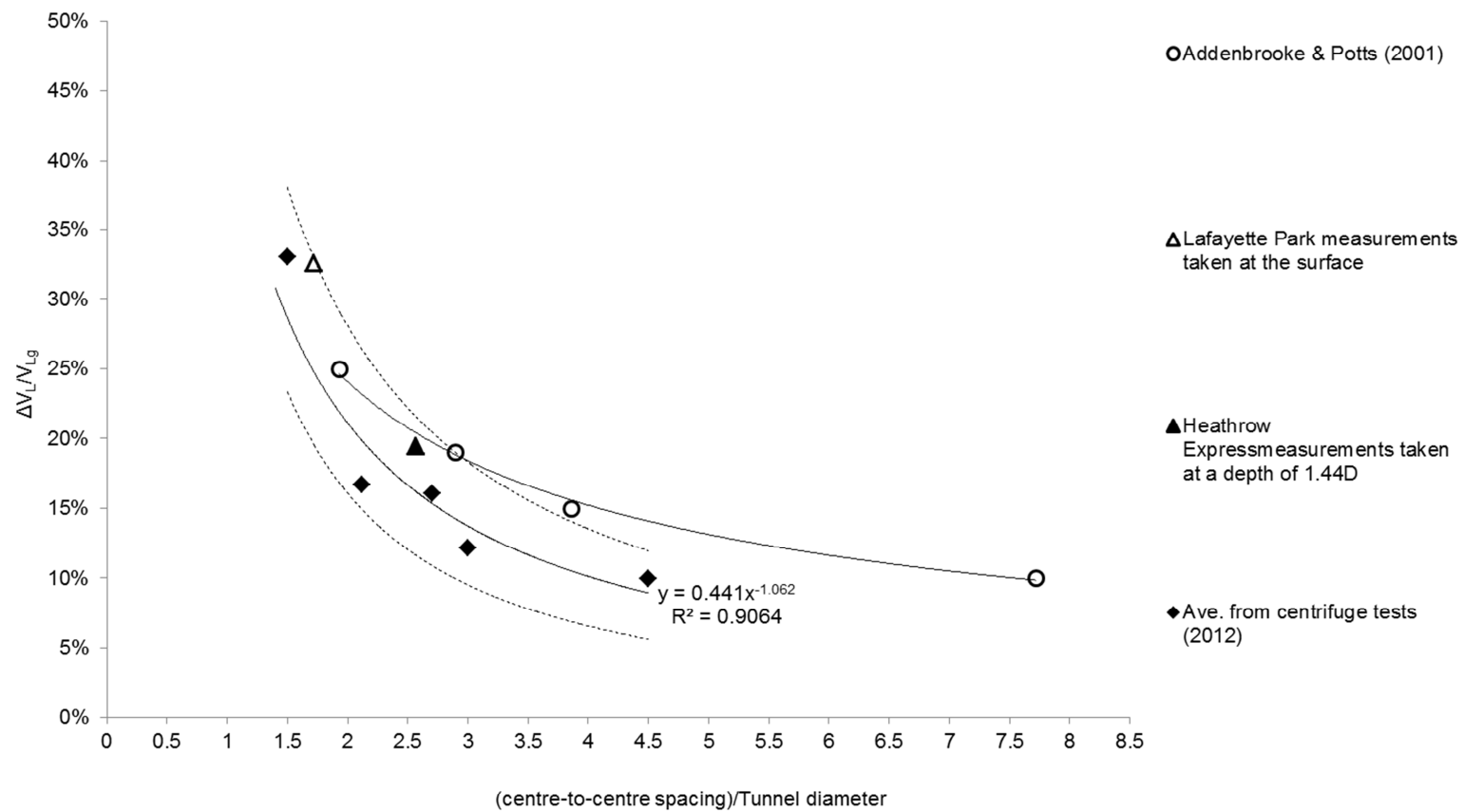


**Figure 9.3:** Volume loss of the second tunnel in regards to distance from the first (Design Chart)

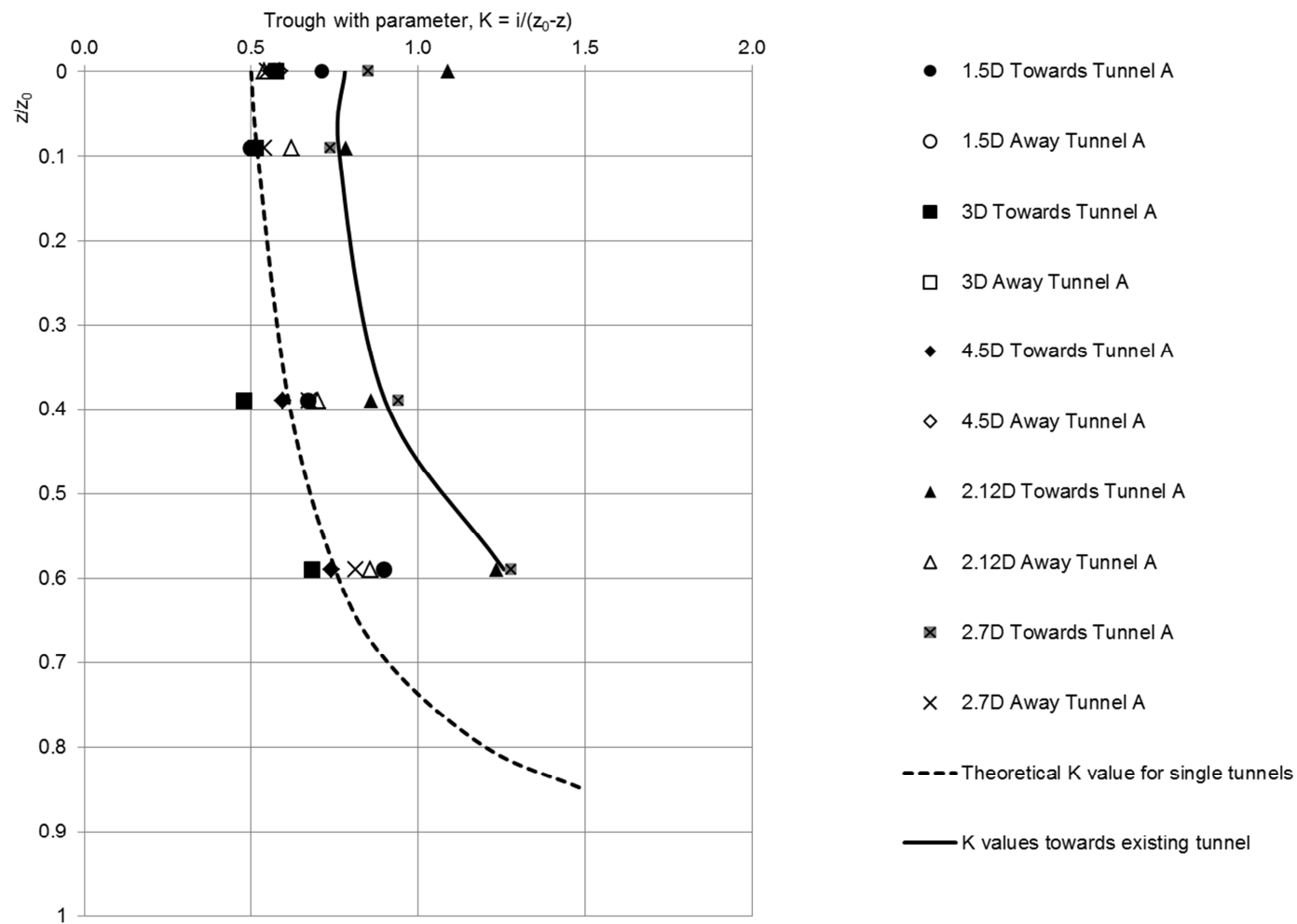


**Figure 9.4:** K with depth for the settlement towards the existing tunnel

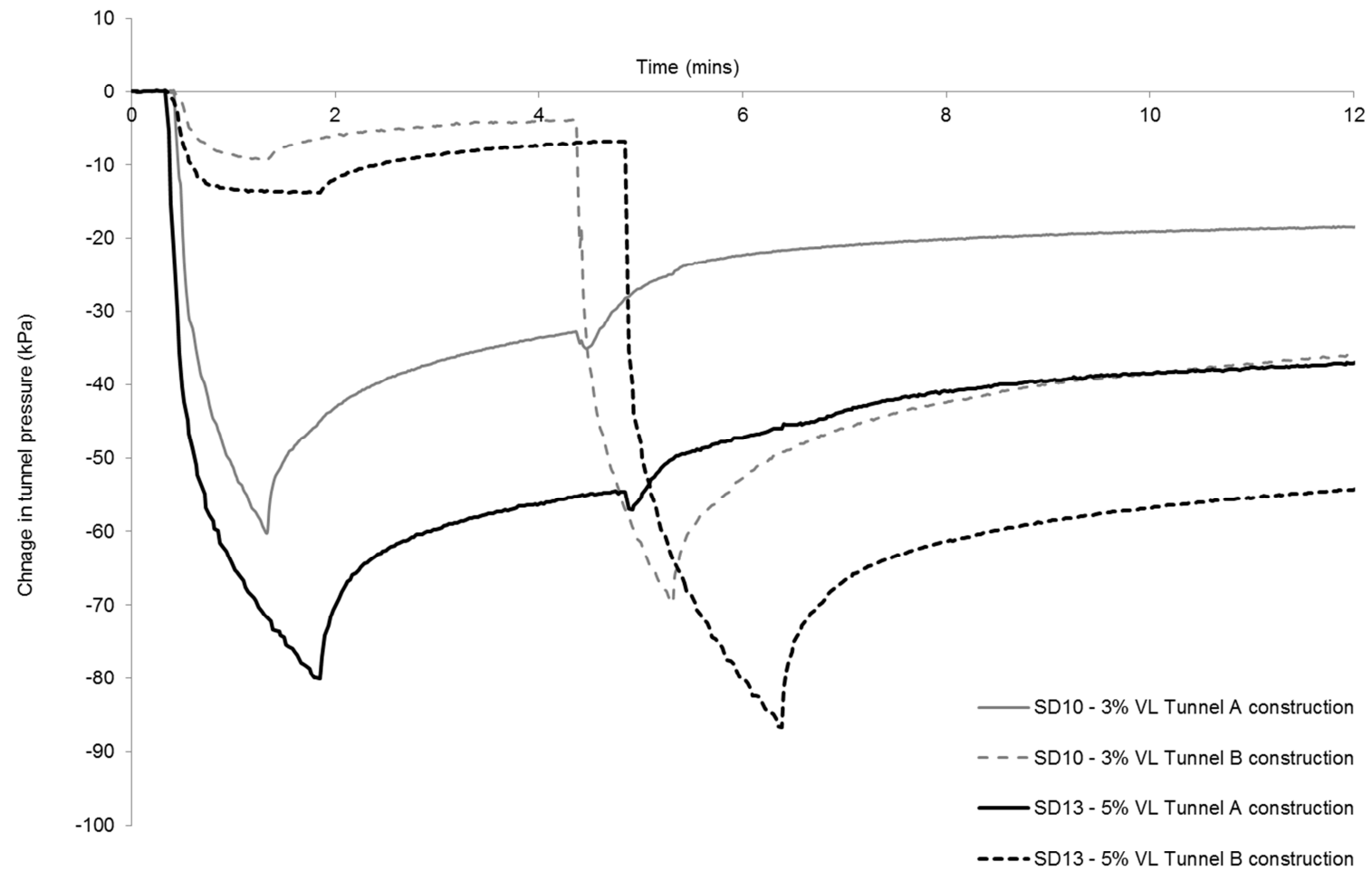


**Figure 9.5:** Pressure data during 1.5D spacing tests

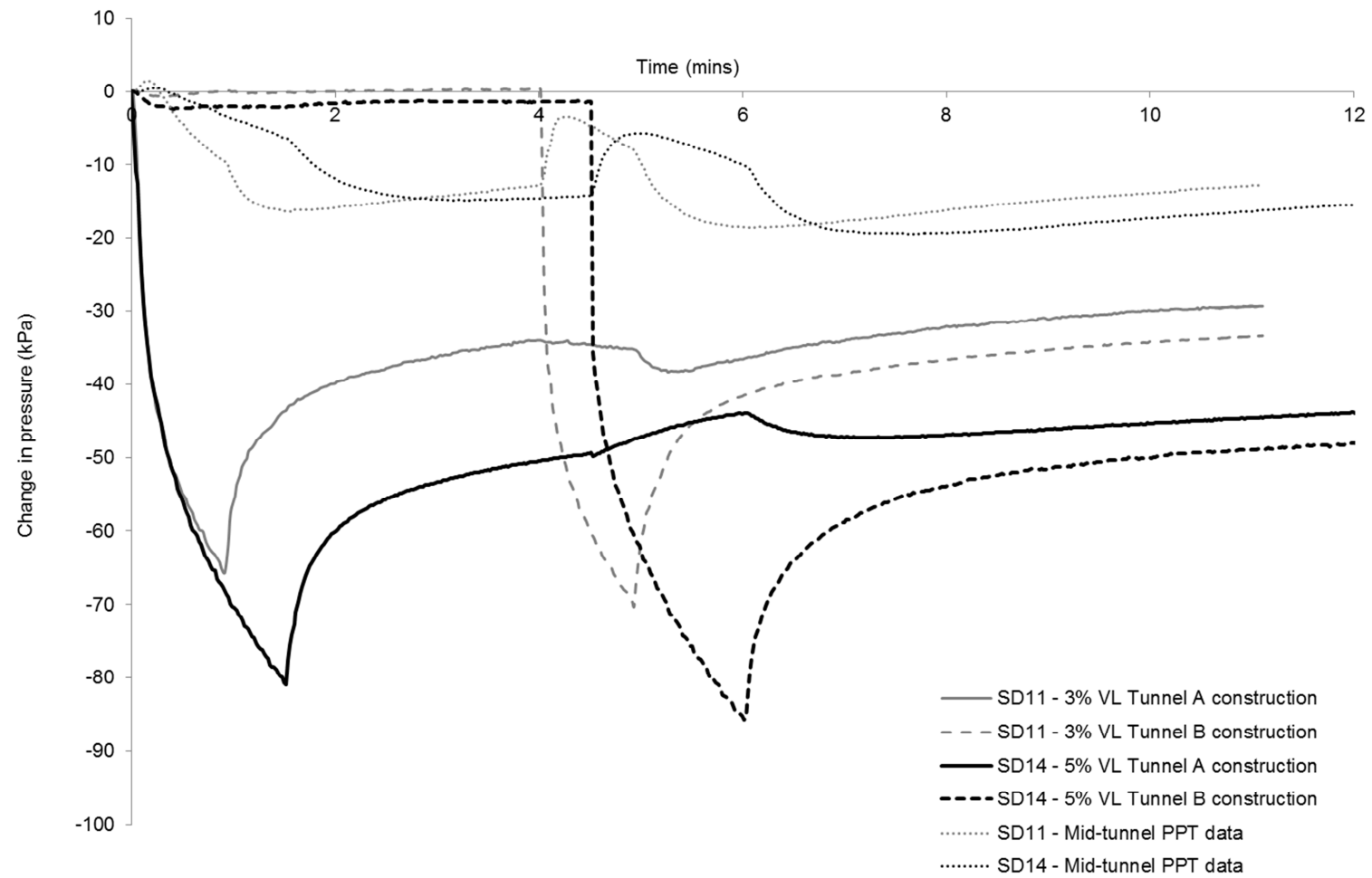


**Figure 9.6:** Pressure data during 3D spacing tests

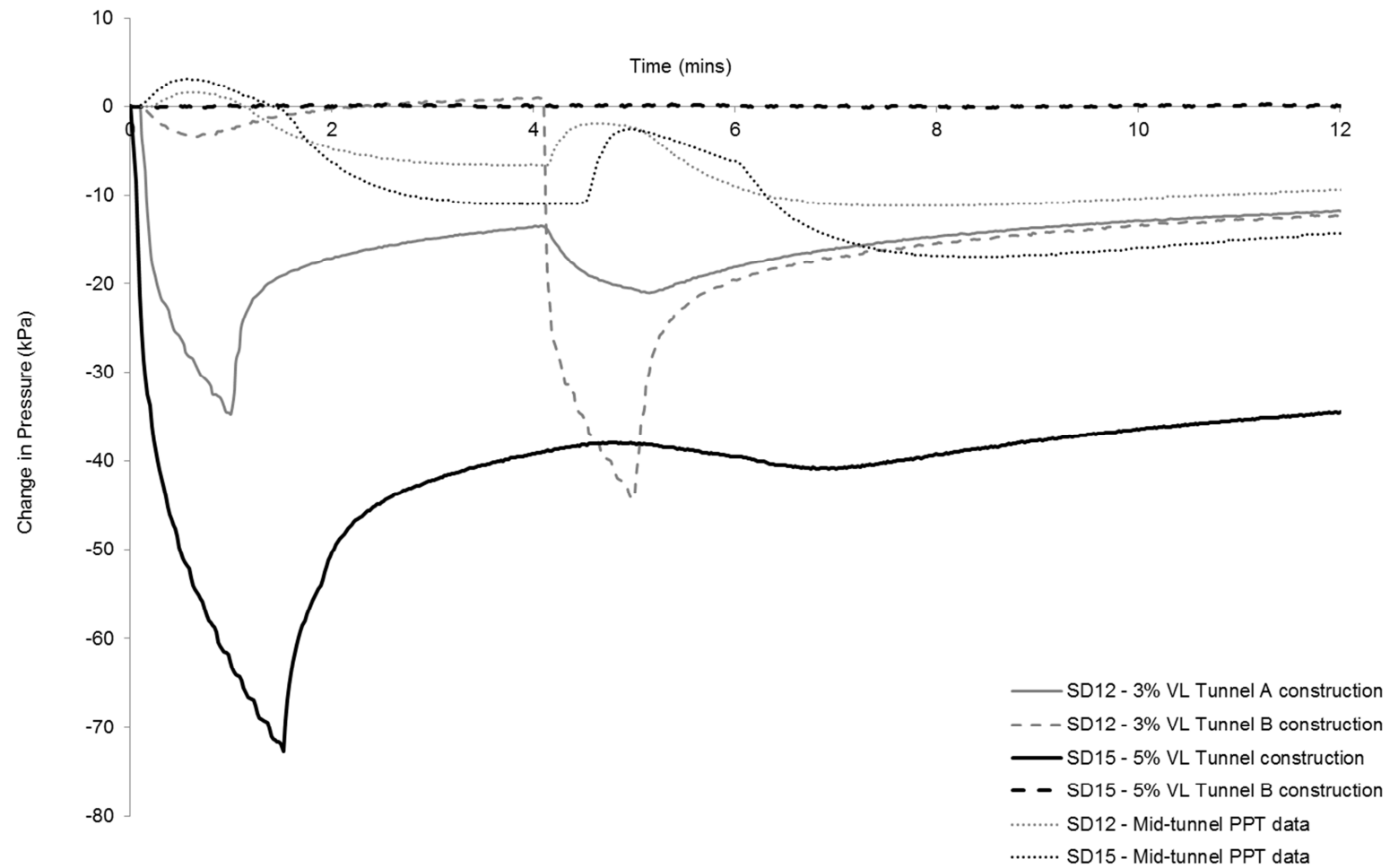
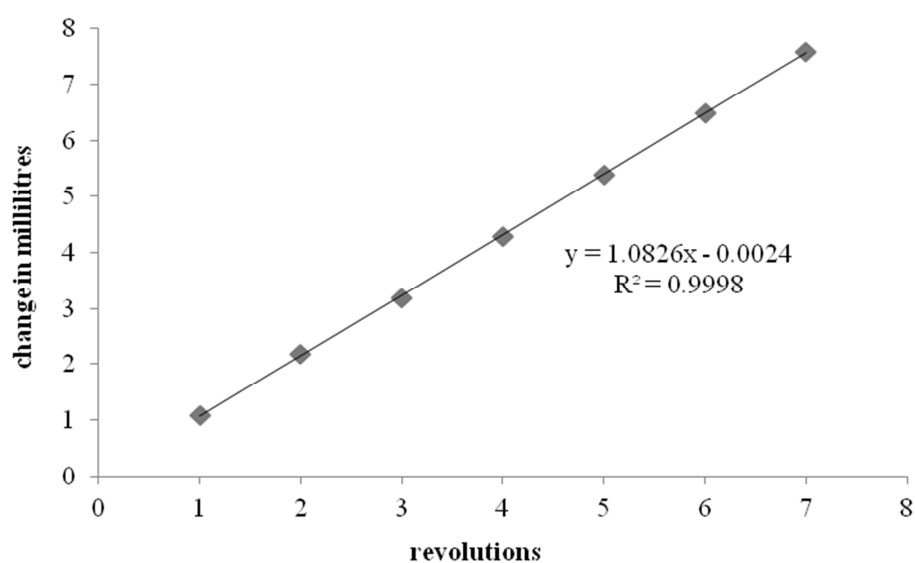


**Figure 9.7:** Pressure data during 4.5D spacing test

## APPENDIX A

The volume controlling apparatus was calibrated by measuring the change in water within a Burette per revolution.

revolutions	$\Delta$ ml
1	1.1
2	2.2
3	3.2
4	4.3
5	5.4
6	6.5
7	7.6



Therefore, 1.0826ml is moved per revolution.

## APPENDIX B

Test ID	Calibration Equations	
	Single Tunnel	Twin-Tunnel
SD13	$y = (1/0.7051)x$	$y = (1/0.7052)x$
SD11	$y = (1/0.3573)x$	$y = (1/0.425)x$
SD15	$y = (1/0.5579)x$	$y = (1/0.5591)x$
SD18	$y = (1/0.4903)x$	$y = (1/0.462)x$
SD17	$y = (1/0.8265)x$	$y = (1/0.9459)x$

Where, in the  $y=mx+c$  form,  $x$  is the vertical displacement from the Image Analysis and  $y$  is vertical displacement taking into account the window-clay surface/marker bead interface.



## APPENDIX C

### Thick cylinder analysis of twin tunnels (Tunnel A)

The calculations below are conducted using  $S_u = 49.8\text{kPa}$ ,  $E = 17500\text{kN/m}^2$ ,  $\gamma = 17.44\text{kN/m}^3$ ,  $\sigma_T = 73.3\text{kPa}$ ,  $a = 2$  and  $N = 2.030$  (taken from test SD11).

#### Linear-elastic perfectly plastic (E – constant)

##### Displacements

Using the stability equation from Mair & Taylor (1993);

$$N = 2 \log_e(c/a) + 1 - (c^2/b^2)$$

If  $b \gg c$  the  $(c^2/b^2)$  tends to zero the above equation becomes;

$$\frac{R_p}{a} = \exp\left(\frac{N-1}{2}\right)$$

And if  $R_p = c$ , then;  $R_p = 3.347\text{m}$ .

Using the equation for displacement from Mair & Taylor (1993);

$$\frac{U_r}{r} = \frac{3 S_u c^2}{2 E r^2}$$

If  $r = a$  in the above equation the result becomes;

$$\frac{U_{ra}}{a} = \frac{3 S_u c^2}{2 E a^2}$$

Therefore,  $U_{ra} = 0.02391\text{m}$ . If this displacement is assumed to be constant around the annulus of the cavity the subsequent volume loss is equal to 2.4%. The measured volume loss via the Gaussian curve fitting exercise was equal to 2.5%.

##### Pore-water pressures

Using the equation for pore pressure change from Mair & Taylor (1993) below;

$$\Delta u = S_u c^2 / b^2$$

If b was the edge of the box and equal to 27.5m (at prototype scale) and c the same value as above then  $\Delta u = 0.738\text{kPa}$ . The pore-water pressure data from the tests show an overall change in pore pressure (measured by the PPTs) of zero.

### **Non-linear-elastic ( $E = E_0(r/x)$ )**

#### Displacements

Using the stability equation from Mair & Taylor (1993);

$$N = 2 \log_e(c/a) + 2 - 2\left(c/b\right)$$

If  $b \gg c$  then  $\left(c/b\right)$  tends to zero the above equation becomes;

$$N/2 = \log_e(c/a) + 1$$

$$\exp(N/2 - 1) = (c/a)$$

And if  $R_{pnl} = c$ , then;  $R_p = 2.030\text{m}$ .

Using the equation for displacement from Mair & Taylor (1993);

$$\frac{U_r}{r} = \frac{3}{2} \frac{r}{E} \frac{S_u}{r} \frac{c}{r}$$

If  $r = a$  and  $b \gg c$  in the above equation the result becomes;

$$\frac{U_r}{r} = \frac{3}{2} \frac{S_u}{E} \frac{a}{r} \exp\left(\frac{N}{2} - 1\right)$$

$$\frac{U_{ra}}{a} = \frac{3}{2} \frac{S_u}{E} \frac{a}{a} \exp\left(\frac{N}{2} - 1\right)$$

Therefore,  $U_{ra} = 0.0086616\text{m}$ . If this displacement is assumed to be constant around the annulus of the cavity the subsequent volume loss is equal to 0.9%. The measured volume loss via the Gaussian curve fitting exercise was equal to 2.5%.

### Pore-water pressures

Using the equation for pore pressure change from Mair & Taylor (1993) below;

$$\Delta u = S_u \left( \frac{2c}{b} - \frac{c}{r} \right)$$

If  $b \gg c$  the above equation becomes,

$$\Delta u = S_u \left( -\frac{c}{r} \right)$$

If  $r$  is the distance to the PPT between the tunnels and equal to 6m (at prototype scale) and  $c = R_{pnl}$  then  $\Delta u = -16.8 \text{ kPa}$ .

### **Thick cylinder analysis of twin tunnels (Tunnel B)**

The calculations below are conducted using  $S_u = 49.8 \text{ kPa}$ ,  $E = 17500 \text{ kN/m}^2$ ,  $\gamma = 17.44 \text{ kN/m}^3$ ,  $\sigma_T = 69.3 \text{ kPa}$ ,  $a = 2$  and  $N = 2.111$  (taken from test SD11).

### **Linear-elastic perfectly plastic (E - constant)**

#### Displacements

Using the stability equation from Mair & Taylor (1993);

$$N = 2 \log_e \left( \frac{c}{a} \right) + 1 - \left( \frac{c^2}{b^2} \right)$$

If  $b \gg c$  the  $\left( \frac{c^2}{b^2} \right)$  tends to zero the above equation becomes;

$$\frac{R_p}{a} = \exp \left( \frac{N - 1}{2} \right)$$

And if  $R_p = c$ , then;  $R_p = 3.485 \text{ m}$ .

Using the equation for displacement from Mair & Taylor (1993);

$$\frac{U_r}{r} = \frac{3 S_u c^2}{2 E r^2}$$

If  $r = a$  in the above equation the result becomes;

$$\frac{U_{ra}}{a} = \frac{3 S_u c^2}{2 E a^2}$$

Therefore,  $U_{ra} = 0.0259\text{m}$ . If this displacement is assumed to be constant around the annulus of the cavity the subsequent volume loss is equal to 2.6%. This value is higher than the value calculated for Tunnel A.

#### Pore-water pressures

Using the equation for pore pressure change from Mair & Taylor (1993) below;

$$\Delta u = S_u c^2 / b^2$$

If  $b$  was the edge of the box and equal to 27.5m (at prototype scale) and  $c$  the same value as above then  $\Delta u = 0.799\text{kPa}$ . The pore-water pressure data from the tests show an overall change in pore pressure (measured by the PPTs) of zero.

#### **Non-linear-elastic ( $E = E_0(r/x)$ )**

#### Displacements

Using the stability equation from Mair & Taylor (1993);

$$N = 2 \log_e(c/a) + 2 - 2\left(\frac{c}{b}\right)$$

If  $b \gg c$  then  $\left(\frac{c}{b}\right)$  tends to zero the above equation becomes;

$$N/2 = \log_e(c/a) + 1$$

$$\exp(N/2 - 1) = (c/a)$$

And if  $R_{pnl} = c$ , then;  $R_p = 2.114\text{m}$ .

Using the equation for displacement from Mair & Taylor (1993);

$$\frac{U_r}{r} = \frac{3 r S_u c}{2 E r r}$$

If  $r = a$  and  $b \gg c$  in the above equation the result becomes;

$$\frac{U_r}{r} = \frac{3}{2} \frac{S_u}{E} \frac{a}{r} \exp\left(\frac{N}{2} - 1\right)$$

$$\frac{U_{ra}}{a} = \frac{3}{2} \frac{S_u}{E} \frac{a}{a} \exp\left(\frac{N}{2} - 1\right)$$

Therefore,  $U_{ra} = 0.004512\text{m}$ . If this displacement is assumed to be constant around the annulus of the cavity the subsequent volume loss is equal to 0.45%.

#### Pore-water pressures

Using the equation for pore pressure change from Mair & Taylor (1993) below;

$$\Delta u = S_u \left( \frac{2c}{b} - \frac{c}{r} \right)$$

If  $b \gg c$  the above equation becomes,

$$\Delta u = S_u \left( -\frac{c}{r} \right)$$

If  $r$  is the distance to the PPT between the tunnels and equal to 6m (at prototype scale) and  $c = R_{pnl}$  then  $\Delta u = -17.5\text{kPa}$ .

## **APPENDIX D**

### **Publications**

Divall, S., Goodey, R.J., and Taylor, R.N. (2012). Ground movements generated by sequential Twin-tunnelling in over-consolidated clay. Proceedings of the 2<sup>nd</sup> European Conference on Physical Modelling in Geotechnics, Delft – online publication by TU Delft Library .

Divall, S. and Goodey, R.J. (2012). Apparatus for centrifuge modelling of sequential twin-tunnel construction. International Journal of Physical Modelling in Geotechnics, Vol. 12, No. 3, pp. 102-111.

Divall, S. & Goodey, R.J. (2012). Novel apparatus for generating ground movements around sequential twin tunnels in over-consolidated clay. Proceedings of the 12<sup>th</sup> BGA Young Geotechnical Engineers Symposium, Leeds, pp. 10-11 – Online publication by Proceedings of the ICE – Geotechnical Engineering.